**University of Groningen**

Substrate and Cation Binding Mechanism of Glutamate Transporter Homologs

Jensen, Sonja

**IMPORTANT NOTE: You are advised to consult the publisher's version (publisher's PDF) if you wish to cite from it. Please check the document version below.**

*Document Version*
Publisher's PDF, also known as Version of record

*Publication date:*
2017

Link to publication in University of Groningen/UMCG research database

*Citation for published version (APA):*
Jensen, S. (2017). *Substrate and Cation Binding Mechanism of Glutamate Transporter Homologs*. University of Groningen.

# Substrate and Cation Binding Mechanism of Glutamate Transporter Homologs

Sonja Jensen

# Substrate and Cation Binding Mechanism of Glutamate Transporter Homologs

**PhD thesis**

to obtain the degree of PhD at the
University of Groningen
on the authority of the
Rector Magnificus Prof. E. Sterken
and in accordance with
the decision by the College of Deans.

This thesis will be defended in public on

Friday 19 May 2017 at 11.00 hours

by

**Sonja Jensen**

born on 24 March 1981
in Hannover, Germany

**Supervisor**
Prof. dr. D.J. Slotboom

**Assessment Committee**
Prof. dr. A.J.M. Driessen
Prof. dr. R. Dutzler
Prof. dr. B. Poolman

# Content

# List of Figures

# List of Tables

# Chapter 1

## General Introduction and Outline of the Thesis

**Sonja Jensen**

**Abstract**

Glutamate transporters and their homologs are integral membrane proteins belonging to the class of secondary active transporters. As such, glutamate transporters fuel the concentrative transport of negatively charged amino acids with the downhill transport of sodium ions and/or protons. In eukaryotes glutamate transporters are involved in excitatory signal transmission and are implied to play a role in neuronal death after ischemia and neurodegenerative diseases such as Alzheimer's, Huntington's and epilepsy. In prokaryotes the same type of transporters enable the up-take of glutamate and aspartate as nutrients. Extensive biochemical, biophysical, X-ray crystallographic, and computational studies aimed to functionally characterize the known transporters and unravel the transport mechanism. This chapter summarizes the current insights on transport mechanism, substrate binding, and ion coupling of glutamate transporters and their homologs.
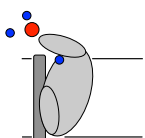
## Membrane Proteins

All living cells are separated from their environment by at least one membrane consisting of a lipid bilayer, which shields the cell content from the exterior. The barrier must allow the uptake of nutrients, extrusion of waste products and toxic compounds, and interaction with signaling molecules in order to grow, divide, orient, and communicate. These processes are mediated by various groups of membrane-associated proteins. While membrane receptor proteins sense and transduce signals from the environment, membrane transport proteins move molecules and ions across the membrane. Depending on the size, charge, abundance, and importance of the transported solute (molecule or ion) many different transporter types and transport mechanisms can be found.

## Passive transporters

Channels and pores allow for passive movement (i.e. diffusion) across the membrane. Both of these transporter types are membrane spanning and display a huge diversity in their selectivity for the cargo. The type of transported solute can vary from small ions to big macromolecules of more than 6 kDa[1] and can be very specific (e.g. potassium channels) or rather unspecific (e.g. mechanosensitive channels of large conductance). Anything that fits can pass, following down its (electro) chemical gradient (downhill transport) into a thermodynamically favorable direction. Therefore, no energy input is required and the transport rates can reach near diffusion limiting rates (e.g. for potassium channels the rate can reach $10^8$ ions per second[2]).

Both pores and channels are simultaneously open to both sides of the membrane during their transporting state. Pores are always open to both sides, and therefore always active. In contrast, channels require a trigger to induce conformational changes that open and activate them. Such a trigger can be the binding of a ligand (e.g. chemical), photon or ion, a change in the electric potential (voltage gated) or mechanical force (stretching of the membrane). Examples for the mentioned channels are acetylcholine receptors (AChR), zinc activated ion channels (ZnC), channelrhodopsin 1 and 2, voltage-gated ion channels, and mechanosensitive channels (for ions (MS) and large conductance (MscL)).
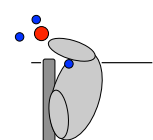
In contrast to channels and pores, carriers never form a continuous opening from one side of the membrane to the other (figure 1.1). As carriers facilitate the movement of solutes, they undergo substantial conformational changes, in which they expose the binding site alternately to the intracellular and extracellular space (alternating access, a term first described by Jardetzky in 1966[3]). In many carrier types, the transported solute may even be completely occluded from the extracellular and the intracellular environment at some stage during the transport cycle. Carriers that transport a substrate down their (electro) chemical gradient (downhill) are called uniporters. The mitochondrial $Ca^+$ uniporter[4] and the glucose transporter GLUT1[5] are examples for this group of transporters. Other carriers facilitate uphill transport of substances and belong to the active transporter proteins (figure 1.1).

**Active transporters**

The translocation into a thermodynamically unfavorable direction (e.g. concentrative transport) requires additional energy and is accomplished by active transport proteins. Active transport proteins can be divided into two classes: primary active transporters and secondary active transporters. Primary active transporters use metabolic or chemically stored energy to transport molecules across the membrane. Most members of the primary active transporters are ATPases, such as <u>A</u>TP <u>b</u>inding <u>c</u>assette (ABC) transporters. They directly use the energy that is released upon the hydrolysis of adenosine triphosphate (ATP) to adenosine diphosphate (ADP) and phosphate (Pi) to fuel the uphill translocation of the transported cargo, which may be an inorganic ion, or a wide variety of molecules[6–8]. But other sources of metabolic energy can be found too. One example is the use of redox energy in the case of the electron transport chain, in which for instance the oxidation of nicotinamide adenine dinucleotide (NADH to $NAD^+$) is utilized to move protons across the inner mitochondrial membrane[9].

Secondary active transporters use the energy stored in electrochemical gradients of one solute to move another solute (the substrate) in a thermodynamically unfavorable direction across the membrane. In this case the energetically unfavorable transport process of the substrate is coupled to the energetically favorable transport of other ions and molecules (driving ion/molecule) down their concentration gradient in such a way that the overall free energy change is still favorable. This coupling can be either by symport (co-transport) or
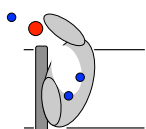
antiport (counter-transport or exchange) of substrate and coupling molecule/ion[10]. The effectiveness of concentrating a certain substrate (concentrative capacity) is related not only to the concentration gradient of the driving ion/molecule, but also to the stoichiometry of coupling ion/molecule to substrate, because of the thermodynamic coupling between driving ion/molecule and substrate transport. That means a higher driving ion/molecule to substrate ratio also leads to an increased concentrative capacity of transport.
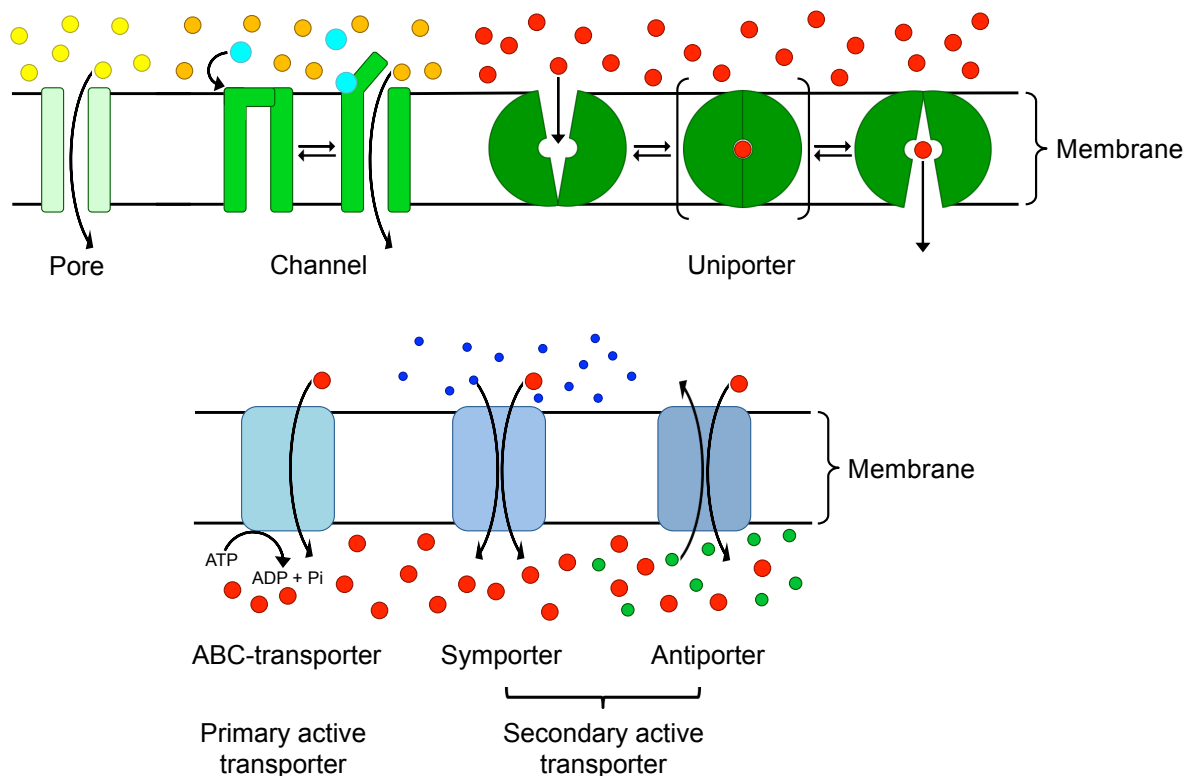


**Figure 1.1) Overview of membrane transport proteins.** Pores, channels and uniporters facilitate passive diffusion across the cell membrane. Primary active and secondary active transporters facilitate concentrative transport across the cell membrane.

Many members of the major facilitator superfamily (MFS) are secondary active transporters[11]. Examples of secondary active transporters of this family are the glycerol 3-phosphate:phosphate exchanger GlpT[12] and the lactose:proton symporter LacY[13].

Even though the driving solute can be a molecule, such as phosphate in the case of GlpT, most secondary transporters exploit pre-existing ion (e.g. sodium or proton) gradients. Because these gradients are created and maintained by primary active transporters (i.e. ion pumps), secondary transporters rely on primary active transporters and are therefore called
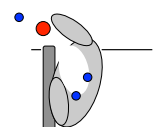
secondary (active) transporters. The members of the Dicarboxylate/Amino Acid:Cation Symporter (DAACS) family are examples of sodium and proton coupled secondary transporters.

## DAACS family

The DAACS family is a widespread family that couples the translocation of various solutes to the thermodynamically favorable co-transport of sodium ions and/or protons. All family members share a similar hydropathy profile[14], with 8 predicted transmembrane segments[15]. Additionally, all family members share a sequence similarity (> 20% identity and > 50% similarity) with the highest conservation for the amino acids involved in coupling ion and substrate binding (figures 1.2 and 5.1 a). According to the substrate preference the DAACS family can be divided into C4-dicarboxylate transporters, negatively charged amino acid transporters and neutral amino acid transporters[14].

C4-dicarboxylate transporters catalyze the transport of Krebs cycle dicarboxylates such as malate, fumarate and succinate. The best characterized transporter of this family is DctA, which can be found in aerobic and anaerobic prokaryotes[16–19]. DctA couples the uptake of its substrates to the symport of protons[16,17].

Neutral amino acid transporters can be found in prokaryotes and eukaryotes, where they catalyze the accumulation of cysteine, alanine, serine, threonine, glutamine and asparagine either by sodium or proton symport[14,20]. The substrate specificity can be relatively narrow as for the cysteine transporters YdjN from *Escherichia coli* and TcyP from *Bacillus subtilis* that transport L-cysteine and L-selenocysteine[21,22]. TcyP couples the substrate translocation to the symport of protons, while for YdjN the coupling ion is yet unknown. The bacterial SstTs facilitate the uptake of serine and threonine together with the co-transport of sodium ions[14,23,24]. A broader spectrum can be found in the mammalian alanine, serine, and cysteine transporters ASCT1 and ASCT2. Both transporters are sodium dependent symporters, that move alanine, serine, and threonine with high affinity across the membrane[25–27]. ASCT1 is also a high affinity cysteine transporter but also transports negatively charged amino acids such as cysteate at low pH (< pH 5.5)[27–30]. Presumably, the protein transports the uncharged version of cysteate, because a substantial fraction of cysteate will be protonated at pH 5.5.

**a**

TMS1    TMS2    TMS3

```
DctA    FQVLTAIAIG----ILLGHFYPE----------IGEQMKPLGDGFVKLIKMIIAPVIFCTVVTGIAGMESMKAVGRTGAVALLY-FEIVSTIALIIGLIIVNVVQPGAGMNVDPATLDAKA  116
SstT    KQILAGLILG----ILLAWISKP----------AAEAVGLLGTLFVGALKAVAPILVLMLV--MASIANHQGQKTNIRPILFLYLLGTFSAALAAVIFSFAF-PSTLH-LS--------  114
ASCT1   LLTVSGVLAG----AGLGAA----LRGLSLSRTQVTYLAFPGEMLLRMLRMIILPLVVCSLVSGAASLDA-SCLGRLGGIAVAY-FGLTTLSASALAVALAFIIKPGSGAQTLQSSDLGLE  156
ASCT2   LLTVVAVVAG----VALGLGVSGAGGALALGPERLSAFVFPGELLLRLLRMIILPLVVCSLSGGAASLDP-GALGRLGAWALLF-FLVTTLLASALGVGLALALQPGAASAAINA-SVGAA  169
EAAT1   LLTVTAVIVG----TILGFTLRP----YRMSYREVKYFSFPGELLMRMLQMLVLPLIISSLVTGMAALDS-KASGKMGMRAVVY-YMTTTIAAVVIGIIIVIIIHPGKGTKEN-MH-----  157
EAAT2   TLTVFGVILG----AVCGGLLRL---ASPIHPDVVMLIAFPGDILMRMLKMLILPLIISSLITGLSGLDA-KASGRLGTRAMVY-YMSTTIAAVLGVILVLAIHPGNPKLKKQLG-----  155
EAAT3   LSTVAAVVLG----ITTGVLVRE---HSNLSTLEKFYFAFPGEILMRMLKLIILPLIISSMITGVAALDS-NVSGKIGLRAVVY-YFCTTIAAVILGIVLVVSIKPGVTQKVGEIA-----  129
EAAT4   LLTVSAVVIG----VSLAFALRP----YQLTYRQIKYFSFPGELLMRMLQMLVLPLIISSLVTGMAALDN-KATGRMGMRAAVY-YMVTTIIAVFIGILMVTIIHPGKGSKEG-LH-----  165
EAAT5   ILSVLSVIVG----CLLGFFLRT----RRLSPQEISYFQFPGELLMRKLMMILPLVVSSLMSGLASLDA-KTSSRLGVLTVAY-YLWTTMAVIVGIFMVSIIHPGSAAQKETTE-----  127
GltT    WQIFIGLILG----IIVGAIFYG-NPK-----VATYLQPIGDIFLRLIKMIVIPIVISSLVVGVASVGDLKKLGKLGGKTIIY-FEIITIAIVVGLLAANIFQPGTGVNMKSLE--KTD  114
GltP    WQILFAMVLG----ILLGSYLHY-HSDSDRWLVVNLLSPAGDIFIHLIKMIVVPIVITSLVVGIAGVGDAKQLGRIGAKTIIY-FEVITIVAIILGITILANVFQPGAGVDMSQLA--TVD  121
GltPh   QKILIGLILGAIVGLILGHYGYA--HA------VHTYVKPFGDLFVRLLCMLVMPIVFASLVVGAASISP-ARLGRVGVKIVVY-YLLTSAFAVTLGIIMARLFNPGAGIHLAVGGQ----  121
GltTk   WKILWGLVLGAVFGLIAGHFGYA--GA------VKTYIKPFGDLFVRLLKMLVMPIVLASLVVGAASISP-ARLGRVGVKIVVY-YLATSAMAVFFGLIVGRLFNVGANVNLGSGTG----  123
        . .: *           .                                     *  :: ::  ::.:   .::         *    *  .    *  .   :
```

TMS4a    TMS4b    TMS4c

```
DctA    VAVY-----ADQAKDQGIVAFIMDVIPASV---IGAFASG-------------------------------------------NILQVLLFAV  158
SstT    ------SSAGDISPPSGIVEVMRGLVMSMVSNPIDALLKG-----------------------------------------NYIGILVWAI  157
ASCT1   DS---GPPPVPKETVDSFLDLARNLFP---SNLVVAAFRTYATDYKVVTQ--------NSSSG-----------NVT-----------THEKIPIGTEIEGMNILGLVLFAV  231
ASCT2   GS---AENAPSKEVLDSFLDLARNIFP---SNLVSAAFRSYSTTYEER--------NIT----------------------GTRVKVPVGQEVEGMNILGLVVFAI  239
EAAT1   -R---EGKIVRVTAADAFLDLIRNMFP---PNLVEACFKQFKTNYEKRSFKVPIQA--NETLVGAVIN------NVSEAMETLTRITEEL--------VPVPGSVNGVNALGLVVFSM  251
EAAT2   -P---GKKNDEVSSLDAFLDLIRNLFP---ENLVQACFQQIQTVKKVLVAPPPDEEANATSAEVSLL------NETVTEVPEETKMVI----------KKGLEFKDGMNVLGLIGFFI  250
EAAT3   -R---TGSTPEVSTVDAMLDLIRNMFP---ENLVQACFQQYKTKREEVKPPSDPEM--NMTEESFTAVMTTAISKNKTKEY----------KIVGMVSDGINVLGLIVFCL  220
EAAT4   -R---EGRIETIPTADAFMDLIRNNMFP---PNLVEACFKQFKTQYSTRVVTRTMVRTENGSEPGASMPPPFSVE--NGTSFLENVTRALGTLQEMLS-FEETVPVPGSANGINALGLVVFSV  276
EAAT5   -Q---SGKPIMSSADALLDLIRNMFP---ANLVEATFKQYRTKTTPVVKSPKVAPEEAPPRRILIYGVQEE---NGSHVQNFALDLTP-----------KSEPGTSDGMNVLGIVFFSA  230
GltT    IQSYVDTTNEVQ--HHSMVETFVNIVP---KNIFESLTKG--------------------------------------------DMLPIIFFSV  159
GltP    ISKYQSTTEAVQSSSHGIMGTILSLVP---TNIVASMAKG----------------------------------------EMLPIIFFS  168
GltPh   --------QFQPHQAPPLVHILLDIVP---TNPFGALANG-------------------------------------------QVLPTIFFAI  159
GltTk   --------KAIEAQPPSLVQTLLNIVP---TNPFASLAKG---------------------------------------------EVLPVIFFAI  161
        ::             :.                                                                          : : ::
```

TMS4c    TMS5    TMS6    HP1a

```
DctA    LFGFALHRLGS--------KGQLIFNVIESFSQVIFGININMIMRLAPIGAFGAMAFTIGKYGV-G-TLVQLGQLIICFYITCILFVVLVLGSI-AKATGFSIFKFIRYI-REELLIVLGTS  267
SstT    GLGFALRHGNE------------TTKNLVNDMSNAVTFMVKLVIHFAPIGIFGLVSSTLATTGFST--LWGYAQLLVVLVGCMLLVALVVNPLLVWWKIRRNPFPLVLLCLRESGVYAFFTR  265
ASCT1   VLGVALKKLGS--------EGEDLIRFFNSLNEATMVLVSWIMWYVPVGIMFLVGSKIVEMKDIIVLVTSLGKYIFASILGHVIHGGIVLPLIYFVFTRKNPFRFLLGL-LAPFATAFATC  343
ASCT2   VFGVALRKLGP--------EGELLIRFFNSFNEATMVLVSWIMWYVPVGIMFLVAGKIVEMEDVGLLFARLGKYILCCLLGHAIHGLLVLPLIYFLFTRKNPYRFLWGI-VTPLATAFGTS  351
EAAT1   CFGFVIGNMKE--------QGQALREFFDSLNEAIMRLVAVIMWYAPVGILFLIAGKIVEMEDMGVIGGQLAMYTVTIVGLLIHAVIVLPLLYFLVTRKNPWVFIGGL-LQALITALGTS  363
EAAT2   AFGIAMGKMGD--------QAKLMVDFFNILNEIVMKLVIMIMWYSPLGIACLICGKIIAIKDLEVVARQLGMYMVTVIIGLIIHGGIFLPLIYFVVTRKNPFSFFAGI-FQAWITALGTA  362
EAAT3   VFGLVIGKMGE--------KGQILVDFFNALSDATMKIVQIIMCYMPLGILFLIAGKIIEVEDWEIF-RKLGLYMATVLTGLAIHSIVILPLIYFIVVRKNPFRFAMGM-AQALLTALMIS  331
EAAT4   AFGLVIGGMKH--------KGRVLRDFFDSLNEAIMRLVGIIIIWYAPVGILFLIAGKILEMEDMAVLGGQLGMYTLTVIVGLFLHAGIVLPLIYFLVTHRNPFPFIGGM-LQALITAMGTS  388
EAAT5   TMGIMLGRMGD--------SGAPLVSFCQLNESVMKIVAVAVWYFPFGIVFLIAGKILEMDDPRAVGKKLGFYSVTVVCGLVLHGFILPLLYFLFITKKNPIVFIRGI-LQALLIALATS  342
GltT    MFGLGVAAIGE--------KGKPVLQFFQGTAEAMFYVTNQIMKFAPFGVFALIGVTVSKFGV-E-SLIPLSKLVIVVYATMVFFIFVVLGGV-AKLFGINIFHIIKIL-KDELILAYSTA  268
GltP    LFGLGLSSLPAT----------HREPLVTVFRSISETMFKVTHMVMRYAPVGVFALIAYMAEGNG-H-VVGELAKVTAAVYVGLTLQILLVYFVL-LKIYGIDPISFIKHA-KDAMLTAFVTR  278
GltPh   ILGIAITYLMNSENEKVRKSAETLLDAINGLAEAMYKIVNGVMQYAPIGVFALIAYMAEQGV-R-VVGPLAKVVGAVYTGLFLQIVITYFIL-LKVFGIDPIKFIRKA-KDAMITAFVTR  278
GltTk   ILGIAITYLMNRNEERVRKSAETLLRVFDGLAEAMYLIVGGVMQYAPIGVFALIAYMAEQGV-R-VVGPLAKVVGAVYTGLFLQIVITYFIL-LKVFGIDPIKFIRKA-KDAMITAFVTR  278
        :*. :              :       :    :  .  :  *.*.   . .         :   :   :      :  .     :    :   .       : : :
```

HP1b    TMS7a    TMS7b    HP2a    HP2b    TMS8

```
DctA    SESALPRMLDKM-EKLGCRKSVVGLVIPTGYSFNLDGTSIYLTMAAVFIAQATNSQMDIVHQITLLIVLLLSKSGAAGVTGSGFIVLAATLSAVGHLPV-------AGLAL-ILGIDRF--  379
SstT    SAANIPVNMALC-EKLNLDRDTYSVSIPLGATINMAGAAITTVLTLAAVNTLGIPVDLPTALLLSVVASLCACGASGVAGGSLLLIPLACNMFG-ISN-------DIAMQVVAVGFIIG  377
ASCT1   SSATLPSMMKCIEENNGVDKRISRFILPIGATVNMDGAAFQCVAAVFIAQLNNVELNAGQIFTILVTATASSVGAAGIPAGGVLTIAIIEAIG-LPT-------HDLPL-ILAVDWI--  455
ASCT2   SSATLPLMMKCIEENNGVDKHISRFILPIGATVNMDGAALFQCVAAVFIAQLSQQSLDFVKIITILVTATASSVGAAGIPAGGVLTLAIILEAVN-LPV-------DHISL-LALDWL--  463
EAAT1   SSATLPITFKCLEENNGVDKRVTRFVLPVGATINMDGTALYEALAAIFIAQVNNFDLNFGQIITISITATAASIGAAGIPQAGLVTMVIVLTSVG-LPT-------DDITL-IIAVDWF--  475
EAAT2   SAGTLPVTFRCLEENLGIDKRVTRFVLPVGATINMDGTALYEAVAAIFIAQMNGVVLDGGQIVNVTVSLTATLATLATLATVG-LPT-------EDISL-LVAVDWL--  474
EAAT3   SSATLPVTFRCAEENNGVDKRITRFVLPVGATINMDGTALYEAVAAIFIAQVNNLDLDLGIGQITITISITATAASVGAAGIPQAGLVTMVIVLSAVG-LPA-------EDVTL-IIAVDWL--  443
EAAT4   SSATLPITFRCLEEGLGVDKRRITRFVLPVGATINMDGTALYEALAAIFIAQVNNYENLNLGQITITISITATAASVGAAGIPQAGLVTMVIVLTSVG-LPT-------EDITL-IIAVDWF--  500
EAAT5   SSATLPITFKCLEENHIDRRIARFVLPVGATINMDGTALYEAVAAIFIAQVNNFELNFGQIITISITATAASIGAAGIPQAGLVTMVIVLTSVG-LPT-------DDITL-IIAVDWL--  513
GltT    SETVLPKIMEKM-ENFGCPKAITSFVIPTGYSFNLDGSTLYQAIAAIFIAQLYGIDMVPISQQISLLLVLMVTSKGIAGVPGVSFVVLLATLGTVG-IPI-------EGLAF-IAGIDRI--  379
GltP    SESVLPRIIEKM-EAYGAPASITSFVVPTGYSFNLDGSTLYQAAIAAIFIAQLYGIDLSIWQEIILVLTLMVTSKGIAGVPGVSFVVLLALLGSVG-IPL-------EGLAF-IAGVDRI--  389
GltPh   SSGTLPVTMRVAK-EMGISEGIYSFTLPLGATINMDGTALYQVATFFIANALGSHLTVGGQLTIVLTAVLASIGTAGVPGAGAIMLCMVLHSVG-LPLTD-PNVAAAYAM-ILGIDAI--  393
GltTk   SSGTLPVTMRVAEEEMGVDKGIFSFTLPLGATINMDGTALYQVTFLVFANAIGHPLTLGGQLVVVLTAVLASIGTAGVPGAGAIMLAMVLQSVG-LDLTPGSPVALAYAM-ILGIDAI--  397
        *  :*     :            . :* *.   :.*  :.*:  *:::  .: .   .:        :      : :  :      :  :   *   *: :      : :.      :: :  :  :
```

TMS8

```
DctA    --MSEARALTNLVGNGVATIVVAKWVKE  404
SstT    VLQDSCETALNSSTDVLFT---AAACQA  402
ASCT1   --VDRTTTVVNVEGDALGAGILHHLNQK  480
ASCT2   --VDRSCTVLNVEGDALGAGLLQNYVDR  488
EAAT1   --LDRLRTTTNVLGDSLGAGIVEHLSRH  500
EAAT2   --LDRMRTSVNVVGDSFGAGIVYHLSKS  499
EAAT3   --LDRFRTMVNVLGDAFGTGIVEHLSRT  469
EAAT4   --LDRLRTMTNVLGDSIGAAVIEHLSQR  525
EAAT5   --LDRFRTMINVLGDALAAGIMAHICRK  538
GltT    --LDMARTAVNVIGNSLAAIIMSKWEGQ  404
GltP    --LDMARTALNVVGNALAVLVIAKWEHK  414
GltPh   --LDMGRTMVNVTGDLTGTAIVAKTEGT  418
GltTk   --LDMGRTMVNVTGDLAGTVIVAKTEKE  422
        .  :     *  *:   :   .   .
```
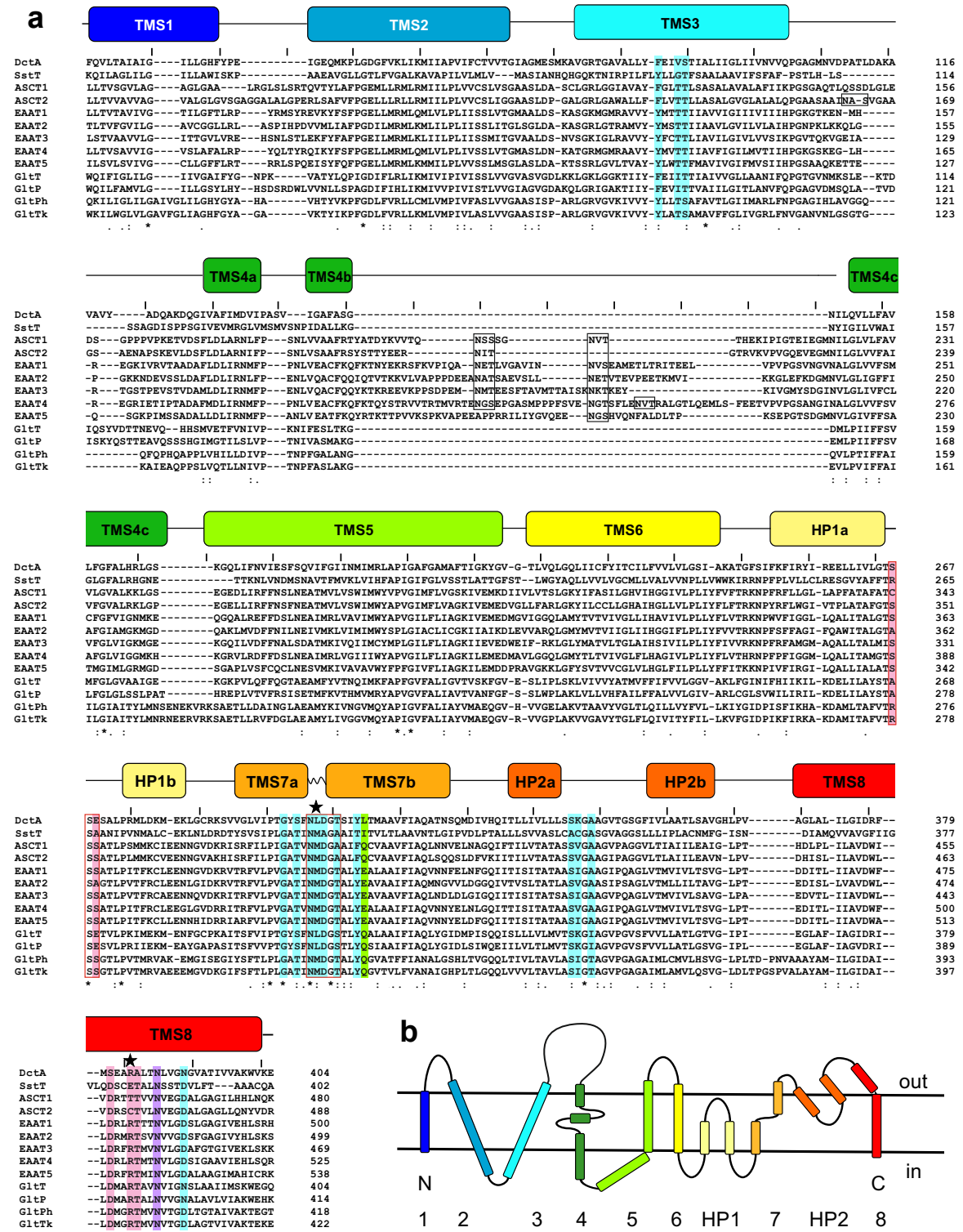
**b**



**Figure 1.2) Sequence alignment of glutamate and neutral amino acid transporters. (a)** Amino acid alignment of the neutral amino acid transporters DctA and SstT from *E. coli* and the human ASCT1 & 2 with the glutamate transporters of the human EAATs 1-5, GltT from *B. stearothermophilus*, GltP from *E. coli* and the aspartate transporters Glt$_{Ph}$ and Glt$_{Tk}$ from *P. horikoshii* and *T. kodakarensis*, respectively. Sequences were truncated at the unordered and unconserved N- and C-terminus. The alignment was made using Clustal Omega[31,32] and manually adjusted. Transmembrane segments (TMS) and the hairpin regions 1 & 2 (HP1 & 2)
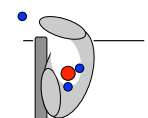
are represented in rainbow colors. Residues involved in substrate binding are highlighted in pink; residues involved in sodium binding are highlighted in blue. Residues involved in potassium and proton binding in the eukaryotic transporters are highlighted in green. Big stars above the sequences indicate residues that undergo the most dramatic change during substrate binding and release. Black boxes mark N-glycosylation sites (NXS/T) of the eukaryotic transporters; red boxes show the conserved serine stretch and NMDGT motif. Characters below the sequence indicate the degree of conservation: a star represents a conserved residue, a colon represents high conservation, a point represents medium conservation, no character represents low to no conservation. **(b)** Schematic representation of the membrane topology of glutamate transporters, adapted from Yernool et al., 2004[15]. Color code of the TMS according to (a).

Different than for ASCT1, cysteine is not a substrate but a strong competitive inhibitor for ASCT2[33]. Nevertheless, ASCT2 has an even broader substrate spectrum than ASCT1 as it also accepts glutamine, asparagine, and with lower affinity glutamate and some other neutral amino acids[27,34,35]. In difference to the closely related ASCT1 and other members of the DAACS family, ASCT2 is an obligate amino acid exchanger.

The negatively charged amino acid or glutamate/aspartate transporters (from now on denoted "glutamate transporters") couple the transport of glutamate and/or aspartate to the symport of sodium ions and protons and can be found in prokaryotes as well as in eukaryotes. They are the best-studied members of the DAACS family and subject of this thesis.

**Glutamate transporters**

Eukaryotic glutamate transporters can be found in nematodes, insects, reptiles, and mammals[36–44] (reviewed in [45]), where they play an important role in signal transmission. All signals from the environment – e.g. visual, taste, scent, pressure, temperature, or sound - have to be transmitted through the brain. At the synapses the electrical signal in the form of an action potential is transformed into a chemical signal by neurotransmitters in order to be further processed. Glutamate is the main excitatory neurotransmitter that is released on one side of the synaptic cleft (presynapse or axon terminal) upon an action potential from an incoming signal. At the other side, at the postsynapse (e.g. dendrite) it activates/excites specific receptors and the signal is passed on. Afterwards the glutamate has to be removed in order to end the signal. If not removed, the elevated levels of glutamate can lead to
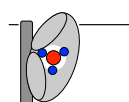
overstimulation or over-excitation, which eventually leads to cell death. Therefore glutamate is excitotoxic[46–49]. If glutamate is not removed it can also diffuse to surrounding or more distant synapses and cause undesired signaling. This is called spill-over and cross-talk[45,50,51]. Glutamate transporters remove the glutamate quickly and efficiently from the synaptic cleft, which leads to its concentration in glia and neurons[52–54]. Reuptake of glutamate does not only end a signal but also prepares the synapses for new signals. Thus, glutamate transporters in eukaryotes are important for sensitive signal transmission. Malfunctioning of glutamate transporters are associated with many neurodegenerative diseases such as Alzheimer's disease[48,55,56], Huntington's disease[57], and epilepsy[58–60] (reviewed in [45]).

Based on the excitatory effect of their substrates, the eukaryotic glutamate transporters are also called Excitatory Amino Acid Transporters (EAATs). So far five different EAATs, EAAT1-5, have been classified[41,44,61–64] (table 1.1 gives an overview of the names of eukaryotic glutamate transporters and their synonyms). All of them transport glutamate and aspartate together with three sodium ions and one proton. After substrate delivery they require the counter-transport of potassium to return to the starting position[65–67].

**Table 1.1) Eukaryotic glutamate transporters**

| Transporter | Synonym |
|---|---|
| EAAT1 | GLAST1, SLC1A3 |
| EAAT2 | GLT-1, SLC1A2 |
| EAAT3 | EAAC1, SLC1A1 |
| EAAT4 | SLC1A6 |
| EAAT5 | AAAT, SLC1A7 |

Glutamate transporters are also found in prokaryotes, where they mediate the uptake of glutamate and aspartate as nutrients[14]. Prokaryotic glutamate transporters couple the translocation of their substrates to either sodium ions or protons but require no potassium transport to reset[24,68–70]. The best studied glutamate transporter is the archaeal aspartate:sodium symporter from *Pyrococcus horikoshii* (Glt$_{Ph}$). This transporter also yielded most of the 3-D crystal structures of glutamate transporters in various states of the transport-cycle. The crystal structures of Glt$_{Ph}$ provided the structural framework to explain
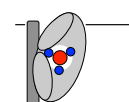
many functional and structural findings on glutamate transporters made before. Recent crystal structures of another archaeal aspartate:sodium symporter from *Thermococcus kodakarensis* ($Glt_{Tk}$), showed high similarity to the available $Glt_{Ph}$ structures[71,72] (chapter 4 and 5). So far crystal structures of $Glt_{Ph}$ and $Glt_{Tk}$ are the only glutamate transporter structures available.

**Architecture of glutamate transporters**

Both prokaryotic and eukaryotic glutamate transporters are homotrimers[15,68,73–76]. However, mixed trimers of EAAT3/EAAT4 have been observed when co-expressed[77]. Because no other EAAT showed the ability to form heterotrimers, this result rather emphasizes the high similarity of EAAT3 and EAAT4. The crystal structure of $Glt_{Ph}$ showed that the trimer is bowl-shaped, with the basin reaching halfway across the lipid bilayer[15](figure 1.3 a-c). Each monomer consists of a trimerization domain and a transport domain, and has eight α-helical transmembrane segments (TMS) and two α-helical hairpin regions (HP)[15] (figures 1.2 b and 1.3 d). The crystal structures also revealed a topology that is similar as suggested by an earlier cysteine based accessibility study on GltT and GLT-1[78,79]. That $Glt_{Ph}$ and the eukaryotic glutamate transporters share similar structural features is also reinforced by cysteine cross-linking experiments on EAAT1 and EAAT2. In the experiments pairs of residues that are in close proximity in the outward-facing state (OFS) $Glt_{Ph}$ crystal structures can be cross-linked in the mammalian transporters[80–82].

The N-terminal part of the protein with TMS1, 2, 4, and 5 forms the trimerization domain and mediates all intersubunit contacts within the trimer. The transport domain is located on the periphery of the transporter and constructed of TMS3, 6, 7, 8, and HP1 and 2 (figure 1.3 a and d). The crystal structure additionally showed that each protomer has its own substrate and ion binding site and translocation pathway[15,69]. The individual transport domains have no contact to one another and are separated by crevices from the other subunits (figure 1.3 a).
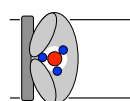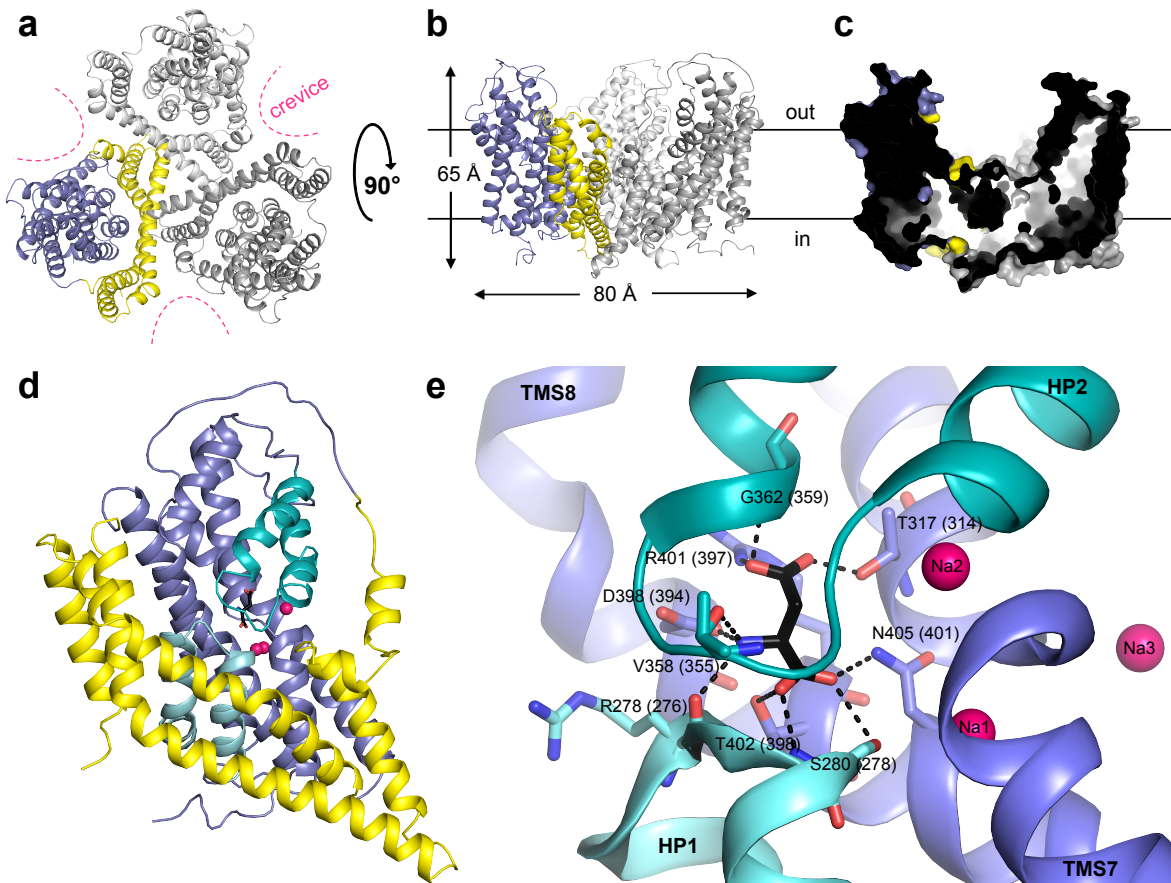
**Figure 1.3) Architecture of glutamate transporters.** Shown is the crystal structure of substrate-loaded Glt$_{Tk}$. **(a)** Topview of the homotrimer; cartoon representation with two monomers presented in grey, one monomer presented in color. The trimerization domain is shown in yellow, the transport domain in blue; intersubunit crevices are indicated with dashed pink lines. **(b)** Sideview of the homotrimer, color scheme as in (a). **(c)** Sideview intersection; surface presentation, highlighting the bowl-shape. **(d)** Sideview of one monomer; color scheme as in (a), with HP1 in light teal and HP2 in teal, L-aspartate presented as sticks in black, and sodium ions (Na1-3) presented as pink spheres. **(e)** Close-up view of the substrate binding site below HP1 and HP2. Color scheme as in (d); amino acids involved in substrate coordination are presented (Glt$_{Tk}$ numbering) as sticks; Glt$_{Ph}$ numbering in parentheses. Interactions with the substrate are indicated with dashed black lines. Figures were made using PYMOL[83].

Eukaryotic glutamate transporters have an additional ~75 amino acid long loop between TMS4b and TMS4c. The loop also contains a set of N-glycosylation sites (see figure 1.2 a)[25–27,44,64,73]. Cysteine accessibility and fluorescence resonance energy transfer (FRET) experiments show that this additional loop is extracellular, protrudes from the center of the trimer, and folds into the intersubunit crevices[84]. The function is not yet known but the authors hypothesize that one of the functions could include the stabilization of the trimer or the mediation of intersubunit sodium cooperativity. However, studies with mixed
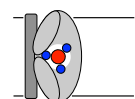
expression of wild type (*wt*) and function-rendered mutant transporters of EAAT3 and EAAT4 as well as FRET, single molecule FRET (smFRET), and electron paramagnetic resonance (EPR) measurements on Glt$_{Ph}$ revealed that each subunit functions independently[76,85–89]. Whether the additional loop participates in transporter stabilization or possibly assists in substrate delivery to the binding site requires further investigation.

**An elevator in a protein**

The first Glt$_{Ph}$ crystal structures showed the transporter in an outward-facing state (OFS) with the substrate close to the extracellular solvent accessible Glt$_{Ph}$-trimer vestibule[15,69]. In the aspartate loaded transporter the substrate is occluded and located between the reentrant regions HP1 and HP2. While HP2 shields the substrate from the extracellular solution, the substrate is separated from the intracellular aqueous phase by a ~20 Å protein layer. An 'open' structure in which the substrate analogue D/L-threo-β-benzyloxyaspartate (TBOA) was bound suggested that HP2 acts as the extracellular gate to the binding site[69]. A broad range of biochemical and computational studies on Glt$_{Ph}$ and the mammalian transporters confirmed the role of HP2 as exterior gate[69,82,90–94]. In order to understand how the substrate is delivered to the interior cross-linking experiments were done. The intersubunit linkage by disulfide bridges along the trimerization domain did not affect the transporter activity and uncovered that the trimerization domain remains rigid upon substrate translocation[95]. Also the more recent double electron-electron resonance (DEER) experiments on Glt$_{Ph}$ support this finding[96]. However, spontaneous intramolecular disulphide bond formation in EAAT1 of residues that are ~20 Å apart in the OFS Glt$_{Ph}$ crystal structure, suggested substantial structural rearrangements upon substrate translocation[97]. Based on inverted repeats of the protein an inward-facing structure (IFS) was proposed for Glt$_{Ph}$[98,99]. In this model the transport domain moves in respect to the trimerization domain towards the intracellular side. Introduction of cysteines and cross-linking experiments on Glt$_{Ph}$ and EAAT3 (Glt$_{Ph}$ V216C M385C, K55C A364A and EAAT3 R61C V420V, K64C V420C) showed that both transporters can adopt such a conformation during the translocation cycle[98,99]. Because Glt$_{Ph}$ K55C A364C corresponds to EAAT3 K64C V420C the experiments additionally demonstrate that prokaryotic and eukaryotic transporters share similar structural features and follow the same transport mechanism. The crystal structures of Glt$_{Ph}$ (V216C M385C and K55C A364A) fixed in the IFS reveal that
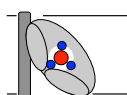
the trimerization domain remains static and forms a scaffold along which the transport domain travels ~15 Å towards the intracellular space[99]. The linkage of trimerization domain and transport domain is mediated via the TMS2-3 loop on the intracellular side and the TMS5-6 and TMS3-4 loops on the extracellular side. Similar to the trimerization domain, the transport domain itself retains its overall structure and displays a rigid body movement[99].

While the transport domain travels to the intracellular side it performs a 37° axial rotation with a minor horizontal translation away from the trimer-center. The movement of the transport domain carries the substrate binding site from a position close to the extracellular aqueous solution to a position near the intracellular side of the membrane. Because this movement of the complete transport domain resembles the motion of an elevator, it was used to give the transport mechanism its name[100]. Glutamate transporters were the first transporters for which such an elevator mechanism was described. However, in the last couple of years more transporter classes have shown to exhibit this elevator-like movement, suggesting that this mechanism is not exceptional amongst transport proteins[101–104].

In the crystallized IFS the substrate binding site of $Glt_{Ph}$ is occluded by HP1 from the hydrophilic environment[99]. In analogy to HP2, HP1 was therefore proposed to be the intracellular gate of the transporter[99,100,105]. Yet no experimental evidence for this hypothesis exists so far. The crystal structure of a fast transporting $Glt_{Ph}$ mutant ($Glt_{Ph}$ R276S M395R) even might undermine this hypothesis[106]. The mutant readily crystallizes in the IFS and shows a stronger swing out of the transport domain away from the trimerization domain, suggestive of a more substantial movement of the transport domain during substrate delivery[106]. In this structure HP2 is close enough to the interior to act as intracellular gate. This suggestion is supported by a previous MD study, which also proposes HP2 as intracellular gate[107]. However, both hypotheses for the intracellular gate are based on crystal structures of mutants and could therefore be biased by an unnatural conformation. Additionally, computational studies are strongly dependent on the available crystal structures and the data quality, an issue that will be addressed later in the section regarding the relevance of crystal structures. To determine which of the HPs forms the internal gate, more structural and biochemical data is required. Future experiments employing
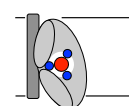
crystallographic methods, smFRET, EPR and electron microscopy (EM) with new generation microscopes and detectors might identify the internal gate.


**Substrate specificity and the substrate binding site**


All glutamate transporters facilitate the concentrative uptake of negatively charged amino acids. Nonetheless, the substrate range and preference can vary amongst the members of this family. The mammalian glutamate transporters EAAT1-5 bind and transport L- and D-glutamate and L-/D-aspartate with similar affinity, but also accept other negatively charged amino acids such as L-cysteine sulfinic acid and L-serine-*O*-sulfate with lower affinity[44,49,108]. EAAC1 even accepts L-cysteine as substrate[109]. The bacterial transporters GltT from *Bacillus caldotenax*, *Bacillus stearothermophilus* (hence $Glt_{BC}$ and $Glt_{BS}$) and *Bacillus subtilis* ($GltT_{Bsu}$), as well as GltP from *E. coli* also accept glutamate and aspartate[24,68,73,74,110–113]. In contrast to this the archaeal glutamate transporter homologs $Glt_{Ph}$ and $Glt_{Tk}$ display a clear preference for L-aspartate and are therefore more correctly called aspartate transporters[69,70] (see also chapter 3). While glutamate, L-serine, and succinate also are low affinity substrates for $Glt_{Ph}$[69] neither of them can bind to $Glt_{Tk}$ (chapter 3). However, $Glt_{Tk}$ does bind L-asparagine with low affinity. Because asparagine resembles aspartate in shape and size, this suggests that the size of the substrate is an important binding criterion (chapter 3). The competitive inhibitor TBOA of the eukaryotic EAATs also binds to $Glt_{Ph}$[69] and $Glt_{Tk}$ (unpublished data) but other EAAT inhibitors such as kainate and dihydrokainate are not accepted by the prokaryotic $Glt_{Ph}$[70]. Identification of the determinants for substrate spectrum and affinity has been - and still is - important in order to get structural information and gain functional insights into the glutamate transporter mechanism.


*The substrate binding site in glutamate transporters*

Structural information on the substrate binding site was obtained by mutational and crystallographic studies. The crystal structures of substrate-loaded $Glt_{Ph}$ and $Glt_{Tk}$ show that in both transporters the same residues are involved in substrate binding (chapter 5 and ref. 69). In this chapter the residue numbering of $Glt_{Ph}$ is followed, for the corresponding $Glt_{Tk}$ numbering see chapter 5. In the crystal structures the aspartate binding site consists of the tips of HP1 and HP2, the conserved NMDGT motif of TMS7 and central hydrophilic residues on TMS8: The α-carboxyl group of the substrate interacts with the side chain of
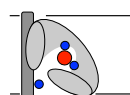
N401 and T398 (TMS8), and the main chain amide NH group of S278 (HP1), while the amino group of the substrate interacts with the side chain of D394 (TMS8) and the backbone carbonyl groups of R276 (HP1) and V355 (HP2). Additionally, the side chains of T314 (TMS7) and R397 (TMS8), and the main chain NH group of G359 (HP2) coordinate the β-carboxyl group of the substrate (figure 1.3 e).

The structures are in good agreement with mutational studies on the eukaryotic transporters (see below, table 1.2 gives a short summary) and demonstrate that the residues involved in substrate coordination are highly conserved amongst the glutamate transporter family (figure 1.2 a). The mutational studies also reveal that all members of the DAACS family share structural and mechanistic features, and that the residues involved in substrate binding determine the substrate selectivity.

*Substrate selectivity*

In EAAT1 cysteine substitutions of the residues corresponding to R276, T314, and N401 in Glt$_{Ph}$ strongly impaired or abolished the transporter function[114,115] indicative for their relevance in substrate coordination. The importance of R397 (Glt$_{Ph}$ numbering) for substrate selectivity has been revealed by mutational studies on EAAT2, EAAT3, and ASCT1[109,116,117]. While the arginine is highly conserved in the glutamate transporters, this residue is a threonine in ASCT1 and a cysteine in ASCT2. Substitution of this arginine to threonine abolished glutamate transport in EAAT2[116]. In EAAT3 uncharged or negatively charged substitutions of the corresponding arginine (R447) likewise diminished the transport of negatively charged amino acids. The ability of this transporter to translocate L-cysteine was not negatively affected by the substitutions but the mutant transporters were additionally able to accumulate L-serine[109], which is a substrate for the neutral amino acid transporters ASCT1, ASCT2 and the SstTs[23,27,117–119]. The mutation of R397 to glutamine enabled EAAT3 even to translocate glutamine. Thus three independent studies concluded that the conserved arginine interacts with the γ-carboxyl group of the substrate[76,109,116]. This conclusion is supported by the converse experiment on ASCT1[117]. The mutants ASCT1 A382T and T459R were able to transport negatively charged amino acids but displayed an impaired transport for neutral amino acids. In Glt$_{Ph}$ the corresponding residues T314 and R397 indeed participate in substrate coordination as revealed by the crystal structures[69].
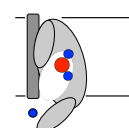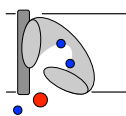
**Table 1.2) Residues involved in substrate binding.**

| Residue in Glt_Ph* | Position | Explored eukaryotic transporter | Mutant | Effect/ conclusions | Study type | Ref. |
|---|---|---|---|---|---|---|
| **R276** | **HP1** | | | Main chain carbonyl interactions with amino group of substrate | X | 69, ch. 5 |
| **S278** | **HP1** | | | Main chain nitrogen interactions with α-carboxyl of substrate | | |
| **T314** | **TMS7** | | | Side chain hydroxyl coordinates β-carboxylate of substrate | | |
| **V355** | **HP2** | | | Main chain carbonyl interactions with amino group of substrate; stabilizes substrate, even in semi opened state | | |
| **G359** | **HP2** | | | Main chain nitrogen coordinates β-carboxylate of substrate | | |
| **D394** | **TMS8** | | | Side chain carboxylate interactions with amino group of substrate | | |
| **R397** | **TMS8** | | | Side chain guanidinium coordinates β-carboxylate of substrate, responsible for negatively charged substrate selectivity | | |
| **T398** | **TMS8** | | | Side chain hydroxyl interactions with α-carboxyl of substrate | | |
| **N401** | **TMS8** | | | Amide nitrogen interactions with α-carboxyl of substrate | | |
| | | EAAT3 | | Supports the conclusions from X-ray crystallography listed above | C | 92, 193, 147, 144 |
| R397 | TMS8 | R447 (EAAC1) | R447C/ E/ G/ S | Becomes a serine/cysteine exchanger | M | 109 |
| | | | R447K | Aspartate accumulation but no serine transport - Recognition of substrate's carboxyl group | | |
| R395 | TMS8 | R445 (EAAC1) | R445M/ Q | Impaired glutamate transport | M | 246 |
| | | | R445K | Transports glutamate - Charge in vicinity of binding site is important | | |
| R397 Q242 | TMS8 | R446 (EAAC1) H295 (EAAC1) | R446Q H295K | Transports glutamine instead of glutamate Reduced glutamate affinity | M | 76 |
| S278 | TMS7 | S363 (EAAT2) | S363C | Impaired transporter | M | 79 |
| R276 | TMS7 | | | Determines substrate specificity by size | C | 122 |

| | | | | | | |
|---|---|---|---|---|---|---|
| D312 | TMS3 | D398 (GLT-1) | D398N/E | Not functional, potential Na$^+$-site | M | 151 |
| Q318 | TMS7 | E404 (GLT-1) | E404D | Impaired substrate transport, prefers L/D-aspartate over L-glutamate, important for selectivity | | |
| D390 | TMS8 | D470 (GLT-1) | D470N/E | Not functional, potential sodium binding site | | |
| T314 | TMS7 | T402 (EAAT1) | T402C | Not functional transporter | M | 114 |
| S278 | HP1 | S365 (EAAT1) | S365C | Impaired transporter | M | 115 |
| R397 | TMS8 | R479 (EAAT1) | R479C | Impaired transporter | | |
| N401 | TMS8 | N483 (EAAT1) | N483C | Impaired transporter | | |
| T314 | TMS7 | A382 (ASCT1) | A382T | Neutral amino acid transporter becomes glutamate transporter | M | 117 |
| R397 | TMS8 | T459 (ASCT1) | T459R | Neutral amino acid transporter becomes glutamate transporter | | |
| S278 | HP1 | S363 (GLT-1) | S364D/N | Not functional | M, C | 212 |
| | | | S364C/A | Reduced substrate affinity, interacts with substrate and via water with Na1 | | |
| D390 | TMS8 | D439 (EAAC1) | D439N | Impaired transporter | M | 140 |
| D394 | TMS8 | D444 (EAAC1) | D444C/S/E | Binds but does not transport succinate | M | 120 |
| | | | | Determinant for negatively charged amino acid binding | | |
| N401 | TMS8 | N451 (EAAC1) | N451S/A/C/D/Q | Na$^+$ cannot be replaced by Li$^+$, reduced transport | M | 136 |
| D394 | TMS8 | N428 (CuqDCT) | N428D | Dicarboxylate transporter becomes a glutamate transporter | M | 121 |
| D394 T398 | TMS8 | D444 T448 (EAAT3) | D444S T448A | Becomes a dicarboxylate transporter | | |
| T314 | TMS7 | T400 (GLT-1) | T400C | Not functional | M | 139 |

CuqDCT: insect dicarboxylate transporter from *Culex quinque-fasciatus*

Minor differences in amino acid numbering of one sort EAAT comes from the species variant used in the mentioned study.

X: crystal structure; M: mutational, C: computational, ch.: chapter, Ref.: reference, *: residues of other prokaryotic transporters are also presented with Glt$_{Ph}$ numbering.
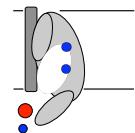
In $Glt_{Ph}$ D394 interacts with the α-carboxylate of the substrate whereas the corresponding residue in DctA is a serine. The substitution of the corresponding residue in EAAT3 to serine impaired the aspartate transport but enabled the transporter to bind the DctA substrate succinate[120]. The reverse was observed in the insect dicarboxylate transporter CuqDCT, which harbors an asparagine at the corresponding position. Replacement of this asparagine to aspartate (N428D) resulted in a change of substrate selectivity towards glutamate[121].

The role of residues that show no direct substrate interaction in the $Glt_{Ph}$ and $Glt_{Tk}$ crystal structures are more difficult to interpret but could have an influence on the size of the binding site or an altered orientation of the substrate coordinating residues. One such example is the R501C mutant of EAAT4 (M395 in $Glt_{Ph}$). This mutant transporter exhibits serine but not glutamate dependent anion currents typical for substrate transport[77]. Interestingly while all eukaryotic glutamate transporters as well as ASCT1 and 2 have an arginine residue at the positions equivalent to EAAT4 R501, a methionine is present in the prokaryotic glutamate transporters, and a serine in the SstTs. Serine and cysteine differ only in their hydroxyl and thiol group, respectively, and are smaller than arginine or methionine. This could increase the accessibility of the binding site for the transported substrate serine. The size of the substrate binding site might also determine the substrate preference for the aspartate transporters. The residues T352 and M362 of $Glt_{Ph}$ are replaced in the eukaryotic transporters by the smaller residues alanine and threonine, respectively. Mutational studies on $Glt_{Ph}$, with T352A and M362T substitutions lead to enhanced glutamate binding[94]. However, the bacterial glutamate transporters $Glt_{BS}$ and GltP[24] possess, just like $Glt_{Ph}$, a threonine and methionine at the positions 352 and 362, respectively, but have a serine replacement at position T314. Also in this case the smaller serine might enlarge the binding site and allow for the binding of larger substrates such as glutamate. Another residue that has been suggested to play a role in substrate size selectivity is R276 ($Glt_{Ph}$). In the homologous EAATs this residue is replaced by the smaller residues alanine or serine[122].

While most residues involved in substrate binding are highly conserved in the glutamate transporter family some variations might explain the apparent differences in the substrate spectrum and affinity amongst these family members. Nevertheless, the molecular determinants for the substrate selectivity are not yet fully understood and more mutational
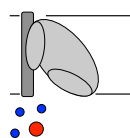
studies and crystal structures of other glutamate transporters and their homologs are required.

## Coupling ions

Glutamate transporters couple the translocation of their substrates to the symport of either sodium ions and/or protons. However, the identity of the coupling ion and the number of symported ions can differ between the family members. For the eukaryotic glutamate transporters a substrate to driving ion stoichiometry was determined by various electrophysical studies[123–125]. In these transporters the translocation of the substrate is coupled to three sodium ions and one proton. Bacterial neutral amino acid transporters (SstTs) and the archaeal aspartate transporters $Glt_{Ph}$ and $Glt_{Tk}$ couple the substrate transport to sodium ions[23,126–128] (also see chapter 2-5). Radiometric transport assays on $Glt_{Ph}$ showed that this transporter translocates one aspartate together with three sodium ions (Na1-3)[128]. Similarly, $Glt_{Tk}$ couples the binding of one aspartate to three sodium ions (chapter 3). Whether the archaeal transporter $Glt_{Ph}$ also additionally requires proton symport is still debated[68,70]. In contrast, the bacterial glutamate transporters $Glt_{Bsu}$, $Glt_{BS}$, $Glt_{BC}$, GltP, and the bacterial dicarboxylate transporters are independent from sodium gradients and couple the substrate translocation to proton symport[16,17,24,68,110,112,113]. Interestingly, for $Glt_{BS}$ and $Glt_{BC}$ the lipidic environment has an influence on the cation selectivity. In general $Glt_{Bs}$ and $Glt_{Bc}$ can utilize sodium and proton gradients to transport their substrate[112,129]. However, in *E. coli* lipids both transporters are strictly proton dependent[110,112]. This led to the proposition that the lipidic environment results in subtle conformational changes that modulate the cation binding sites[110].

### *Sodium and proton binding*

The residues involved in sodium binding are conserved amongst the eukaryotic and prokaryotic sodium-coupled transporters, with only minor changes in the proton driven glutamate transporters (figure 1.2 a). In many prokaryotic and eukaryotic glutamate transporters lithium ions can replace sodium ions and support substrate translocation[69,130,131] (chapter 3). In contrast, $Li^+$ replacement cannot induce substrate transport in EAAT2[132]. This property was used in a couple of mutational studies to determine residues, that are involved in coupling ion selectivity and thus, most likely form part of the sodium binding
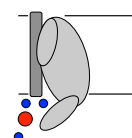
sites in the eukaryotic transporters[130,133–136]. However, even residues not directly involved in cation binding can have an influence on the cation selectivity. One such residue is S440 in EAAT2. In EAAT1, 3, 4, 5, and Glt$_{Ph}$ the corresponding residue is a glycine. S440G substitution in EAAT2 allowed Li$^+$ to drive substrate-translocation[134]. The counter-experiments with serine substitution of the corresponding glycine in EAAT1 and 3 supported the relevance of this residue in cation selectivity[130,137]. In the mutants the ability to couple Li$^+$ transport to substrate symport was abolished[130]. Yet the crystal structures of ion and substrate loaded transporters[69] (chapter 5) revealed that this residue is not directly involved in cation coordination.

The crystal structure of Glt$_{Ph}$ in complex with thallium ions revealed the first two sodium binding sites. Thallium ions have stronger anomalous scattering properties and can replace sodium and potassium ions in glutamate transporters[69,138]. According to the order of discovery these sodium binding sites were called Na1 and Na2.

In the crystal structure Na1 is located below the bound substrate and coordinated by the main chain carbonyls of G306 and N310 (TMS7), N401 (TMS8), and the main and side chain carbonyls of D405 (TMS8)[69]. This is in agreement with mutational studies on the mammalian transporters EAAT2, EAAT3, and ASCT1 (see table 1.3). The substitution of the corresponding residues of N310, N401, and D405 led to reduced sodium affinity, impaired transport, or left the transporter non-functional[135,136,138–141]. The crystal structure of the Tl$^+$ soaked Glt$_{Ph}$ D405N mutant emphasized the importance of D405 in sodium coordination: the derived structure displayed a strong anomalous signal in the Na2 site but showed no signal for Tl$^+$ at the Na1 binding site[69].

The Na2 site, as revealed by the wild type crystal structure, consists of the tip of HP2 and central residues of TMS7[69]. Carbonyl groups of T308 (TMS7), S349, I350, and T352 (HP2) coordinate the sodium ion, whereas M311 (TMS7) separates Na1 from Na2. M311 is a functionally important residue as the mutation of the corresponding M397 in GLT-1 rendered the transporter non-functional[139]. Additionally, the comparison of crystal structures of the substrate-free transporters and substrate-loaded transporters of Glt$_{Tk}$ and Glt$_{Ph}$ revealed, that this residue is one of the key residues for allosteric ion and substrate binding[71,142] (chapter 4 and 5).
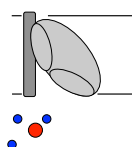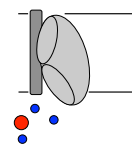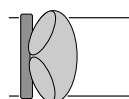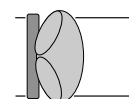
**Table 1.3) Amino acid residues involved in Na1 coordination.**

| Residue in Glt$_{Ph}$ * | Position | Explored eukaryotic transporter | Mutant | Effect/ conclusions | Study type | Ref. |
|---|---|---|---|---|---|---|
| **G306** | **TMS7** | | | All main chain carbonyls coordinate Na1, N401 also coordinates Na1 via β-carboxyl group | X, M | 69, ch. 5 |
| **N310** | **TMS7** | | | | | |
| **N401** | **TMS8** | | | | | |
| **D405** | **TMS8** | | D405N | Reduced Asp affinity, in the crystal structure Tl$^+$ bound in Na2 not Na1 | | |
| | | | | Supports the conclusions from X-ray crystallography listed above | C | 92, 144, 145 |
| D405 | TMS8 | D455 (EAAT3) | | | C | 146 |
| D312 | TMS7 | D368 (EAAT3) | | | | |
| N401 | TMS8 | N451 (EAAT3) | | | | |
| G306 | TMS7 | G362 (EAAT3) | | | | |
| N310 | TMS7 | N366 (EAAT3) | | | | |
| G354 | HP2 | G410 (EAAC1) | G410S | Li$^+$ cannot replace Na$^+$ | M | 130 |
| D405 | TMS8 | D467 (ASCT1) | D467S | Not functional, binding unaffected | C, M | 141 |
| D405 | TMS8 | D454 (EAAC1) | D454N/ S/ A | Reduced Na$^+$ affinity | M | 124, 140 |
| D405 | TMS8 | D455 (GLT-1) & (EAAC1)$^{#}$ | D455S/ C D455E / A | Impaired transporter, Li$^+$ cannot replace Na$^+$ Impaired transporter, Li$^+$ can replace Na$^+$ | M | 135 |
| N401 | TMS8 | N451 (EAAC1) | N451A/ C/ D/ Q N451S | Not functional Impaired transporter, Li$^+$ cannot replace Na$^+$ | M | 136 |
| N310 | TMS7 | N396 (GLT-1) | N396C | Not functional | M | 139 |

Minor differences in amino acid numbering of one sort EAAT comes from the species variant used in the mentioned study.

X: crystal structure; M: mutational; C: computational; ch.: chapter; Ref.: reference; in red: residue is involved in substrate binding; *: residues of other prokaryotic transporters are also presented with Glt$_{Ph}$ numbering; $^{#}$: EAAC1 numbering presented only.
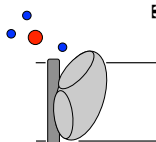
**Table 1.4) Amino acid residues involved in Na2 coordination.**

| Residue in Glt$_{Ph}$* | Position | Explored eukaryotic transporter | Mutant | Effect/ conclusions | Study type | Ref. |
|---|---|---|---|---|---|---|
| **T308** | **TMS7** | | | The Na2 site sits below HP2; Na2 is coordinated by the carbonyl groups of T308, S349, I350, T352 by dipole moment; M311 separates Na1 and Na2 | X, C | 69, ch. 5, 144 |
| **M311** | **TMS7** | | | | | |
| **S349** | **HP2** | | | | | |
| **I350** | **HP2** | | | | | |
| **T352** | **HP2** | | | | | |
| I309 | TMS7 | | | Carbonyl oxygens of the C-terminal TMS7 helix & the first helix of the HP2 loop coordinate Na2 stably together with the sulfur atom of M311 | C, M | 143 |
| N310 | TMS7 | | | | | |
| M311 | TMS7 | | | | | |
| S349 | HP2 | | | Na2 of the crystal structure is just an intermediate binding site (Na2') | | |
| I350 | HP2 | | | | | |
| T352 | HP2 | | | | | |
| T308 | TMS7 | | | | | |
| T308 | TMS7 | | T308W | Not functional | | |
| | | | T308A/ V | Reduced L-Asp and Na$^+$ affinity and reduced amount of Na$^+$ binding sites | | |
| | | | T308S | L-Asp, Na$^+$ affinity and Hill coefficient unaffected but reduced $v_{max}$ | | |
| T308 | TMS7 | T364 (EAAT3) | T364A/ S/ V/ W | Reduced L-Asp affinity | | |
| S278 | HP1 | | | | C | 145 |
| N401 | TMS8 | | | | | |
| T308 | TMS7 | T364 (EAAT3) | | Na2 of the crystal structure is just an intermediate binding site (Na2') | C | 147 |
| I350 | HP2 | I406 (EAAT3) | | | | |
| T352 | HP2 | A408 (EAAT3) | | | | |

*Chapter 1*

| | | | | | | |
|---|---|---|---|---|---|---|
| T308 | TMS7 | T364 (EAAT3) | | The carbonyl oxygen atoms coordinate Na2 | C | 146 |
| I309 | TMS7 | I365 (EAAT3) | | | | |
| S349 | HP2 | S405 (EAAT3) | | | | |
| I350 | HP2 | I406 (EAAT3) | | | | |
| T352 | HP2 | A408 (EAAT3) | | | | |
| M311 | TMS7 | M397 (GLT-1) | M397C | Not functional | M | 139 |
| M311 | TMS7 | | M311A | $Na^+$:L-Asp stoichiometry of 2:1 | M | 142 |
| | | | M311L | $Na^+$:L-Asp stoichiometry comparable to *wt*-$Glt_{Ph}$ | | |
| M311 | TMS7 | M367 (EAAC1) | M367L/C/S | Change in substrate selectivity (L-Asp over L-Glu) and impaired L-Glu, L-Asp and D-Asp transport | M | 226 |
| M311 | TMS7 | M367 (EAAC1) | M367C | Impaired L-Asp transport | M | 130 |
| M311 | TMS7 | M399 (EAAT1) | M399C | Not functional | M | 114 |

Minor differences in amino acid numbering of one sort EAAT comes from the species variant used in the mentioned study.

X: crystal structure; M: mutational; C: computational; ch.: chapter; Ref.: reference; *: residues of other prokaryotic transporters are also presented with $Glt_{Ph}$ numbering.

**Table 1.5) Amino acid residues involved in Na3 coordination.**

| Residue in Glt$_{Ph}$* | Position | Explored eukaryotic transporter | Mutant | Effect/ conclusions | Study type | Ref. |
|---|---|---|---|---|---|---|
| **Y89** | **TMS3** | | | Main chain carbonyl interaction | X, C | ch. 5, 148 |
| **T92** | **TMS3** | | | Hydroxyl coordination | | |
| **S93** | **TMS3** | | | Hydroxyl coordination | | |
| **N310** | **TMS7** | | | Carboxamide interaction, N310 shields Na3 from Na1 | | |
| **D312** | **TMS7** | | | Side chain carboxyl interaction | | |
| T92 | TMS3 | | T92A | Reduced Na$^+$ affinity | M | 148 |
| S93 | TMS3 | | S93A | Reduced Na$^+$ affinity | | |
| N310 | TMS7 | | N310A | Not functional | | |
| D312 | TMS7 | | D312A | Not functional | | |
| T92 | TMS3 | T130 (EAAT1) | T130A | Reduced Na$^+$ affinity | | |
| S93 | TMS3 | T131 (EAAT1) | T131A | Reduced Na$^+$ affinity | | |
| Y89 | TMS3 | | | Main chain interactions | C | 122 |
| T92 | TMS3 | | | Amino acid oxygen interacts with Na3 | | |
| S93 | TMS3 | | | Main chain interactions | | |
| N310 | TMS7 | | | Carboxamide oxygen interacts with Na3 | | |
| D312 | TMS7 | | | Carboxamide oxygen interacts with Na3 | | |
| D394 | TMS8 | D444 (EAAT3) | | | C | 147 |
| R397 | TMS8 | R447 (EAAT3) | | | | |
| D312 | TMS7 | | | D405, D312, and N310 form an intermediate Na3 site (Na3') | C | 149 |
| T92 | TMS3 | | | | | |
| N310 | TMS7 | | | | | |

| Residue | TMS | Variant | Mutation | Description | Method | Ref |
|---|---|---|---|---|---|---|
| T314 | TMS7 | T370 (EAAT3) | | Na$^+$ binding precedes substrate binding but the substrate's oxygen atoms form part of the Na3 site | C | 146 |
| N401 | TMS8 | N451 (EAAT3) | | T92 and D312 form a transient Na3 site (Na3') | | |
| D312 | TMS7 | D398 (GLT-1) | D398N/E | Not functional, potential Na$^+$ binding-site | M | 151 |
| N310 | TMS7 | N366 (EAAC1) | N366D/A | Not functional | M | 152 |
| D312 | TMS7 | D368 (EAAC1) | D368N/A | Not functional | | |
| N310 | TMS7 | N396 (GLT1), | N396D D398N | Not functional | | |
| D312 | TMS7 | D398 (GLT1) | | | | |
| T92 | TMS3 | T124 (ASCT1) | T124A | Reduced Na$^+$ affinity | C, M | 141 |
| D312 | TMS7 | D380 (ASCT1) | D380A | Reduced Na$^+$ affinity | | |
| | | | D380N | No transport, binding unaffected | | |
| D312 | TMS7 | D367 (EAAC1) | D367N | Reduced Na$^+$ affinity, residue functions as charge compensator | M | 140, 151 |
| T92 | TMS3 | T101 (EAAC1) | T101A | Reduced Na$^+$ affinity | C, M | 150 |
| D312 | TMS7 | D367 (EAAC1) | T101A D367N | Not functional | | |
| T314 | TMS7 | T370 (EAAC1) | T370S | Na$^+$ cannot be replaced by Li$^+$, impaired transport | M | 136 |
| N401 | TMS8 | N451 (EAAC1) | N451S | Na$^+$ cannot be replaced by Li$^+$, impaired transport | | |
| | | | | T370, N451 (EAAC1), and substrate form Na3 | | |
| N310 | TMS7 | N396 (GLT-1) | N396C | Not functional | M | 139 |
| D312 | TMS7 | D398 (GLT-1) | D398C | Not functional | | |

Minor differences in amino acid numbering of one sort EAAT comes from the species variant used in the mentioned study.

X: crystal structure; M: mutational; C: computational; ch.: chapter; Ref.: reference; in red: residue is involved in substrate binding; in blue: residue is involved in Na1 binding; *: residues of other prokaryotic transporters are also presented with Glt$_{Ph}$ numbering.
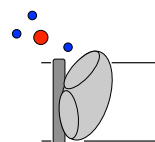
Mutational studies on the mammalian transporter EAAT3 confirmed the relevance of T308 ($Glt_{Ph}$ numbering) in $Na^+$ binding: alterations of the corresponding residue resulted in impaired sodium affinity[143].

Because thallium ions might bind differently in glutamate transporters than sodium ions, computational studies were conducted to evaluate the $Tl^+$ derived structures. Various MD and electrostatic interaction studies confirmed the Na1 site as proposed by the $Glt_{Ph}$ crystal structure[92,144,145] and reinforced that the same residues form the Na1 site in the eukaryotic transporters[141,146]. For Na2 the computational studies came to unequal conclusions. While two MD studies generally agree with the crystal structure[144,146], three other computational studies suggest different solutions[147,145,143]. Venkatesan et al.[143] and Heinzelmann et al.[147] propose both that the Na2 of the crystal structure is only an intermediate state but disagree on the position of Na2. However, in both solutions residues that form the Na2 site in the crystal structure also are part of the computationally predicted Na2 site. A summary of computational and mutational studies on Na2 is given in table 1.4.

Different to Na1 and Na2, the position of the third sodium binding site (Na3) was not revealed in the $Tl^+$ soaked $Glt_{Ph}$ crystal structure, possibly because thallium ions have a bigger size than sodium ions (1.64 Å vs 1.16 Å, ionic radius)[72]. Therefore, many mutational and computational studies on $Glt_{Ph}$ and EAAT1-3 explored potential Na3 sites. The results of the computational studies are diverse[122,141,144,146–150] but several mutational studies revealed the importance of T92, S93, N310, D312[138,139,141,148,151–153,150]. Mutation of these residues resulted in impaired sodium affinity or rendered the transporter non-functional (see table 1.5 for a summary of the computational and mutational studies). Only recently the crystal structure of sodium and substrate-loaded $Glt_{Tk}$ was solved, with resolution high enough to reveal the third sodium binding site (chapter 5). In the structure Na3 is coordinated by the main chain carbonyl of Y89 (TMS3), side chain hydroxyls of T92 (TMS3), S93 (TMS3), the side chain carboxyl of D312 (TMS7) and the carboxamide of N310 (TMS7; $Glt_{Ph}$ numbering, for the corresponding $Glt_{Tk}$ numbering see chapter 5). This is in line with the mutational studies and the computational studies from Bastug et al.[148] and Heinzelmann et al.[122].
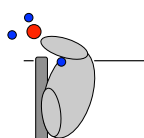
*Proton binding site*

In mammalian glutamate transporters glutamate translocation is accompanied by an intracellular acidification[124,154,155]. Because mainly the neutral cysteine is transported in EAAC1 at neutral pH (pH 7.4) without associated pH change, Zerangue et al. concluded, that a proton is co-translocated together with the substrate[156]. Additionally, it was hypothesized, that the proton is transported by the protonated form of the substrate[14,156]. However, an electrophysical study using laser-pulse photolysis revealed that proton binding precedes the substrate binding at an ionizable residue with an apparent $pK_a$ of 8[157].

A conserved histidine in TMS6 of EAATs was first proposed as possible proton acceptor, because arginine, lysine, and threonine substitutions of H326 in EAAT2 resulted in strongly impaired substrate transport[158]. Additionally, histidine was shown to be involved in proton transport of the *lac*-permease of *E. coli*[159]. However, later mutational studies on EAAT2 revealed that the respective histidine is not protonated at physiological pH and thus not involved in proton binding[160]. Differently, three independent mutational studies identify E374 from EAAT3 as the proton acceptor, as glutamine and asparagine substitutions yielded pH independent carriers[140,160,161]. This finding was confirmed by the reciprocal mutation of ASCT2 (Q392E), which rendered the proton independent transporter pH sensitive[161]. Also Molecular Dynamics simulations predict the proton to bind at E364 in the presence of Na2 via D368 and D455 in EAAT3[162]. The same computational study also predicts that the proton is replaced by one potassium ion after substrate delivery.

*Potassium binding*

After substrate delivery, eukaryotic glutamate transporters require the counter transport of potassium in order to reset. However, prokaryotic glutamate transporters, as $Glt_{Ph}$, are potassium independent and reorient spontaneously[68,70]. Accordingly, the $Glt_{Ph}$ crystal structures did not reveal the potassium binding site. Computational studies resulted in different predicted binding sites for $K^{+}$ [144,150,162]. Mutational studies on EAAT2 and EAAT3 revealed a broad range of amino acids that might be involved in potassium binding. Corresponding residues to Y317, R397, D405, N310, D312, D390, and Q318 in $Glt_{Ph}$ were implicated in potassium coordination[66,109,133,135,138–140,152,163,164] (see table 1.6). EAAT2 and EAAT3 with alteration of either of these residues were not functional and became electroneutral amino acid exchangers. Substrate transport to the intracellular was still
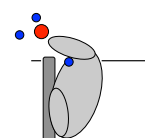
**Table 1.6) Amino acid residues implicated in potassium binding.**

| Residue in Glt$_{Ph}$* | Position | Explored eukaryotic transporter | Mutant | Effect/ conclusions | Study type | Ref. |
|---|---|---|---|---|---|---|
| D394 | TMS8 | D444 (EAAT3) | | Carboxyl interactions with K$^+$ | C | 144 |
| Q318 | TMS7 | E404 (EAAT2) | E404D | Becomes an electroneutral amino acid exchanger due to abolished K$^+$ binding | M | 66 |
| Y317 | TMS7 | Y403 (GLT-1) | Y403F | Becomes an electroneutral amino acid exchanger due to abolished K$^+$ binding | M | 133 |
| Y317 | TMS7 | Y403 (GLT-1) | Y403C | Not functional | M | 139 |
| Q318 | TMS7 | E374 (EAAT3) | | K$^+$ replaces H$^+$ after substrate delivery. K$^+$ can also replace Na1 or Na3, transporter does not require the inward *apo* state | C | 162 |
| R397 | TMS8 | R447 (EAAC1) | R447C | Becomes an electroneutral amino acid exchanger due to abolished K$^+$ binding | M | 109 |
| D405 | TMS8 | D454 (EAAC1) | D454N | Turned into an exchanger, overlapping Na1 and K$^+$-sites | M | 163 |
| N310 | TMS7 | N366 (EAAC1) | N366Q/E N366D/A | Impaired transport. Not functional | M | 152 |
| D312 | TMS7 | D368 (EAAC1) | D368N/A | Not functional | | |
| N310 | TMS7 | N396 (GLT-1) | N396D D398N | Not functional, impaired K$^+$ binding | | |
| D312 | TMS7 | D398 (GLT-1) | | | | |
| D390 | TMS8 | D440 (EAAC1) | D440E | Decreased K$^+$ affinity, cannot relocate after substrate delivery, becomes amino acid exchanger | M | 164 |
| Q318 | TMS7 | E373 (EAAC1) | E373Q | Not functional, possibly affected H$^+$ or K$^+$ binding | M | 124, 141 |
| D405 | TMS8 | D454 (EAAC1) | D454N | Not functional, possibly affected H$^+$ or K$^+$ binding | | |
| D312 | TMS7 | | | Potential but not optimal K$^+$ binding site | C | 150 |
| T92 | TMS3 | | | | | |
| N310 | TMS7 | | | | | |
| Y88 | TMS3 | | | | | |
| G404 | TMS8 | | | | | |

| Residue | TMS/HP | Equivalent residue | Mutation | Description | Method | Ref |
|---|---|---|---|---|---|---|
| D405 | TMS8 | D455 (GLT-1 & EAAC1)# | D455A/S/C/N/E | $Na^+$ dependent exchanger due to impaired $K^+$ binding | M | 135 |
| D394 | TMS8 | D444 (EAAT3) | D444S | D444S T448A shows impaired electrophysical response of $K^+$ binding | M | 121 |
| D394 | TMS8 | N428 (CuqDCT) | N428D | Conferred electrophysical response of $K^+$ binding | M | |
| R276 | HP1 | | | IFS $Glt_{Ph}$ in complex with $Tl^+$, $Tl^+$ density mimics $K^+$ – site of EAATs, however $Tl^+$ could not be outcompeted by $Na^+$ or $K^+$ | X | 142 |
| V355 | TMS7 | | | | | |
| P356 | TMS7 | | | | | |
| D394 | TMS8 | | | | | |
| T398 | TMS8 | | | | | |
| Y317 | TMS7 | | | Potential $K^+$ binding site in the EAATs | X | ch. 4 |
| Q318 | TMS7 | | | | | |
| T314 | TMS7 | | | | | |

Minor differences in amino acid numbering of one sort EAAT comes from the species variant used in the mentioned study.

X: crystal structure; M: mutational; C: computational; ch.: chapter; Ref.: reference; in red: residue is involved in substrate binding; in blue: residue is involved in sodium binding; *: residues of other prokaryotic transporters are also presented with $Glt_{Ph}$ numbering; #: EAAC1 numbering presented only.
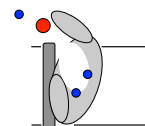
possible, but the mutant transporters were not able to relocate after substrate delivery. Therefore, it was assumed that potassium binding was abolished in the mutants. While most of the residues suggested in potassium binding are conserved in $Glt_{Ph}$ and the eukaryotic transporters, the neutral residue Q318 of $Glt_{Ph}$ is a glutamate in the EAATs (E374 in EAAT3). The negatively charged residue of eukaryotic transporters might therefore be part of the potassium binding site. Remarkably, E374 from EAAT3 is also the proton acceptor in the eukaryotic glutamate transporters. After substrate delivery, potassium could possibly replace the proton at this binding site.

The crystal structure of an aspartate-free transporter (chapter 4) showed how a possible potassium binding site could be created after substrate delivery. The substrate-free structure revealed a potential cation binding site between Y317, Q318 and T314 ($Glt_{Ph}$ numbering). This is in line with mutational studies on mammalian glutamate transporters, in which mutations of either of these residues resulted in transporters deficient in potassium binding [66,140,139,133,138], and is additionally supported by a recent computational study[147]. Differently, the crystal structure of an IFS $Glt_{Ph}$ mutant in complex with thallium suggests an alternative location for the potassium binding site, consisting of T398, R276, D394, V355 and P356[142]. This proposed potassium binding site is supported by a computational study[144] and one mutational study on an insect dicarboxylate transporter[121]. At position of D394 this transporter has an asparagine. Mutation of this residue to aspartate changed the transporter into a glutamate transporter with increased $K^+$ induced currents[121]. However, the $K^+$ binding site was determined by the use of $Tl^+$ ions that supposedly mimic $K^+$. Yet, neither the excess of $K^+$ nor $Na^+$ was able to outcompete the bound $Tl^+$ in the $Glt_{Ph}$ crystal structure.

Another computational study[162] proposed that the potassium ion can bind to multiple sites, among which the proton binding site, the substrate binding site, and the sodium binding sites 1 and 3. Consequently, eukaryotic glutamate transporters do not require reaching the inward *apo*-state. The authors hypothesize, that this enables the extremely fast translocation rates of eukaryotic glutamate transporters.
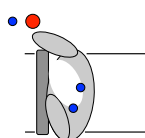
## Uncoupled chloride conductance

Besides the cation coupled substrate translocation, eukaryotic glutamate and neutral amino acid transporters also display chloride currents and act as chloride channels[63,119,165–168]. Even though the chloride conductance is activated by sodium ions and increased by substrate binding[165,169–171], it is uncoupled from substrate transport. Mutations and modifications in HP2 that abolished the uptake of substrate did not diminish chloride currents[1725–175]. Vice-versa, mutants of EAAT1 with altered chloride conductance displayed unchanged or only minimally affected substrate transport[97,176]. Binding of the substrate analog TBOA, that prevents the closure of HP2[69] and therewith locks the transporter in the OFS, resulted in abolished chloride conductance[97,177]. This exemplifies that the anion conducting state is not linked to the binding of substrate but to a subsequent conformation during substrate translocation[131,178]. Thus, while the substrate is transported across the membrane a channel opens that mediates the chloride currents[63,166,175,179–181]. Fluorescence, electrophysiology, and rapid solution exchange experiments revealed that each protomer has its own independent chloride permeation pathway[76,88,89,97].

Besides chloride, also other anions are conducted with following order: $SCN^- > ClO^- > NO^- > I^- > Br^- > Cl^- \gg F^{-}$[166,178]. Therefore, the chloride channel of glutamate transporters is more applicably an anion channel. Based on the preference of conducted anions the pore size of the anion channel was proposed to have a diameter of ~5 Å[175,182]. An uncoupled chloride conductance was also described for the prokaryotic transporter $Glt_{Ph}$[183].

The physiological function of the uncoupled anion conductance is not fully understood yet. However, transport assays on $Glt_{Ph}$ suggest, that anion influx during substrate and cation translocation prevents depolarization of the membrane at least in part[183]. The experiments showed that in the presence of permeable anions substrate transport is maintained for a longer time period. Additionally, chloride permeation by EAAT5 of rat retinal rod bipolar cells and mouse bipolar axon terminals was reported to reduce glutamate release into the synaptic cleft by hyperpolarization[184,185]. It was suggested that anion channel activity serves as inhibitory feedback mechanism to prevent neurotoxic glutamate release[63,171,184–186].

The ratio of anion conductance to glutamate transport differs greatly amongst the various eukayotic glutamate transporters: EAAT1-3 display only minor anion currents, whereas
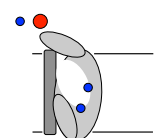
EAAT4-5 are believed to function mainly as anion channels[187,188]. Additionally, EAAT1-3 are low affinity transporters with high capacity. On contrast, EAAT4-5 rather are high affinity transporters with low capacity. Therefore Mim et al. suggested that these transporters complement each other for effective glutamate removal[187].

The first structural indication on the localization of the anion channel came from a crystal structure of $Glt_{Ph}$ with one protomer in an intermediate OFS[189]. The structure revealed a water filled cavity at the interface of trimerization and transport domain. An extended study, combining MD simulations and functional methods proposed that the formation of a transient state, involving a lateral movement of the transport domain away from the intermediate OFS of the crystal structure, results in the opening of the anion channel[167]. This channel runs nearly perpendicular through the transporter and is located between the interface of the trimerization and transport domain. The following pore lining residues were identified: V12, L13, I16, L20, F50, V51, L54, V198, M202, A205, P206, G208, V209, L212, I213, T271, V274, T275, R276, S278, T281, V284, P356, A358, I361, L387, D390, A391, D394 ($Glt_{Ph}$ numbering)[167].

Interestingly, the previously defined anion selectivity filter residue S65 is not part of the proposed anion pathway. The mutation of this serine, which is conserved in glutamate transporters, to valine resulted in an altered chloride permeation behavior and a changed anion permeability sequence in $Glt_{Ph}$ and EAAT1 (S65V and S103V), respectively[97,183]. Also residues surrounding S65 were shown to have an influence on the chloride conductance[97,176,181,183,190,191]. However, even residues not directly involved in anion conductance might indirectly have an influence on the functionality by creating local rearrangements and steric hindrances. Additionally, the substrate translocation might sample conformational changes that transform the anion channel as proposed by Machtens et al. into a pathway that also contains S65[186]. Future experiments and more crystal structures of intermediate states and/or the mutants are required for a more detailed understanding.

**Transport mechanism**

The combination of functional, crystallographic and computational data has greatly improved our understanding of the glutamate transport mechanism. EPR experiments on
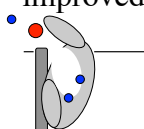
Glt$_{Ph}$ revealed that, even in the unloaded transporter, the transport domain is very dynamic[86,96]. It undergoes multiple conformations and travels the membrane to visit inward and outward-facing states. The high dynamics are enabled by the similarity in the energy of IFS and OFS as well as for the substrate-loaded and the empty transporter[86,192]. EPR data revealed that in the substrate unbound state the external gate HP2 is in a closed conformation[91]. In the same study it was found that sodium binding resulted in the opening of HP2 (figure 1.4 a-b). Subsequent substrate binding resulted in the closure of HP2 (figure 1.4 c-d).

Experimental data, presented in this thesis, show that sodium binding has to precede aspartate binding in Glt$_{Ph}$ and is accompanied by large conformational changes (chapter 2). This is in line with experimental studies on EAAT2 and EAAT3 using voltage-clamp fluorometry and glutamate transport dependent currents, respectively[84,177]: both studies conclude that two sodium ions bind prior to glutamate binding. Computational studies suggest that sodium binds first to the Na1[92,149] or Na3-site[122]. Na3 exhibits the highest sodium affinity amongst the three sodium-sites[72,122,193] (see also chapter 5), which might indicate that this site is occupied first. Nevertheless, MD simulations based on substrate-loaded Glt$_{Ph}$ structures indicate that only Na1 is water and sodium accessible in the substrate-free state[149]. Therefore, Huang et al. suggest that Na$^+$ binding to Na1 results in conformational changes, that enable extracellular water and Na$^+$ to reach D312 (part of the Na3-site) via a pathway lined by the conserved amino acids G306, N310, M311, N401, G404, and D405[149]. The same study suggests, that Na3 is then filled by a second Na$^+$ diffusing via this water accessible pathway or by knock-off mechanism. This mechanism suggests that Na1 moves towards to Na3 while another sodium ion fills Na1.

However, in the *apo*-state neither the Na1 nor the Na3-site are present (chapter 4). It is therefore not clear which sodium ion binds first, but based on the location and the structural linkage of the binding sites it is plausible that binding of either Na1 or Na3 results in the formation of the second sodium binding site (figure 1.4 b). Binding of both sodium ions results in structural rearrangements of key residues in TMS7, 8, and 3 and the formation of a high affinity substrate binding site (figure 1.4 c) and is described in more detail in chapter 5. Subsequent substrate binding partially closes HP2 and creates the Na2 binding site[92] (figure 1.4 d). Even though the transport domain is highly dynamic and visits the IFS also in partially loaded-states[85,96] (figure 1.4 m), the binding of the last sodium ion
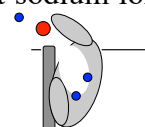
is required for substrate delivery[84,177]. Computational studies propose that binding of Na2 closes the outer lid and locks HP2 in a closed conformation[92,122] (figure 1.4 d). This most likely allows subsequently for productive transport (figure 1.4 e-f). Because Na^{+} in Na2 was unstable during MD simulations[72,122,143] (chapter 5), two computational studies propose that the position of Na2 as determined by the crystal structure, is only an intermediate Na2'-site[122,143]. Both studies suggest that Na2 matures during the transport process but come to different solutions close to the initial Na2 binding site.

Crystal structures of fully loaded Glt$_{Ph}$ in OFS[69], intermediate state[189] and IFS[99] show that the transport domain travels with a rigid body movement, like an elevator, to the other side of the membrane (figure 1.4 e-f). Simulations based on crystal structures of Glt$_{Ph}$ in the IFS suggest an intrinsic flexibility of HP2, which results in spontaneous Na2 release to the cytoplasm after the translocation[100] (figure 1.4 g). As the gatekeeper Na2 dissociates and HP2 slightly opens, water molecules enter the substrate binding site. The water-influx destabilizes the substrate interactions to residues on TMS8 and leads to substrate dislocation. Strong hydrogen bonds between substrate and the conserved serine stretch in HP2 (Glt$_{Ph}$ S276-278) prevent the immediate substrate release. The opening of HP1 subsequently results in the release of the substrate to the interior (figure 1.4 h, uncolored panel). In this model HP2 is only the initiator for substrate release, while HP1 is the internal gate[100].

Another computational study proposes that HP2 is not only the extracellular gate but also the intracellular gate[107] (figure 1.4 h, yellow panel). Also in this model the opening of the internal gate results in substrate release. However, this model requires a stronger translational movement or 'swing-out' of the transport domain than observed in the IFS crystal structures of IFS cross-linked Glt$_{Ph}$. Notably, Glt$_{Ph}$ R276S M395R crystallizes readily in such a conformation. Therefore, HP1 as well as HP2 might likely form the internal gate. In the future crystal structures with the internal gate in an open conformation might solve this question.
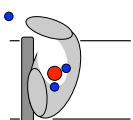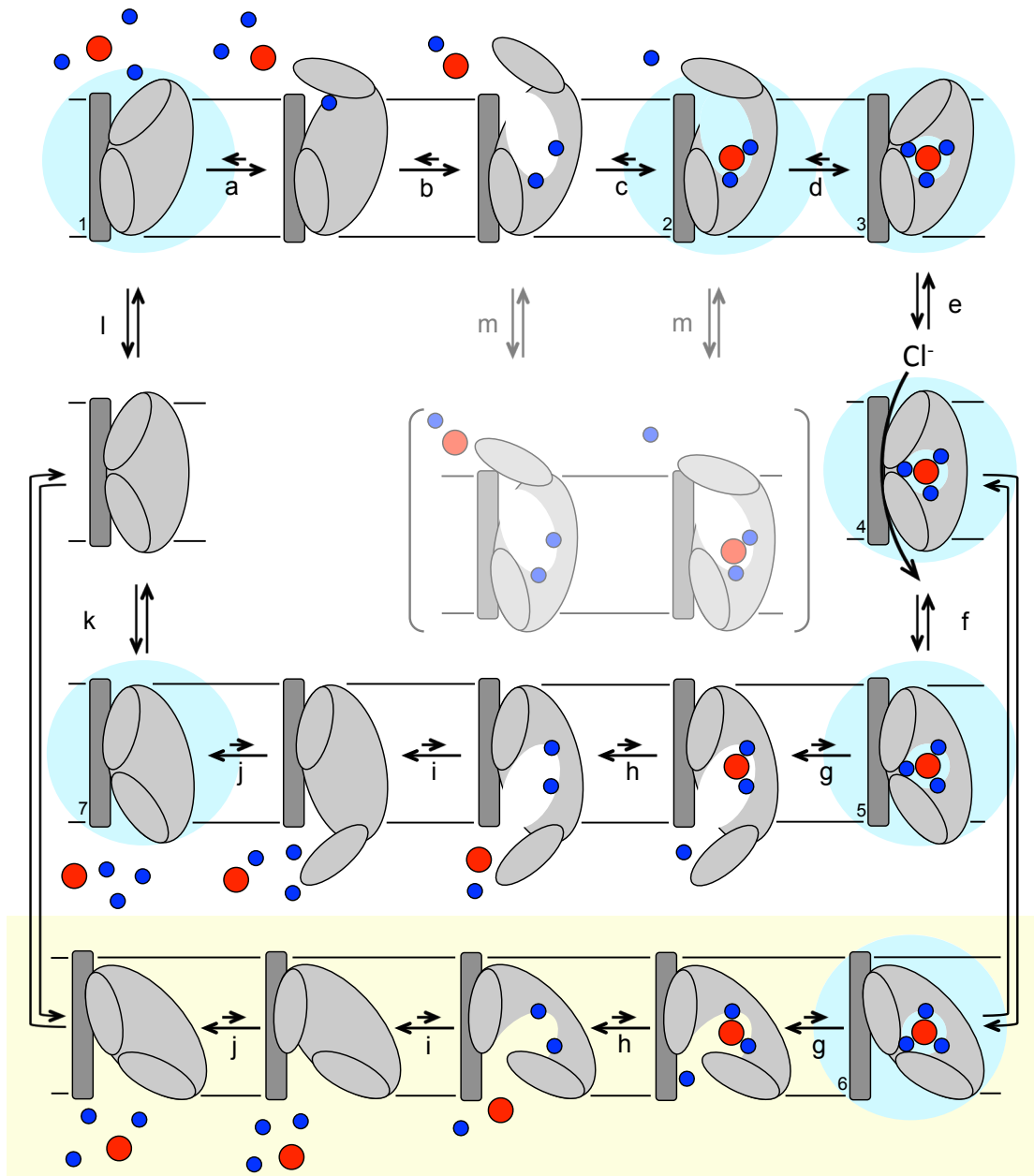
**Figure 1.4) Schematic translocation cycle of archaeal glutamate transporter homologs based on the available crystal structures, biochemical, and computational data.** Shown is one protomer in the membrane plane in side-view presentation. The translocation domain with HP1 and 2 are shown in light grey, the trimerization domain is shown in dark grey; sodium ions and L-aspartate are represented as blue and red spheres, respectively. Light blue colored circles indicate states with available crystal structures. Crystal structure PDB codes: **(1)** 4KY0[71], 4OYE[142]; **(2)** 2NWW[69]; **(3)** 5E9S[72], 2NWX[69]; **(4)** 3V8G[189]; **(5)** 3KBC[99], 3V8F[189]; **(6)** 4X2S[106]; **(7)** 4P3J[142]. **(a)**-**(d)** Indicate transitions during $Na^+$ and L-aspartate loading in the OFS. **(m)**, **(e)**-**(f)**, **(l)**-**(k)** indicate elevator-like movements of the transport domain in empty and loaded states across the membrane; **(g)**-**(j)** indicates transitions during $Na^+$ and L-aspartate unloading in the IFS. Substrate and cation release in IFS with HP1 as intracellular gate as proposed by[99,100,105] are shown without colored background; the yellow colored background shows substrate and cation release in IFS with HP2 as intracellular gate as proposed by[106,107]. Unproductive translocations and states are depicted in lighter shades.
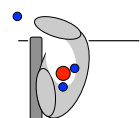
While the internal gate opens and the substrate leaves the binding site a conserved arginine of TMS8 ($Glt_{Tk}$ R401) fills the site occupied by the substrate in the substrate-loaded transporter[71] (chapter 4). This motion also relocates the Na1 and Na3 coordinating residues in TMS3, 7, and 8. The structural rearrangements then distort the known sodium binding sites. Because Na1 is less strong bound to the transporter it presumably leaves the binding site before Na3. Na3 binds with much higher affinity and was therefore proposed to unbind last[193] (figure 1.4 i). After substrate and coupling ion release all binding sites are distorted, occluded and the transport domain is as compact as in the outward facing empty transporter or the fully loaded transporter[71,142] (figure 1.4 j). This most likely enables the transport domain to travel across the membrane into the OFS in the same way as it did to the IFS while being substrate-loaded[71] (figure 1.4 k-l).

The transport mechanism above describes the relevant translocation steps that are identical for prokaryotic and eukaryotic glutamate transporters. However, the transport mechanism of eukaryotic glutamate transporters is slightly more complex and requires some additional steps: after Na1 and Na3 binding, one proton binds to the transporter followed by high affinity substrate binding[147,157,194]. MD simulations on EAAT3 suggest that after the substrate translocation and Na2 release, hydration of the substrate and proton binding site results in deprotonation[162]. According to this study subsequent substrate, Na1 and Na3 dissociation would result in re-protonation of the proton binding site by the side chains of EAAT3 D368 and D455. The MD simulation showed that $K^+$ binding in the proton binding site prevents re-protonation at this step. Yet also other potassium binding sites were proposed[66,109,133,135,138–140,152,162–164], and whether potassium binding occurs after the release of substrate and coupling ions is still debated[147,162].

**The relevance of crystal structures**

The primary structure of a protein and alignments of amino acid sequences of related proteins can reveal secondary, tertiary, and quaternary structure motifs[195]. It even can give some functional insight in cases of high similarity and well-characterized homologs. Additionally, biochemical data and mutational studies can provide crucial information about the functionality of proteins, localize the active site, and provide some structural information. However, not all details can be solved in this way and mutational studies can
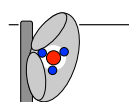
be difficult to interpret. In order to gain detailed structural insights into proteins and to gain better mechanistic insights X-ray crystallography can be a powerful tool. X-ray crystallography can deliver a high-resolution analysis of the three dimensional structure of a protein. Yet a crystal structure reveals only a snapshot of one well ordered state that is stable under the crystallization condition. As the crystallization conditions usually differ very much from the natural environment of the protein, this may have an influence on the protein structure. Interactions with precipitants, salts, or other compounds in the crystallization condition might affect the fold, size, or conformation of the protein. Also, the crystal packing can result in altered conformations. Therefore, the crystallized state potentially might represent a crystallographic artifact instead of a physiological relevant state[196]. Additionally, crystal packing and unordered or dynamic regions in the structure influence data quality, and can result in incomplete data and low-resolution, which complicates or impedes the data interpretation. Many of the currently available crystal structures of glutamate transporter homologs suffer from medium resolution (> 3 Å) and partially low completeness (table 1.7).

Especially the $Glt_{Ph}$ structures with PDB code 3V8G (intermediate state), 4IZM (OFS cross-linked), 4P6H (IFS cross-linked), 4OYE (*apo*-OFS), 4X2S (IFS $Glt_{Ph}$ R276S M395R) display resolutions equal or worse than 4 Å. Roughly, resolutions worse than 4 Å only allow for secondary structure motive identifications[197]. Differently, resolutions of 3-4 Å allow for tertiary and quaternary structure identifications but are very likely to include erroneous side chain rotamers[197]. In general the higher the resolution the more detailed the structure and the lower the amount of wrong rotamers. Highest resolution so far is reported for substrate-free and substrate-loaded OFS structures from $Glt_{Tk}$[71,72] (chapter 4-5). The structures are comparable to the corresponding $Glt_{Ph}$ structures. Therefore, they do not only reinforce the similarity between the homologous transporters but also indicate that the crystalized states most likely are of physiological relevance: the likelihood of a crystal structure to be of physiological relevance increases when more homologs or structures with different packing units share the same fold and state.

**Table 1.7) List of the available glutamate/aspartate transporter crystal structures.**

| PDB code (Ref.) | Transporter | Description | Resolution (Å) | Completeness* (%) | Remark/ Conclusion |
|---|---|---|---|---|---|
| 1XFH (15) | $Glt_{Ph}$ 7H | OFS | 3.5 | 97.1 (98) | Homotrimeric, bowl shaped organization |
| 2NWL (69) | $Glt_{Ph}$ 7H | OFS, +L–Asp | 2.96 | 69.3 (47.8) | Substrate binding site |
| 2NWW (69) | $Glt_{Ph}$ 7H | OFS, +TBOA | 3.2 | 74.8 (33.2) | HP2 is the extracellular gate |
| 2NWX (69) | $Glt_{Ph}$ 7H | OFS, +L–Asp, $Na^+$ | 3.29 | 69.2 (30.2) | Na1 and Na2 binding site |
| 3V8G (189) | $Glt_{Ph}$ 7H V198C M300C | Two protomers in IFS, one protomer in intermediate OFS, $Hg^{2+}$ cross-linked, +L–Asp & $Na^+$ | 4.66 | 73.5 (9) | Intermediate OFS |
| 3V8F (189) | $Glt_{Ph}$ 7H V216C M385C | IFS, $Hg^{2+}$ cross-linked, +L–Asp & $Na^+$ | 3.8 | 99.4 (99.8) | IFS, elevator-like transport mechanism |
| 3KBC (99) | $Glt_{Ph}$ 7H K55C A364C | IFS, $Hg^{2+}$ cross-linked, +L–Asp & $Na^+$ | 3.51 | 97.2 (92.2) | IFS, elevator-like transport mechanism |
| 4IZM (192) | $Glt_{Ph}$ 7H L66C A300C | OFS, $Hg^{2+}$ cross-linked, +L–Asp & $Na^+$ | 4.5 | 99.7 (100) | OFS structure comparable to uncross-linked $wt$-$Glt_{Ph}$ |
| 4P1A (142) | $Glt_{Ph}$ 7H K55C A364C | IFS, $Hg^{2+}$ cross-linked, +$Tl^+$ (apo-conformation) | 3.75 | 99.7 (99.8) | Potential $K^+$ binding site (see table 1.6) |
| 4P19 (142) | $Glt_{Ph}$ 7H K55C A364C | apo-IFS, Hg2+ cross-linked | 3.25 | 99.0 (88.1) | Alkali containing crystallization condition |
| 4P3J (142) | $Glt_{Ph}$ 7H K55C A364C | apo-IFS, $Hg^{2+}$ cross-linked | 3.5 | 95.5 (92.7) | Structure of transport domain comparable to 4KY0 |
| 4P6H (142) | $Glt_{Ph}$ 7H K55C A364C | apo-IFS, $Hg^{2+}$ cross-linked, substrate-bound conformation | 4.08 | 67.4 (6.5) | |
| 4OYE (142) | $Glt_{Ph}$ 6H R397A | apo-OFS | 4.0 | 67.9 (13.0) | Structure comparable to 4KY0 |
| 4OYF (142) | $Glt_{Ph}$ 6H R397A | OFS, +$Na^+$ | 3.41 | 87.3 (12.0) | |
| 5CFY replacing 4OYG (142) | $Glt_{Ph}$ 6H R397A | OFS, +L–Asp & $Na^+$ | 3.5 | 97.1 (96.6) | |

| | | | | | |
|---|---|---|---|---|---|
| 4X2S (106) | Glt$_{Ph}$ 7H R276S M395R | IFS, +L–Asp & Na$^+$ | 4.21 | 83.2 | Increased hydration of transport and trimerization domain interface increases the substrate transport rate |
| 4KY0 (71) | Glt$_{Tk}$ | *apo*-OFS | 3.0 | 99.8 | Structure of the *apo*-OFS, potential cation binding site (see table 1.6) |
| 5DWY (ch. 5) | Glt$_{Tk}$ | *apo*-OFS | 2.7 | 79 (17.9) | Improvement of 4KY0 |
| 5E9S (ch. 5) | Glt$_{Tk}$ | OFS, +L–Asp & Na$^+$ | 2.8 | 97.5 (96.0) | Na3 binding site |
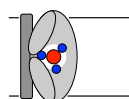
Glt$_{Ph}$ 6H and 7H: glutamate transporter homologs from the archaeon *P. horikoshii* with 6 and 7 histidine substitutions, respectively

Glt$_{Tk}$: archaeal glutamate transporter homolog from *T. kodakarensis*; IFS: inward facing state; OFS: outward facing state; ch: chapter.

*: Values for completeness mean the overall completeness of the dataset. Values in parentheses give the completeness for the highest resolution shell.

In grey: values are for the highest resolution shell as given in the literature, overall resolution and completeness however differs from the PDB data refinement statistics.

For the overall completeness and resolution the PDB values were used.
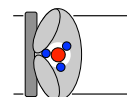
Determining only one state of a transporter can give valuable mechanistic insights but cannot unravel the structural basis of the complete transport mechanism. For this many structures of various conformations are required. Even though structures of glutamate transporters in many conformations are available, not all steps of the transport cycle are yet crystallized (see table 1.7 and figure 1.4). Additionally, crystal structures still are just static snap-shots of particular states. The function of proteins however involves dynamic processes. Yet there are no experimental techniques so far that enable dynamic studies at atomic level resolution and at physiological relevant time frames. Computer simulations can reveal such dynamic insights but also require an initial experimentally determined structure[198,199]. The same accounts for current computational drug discovery and design tools[200].

Also for glutamate transporters many computational studies complemented the biochemical and structural data. Most MD simulations used the available substrate-loaded $Glt_{Ph}$ structures of medium quality. Resolving more high-resolution crystal structures of yet unsolved states and other glutamate transporter homologs can only lead to an improvement of our understanding of the glutamate transporter family, help to unravel the complete transport mechanism, and foster drug-design in the future.
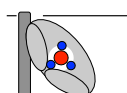
## Outline of this thesis

By the time I started my PhD, there was a vast amount of functional and structural information on glutamate transporters available. However, many mechanistic questions were still unknown or debated. There was no structure yet of a substrate-free transporter. Thus the question was how the empty transporter would look like and how it might reorient after substrate delivery. Also the third sodium binding site was not found yet, since the crystal structures of thallium and substrate-bound $Glt_{Ph}$ only revealed two potential sodium binding sites. Another point of interest was how glutamate transporters were coupling the substrate binding to ion binding and how specificity is mediated and leaks avoided. This is not only a question of importance for glutamate transporters but relevant for any secondary active transporter. Glutamate transporters could serve therefore as a model for other secondary active transporters.

**Chapter 1** gives a general introduction on membrane proteins and the position glutamate transporter take amongst them. In this chapter the main functional and structural information is summarized and the objective of my PhD is defined.

**Chapter 2** describes the binding kinetics of sodium and aspartate using the fluorescence of tryptophan $Glt_{Ph}$ mutants. It shows that sodium and aspartate binding is mutually dependent. The results show that aspartate binding is fast and involves only smaller conformational changes. In contrast to this, sodium binding is slow, of low affinity and involves big conformational changes, which most likely makes sodium binding the rate-limiting step in substrate binding.

**Chapter 3** presents a biochemical characterization of $Glt_{Tk}$ in respect to substrate binding. It shows that $Glt_{Ph}$ and $Glt_{Tk}$ share ~77% sequence identity and many functional properties. However, there are also significant differences in substrate specificity and binding affinities. Initial transport assays show the importance of the lipidic environment of the transporter and reveal that $Glt_{Tk}$ is a much faster transporter than $Glt_{Ph}$.

In **chapter 4** the crystal structure of substrate-free $Glt_{Tk}$ is described. In the empty transporter the highly conserved residue R401 fills the site occupied by the substrate in the substrate-loaded transporter. As consequence the interaction with Y320 in TMS7 is
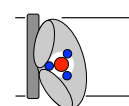
interrupted and the functionally important residue M314 relocated. The structural rearrangements distort the known sodium binding sites. The presented structure gives insights over how the empty transporter might reorient after substrate delivery.

In **chapter 5** the third sodium binding site is revealed. In the substrate-loaded structure Na3 is coordinated by T94, S95, N31, D315, and Y91. The structure shows that binding of Na3 facilitates and reinforces the formation of the aspartate binding site. MD studies based on the substrate-loaded $Glt_{Tk}$ structure and the *apo*-$Glt_{Tk}$ structure are consistent with a transport-model, in which Na3 and Na1 bind before aspartate with subsequent Na2 binding.

When taken together **chapters 2 to 5** show how the coupling between sodium and aspartate is realized, maintained and how substrate leakage is avoided in the aspartate:sodium symporters $Glt_{Ph}$ and $Glt_{Tk}$.
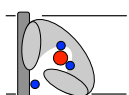
# Chapter 2

# Low Affinity and Slow Na$^+$ Binding Precedes High Affinity Aspartate Binding in the Secondary-active Transporter Glt$_{Ph}$

**Inga Hänelt[#], Sonja Jensen[#], Dorith Wunnicke and Dirk Jan Slotboom**
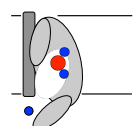
**Abstract**

Glt$_{Ph}$ from *Pyrococcus horikoshii* is a homotrimeric Na$^+$-coupled aspartate transporter. It belongs to the widespread family of glutamate transporters, which also includes the mammalian excitatory amino acid transporters (EAATs) that take up the neurotransmitter glutamate. Each protomer in Glt$_{Ph}$ consists of a trimerization domain involved in subunit interactions, and a transport domain containing the substrate binding site. Here, we have studied the dynamics of Na$^+$ and aspartate binding to Glt$_{Ph}$. Tryptophan fluorescence measurements on the fully active single tryptophan mutant F273W revealed that Na$^+$ binds with low affinity to the *apo*-protein ($K_d$ 120 mM), with a particularly low $k_{on}$ value (5 M$^{-1}$s$^{-1}$). At least two Na$^+$ ions bind prior to aspartate. The binding of Na$^+$ requires a very high activation energy ($E_a$ 106.8 kJmol$^{-1}$) and consequently has a large $Q_{10}$ value of 4.5, indicative of substantial conformational changes before or after the initial binding event. The apparent affinity for aspartate binding depended on the Na$^+$ concentration present. Binding of aspartate was not observed in the absence of Na$^+$, whereas in the presence of high Na$^+$ concentrations (above the $K_d$ for Na$^+$) the dissociation constants for aspartate were in the nanomolar range and the aspartate binding was fast ($k_{on}$ of 1.4*10$^5$ M$^{-1}$s$^{-1}$), with low $E_a$ and $Q_{10}$ values (42.6 KJmol$^{-1}$ and 1.8, respectively). We conclude that Na$^+$ binding is most likely the rate-limiting step for substrate binding.

Low Affintiy and Slow Na$^+$ Binding Precedes High Affinity Asapartate Binding in the Secondary-active Transporter Glt$_{Ph}$

53
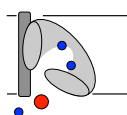
## Introduction

Glutamate is the main excitatory neurotransmitter in the central nervous system. Glutamate transporters take up extracellular glutamate into glial cells and neurons surrounding the synaptic cleft, and thus help to prevent prolonged elevated, neurotoxic extracellular concentrations of the neurotransmitter and maintain efficient synaptic communication between the neurons[45,201]. Five mammalian subtypes of glutamate transporters (excitatory amino acid transporters (EAAT)[45,65,70,124,201] each couple glutamate transport to the co- and counter-transport of cations[65]. Three Na$^+$ ions and one proton are co-transported with a glutamate molecule, whereas the transport cycle is completed by the counter-transport of one K$^+$ ion[124].

The only glutamate transporter homologs for which high-resolution crystal structures have been solved are the archaeal Na$^+$-coupled aspartate transporters Glt$_{Ph}$ from *Pyrococcus horikoshii*[70] and Glt$_{Tk}$ from *Thermococcus kodakarensis*[71]. Crystal structures in different conformations revealed that the protomers in the homotrimeric proteins consist of a trimerization domain involved in the subunit interactions and a transport domain, which contains the binding sites for aspartate and sodium ions. A transport mechanism has been proposed in which the transport domains move across the membrane like an elevator to expose the binding site alternately to the intracellular or extracellular space[15,69,99,189]. Two helical hairpin regions (HP1 and HP2) form the inner and outer lids on the binding site, respectively, that may open when the transporting domain is located in the inward or outward-facing conformation. Although three Na$^+$ ions are co-transported with one aspartate[128], the crystal structures revealed only two Na$^+$ ion binding sites (Na1 and Na2) within each protomer[69]. The binding site for the third Na$^+$ ion is still debated[136,144,146,148,149,152,150]. Experiments and simulations on Glt$_{Ph}$ and EAAT3 have suggested that the third Na$^+$ ion (Na3) may be coordinated by Thr314 and Asn401 in Glt$_{Ph}$[146]. This location is in line with previous experimental data[130,153]. Simulations also indicated that binding to Na1 and Na3 takes place before glutamate/aspartate binding[146,148], whereas the third Na$^+$ ion binds to the Na2 site only after the amino acid substrate has bound[69]. These results again are in agreement with former experimental and computational studies on several glutamate transporters[92,149,153,166,194,202,203]. In previous characterizations of Glt$_{Ph}$ using tryptophan fluorescence measurements with a single tryptophan introduced at
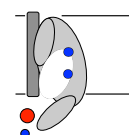
position Leu130 (figure 2.1), the affinity for aspartate binding was shown to strictly depend on the Na$^+$ concentration and vice versa[69]. The L130W mutant has several disadvantages for functional studies because its transport activity is severely reduced compared with the wild-type (*wt*) protein, and it only reports fluorescence changes upon binding of both aspartate and sodium ions.

Here we constructed novel single tryptophan mutants with the aim to dissect Na$^+$ and aspartate binding events in Glt$_{Ph}$. Using steady-state and stopped-flow fluorescence measurements, we show that sodium binding to the *apo*-protein is of low affinity and is accompanied by large conformational changes. Sodium binding precedes aspartate binding, which is fast and of high affinity as long as sodium is present.
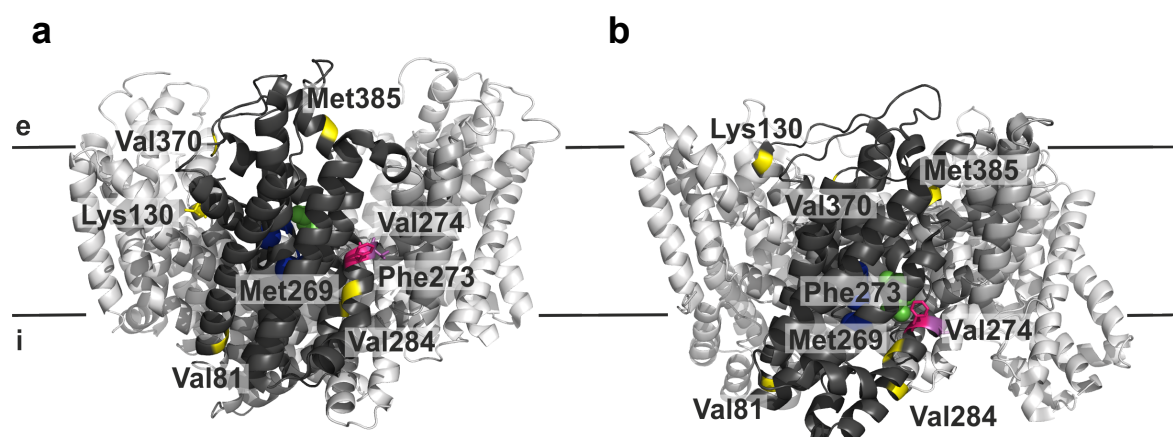


**Figure 2.1 Schematic representation of the residues selected for tryptophan fluorescence measurement.** **(a)** and **(b)** show a side view of the trimeric protein in the outward-facing (PDB code 2NWL)[69] **(a)** and inward-facing (PDB code 3KBC)[99] **(b)** crystal structures, respectively, with one protomer highlighted in dark grey. Glt$_{Ph}$ with tryptophan substitutions of residues Val81, Lys130, Met269, Val284, Val370, and Met385 marked yellow showed no fluorescence change (Val81, Val284) or changes only when both Na$^+$ and aspartate were added. Glt$_{Ph}$ with tryptophan substitutions of residues Phe273 (pink) and Val274 (magenta) reported both aspartate-independent Na$^+$ binding and Na$^+$-dependent aspartate binding. Bound aspartate is shown in green, and three putative Na$^+$ binding sites are labeled in blue[18]. Black lines represent the membrane with the extracellular (e) and intracellular (i) side indicated.

**Experimental Procedures**

*Mutagenesis, Expression, and Purification of Glt$_{Ph}$*

Mutations for single tryptophan variants were introduced in recombinant Glt$_{Ph}$ possessing a C-terminal eight-histidine tag using site-directed mutagenesis. DNA sequencing confirmed

Low Affintiy and Slow Na+ Binding Precedes High Affinity Asapartate Binding in the Secondary-active Transporter Glt$_{Ph}$

55
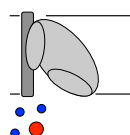
the presence of only the desired mutations. Glt$_{Ph}$ was produced in *Escherichia coli* MC1061 and purified as previously described[128] with slight modifications. Buffer A containing 50 mM Tris-HCl, pH 8.0, 300 mM KCl, and 0.04% (w/v) DDM (Anatrace) was used throughout the whole purification after solubilization including size exclusion chromatography on a Superdex 200 10/300 GL column (GE Healthcare). Protein concentrations were determined using the calculated extinction coefficients of the variants.

*Fluorescence Measurements*

Steady-state fluorescence of purified, detergent-solubilized protein was monitored at 25 °C on a Spex® Fluorolog® 322 fluorescence spectrophotometer (Jobin Yvon). Fluorescence spectra were recorded with an excitation wavelength of 295 nm. For titration experiments with increasing Na+ or aspartate concentrations, emission was measured at 343 nm with excitation at 295 nm. Aspartate and sodium were titrated to 1 μM protein in 1 mL of buffer A as described in Erkens and Slotboom[204]. The resulting curves were fitted in Origin 7.0 (OriginLab) to an equation describing equilibrium binding[204] or to the Hill equation. Stopped-flow measurements were performed on an Applied Photophysics SX20 spectrometer. An excitation wavelength of 295 nm and a cut-off filter of either 310 or 305 nm were used. All experiments were carried out in buffer A with 1.5–2 μM protein at temperatures as indicated. The protein was mixed with substrate containing buffer A in a 1:1 ratio. 3–15 traces per concentration were recorded and averaged per condition. All indicated concentrations are final after mixing. Pseudo-first-order reactions were assumed when the substrates (Na+, L-aspartate, D-aspartate, or L-cysteine sulfinic acid) were at least in 5-fold excess compared with the protein. The data were fitted to a single exponential model using Origin 7.0 (OriginLab). In the cases of very long measurements slightly poorer fits were obtained using the single exponential model and double exponential models were used (indicated in the figure legends). The presence of the additional component, which had a small amplitude, depended on the measuring time and became more apparent in the slower reactions that required longer time range measurements (> 5 s). We assume that bleaching accounts for this component. When double exponential models were used for one trace in a series, we chose to use it for all traces in the series (concentration-dependent L-aspartate, D-aspartate, and L-cysteine sulfinic acid binding data).
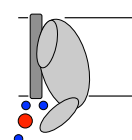
*Isothermal Titration Calorimetry (ITC)*

ITC experiments were performed using an iTC200 calorimeter (MicroCal). 100 μM aspartate (in buffer A with indicated sodium concentrations) was titrated into the thermally equilibrated ITC cell filled with 200 μL of mutant $Glt_{Ph}$ (13–20 μM) in the presence of 10 or 200 mM NaCl. Temperature was kept constant at 25 °C. Data were analyzed using the Origin-based software provided by MicroCal.

*Protein Reconstitution and Transport of [$^{14}$C]-Aspartate into Proteoliposomes*

Reconstitution and transport of [$^{14}$C]-aspartate were performed as previously described [11] with the following modifications: Tryptophan variants were reconstituted 1:250 (w/w) into a mixture of synthetic lipids (Avanti Polar Lipids, Inc.) of a 3:1:1 weight ratio of 1,2-dioleoyl-sn-glycero-3-phosphoethanolamine (DOPE):1,2-dioleoyl-sn-glycero-3-phosphocholine (DOPC):1,2-dioleoyl-sn-glycero-3-phospho- (1'-rac-glycerol) (DOPG). The transport of aspartate was initialized by diluting 2 μL of proteoliposomes (125 μg/μL lipid concentration) loaded with 50 mM potassium phosphate buffer, pH 7, into 200 μL of 50 mM sodium phosphate buffer, pH 7, containing 0.69 μM [$^{14}$C]-aspartate and 0.5 μM valinomycin.

**Results**

*Construction of Single Tryptophan Variants of $Glt_{Ph}$*

To detect the binding of aspartate and sodium ions to $Glt_{Ph}$, we constructed single tryptophan variants of the protein. We chose positions where the environment was expected to change upon binding of $Na^+$ and aspartate based on the available crystal structures. Residues Val81 (at the cytoplasmic end of helix 3), Met269, Phe273, Val274, Val284 (all HP1), Val370 (HP2), and Met385 (periplasmic end of helix 8) were mutated (figure 2.1).

We purified the single tryptophan variants in the *apo*-state (sodium- and aspartate-free), recorded fluorescence spectra in detergent solution, and tested whether the tryptophan fluorescence was sensitive to the addition of sodium ions and aspartate. The fluorescence properties of the variants fell into three groups as follows: V81W and V284W did not show any fluorescence changes upon substrate and coupling ion binding and were not analyzed

Low Affintiy and Slow Na⁺ Binding Precedes High Affinity Asapartate Binding in the Secondary-active Transporter Glt$_{Ph}$

57
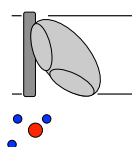
further (data not shown). The tryptophan fluorescence of M269W, V370W, and M385W did not change upon the addition of either sodium ions or aspartate alone, but it was affected when both Na⁺ and aspartate were present (data not shown). This behavior is very similar to L130W (periplasmic end of helix 4), which was shown previously to report binding of aspartate and sodium ions[69]. We chose L130W as representative for this group of mutants because it showed the most pronounced changes in fluorescence levels upon aspartate and sodium ion binding (figure 2.2 a and b). The fluorescence of F273W and V274W was affected by the binding of sodium ions alone to the *apo*-protein, as well as by subsequent binding of aspartate to the Na⁺-bound protein (figure 2.3 a). We chose F273W as representative for this group, because (i) it showed the most pronounced changes in fluorescence levels upon Na⁺ and aspartate binding, and (ii) it was fully active in transport (figure 2.3 e), in contrast to V274W.

*Steady-State Binding of Na⁺ to Glt$_{Ph}$*

For all binding experiments detergent-solubilized proteins were used, and consequently, binding could take place to the outward- or inward-facing states. Because the binding affinities of the two states for the substrates are identical[192], the lack of sidedness is not expected to affect the steady-state $K_d$ determinations. The tryptophan in F273W is located in HP1, close to the binding sites for aspartate and two Na⁺ ions. The addition of Na⁺ to the purified, detergent-solubilized *apo*-form of this variant resulted in an increase of the steady-state tryptophan fluorescence intensity, which allowed us to determine the affinity of Glt$_{Ph}$ for sodium ions in the absence of aspartate (figure 2.3 a). Na⁺ binding was cooperative and of low affinity ($K_d$ of 120 mM, Hill coefficient of 2.1 (figure 2.3 c). The Hill coefficient suggests that at least two sodium ions bind to the protein in a cooperative way in the absence of aspartate.

The apparent affinity for sodium was higher when aspartate was present. In the presence of 100 μM aspartate F273W bound Na⁺ with a $K_d$ of 25 mM and a Hill coefficient of 2.4 (figure 2.3 d). In the presence of aspartate the affinity for Na⁺ could also be determined in mutant L130W. The fluorescence of L130W increased when both Na⁺ and aspartate bound to the protein (figure 2.2 a and b). We found a $K_d$ value of 9 mM for Na⁺ binding to L130W in presence of 100 μM aspartate and a Hill coefficient of 2.2 (figure 2.2 e). These numbers compare well with previous data on the binding of sodium to variant L130W[69,205].
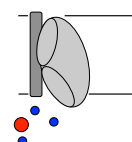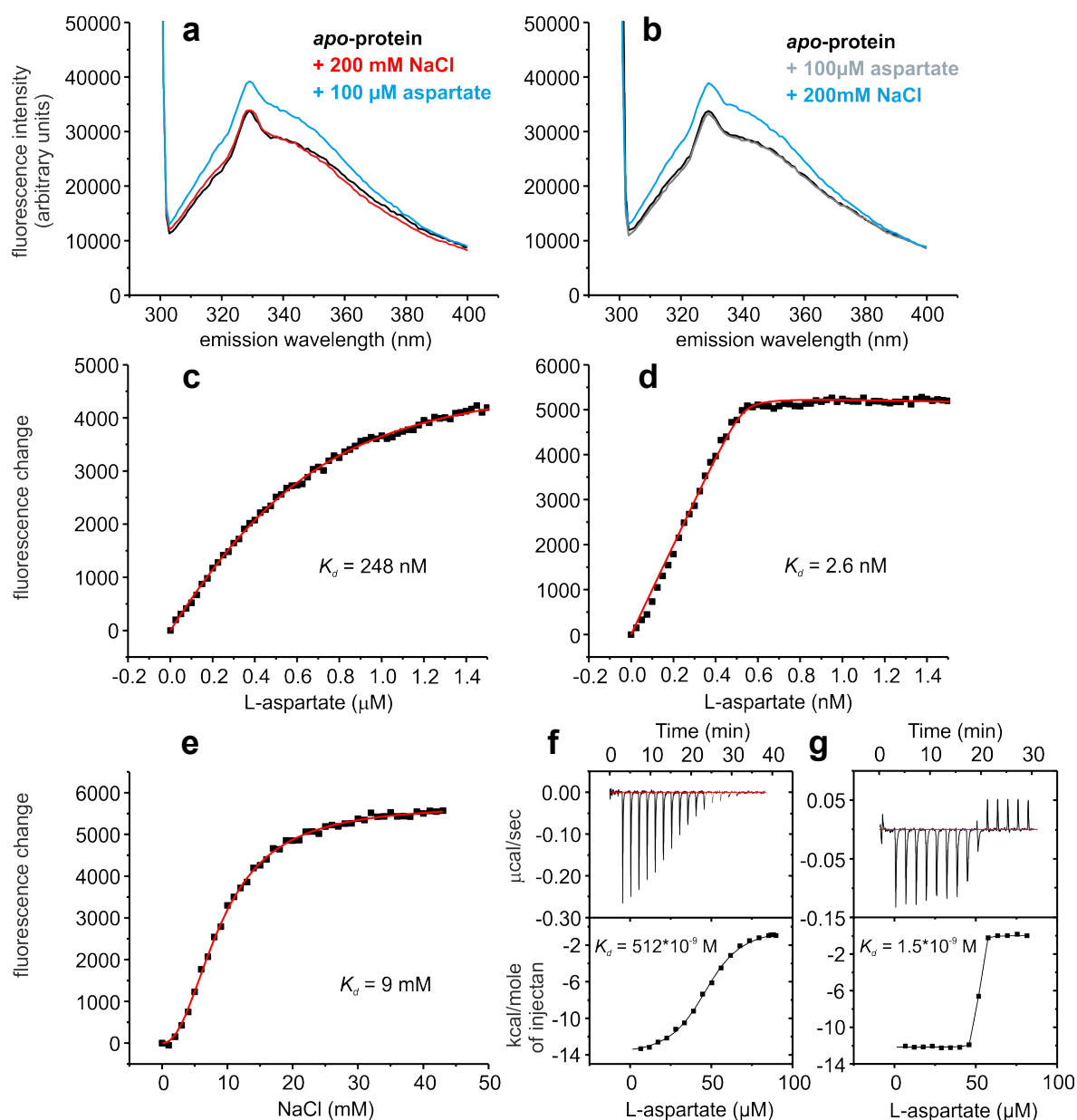
**Figure 2.2) Tryptophan fluorescence of Glt$_{Ph}$ variant L130W. (a)** Fluorescence emission spectra of the *apo*-protein (black) and after the addition of 200 mM NaCl (red), followed by the addition of 100 μM aspartate (blue). **(b)** Reverse order of additions: *apo*-protein (black), with 100 μM aspartate (gray), followed by the addition of 200 mM NaCl. A fluorescence increase was observed only when both substrates were present. In panels **(c)** and **(d)** titrations of aspartate in the presence of 10 mM and 200 mM NaCl, respectively, are shown, whereas in **(e)** the fluorescence changes by the addition of NaCl in the presence of 100 μM aspartate are plotted. The dots represent the average fluorescence levels corrected for dilution measured at the indicated aspartate and NaCl concentrations. The red line is the best fit to a one-site binding equation[204] or the Hill equation. In panels **(f)** and **(g)** ITC measurements of aspartate in presence of 10 mM **(f)** and 200 mM **(g)** NaCl are shown. The determined $K_d$ values were 512 nM and 2 nM, respectively.

Low Affintiy and Slow Na$^+$ Binding Precedes High Affinity Asapartate Binding in the Secondary-active Transporter Glt$_{Ph}$

59
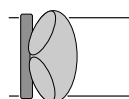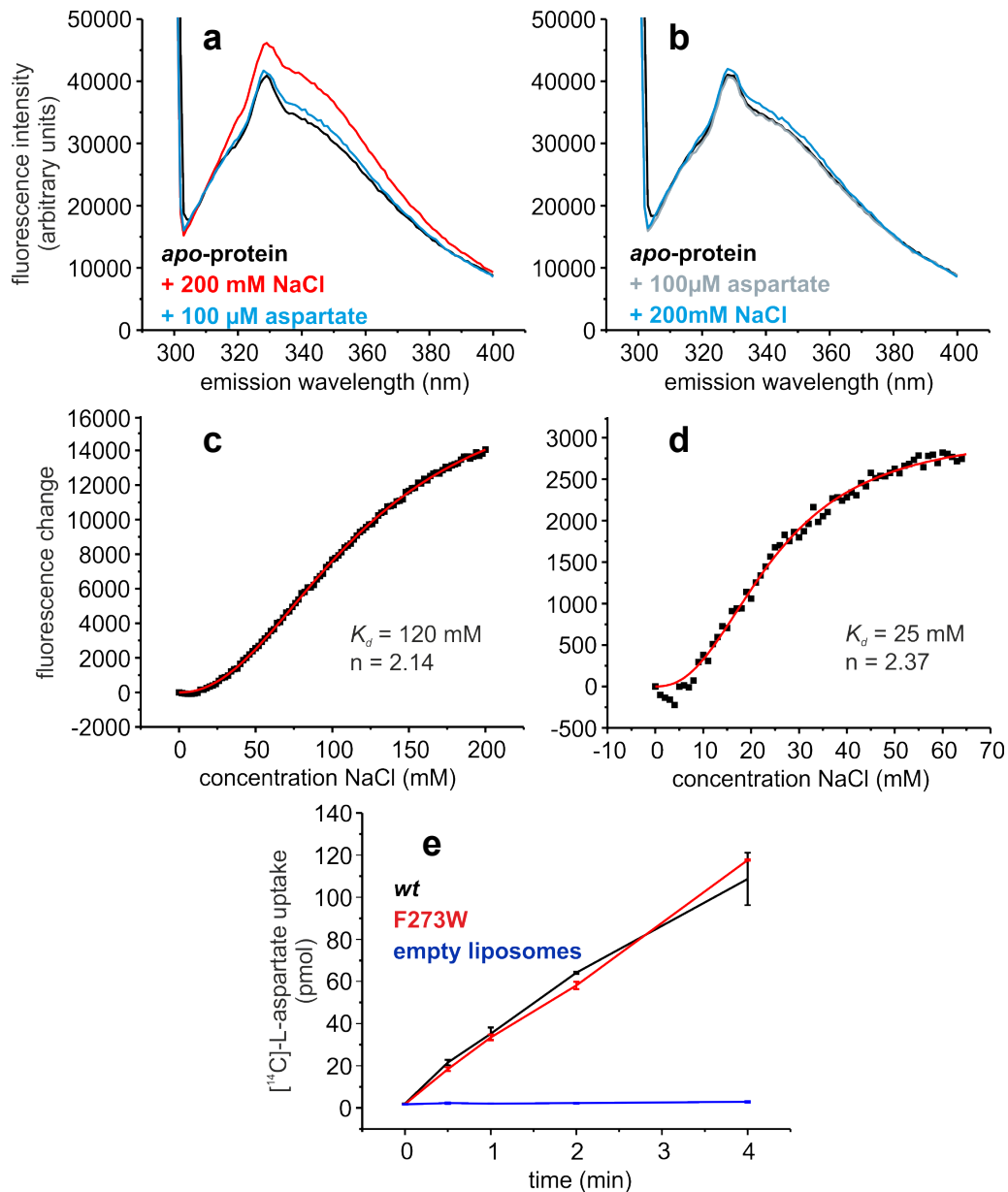
**Figure 2.3) Tryptophan fluorescence and transport activity of Glt$_{Ph}$ variant F273W.** (a) Fluorescence emission spectra of the *apo*-protein (black) after the addition of 200 mM NaCl (red) and after subsequent addition of 100 μM aspartate (blue). In panel (b) the order of additions was reversed: fluorescence emission spectra of the *apo*-protein (black) after the addition of 100 μM aspartate (gray) and after the subsequent addition of 200 mM NaCl (blue). In panels (c) and (d) the fluorescence changes as a function of Na$^+$ concentration are shown in the absence of aspartate and in the presence of 100 μM aspartate, respectively. The dots represent the average fluorescence levels corrected for dilution measured at the indicated NaCl concentrations. The red lines are best fits to the Hill equation. (e) [$^{14}$C]-L-aspartate uptake of Glt$_{Ph}$ variant F273W (red) and wild-type Glt$_{Ph}$ (*wt*, black) in proteoliposomes and in control liposomes without protein (blue).
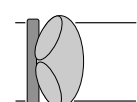
*Steady-State Binding of Aspartate to Glt$_{Ph}$*

Whereas the binding of Na$^+$ to Glt$_{Ph}$ F273W resulted in a concentration-dependent increase in the fluorescence intensity, the subsequent binding of aspartate caused a decrease in intensity. The level of fluorescence with both substrates bound was slightly higher than that of the *apo*-protein (figure 2.3 a). The change in fluorescence upon the addition of aspartate to Glt$_{Ph}$ preincubated with sodium depended strongly on the concentration of sodium used. In the presence of 200 mM Na$^+$, the addition of aspartate to F273W caused a relatively large decrease in fluorescence intensity. However, in the presence of lower concentrations of sodium (50 and 100 mM NaCl, which is below the $K_d$ for sodium) the decrease was less pronounced. At these Na$^+$ concentrations the protein is not fully occupied with Na$^+$, and therefore, the reference level of fluorescence before the addition of aspartate is lower than in the presence of saturating sodium concentrations. Because the final level of fluorescence after the addition of aspartate was the same regardless of the sodium concentration, the decrease in fluorescence by aspartate binding was less pronounced at lower sodium concentrations (figure 2.4). At very low sodium concentrations (10 and 20 mM NaCl, respectively) the initial occupancy by sodium ions was so low that there was an increase rather than a decrease of fluorescence intensity upon the addition of aspartate. Nonetheless, in all cases the same end level of fluorescence was reached, indicating that aspartate pulls the carrier to the fully occupied state, and sodium and aspartate binding is mutually cooperative.

When we added the substrates in the reverse order, the addition of aspartate did not cause a change in fluorescence, suggesting that aspartate does not bind to Glt$_{Ph}$ in the absence of Na$^+$, whereas subsequent addition of Na$^+$ caused a slight increase (figure 2.3 b). Regardless of the order of additions, the same end level of fluorescence intensity was reached (*cf.* figure 2.3 a and b).
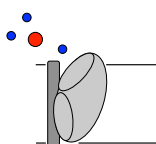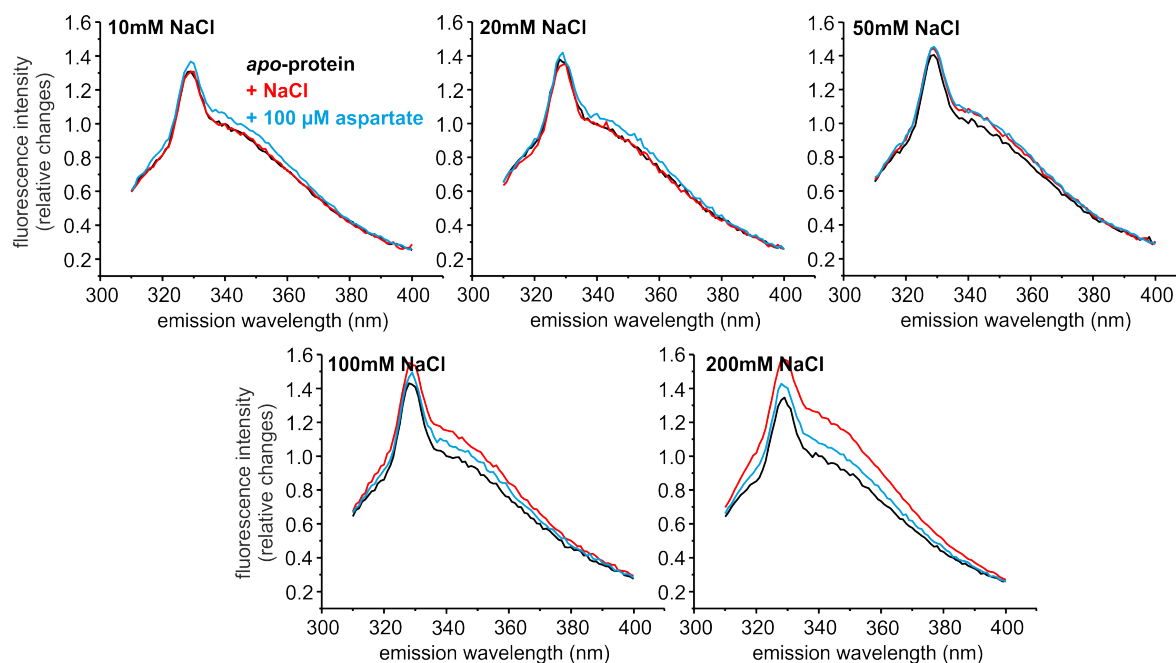
**Figure 2.4) Tryptophan fluorescence spectra of Glt_Ph variant F273W in the presence of different NaCl concentrations.** Fluorescence spectra of the *apo*-protein (black) after the addition of NaCl (red; concentrations as indicated) and after subsequent addition of 100 μM aspartate (blue). For better comparison the spectra were normalized taking the fluorescence of the *apo*-protein as 1.

Because the changes in fluorescence intensity upon aspartate binding to F273W depended strongly on the sodium concentration and were very small in the presence of low sodium concentrations, we could not use the changes in fluorescence intensity to determine binding affinities for aspartate. Instead we used ITC measurements. The apparent affinity for aspartate depended on the NaCl concentration; with 10 mM NaCl present the $K_d$ was 4 μM (figure 2.5 a), whereas the affinity increased 3 orders of magnitude with 200 mM NaCl added ($K_d$ of 2.7 nM; figure 2.5 b). Taking into account that $K_d$ values in the low nanomolar range obtained from ITC or fluorescence measurements are difficult to determine accurately, these numbers compare well with previous data on L130W[99]. Using ITC measurements for L130W, we found a $K_d$ of 512 nM for aspartate with 10 mM NaCl present (figure 2.2 f) and a $K_d$ of 1.5 nM with 200 mM NaCl present (figure 2.2 g). Similar $K_d$ values of 248 and 2.6 nM in the presence of 10 mM and 200 mM NaCl, respectively, were obtained from steady-state fluorescence measurements on L130W (figure 2.2 c and d).
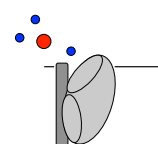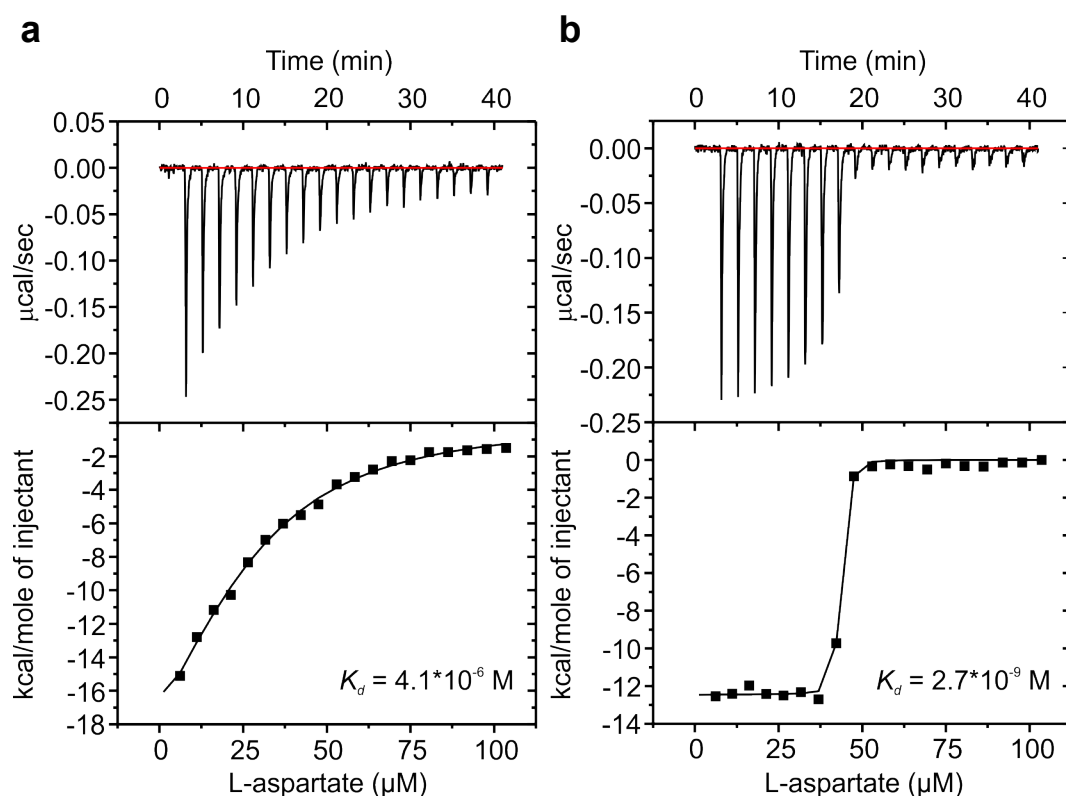
**Figure 2.5) ITC measurements of Glt$_{Ph}$ variant F273W.** Aspartate titration in the presence of 10 mM **(a)** and 200 mM **(b)** NaCl. Determined $K_d$ values for aspartate binding were 4 μM and 3 nM, respectively.

*Rates of Na$^+$ and Aspartate Binding to Glt$_{Ph}$ F273W*

We performed tryptophan fluorescence-based stopped-flow measurements on Glt$_{Ph}$ F273W in detergent solution to record the substrate-induced fluorescence changes over time. Although in detergent solution there is no sidedness and binding could in principle take place to both the outward- or inward-facing states, the data fitted well to a single exponential model. Therefore, it is likely that we observed a single type of event.

Fast mixing experiments on the binding of Na$^+$ to the F273W variant revealed a very low $k_{on}$ value for Na$^+$ of 5.1 M$^{-1}$ s$^{-1}$ (figure 2.6 a, table 2.1). The kinetics data are consistent with the low affinity of Glt$_{Ph}$ for Na$^+$ in the absence of aspartate measured in the steady-state experiments (*cf*. figure 2.3 a and 2.6 a). In the experiments the ionic strength was kept constant at 1 M by the addition of the appropriate concentrations of KCl to compensate for the different NaCl concentrations used. It must be noted though that the rate constants were identical in the absence of compensating KCl additions showing that differences in ionic strength had no detectable effect (data not shown). Rate constants were also determined at different temperatures between 6 °C and 30 °C. From these data values for the activation

Low Affintiy and Slow Na$^+$ Binding Precedes High Affinity Asapartate Binding in the Secondary-active Transporter Glt$_{Ph}$

63
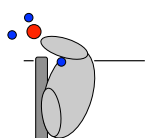
energy, $E_a$ and $Q_{10}$ of 106.8 kJmol$^{-1}$ and 4.5, respectively, were derived (figure 2.6 b). These values suggest a relatively big conformational change either before or after binding of Na$^+$. Nonetheless, the stopped-flow measurements with increasing Na$^+$ concentrations (figure 2.6 a) did not result in a saturation of the $k_{obs}$ values. A possible explanation for the lack of saturation is that the concentrations of Na$^+$ required to reach saturation are too high to be compatible with the experimental setup.

**Table 2.1) Rates of substrate and Na$^+$ binding to variant F273W as derived from stopped-flow quantities.**

| Substrate | $k_{on}$ M$^{-1}$s$^{-1}$ | $k_{off}$ s$^{-1}$ | $K_d^a$ M |
|---|---|---|---|
| Na$^{+b}$ | 5.1 ($\pm$ 0.237) | 3.9 ($\pm$ 0.134) | 0.76 |
| L-Aspartate$^c$ | $1.4*10^5$ ($\pm 4.7*10^3$) | 0.25 ($\pm$ 3.3) | $1.8*10^{-5}$ |
| D-Aspartate$^c$ | $6.8*10^4$ ($\pm 4.1\pm*10^3$) | 2.2 ($\pm$ 1.6) | $3.2*10^{-5}$ |
| L-CS$^c$ | $9.5*10^4$ ($\pm3.9*10^3$) | 2.9 ($\pm$ 1.6) | $3.1*10^{-5}$ |

$^a$ Derived from $k_{off}/k_{on}$.

$^b$ Measurements were performed at room temperature.

$^c$ Measurements were performed at 6 °C.

L-CS: L-cysteine sulfinic acid

*Rates of Na$^+$ Binding to Glt$_{Ph}$ F273W in the Presence of Aspartate*

Na$^+$ binding was also monitored in the presence of three different aspartate concentrations of 1 μM, 10 μM, and 100 μM. At some aspartate-to-Na$^+$ ratios (combinations of high Na$^+$ and low aspartate concentrations) two phases became apparent (figure 2.7): a fast increase in tryptophan fluorescence followed by a slower decrease. The two observed rate constants $k_{obs}$ were in good agreement with the corresponding rates of Na$^+$ binding to *apo*-Glt$_{Ph}$ and aspartate binding to the Na$^+$-loaded protein, indicating that the observed phases describe the binding of Na$^+$ (fast at high Na$^+$ concentration) before the binding of aspartate (slow at low aspartate concentration). At low sodium ion concentrations a single phase only was observed, corresponding to slow and rate-determining sodium binding. The subsequent aspartate binding was much faster in this condition.
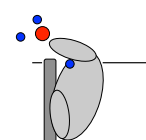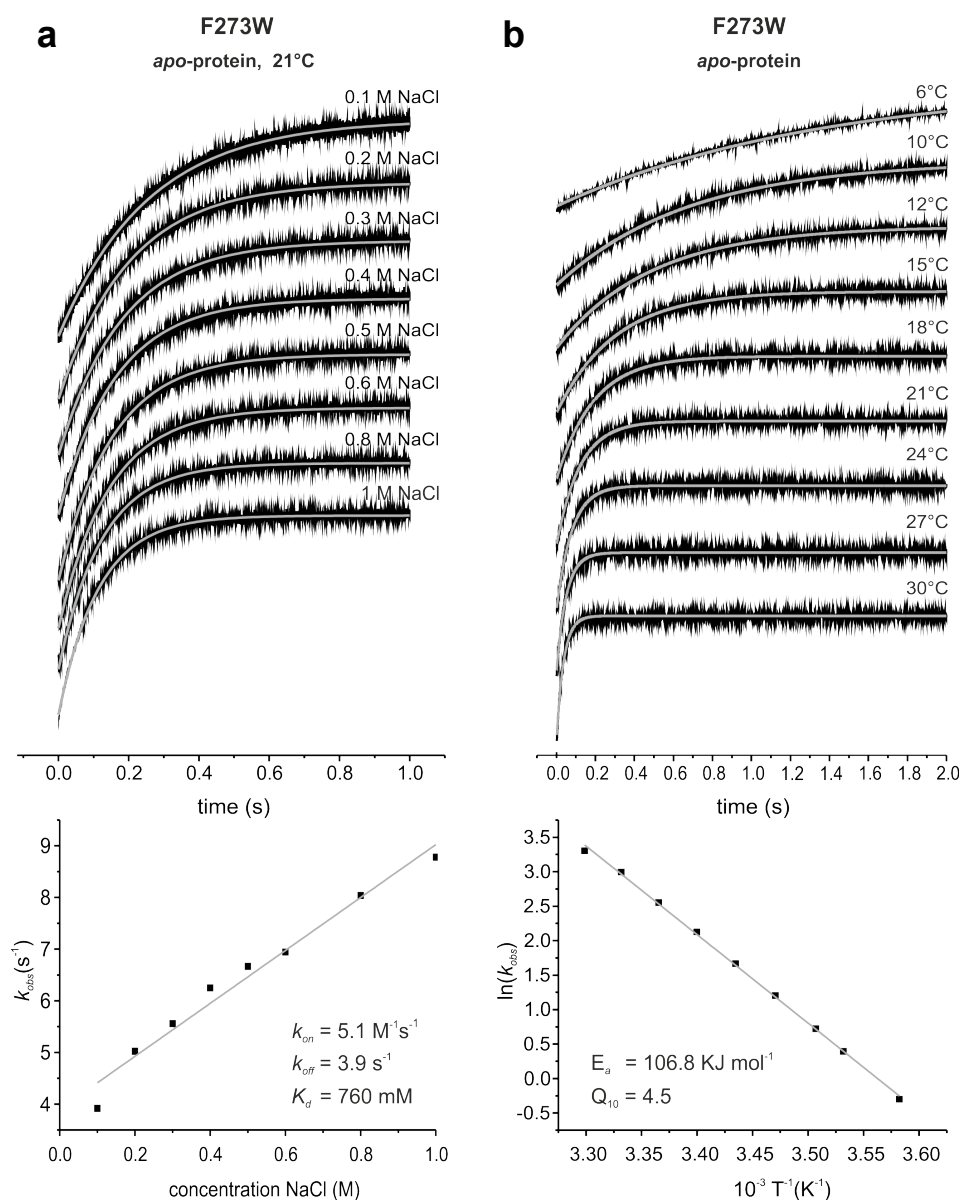
**Figure 2.6) Rates of Na+ binding to Glt_Ph F273W.** The top panels show the stopped-flow fluorescence measurements. Each trace (black) represents an average of 6-15 individual traces, fitted with a single exponential equation (gray). **(a)** 1.5 μM Glt_Ph F273W *apo*-protein was mixed with solutions of the indicated concentrations of NaCl; KCl was present so that the sum of the NaCl and KCl concentration was 1 M. All measurements were performed at room temperature. The bottom panel shows the $k_{obs}$ values plotted against the corresponding NaCl concentrations. The slope of the linear fit gives the $k_{on}$, and the intercept with the $k_{obs}$ axis gives the $k_{off}$ value. **(b)** 1.5 μM Glt_Ph F273W *apo*-protein was mixed with 1 M NaCl at different temperatures as indicated, and the bottom panel shows the Arrhenius plot of the derived $k_{obs}$. The gray line is a linear fit of the data according the Arrhenius equation $\ln(k) = B + (\ln(E_a)/RT)$, with $E_a$ representing the activation energy, $B$ representing the frequency factor, T representing the absolute temperature in Kelvin, and R representing the gas constant. The linear fit results in an $E_a = 106.8$ KJ mol$^{-1}$.

Low Affintiy and Slow Na⁺ Binding Precedes High Affinity Asapartate Binding in the Secondary-active Transporter Glt$_{Ph}$

65
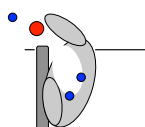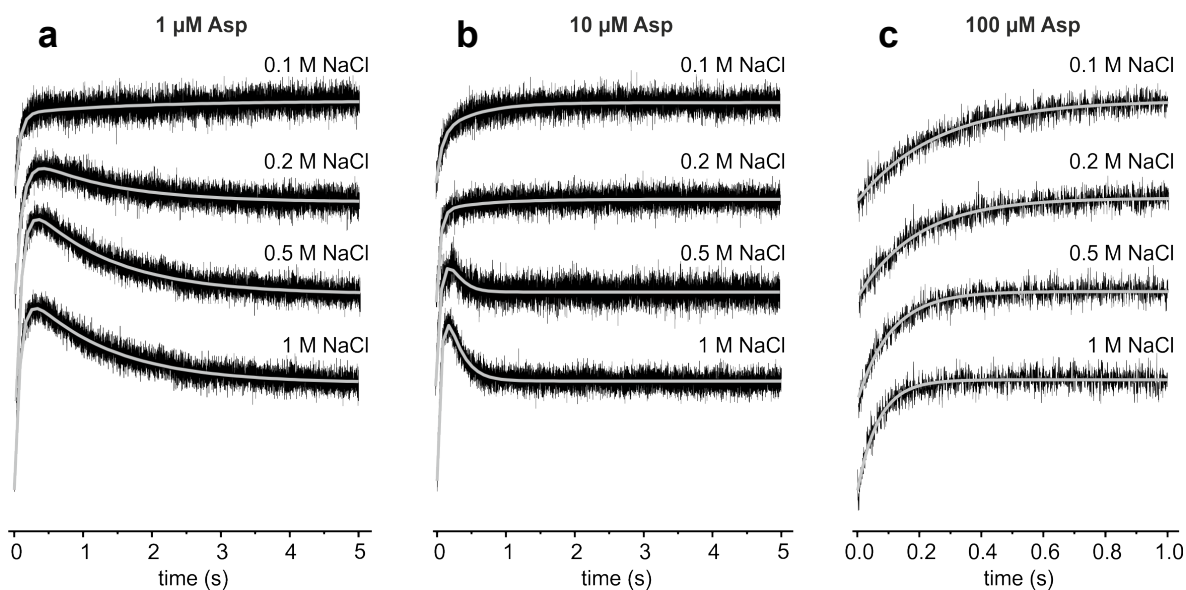


**Figure 2.7) Sodium binding to Glt$_{Ph}$ variant F273W in the presence of different aspartate concentrations.** Stopped-flow traces of the tryptophan fluorescence started by mixing 2 μM protein with different NaCl concentrations in presence of 1 μM **(a)**, 10 μM **(b)**, and 100 μM **(c)** aspartate, respectively. Each trace (black) represents an average of 10–15 individual traces, fitted with a double exponential equation (gray).

*Rates of Aspartate Binding to Na⁺-loaded Glt$_{Ph}$ F273W*

The binding of L-aspartate to F273W at room temperature was too fast for accurate determination of the rate constants at high aspartate concentrations. Therefore, binding rates for L-aspartate using Glt$_{Ph}$ pre-incubated with 1 M Na⁺ were determined at 6 °C and yielded $k_{on}$ and $k_{off}$ values of $1.4*10^5$ M⁻¹s⁻¹ and 0.25 s⁻¹, respectively (figure 2.8 a). The activation energy for binding of L-aspartate to Glt$_{Ph}$ F273W was 42.6 kJ mol⁻¹ with a correlating $Q_{10}$ value of 1.8 (figure 2.8 b). The substantial activation energy and the small $k_{on}$ value, which is well below rate constant for diffusion limited binding, indicate that F273W reports a conformational change rather than the initial aspartate binding event. This observation is consistent with aspartate binding data for L130W, indicating an induced-fit mechanism[205]. However, there are also differences between L130W and F273W. For F273W we did not observe saturation of $k_{obs}$ at high L-aspartate concentrations in contrast to previous data for L130W[205]. Similarly, we did not observe saturation of $k_{obs}$ at high concentrations of the alternative substrates D-aspartate and L-cysteine sulfinic acid, again in contrast with the reported work on L130W (figures 2.8 a, 2.9 a and b, respectively).
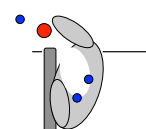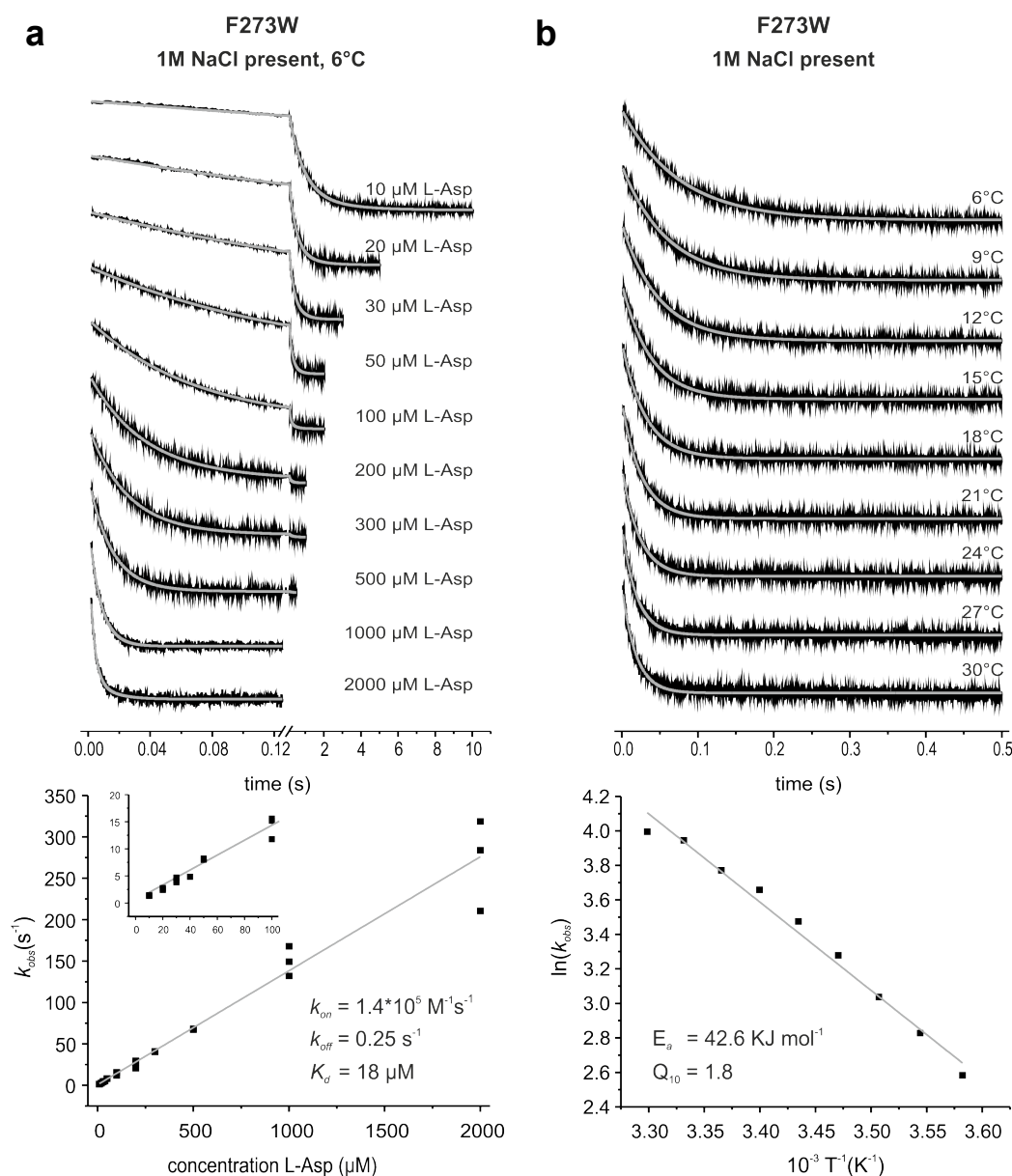
**Figure 2.8) Rates of L-aspartate binding to Glt$_{Ph}$ F273W in the presence of 1 M NaCl.** The top panels show the stopped-flow fluorescence measurements. Each trace (black) represents an average of 6–10 individual traces. **(a)** 1.5 μM F273W was mixed with varying L-asparte concentrations as indicated, and individual traces were fitted with a double exponential equation (gray). In the bottom panel the $k_{obs}$ values resulting from the fits with assumed pseudo-first-order reaction are plotted against the corresponding aspartate concentrations. The slope of the linear fit gives the $k_{on}$, and the intercept with the $k_{obs}$ axis gives the $k_{off}$ value. The inset shows the data at low aspartate concentrations. **(b)** 1.5 μM F273W was mixed with 100 μM L-aspartate at different temperatures as indicated, and individual traces were fitted with a single exponential equation. The bottom panel shows the Arrhenius plot of the derived $k_{obs}$. The gray line demonstrates the linear fit of the data according to the Arrhenius equation $\ln(k) = B + (\ln(E_a)/RT)$, with $E_a$ representing the activation energy, $B$ representing the frequency factor, T representing the absolute temperature in Kelvin, and R representing the gas constant. The linear fit results in an $E_a$ = 42.6 kJ mol$^{-1}$.

Low Affintiy and Slow Na⁺ Binding Precedes High Affinity Asapartate Binding in the Secondary-
active Transporter Glt$_{Ph}$

67
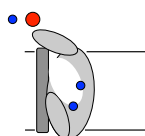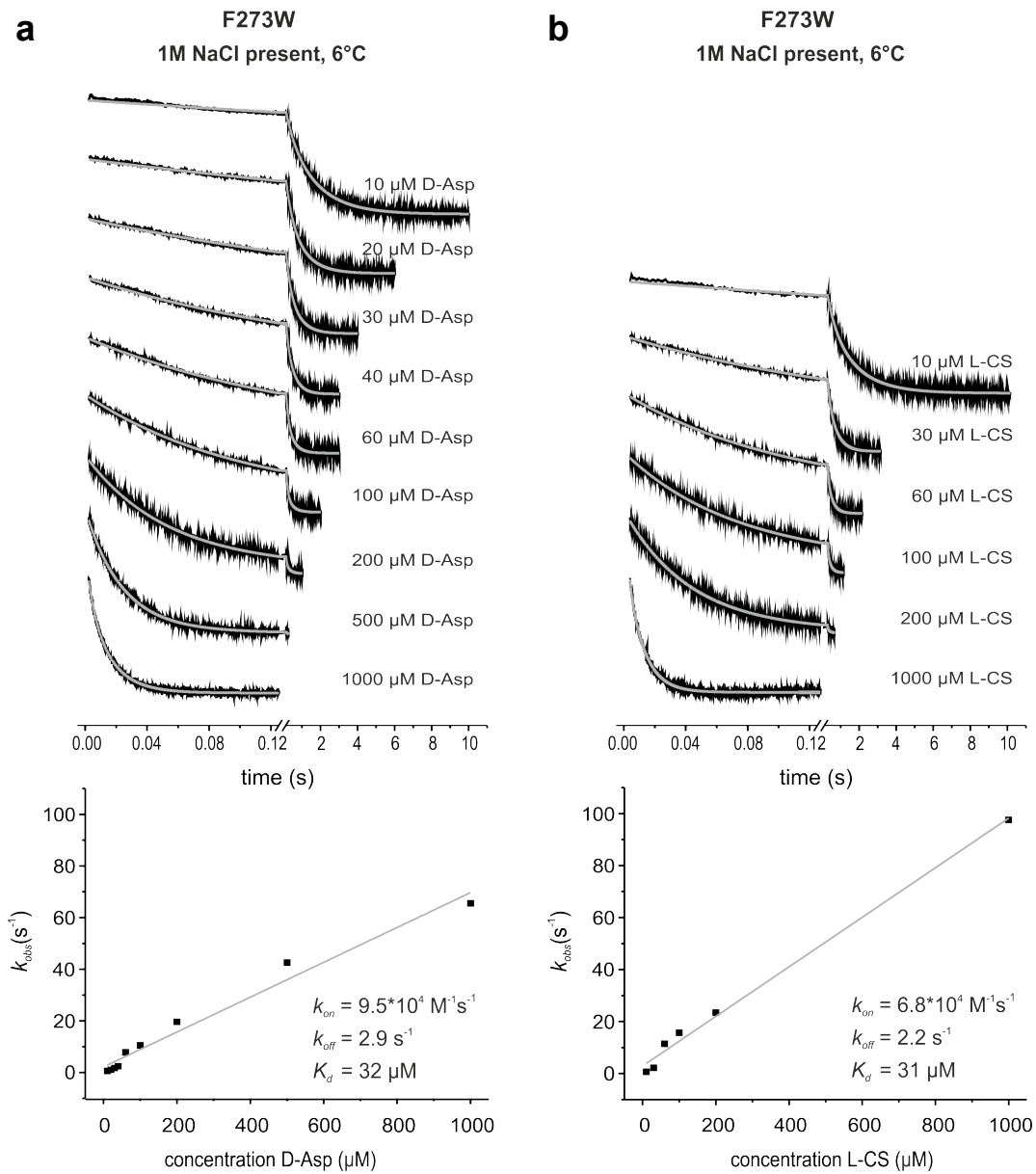
**Figure 2.9) Rates of D-aspartate and L-cysteine sulfinic acid binding to Glt$_{Ph}$ F273W in the presence of 1 M NaCl.** The top panels show the stopped-flow fluorescence measurements. Each trace (black) represents an average of 3–8 individual traces, fitted with a double exponential equation (gray). In the bottom panels the $k_{obs}$ values resulting from the fits with assumed pseudo-first-order reaction are plotted against the corresponding substrate concentrations. All measurements were performed at 6 °C. The slopes of the linear fits give the $k_{on}$, and the intercepts with the $k_{obs}$ axis give the $k_{off}$ values. **(a)** 1.5 μM F273W was mixed with varying D-aspartate (D-Asp) concentrations as indicated. **(b)** 1.5 μM F273W was mixed with varying L-cysteine sulfinic acid (L-CS) concentrations as indicated.

It is not clear why saturation was not observed for F273W, but it is possible that higher L-aspartate concentrations were required to reach saturation. However, at higher concentrations the rates were too high to measure accurately using our experimental setup.
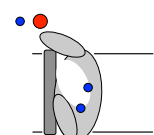
In addition, variant L130W showed greatly reduced transport activity, in contrast to F273W (*cf*. ref. 69 and figure 2.3 e), and therefore, L130W may have a more limited conformational flexibility than F273W, which becomes rate limiting at lower substrate concentrations.

**Discussion**

The change in tryptophan fluorescence upon Na$^+$ binding to Glt$_{ph}$ F273W and the kinetics of binding as well as the temperature dependence indicate that a substantial conformational change is associated with the binding of sodium ions to the *apo*-protein. The change in fluorescence may arise either from local conformational changes before or upon the initial binding to the exposed binding site or by the subsequent redistribution of conformational states of the whole transport domain. Distinct local conformational changes forming the binding pocket for aspartate were proposed by molecular dynamic simulations[146,148] and binding studies on Glt$_{Ph}$[192,205]. Comparison of the recent crystal structures of *apo*-Glt$_{Ph}$[142] and the closely related protein *apo*-Glt$_{Tk}$[71] with the Na$^+$ and aspartate-bound proteins[69,99] are also consistent with a large local conformational change associated with sodium binding. Because the tryptophan residue in F273W is located in close proximity to the Na$^+$ binding sites, this possibility is plausible. But also a Na$^+$-induced overall movement of the transport domain as shown by EPR and single-molecule FRET studies[85,86,96,206] would be consistent with the present fluorescence data.

Similarly, the fluorescence decrease upon binding of aspartate to the Na$^+$-loaded carrier is likely related to a conformational change. A previous EPR study showed that binding of aspartate to the Na$^+$-saturated carrier caused a minor change in the occupancy of the conformational states of the transporting domain compared with the Na$^+$-induced changes[96], whereas the molecular dynamic simulation again suggested a local rearrangement enabling the binding of the third sodium ion[146]. The fluorescence measurements revealed that binding of Na$^+$ takes place before aspartate binding. This is consistent with previous data[136,142,144,146,148,149,152,150,192,207]. However, our measurements allow no speculations about the binding of the third sodium ion.

*Apo*-Glt$_{Ph}$ has a very low affinity for sodium ions ($K_d$ = 120 mM). This value compares well with experiments in which a voltage-sensitive dye was used to measure Na$^+$ binding to

Low Affintiy and Slow Na$^+$ Binding Precedes High Affinity Asapartate Binding in the Secondary-active Transporter Glt$_{Ph}$

69
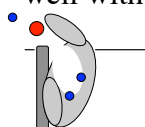
wild-type Glt$_{Ph}$ ($K_d$ = 99 mM)[192] but differs to a larger extent from the $K_d$ for Na$^+$ determined by tyrosine fluorescence changes upon sodium binding to wild-type Glt$_{Ph}$ (25 mM)[205]. The basis for these differences is not known. Nonetheless, in any case the $K_d$ is in the physiologically relevant range, considering that the natural environment of *P. horikoshii* is seawater containing about 0.5 M NaCl. The $k_{on}$ value for sodium binding was only ~5 M$^{-1}$s$^{-1}$, but at physiological Na$^+$ concentrations relatively fast binding of the coupling ions is ensured ($k_{obs}$ values ~7 s$^{-1}$). In addition, this rate is in good agreement with rates previously determined for the human EAAT5[188], in which case sodium binding preceded fast glutamate binding. The data are also consistent with several studies on glutamate transporters showing that slow binding of two Na$^+$ is followed by fast binding of substrate and subsequently the third coupling ion[177,194].

The change in fluorescence upon binding of aspartate to the Na$^+$-loaded carrier L130W has been shown to report an induced fit event. The low rate constants of fluorescence changes upon aspartate binding to variant F273W ($k_{on}$ of 1.4*10$^5$ M$^{-1}$s$^{-1}$) are consistent with an induced fit mechanism. We hypothesize that the fluorescence of F273W reports a conformational change induced by substrate binding rather than the initial binding event. The conformational change reported by F273W is significantly slower than the initial substrate binding ($k_{on}$), which is manifested by the difference between the $K_d$ values calculated from the rate constants by stopped-flow fluorescence measurements and thermodynamics using ITC measurements (18 μM versus 2.7 nM, respectively). The conformation change could for example be associated with an opening of the inward-facing lid HP1[100,105] or a reorientation of the whole transport domain after binding of both Na$^+$ and aspartate[85]. However, for the F273W mutant the $k_{obs}$ values of aspartate binding did not saturate at high aspartate concentration, in contrast to L130W[205]. Because L130W is much less active in transport than the wild-type or F273W[69], it is possible that the kinetics of the reported conformational changes are different and may become rate-limiting only in L130W at high aspartate concentrations.

In summary, this study provides new insights into the molecular mechanism of substrate binding in the archaeal aspartate transporter Glt$_{Ph}$. Na$^+$ binding is slow and involves conformational rearrangements that are essential for subsequent high affinity aspartate binding, which ensures the coupled uptake of cations and substrate as necessary for the transporter. Na$^+$ binding is likely the rate-limiting step for substrate binding.
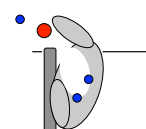
## Acknowledgments
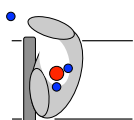
# Chapter 3

Substrate Binding to the Archaeal Glutamate Transporter Homolog $Glt_{Tk}$ from *Thermococcus kodakarensis*

**Sonja Jensen, Stephan Rempel, Nynke van der Veer, Łukasz R. Winkler, and Dirk Jan Slotboom**
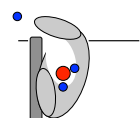
**Abstract**

Glutamate transporters are trimeric membrane proteins that couple the uptake of aspartate and glutamate to the symport of cations. In mammals glutamate transporters remove the neurotransmitter glutamate after signal transmission and prevent excitotoxicity. Up to date structural information is only available for two prokaryotic glutamate transporter homologs, $Glt_{Ph}$ and $Glt_{Tk}$. The structures of $Glt_{Tk}$ are of high resolution and data quality, but the protein is not well-characterized biochemically. Here we studied the substrate and cation binding properties of $Glt_{Tk}$. Our results show that $Glt_{Tk}$ binds aspartate as the preferred substrate and couples the high affinity binding of aspartate to the binding of 3 sodium ions. In contrast to the related transporter $Glt_{Ph}$, $Glt_{Tk}$ also accepts the neutral amino acid L-asparagine as substrate, albeit with lower affinity. In addition to the slightly different substrate spectrum than $Glt_{Ph}$, $Glt_{Tk}$ is also a faster transporter with an apparent aspartate turnover number of 4-5 $s^{-1}$ compared to 0.0048 $s^{-1}$ for $Glt_{Ph}$.
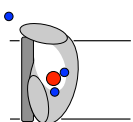
## Introduction

Glutamate transporters and their homologs are secondary active transporters that co-translocate negatively charged amino acids together with sodium ions and/or protons. These homotrimeric transporters can be found in eukaryotes as well as in bacteria and archaea[15,68,73,74].

The mammalian glutamate transporters, called excitatory amino acid transporters (EAATs), clear the synaptic cleft of the neurotransmitter glutamate after signal transduction. In this way they enable sensitive signal transmission and prevent excitotoxicity[45]. There are five sub-classes of mammalian glutamate transporters: EAAT 1-5. All of them couple glutamate uptake to the symport of three sodium ions and one proton[65]. After the substrate delivery mammalian glutamate transporters require the counter-transport of one K$^+$ in order to return to the starting position and to complete the transport cycle[124, 123]. Homologs of the mammalian EAATs can be found in bacteria and archaea, where they facilitate the uptake of glutamate and aspartate as nutrients[14]. Many bacterial glutamate transporters such as GltT from *Bacillus stereothermophilus*, GltP from *Escherichia coli*, and Glt$_{Bsu}$ from *Bacillus subtilis* are proton dependent glutamate transporters[110,112,113]. In contrast the archaeal glutamate transporter homolog from *Pyrococcus horikoshii* (Glt$_{Ph}$) couples the transport of aspartate to the symport of Na$^+$ [15,69]. The prokaryotic transporters do not require the counter-transport of K$^+$ to reorient after substrate transmission.

The best-studied member of the glutamate transporter family is the archaeal aspartate transporter from Glt$_{Ph}$. This transporter couples the uptake of aspartate to the translocation of Na$^+$ in a stoichiometry of 1:3[128]. Much information of the transport mechanism of glutamate transporters comes from a series of crystal structures of Glt$_{Ph}$ in various states of the transport cycle. The first crystal structure of this transporter was in an outward-oriented conformation with the substrate binding site occluded[15]. Later, structures of the open outward-oriented state, inward-oriented occluded, and intermediate occluded state followed[69,99,142,189,192]. The structures revealed that Glt$_{Ph}$ is a homotrimer with each protomer consisting of two domains: a trimerization domain that mediates inter-subunit interactions, and a transport domain that contains the substrate binding site[15] with two hairpin regions, HP1 and HP2, that are believed to form the interior and exterior gate, respectively[15,81,99,100,105].
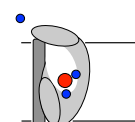
The crystal structures suggested that the trimerization domain forms a rigid framework. This finding was consistent with experiments showing that cysteine cross-linking of the trimerization domains of GltT to each other in the homotrimer did not affect the binding and transport properties of the transporter[95]. Unlike the trimerization domain the translocation domain undergoes great movement as it elevates across the membrane during substrate translocation[90,96,99,142,189]. Although glutamate transporters exist as trimers, each of the protomers functions independently[76,77,85–88,95,].

Published in 2013, the structure of a substrate-free glutamate transporter homolog from *Thermoccoccus kodakarensis* ($Glt_{Tk}$)[71] showed high similarity to $Glt_{Ph}$. Together with a recent EPR study[96] on $Glt_{Ph}$ this structure suggested that the empty transporter crosses the membrane the same way in order to reorient as it does when it shuttles its substrates from the outside to the inside (chapter 4).

Even though glutamate transporters have been studied extensively, the transport mechanism is still not fully understood. Structural information so far is only available from the two glutamate transporter homologs $Glt_{Ph}$ and $Glt_{Tk}$. In order to be able to conclusively compare them to one another and to correlate $Glt_{Tk}$ to other members of the glutamate transporter family, a biochemical characterization of $Glt_{Tk}$ is required. This will also help to deduce common features for the whole glutamate transporter family.

Here we characterize the substrate binding properties of $Glt_{Tk}$. Using isothermal titration calorimetry (ITC) we determined the binding affinities for various amino acid substrates in the presence of sodium and determined the binding stoichiometry of aspartate and sodium.

ITC measurements and preliminary uptake assays with radiolabeled substrates revealed that, similar to $Glt_{Ph}$, $Glt_{Tk}$ is a high affinity aspartate transporter with a binding stoichiometry of sodium to aspartate of 3:1. The binding affinities of $Glt_{Tk}$ for sodium and substrate are lower compared to $Glt_{Ph}$, and the turnover rates of substrates by $Glt_{Tk}$ are much higher.
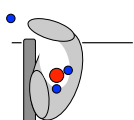
## Materials and Methods

*Chemicals*

Restriction enzymes and Pfu polymerase were purchased from New England Biolabs (NEB) and Agilent Technologies respectively. [$^{14}$C]-L-aspartate (1.85 MBq, 7.4 GBq/mmol), [$^{3}$H]-L-aspartate (35 MBq, 0.477 TBq/mmol) and [$^{3}$H]-D-aspartate (37 MBq, 0.488 TBq/mmol) were purchased from PerkinElmer. Lipids were purchased from Avanti polar lipids. L-arabinose, L-aspartate, D-aspartate, L-cysteine sulfinic acid, L-asparagine, D-asparagine, L-glutamate and ampicillin sodium salt were bought from Sigma-Aldrich. All chemicals were analytical grade pure.

*DNA manipulation, protein production, purification and concentration determination*

Double cysteine mutations were introduced into C-terminal His8-tagged Glt$_{Tk}$[1] using QuickChange. *E. coli* MC1061 cells containing pBAD24 plasmid carrying wild type (*wt*) Glt$_{Tk}$ and mutant Glt$_{Tk}$ were cultivated in LB medium supplemented with 100 μg/mL ampicillin at 37 °C and 200 rpm. Protein production was induced at OD$_{600}$ of 0.8-1 with 0.05 % L-arabinose for 3 h. Cell harvesting, membrane vesicle preparation and protein purification were performed as previously described by Jensen et al.[71]. The protein concentration of purified mutant and *wt*-Glt$_{Tk}$ was determined by NanoDrop, using molecular weight and extinction factor calculated by the Expasy Protparam tool (web.expasy.org/protparam/). The concentration of Hg$^{2+}$ cross-linked protein was determined by BCA assay (ThermoFisher Scientific) according to the producer's manual.

*Cross-linking of Glt$_{Tk}$*

To cross-link Glt$_{Tk}$ in the inward-facing conformation purified Glt$_{Tk}$ was incubated with 2 mM of various Cross-linkers. The best cross-linking conditions were: Cu$^{2+}$ and CuPh for 2 h at 30 °C or 2 mM HgCl$_2$ for 1 h at 30 °C. After cross-linking Glt$_{Tk}$ was subjected to buffer exchange in order to remove excess cross-linker, using a NAP10 column (GE Healthcare Life Sciences) according to the manufacturer's instructions.

*Isothermal titration calorimetry (ITC)*

ITC experiments were performed at a constant temperature of 25 °C using an iTC200 calorimeter (MicroCal). Varying concentrations of the indicated substrates (in 10 mM
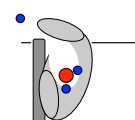
Hepes KOH pH 8, 100 mM KCl, 0.15 % DM and indicated sodium concentrations) were titrated into a thermally equilibrated ITC cell filled with 250 μL of 3-20 μM $Glt_{Tk}$ supplemented with 0 to 750 mM NaCl, 500 mM LiCl or 500 mM $NaNO_3$. Data were analyzed using the ORIGIN-based software provided by MicroCal.

*Reconstitution of purified protein and luminal buffer exchange*

$Glt_{Tk}$ was reconstituted into liposomes consisting of either a 3:1:1 mixture of 1,2-Dioleoyl-sn-Glycero-3-Phosphoethanolamine *(*DOPE): 1,2-dioleoyl-sn-glycero-3-phosphocholine *(*DOPC): 1,2-di-(9Z-octadecenoyl)-sn-glycero-3-phospho-(1'-rac-glycerol) (DOPG) or a 3:1 mixture of *E. coli* polar lipids and egg phosphatidylcholine (PC) following the reconstitution procedure as described by Hänelt et al.[96] in a protein to lipid ratio of 1:125-1:1600. After reconstitution, the buffer was exchanged. For this purpose proteoliposomes were spun down at 80,000 rpm, 4 °C in a Beckman TLA 80.2 rotor for 20 minutes. The pellet was washed with the buffer of interest, resuspended in the buffer of interest and subjected to three freeze-thaw cycles before being stored in liquid $N_2$.

*Transport assays*

Proteoliposomes were thawed and extruded 11x through a 400 nm pore size filter, centrifuged (80,000 rpm, 4 °C, Beckman TLA 80.2 rotor for 20 min.) and resuspended in luminal buffer to a protein concentration of 0.125-1 μg/μL. Transport reactions were started by adding 2 μL of proteoliposomes into 200 μL external buffer (as indicated in the result section) supplemented with 3 mM valinomycin (val). All assays were done at 30 °C with stirring, under iso-osmotic conditions. Transport reactions were stopped by the addition of 2 mL ice-cold 0.1 M LiCl, followed by rapid filtration over 0.45 μm pore size Whatman®Protran® BA-85 nitrocellulose filters (Sigma-Aldrich), including an additional wash step with 2 mL ice-cold 0.1 M LiCl. Then the filters were dissolved in 2 mL of Emulsifier Scintillator Plus liquid (Perkin Elmer). Subsequently the amount of radioactivity was measured in a Perkin Elmer Tricarb 2800 TR isotope counter.

For substrate competition experiments, a 400-fold excess of unlabeled amino acids was added to the 0.23 μM [$^{14}$C]-L-aspartate-containing outside buffer. Uptake reactions were stopped after 1.5 minutes.
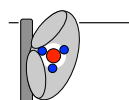
## Results

*Substrate Binding as Determined by Isothermal Titration Calorimetry (ITC)*

Using ITC measurements we determined the binding affinities of various substrates to Glt$_{Tk}$ in the presence of Na$^+$. A previous publication (chapter 4) showed that the protein alone does not bind its amino acid substrates in the absence of sodium ions[71]. Our studies showed that in the presence of high amounts of Na$^+$ (300 and 500 mM) the preferred substrate is L-aspartate with a $K_d$ in the nanomolar range (figure 3.1). Similarly to Glt$_{Ph}$, Glt$_{Tk}$ also binds D-aspartate, with a five-fold lower affinity than the L-form and also accepts L-cysteine sulfinic acid (L-CS) as substrate (~13-fold lower affinity). In contrast to Glt$_{Ph}$, Glt$_{Tk}$ binds the neutral amino acid L-asparagine with low affinity ($\mu$M range) but neither L- nor D-glutamate (data not shown).
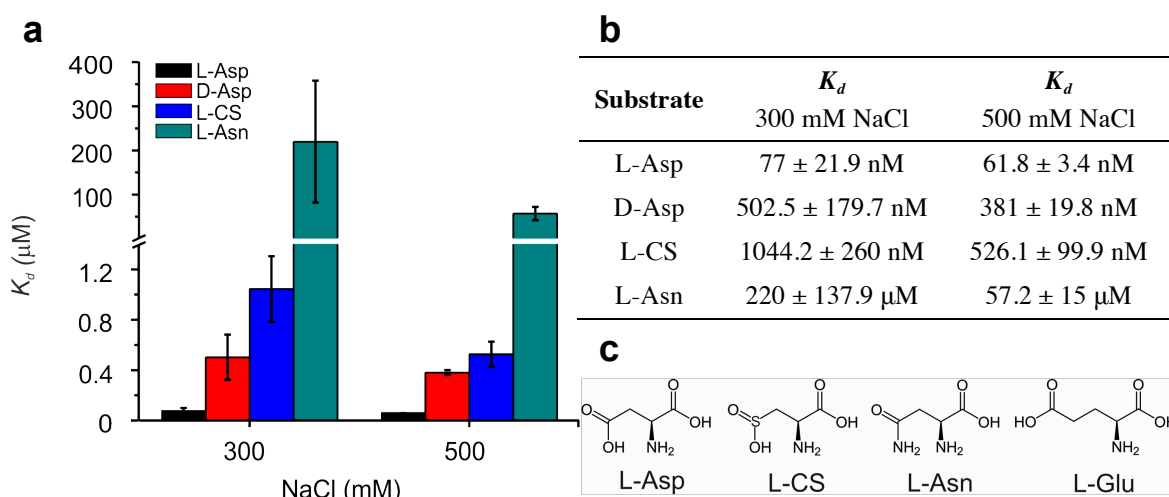


**Figure 3.1) Substrate binding to Glt$_{Tk}$.** Comparison of dissociation constants ($K_d$) for L-aspartate (L-Asp), D-aspartate (D-Asp), L-cysteine sulfinic acid (L-CS) and L-asparagine (L-Asn) in the presence of 300 mM and 500 mM Na$^+$ as derived by ITC. Measurements were performed at 25 °C and data shown are means ± SD (error bars). All experiments were performed in 3-5 independent replicates. **(a)** bar chart, **(b)** derived $K_d$ values. **(c)** Chemical representation of L-aspartate (L-Asp), L-cysteine sulfinic acid (L-CS), L-asparagine (L-Asn), and L-glutamate (L-Glu).

| Substrate | $K_d$ 300 mM NaCl | $K_d$ 500 mM NaCl |
|---|---|---|
| L-Asp | 77 ± 21.9 nM | 61.8 ± 3.4 nM |
| D-Asp | 502.5 ± 179.7 nM | 381 ± 19.8 nM |
| L-CS | 1044.2 ± 260 nM | 526.1 ± 99.9 nM |
| L-Asn | 220 ± 137.9 µM | 57.2 ± 15 µM |

In order to test whether Li$^+$ could replace Na$^+$ as coupling ion, we also determined the binding affinity of L-aspartate in the presence of 500 mM LiCl. The results show that Glt$_{Tk}$ still binds L-aspartate although the affinity is decreased by more than 250-fold (~62 nM in the presence of 500 mM NaCl, ~32 µM in the presence of 500 mM LiCl, figure 3.2 a and b, respectively). This finding is in good agreement with previous transport studies on Glt$_{Ph}$
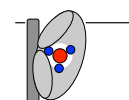
and the mammalian glutamate transporters[69,130,131], in which $Li^+$ replacement still supported substrate transport, but with reduced transport rates. Because the used LiCl was > 99% pure and the L-aspartate affinity in the presence of 500 mM LiCl is comparable to the affinity of L-aspartate in the presence of 25 mM NaCl (34 ± 12 µM) the observed affinity is too high to be caused by trace amounts of contaminating sodium in the used conditions.

Many glutamate transporters display an uncoupled anion channel activity. To test the influence of different conducted anions on the substrate binding we also determined the $K_d$ of L-aspartate binding in the presence of 500 mM $NaNO_3$ instead of NaCl. Strikingly, the $K_d$ was lowered by ~5.5-fold in the presence of $NO_3^-$ compared with $Cl^-$ (345 nM instead of 62 nM, figure 3.2 c). Because the coupling ion is the same, yet the affinity is much lower than in the presence of $Cl^-$, this result indicates an interaction between the anion and the transporter.
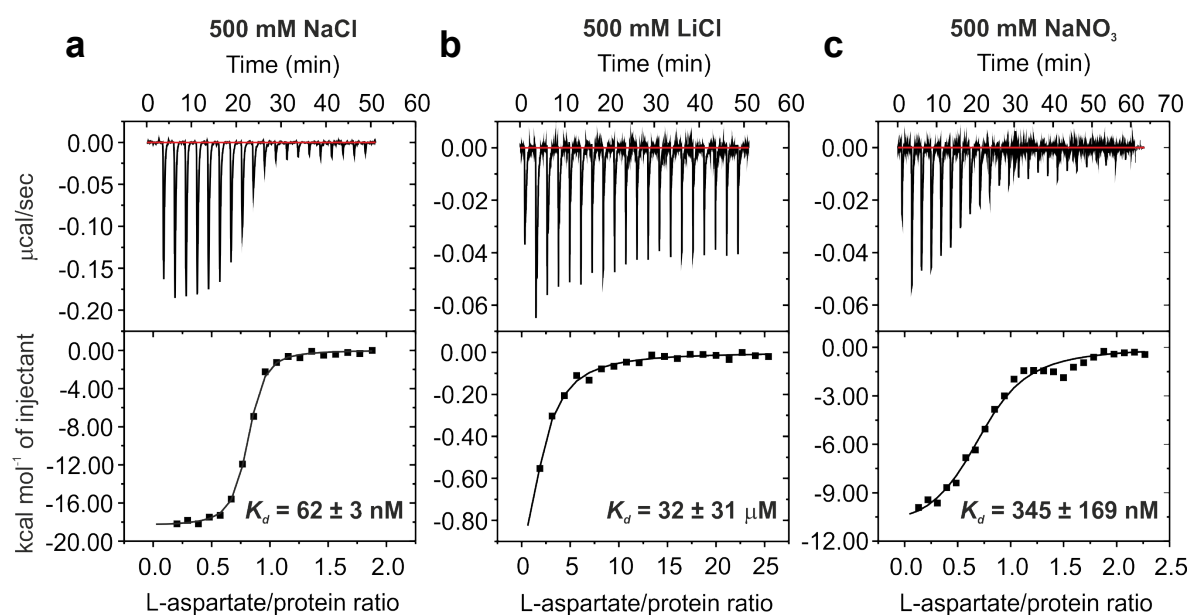


**Figure 3.2) Influence of ions on aspartate binding to Glt$_{Tk}$.** Isothermal titration calorimetry (ITC) of L-aspartate to Glt$_{Tk}$ in the presence of **(a)** 500 mM NaCl, **(b)** 500 mM LiCl, **(c)** 500 mM $NaNO_3$. ITC mesurements were performed in triplicate (n = 3-5) at 25 °C with 5-20 µM of protein. The upper panels show the raw data of heat release upon aspartate binding to the protein. The bottom panels show the non-linear least square fit of the peak area under each injection signal fitted to a single-binding-site-model (solid lines) with the software provided by MicroCal. The given $K_d$ values represent an average ± SD from 3-5 independent measurements.
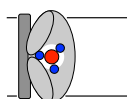
In order to determine the binding stoichiometry of aspartate to $Na^+$, we titrated L- and D-aspartate in the presence of varying $Na^+$ concentrations. When plotting the sodium concentration against the observed $K_d$ values, both in logarithmic scale, at the very lowest sodium concentration limit the negative slope of a linear fit corresponds to the number of ions that bind together with the substrate[69,208]. For both L- and D-aspartate, the $K_d$ for aspartate binding was dependent on the $Na^+$ concentration and showed that at least three $Na^+$ bind per L-aspartate, as can be seen in figure 3.3. Our data suggests that D-aspartate couples its binding to three to four sodium ions (figure 3.3).
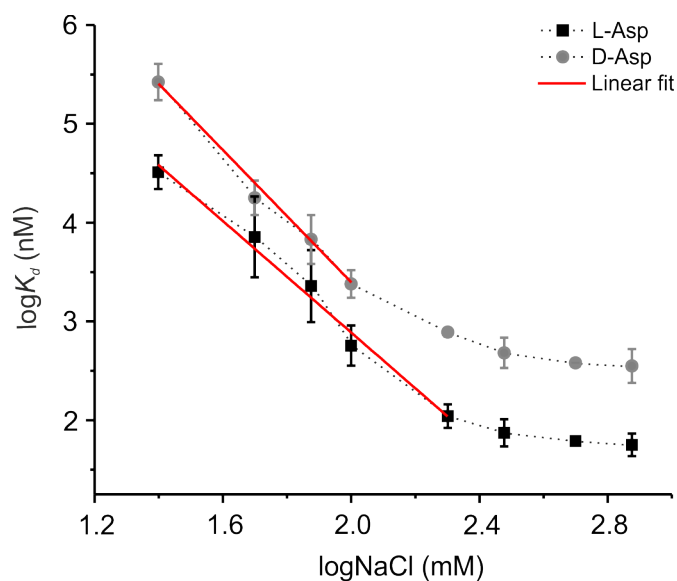


**Figure 3.3) Sodium and aspartate binding stoichiometry.** Logarithmic plot of L-aspartate $K_d$ (black squares) and D-aspartate $K_d$ (grey circles) in dependence of various sodium concentrations. Close to the limit of low sodium concentrations the negative slope of the double logarithmic plot (red line) approaches the number of sodium ions that bind together with aspartate. For L-aspartate the slope is -2.8 ± 0.2 and for D-aspartate -3.3 ± 0.2. Error bars represent the standard deviation from at least 3 independent measurements.

*Cross Linking of $Glt_{Tk}$ K57C A367C in the Inward-Facing Conformation*

Previously it was shown that $Glt_{Ph}$ with two engineered cysteines (K55C A364C) can be cross-linked and fixed in an inward facing-state[99]. In analogy to $Glt_{Ph}$ we constructed a similar double cysteine mutant of $Glt_{Tk}$ (K57C A367C). The double cysteine mutant was cross-linked with various cross-linkers in the presence and absence of aspartate and $Na^+$. We assessed the cross-linking efficiency by analysis of the electrophoretic migration in gels. The uncross-linked transporter migrates slower in the gel (upper band) than the cross-linked species (lower band), which likely is more compact. Besides bands for monomeric
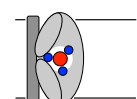
$Glt_{Tk}$ also bands corresponding to the trimeric transporter were visible, possibly representative for the strong stability of the trimeric transporter. However, cross-linking seems to destabilize the trimer and leads to the appearance of a small fraction of dimers (figure 3.4 a-c). The reason is yet unclear, but perhaps inter-subunit cross-links can be formed upon denaturation in SDS.

The best cross-linking results were obtained with 2 mM $HgCl_2$ (~100% cross-link), 2 mM $CuCl_2$, $CuSO_4$ (~80% cross-link), and CuPh (~75% cross-link) (figure 3.4).

In all Cu-containing cross-linkers ($CuCl_2$, $CuSO_4$, and CuPh) $Cu^{2+}$ is the active cross-linker. $CuCl_2$ and $CuSO_4$ show the same cross-linking efficiency but in both cases $Cu^{2+}$ is not stable in solution at approximately neutral pH and tends to precipitate. In CuPh, 1,10-phenanthroline stabilizes $Cu^{2+}$ even at higher pH (> pH 7). The lowered cross-linking efficiency of CuPh might be due to a lowered amount of reactive $Cu^{2+}$, but because of the higher stability of $Cu^{2+}$ in CuPh this condition was chosen for further cross-linking experiments.

Cross-linking with $Hg^{2+}$ was quick (reaction completed within 1 minute) with equal efficiency in presence and absence of substrates (figure 3.4 c). The cross-link was reversible by the addition of 10 mM 2-mercaptoethanol. In contrast, the cross-linking with CuPh was much slower, incomplete and the efficiency differed between the substrate-free and substrate-loaded carrier (figure 3.4 b): The cross linking efficiency was highest in the absence of substrates and presence of sodium only, with about 70-80% of the transporters fixed by disulfide bridge formation in presumably the inward-facing state. The substrate-free transporter reached the maximal cross-linking levels within 5 minutes, whereas the sodium-loaded transporter reached equal levels only after 15 minutes. Cross-linking of the fully substrate-loaded transporter was much slower with a final cross-linking efficiency of 50% only (figure 3.4 b). The Copper induced cross-link could not be removed by excess amounts of 2-mercaptoethanol  (up to 1 M) or dithiothreitol (up to 100 mM).
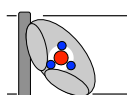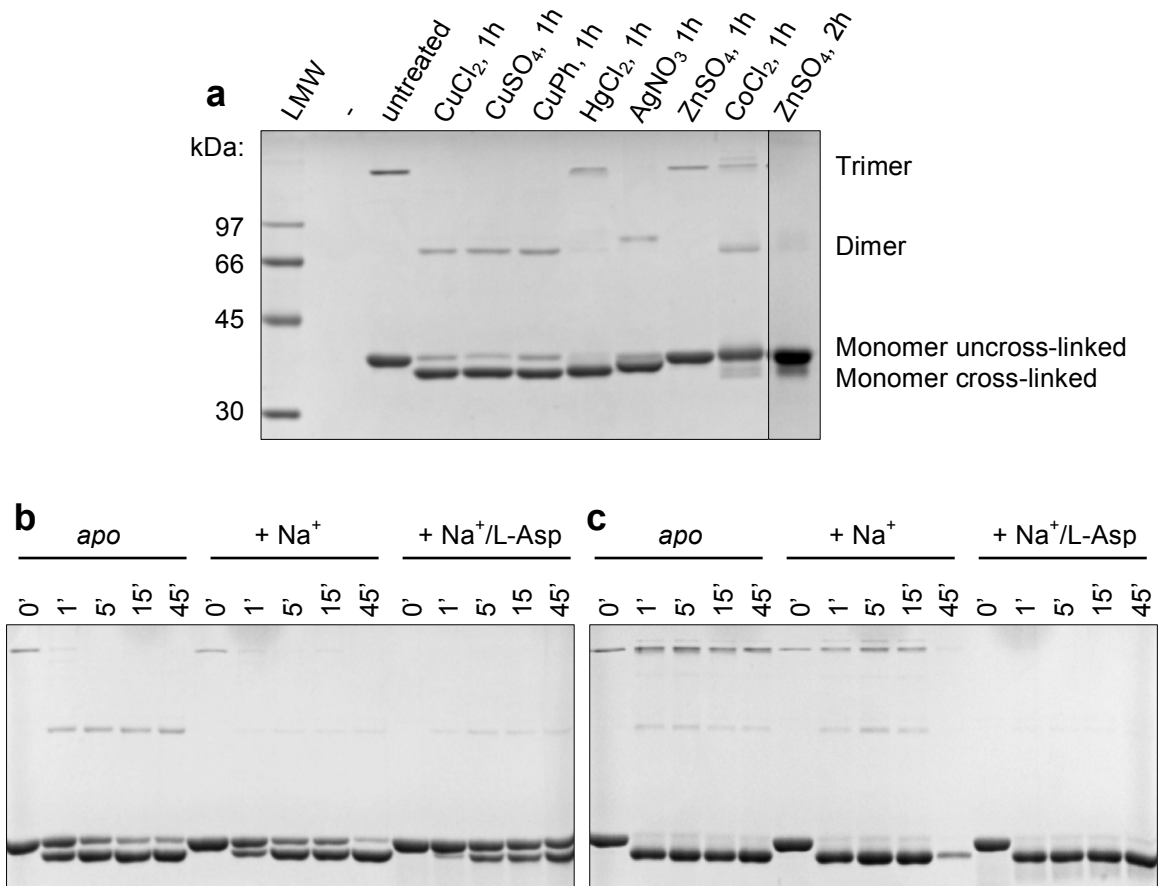
**Figure 3.4) Cross-linking of Glt$_{Tk}$ K57C A367C in the inward facing-conformation. (a)** For cross-linking the purified protein was incubated with each 2 mM of the mentioned cross-linker for one to two hours at 30 °C. The cross-linked protein was run against an untreated sample as negative control and LMW (Fermentas) as standard; CuPh: 1,10-Copperphenanthroline **(b)** Cross-linking time-course of Glt$_{Tk}$ K57C A367C with 2 mM CuPh at 30 °C in the absence (*apo*) and presence of substrates (+ Na$^+$, + Na$^+$/L-Asp). At the indicated time points the reaction was quenched with 20 mM NEM. **(c)** Cross-linking time-course of Glt$_{Tk}$ K57C A367C with 2 mM HgCl$_2$ at 30 °C in the absence (*apo*) and presence of substrates (+ Na$^+$, + Na$^+$/L-Asp). At the indicated time points the reaction was quenched with 20 mM NEM. + Na$^+$: in the presence of 300 mM NaCl; + Na$^+$/L-Asp: in the presence of 300 mM NaCl and 100 µM L-Asp; NEM: N-Ethylmaleimide; ': minutes.

*Binding properties of Glt$_{Tk}$ K57C 367C*

Since the inward facing fixation mediated by Hg$^{2+}$ was very fast, the binding of this cross-linker was determined by ITC measurements. It must be noted that Glt$_{Tk}$ K57C A367C has the tendency to aggregate in the presence of Hg$^{2+}$ (and Cu$^{2+}$). This effect was less pronounced for the fully loaded transporter than for the *apo*-protein. For the fully loaded transporter the high binding affinity of Hg$^{2+}$ could be determined with a $K_d$ of 12 nM (figure 3.5 b).
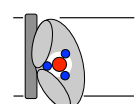
The $Hg^{2+}$ mediated cross-link had no effect on the number of binding sites (N). The affinity for aspartate to the mutant (*mut*) cross-linked with $Hg^{2+}$ was the same as in the wild type (*wt*) ($K_{d\,wt}$ = 77 nM, $N_{wt}$ = 0.78, $K_{d\,mut}$ = 60 nM, $N_{mut}$ = 0.65; figures 3.1 b and 3.5 c) but the uncross-linked $Glt_{Tk}$ K57C A367C had a four-fold lower affinity for aspartate ($K_d$ = 251 nM, N = 0.74, figure 3.5 a).
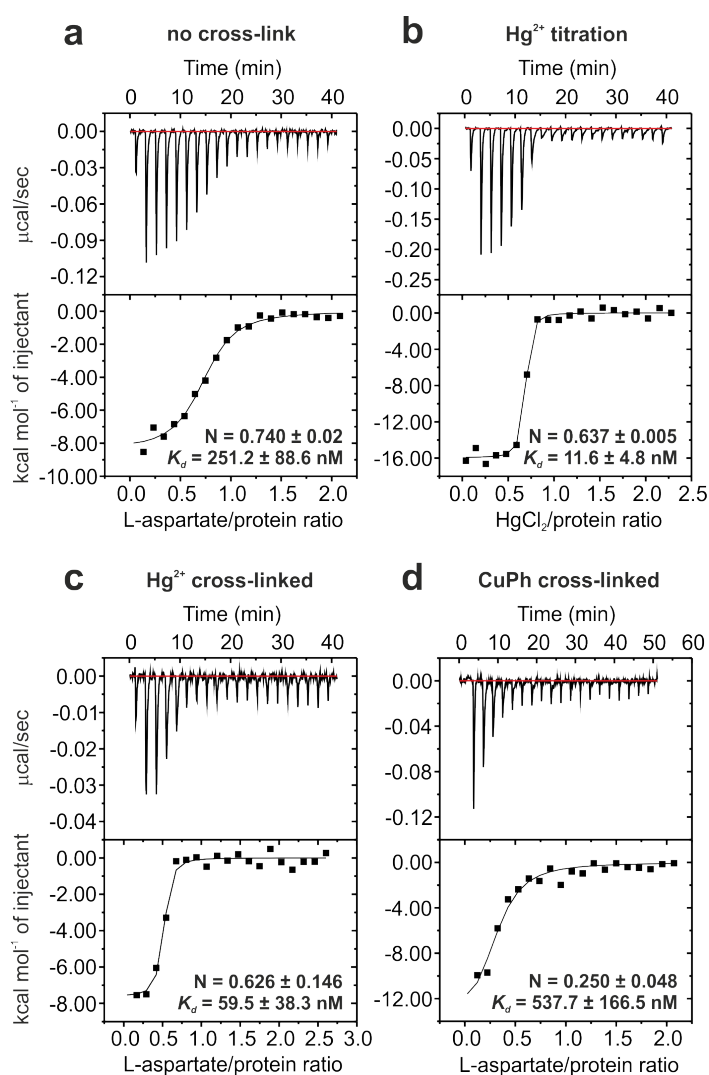


**Figure 3.5) Substrate and $Hg^{2+}$ binding to $Glt_{Tk}$ K57C A367C by ITC. (a)** L-Asp binding to $Glt_{Tk}$ K57C A367C in the presence of 300 mM NaCl, **(b)** $HgCl_2$ titration to $Glt_{Tk}$ K57C A367C in the presence of 300 mM NaCl and 100 μM L-Asp, single measurement; N and $K_d$ values with fitting error, **(c)** L-Asp binding to $Hg^{2+}$ cross-linked $Glt_{Tk}$ K57C A367C in the presence of 300 mM NaCl, **(d)** L-Asp binding to CuPh cross-linked $Glt_{Tk}$ K57C A367C in the presence of 300 mM NaCl. ITC measurements were performed at 25°C with 3-10 μM protein. The upper panels show the raw data of heat release upon aspartate or $Hg^{2+}$ binding to the protein. The bottom panels show the non-linear least square fit of the peak area under each injection signal fitted to a single-binding-site-model (solid lines). Fitting was done with the software provided by MicroCal. The given N and $K_d$ values represent means ± SD from 3 independent replicates if not stated otherwise.
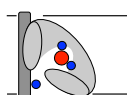
Different to Hg$^{2+}$ the CuPh treated mutant displayed a reduction of the number of binding sites to ~25% of the uncross-linked protein, which correlates well with the cross-linking efficiency of ~75%. Additionally, the affinity was 50% lower than the uncross-linked mutant or ~7-fold decreased when compared with the wild type (538 nM; figure 3.5 d).

### Glt$_{Tk}$ is an aspartate transporter that competitively binds asparagine

In chapter 4 we show that Glt$_{Tk}$ is an aspartate transporter. In order to test whether other substrates may also bind to the transporter, we performed transport assays using protein reconstituted in liposomes. Competition assays were performed with 400-fold excess of unlabeled molecules. Only L-/D-aspartate and L-asparagine were found to inhibit the uptake of radiolabeled aspartate (figure 3.6), which confirms the ITC binding data presented in this study.
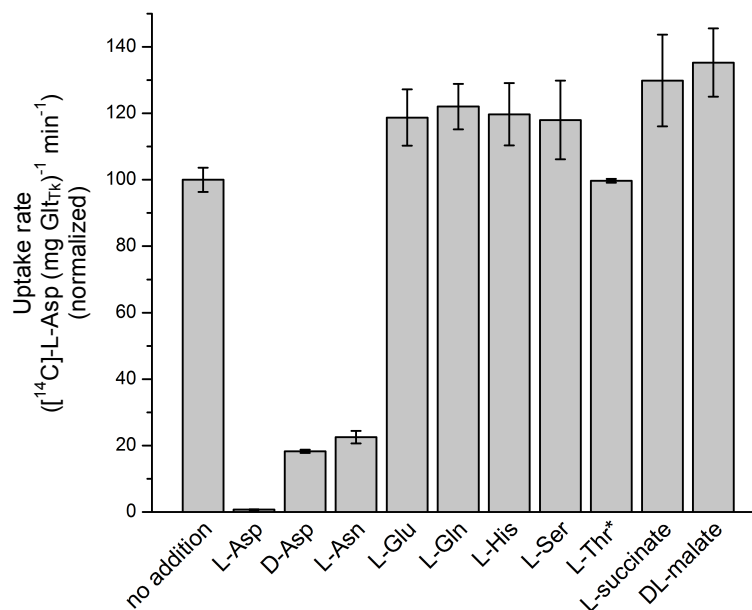


**Figure 3.6) Substrate specificity of Glt$_{Tk}$.** Competition experiment with 400-fold excess of the indicated amino acid/dicarboxylic acid, added to the external buffer. Excess of L-aspartate abolishes [$^{14}$C]-L-aspartate uptake, whereas D- aspartate and L-asparagine decrease the uptake rate. The higher uptake rates for the not competing compounds (except L-Thr) could be due to a slightly altered osmolality or membrane potential. Measurements were performed at 30 °C, reactions were stopped after 90 seconds. Data shown are means ± SEM (error bars) from technical triplicates, *: duplicate only.
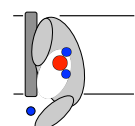
*The Influence of Lipids on Glt$_{Tk}$*

Because the lipidic environment can have influence on the function of glutamate transporters[209] we compared the substrate uptake by Glt$_{Tk}$ reconstituted in either synthetic lipids (SL; consisting of a 3:1:1 ratio of DOPE:DOPC:DOPG) or *E. coli* polar lipid extract (EL; consisting of a 3:1 mixture of *E. coli* lipids:egg phosphatidylcholine). Our results show that there is a big effect of the lipid environment on the transporter function (figure 3.7 a and b). Glt$_{Tk}$ reconstituted in SL exhibited a much slower transport rate than Glt$_{Tk}$ reconstituted in EL. In EL the transporter translocated the radiolabeled substrate with such high rate that within 15 seconds the accumulation was completed. Only with a much lower protein:lipid reconstitution ratio and dilution of the radiolabeled substrate with unlabeled substrate an uptake curve was obtained that allowed for the determination of an initial transport rate. The best results were achieved with a reconstitution ratio of 1:1600 (Glt$_{Tk}$:EL, *w:w*) and 20 μM L-aspartate (40x dilution with unlabeled substrate) (figure 3.7 c). Even under these conditions the linear phase was ≤15 seconds and a preliminary uptake rate was determined for the uptake within this time limit. The deduced apparent turnover for Glt$_{Tk}$ reconstituted in a protein to EL ratio of 1:800 and 1:1600 is nearly identical, with 4 and 5 s$^{-1}$, respectively. However, after the first 15 seconds the uptake for L-aspartate at a reconstitution ratio of 1:800 slows down much faster and seems to reach a much lower uptake level than for the reconstitution rate of 1:1600. Proteoliposomes with a reconstitution rate of 1:1600 contain more proteoliposomes per μg protein compared to proteoliposomes with a reconstitution rate of 1:800. Therefore, it is most likely that the total volume of the proteoliposomes limits the final uptake level in our assays.
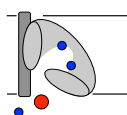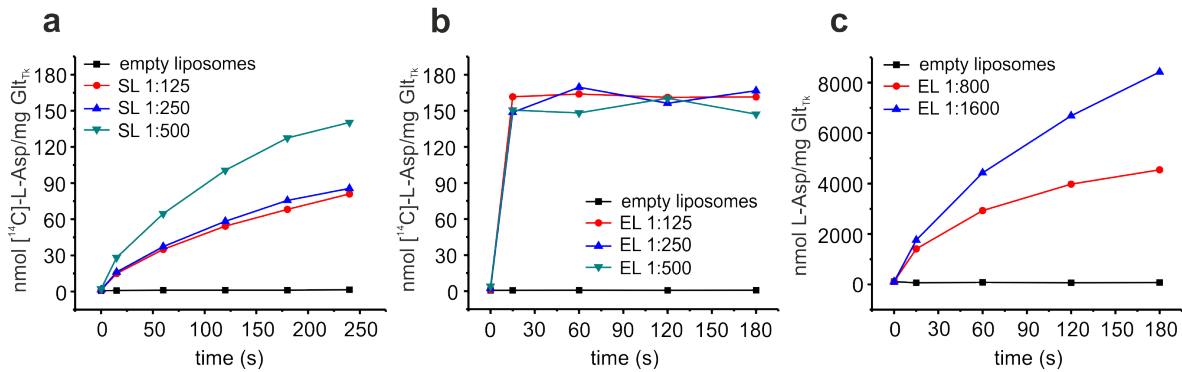
**Figure 3.7) Importance of the lipidic environment for the function of $Glt_{Tk}$.** Radiometric transport assays with [14C]-L-aspartate accumulation into $Glt_{Tk}$ containing proteoliposomes over time. **(a)** [14C]-L-aspartate uptake by $Glt_{Tk}$ reconstituted in synthetic lipids (SL; DOPE:DOPC:DOPG in 3:1:1 ratio) Reconstitution ratios of protein: lipids of 1:125, 1:250, and 1:500 were tested. **(b)** [14C]-L-aspartate uptake by $Glt_{Tk}$ reconstituted in *E. coli* lipids (EL; 3:1 mix of *E. coli* lipids and egg phosphatidylcholine) Reconstitution ratios of protein: lipids of 1:125, 1:250, and 1:500 were tested. After 15 sec. uptake was completed and all radiolabelled substrate was accumulated in the proteoliposomes. **(c)** Optimized uptake conditions for in *E. coli* lipids reconstituted $Glt_{Tk}$. Uptake of 0.5 μg [14C]-L-aspartate + 19.5 μg L-aspartate by $Glt_{Tk}$ reconstituted in a ratio of 1:800 and 1:1600. Only the 15-second data point was used for the determination of the turnover. $Glt_{Tk}$ 1:800 has a turnover of of 4 s$^{-1}$ $Glt_{Tk}$ 1:1600 has a turnover of 5 s$^{-1}$. Data results from single experiments only.

## Discussion

### $Glt_{Tk}$ is an aspartate transporter that binds aspartate with high affinity

In chapter 4 we show that $Glt_{Tk}$ is a sodium dependent aspartate transporter[71]. The results in this chapter are in-line with this finding. Besides L-aspartate also D-aspartate and the neutral amino acid L-asparagine inhibited aspartate transport albeit to a lower extent. This shows that arginine either competitively or allosterically (non-competitively) inhibits aspartate binding. Due to the similarities of aspartate and asparagine it is very likely that arginine binds to the same binding site as aspartate. However, this conclusion cannot be drawn from the current results. Future binding assays deploying displacement ITC could validate this question. Whether $Glt_{Tk}$ also transports L-asparagine requires further investigation using radiometric transport assays.

Additionally, our binding studies show that the negatively charged amino acids L-, D-aspartate and L-cysteine sulfinic acid bind with relatively high affinity but L-asparagine with low affinity. This is in clear contrast to $Glt_{Ph}$, which does not bind asparagine[70], yet the
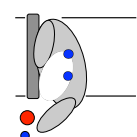
amino acid residues that form the substrate binding site are conserved in Glt$_{Tk}$ and Glt$_{Ph}$. In glutamate transporters the γ-/β-carboxyl group of glutamate and aspartate, respectively, is coordinated by the highly conserved amino acids T317 (TMS7), G362 (HP2), and R401 (TMS8) (Glt$_{Tk}$ numbering with the corresponding amino acids T314, G359, and R397 in Glt$_{Ph}$, respectively)[15,109,144]. Additional interactions between the amino group of the substrate and residues R278, V358, D398 (R276, V355, and D394 in Glt$_{Ph}$, respectively)[69] position the substrate and increase the affinity. In D-aspartate the amino group is turned. Thus binding to the same binding site as L-aspartate with the same interaction partners is less optimal. Interaction distances most likely are slightly different and presumably lead to weaker interactions and subsequent lower binding affinity. Another possibility is that D-aspartate binds at the same binding site as L-aspartate but with the amino group turned. Consequently the interactions with R278, V358, and D398 would be abolished. Yet the amino group could interact with the α-carboxyl of N405. This would interrupt the interaction between the amino group of N405 and the α-carboxyl of the substrate, which would move more towards its interaction partners S280 and T402 (S278 and T398 in Glt$_{Ph}$, respectively). Even though the interactions between the α-carboxyl of D-aspartate and S280 and T402 potentially increase, this can not compensate for the reduced interactions and could explain the preference for L- over D-aspartate and the lack of affinity for asparagine in Glt$_{Ph}$. Why Glt$_{Tk}$ can also bind L-asparagine with low affinity is not clear from the crystal structures (ref. 69 and chapter 5) and the residues involved in substrate and ion binding are conserved in Glt$_{Ph}$ and Glt$_{Tk}$. Possibly, subtle differences in the size of the binding site, the positioning of the binding site lining amino acids, or in flexibility might yield more space to accommodate L-asparagine binding.

Besides a spacial preference for L-aspartate in the binding site an MD study suggested that the β-carboxyl group of L-aspartate together with HP2 interact with Na3[144]. As a result substrate and coupling ion would stabilize each other. Replacing the carboxyl group for a neutral one would therefore not only drastically distort the substrate binding but also the binding of Na3. However, the structure of substrate-loaded Glt$_{Tk}$ (chapter 5) localizes Na3 at a different position: in the substrate loaded Glt$_{Tk}$ crystal structure Na3 exhibits interactions with the carboxamide group of N313, the hydroxyl groups of T94 and S95 (TMS3), the side chain carboxyl of D315 and the main chain carbonyl of Y91. This is in line with a recent free-energy simulation[148] and supported by various mutational studies on
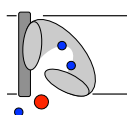
Glt$_{Ph}$ and mammalian transporters in which mutations of the stated residues reduced the affinity for Na$^+$ or even rendered the protein inactive[139,148,153,150]. Residue N313 does not only coordinate Na3 but also interacts with Na1, which means that binding sodium at either Na1 or Na3 site would stabilize the formation of the following Na-site and enhance the binding of the following sodium at the other position. This in turn creates the substrate-binding site, since T317, which is involved in the substrate coordination, is in direct proximity to the residues interacting with Na1 and Na3. Therefore, both sodium and substrate binding again stabilize each other. Weaker interactions of the substrate could result in the deformation or loss of one sodium binding site. Due to the low affinity of asparagine to Glt$_{Tk}$ it was not possible to determine the L-asparagine to sodium stoichiometry. For this reason it remains unsolved if the Na3-site, during L-asparagine binding, is unchanged, shifted, or completely destroyed. But the last two scenarios would probably also lead to a much lower affinity; as observed for L-asparagine binding in Glt$_{Tk}$.

L-cysteine sulfinic acid resembles L-aspartate in size and also has a negatively charged side chain. It binds to Glt$_{Tk}$ with ~13-fold lower affinity than L-aspartate. This also indicates that the charge of the β-carboxyl/sulfinic acid group has an influence on the substrate binding. Besides charge the size of the amino acid residue of the substrate plays a crucial role: aspartate, asparagine and cysteine sulfinic acid are of similar size and composition (see figure 3.1 c) but glutamate, which is slightly bigger than aspartate, does not bind (figure 3.1 a-c and figure 3.6). The amino acid residues of glutamate transporters that interact with the substrates are highly conserved amongst mammalian and prokaryal transporters. Therefore, residues surrounding the binding pocket limit the size of the substrate. In the mammalian transporters the residues T355 and M365 (T352 and M362 in Glt$_{Ph}$) are replaced by the smaller residues alanine and threonine, respectively. Mutational studies on Glt$_{Ph}$, with T352A and M362T replacements resulted in transporters with enhanced glutamate binding[94]. The bacterial glutamate transporters GltT and GltP (Groeneveld, Duurkens, Slotboom, unpublished data) possess, just like Glt$_{Tk}$ and Glt$_{Ph}$, a threonine and methionine at the positions 355 and 365, respectively, but have a serine replacement at position T317 (Glt$_{Tk}$ numbering). The presence of the smaller serine might enlarge the binding site and allow for the binding of larger substrates such as glutamate. Interestingly, in the neutral amino acid transporters SstT from *E. coli* and the mammalian transporters ASCT1 and ASCT2 the T317 is replaced with an alanine. This indicates that
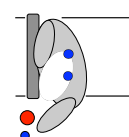
this residue plays a crucial role in substrate binding and selectivity. The hydroxyl group of serine or threonine could interact with the charged amino acid residue (γ- or β-carboxylate) of glutamate and aspartate, respectively. This hypothesis is supported by the available crystal structures from substrate-loaded $Glt_{Ph}$ and $Glt_{Tk}$ (ref. 69 and chapter 5, respectively). In both transporters the hydroxyl group of T317 ($Glt_{Tk}$ numbering) interacts with the β-carboxylate group of aspartate. It also exemplifies that the size of the binding site rather than one specific residue dictates the size of the substrate that can be accepted.

*$Glt_{Tk}$ couples the binding of aspartate to three sodium ions*

Besides the substrate specificity of $Glt_{Tk}$ we were also interested in the number of sodium ions that are involved in substrate binding. Because the binding of aspartate and sodium is mutually dependent on each other (chapter 2)[210] we could determine the stoichiometry by plotting the apparent aspartate affinities in the presence of various sodium concentrations, as has been described for $Glt_{Ph}$[69,208] before. Our results show that $Glt_{Tk}$ just like $Glt_{Ph}$[128] binds three sodium ions together with one aspartate. This shows that $Glt_{Tk}$ and $Glt_{Ph}$ do not only share high sequence similarity but are also very similar with respect to substrate and ion binding suggesting that they share the same functional properties and therefore allow for direct comparison of the structural data. Additionally, our data show that, even though the affinity for D-aspartate is lower than for L-aspartate, the binding of D-aspartate is not accompanied by a loss of sodium binding sites, which is in line with the observation that none of the sodium binding sites are directly coordinated by the substrate L-aspartate. While L-aspartate binding is coupled to the binding of three sodium ions D-aspartate binding involves the binding of three to four coupling ions. When L-aspartate is bound to $Glt_{Tk}$ the amino group interacts with R278, V358, and D398 (R276, V355, D394 in $Glt_{Ph}$, respectively). D-aspartate might bind to the same binding site and interact with the same amino acids. In this case the number and location of cation binding sites most likely are equal to those for L-aspartate. However, if D-aspartate binds with its amino group pointing away from the residues that coordinate the amino group of L-aspartate, this might create sufficient space to allow for binding of a fourth sodium at that position. Future crystal structures of $Glt_{Tk}$ loaded with D-aspartate and sodium might reveal the positioning of D-aspartate in the binding site as well as the associated amount of coupling ions.
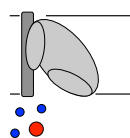
*Interactions with coupling ions and anions*

In $Glt_{Tk}$ $Li^+$ can replace $Na^+$ and promote the binding of aspartate but with ~250-fold lower affinity. This is similar to results for other glutamate and aspartate transporters, including $Glt_{Ph}$[69,130,132–135,137,211,212]. One explanation for this data is the smaller size of $Li^+$ (0.9 Å vs. 1.16 Å for $Na^+$), which might result in a much weaker binding of the coupling ion, dislocation of the cation binding sites or loss of one or more cation binding sites. Because of the low affinity for aspartate in the presence of $Li^+$ it was not possible to determine the stoichiometry of $Li^+$:aspartate. It therefore remains unclear if substrate binding in $Glt_{Tk}$ is accompanied by the binding of one, two, or three $Li^+$.

Our binding data additionally show that the cation accompanying anions also have a crucial impact on the transporter: In the presence of $NO_3^-$ instead of $Cl^-$ the $K_d$ for aspartate binding is increased ~seven-fold, while in both cases the coupling ion was $Na^+$. This result is indicative for an interaction of the anion with the protein. This interaction could occur on the surface of the transporter or within the protein, where it might hinder structural rearrangements connected with substrate binding. Interestingly, substrate binding promotes an uncoupled anion conductance in mammalian transporters[88,89,166,173,174,186,213–215] and $Glt_{Ph}$[183]. In EAAT1-3 $NO_3^-$ is more permeable than $Cl^-$, but the permeation sequence could be different in $Glt_{Tk}$. Another explanation for the observed effect of $NO_3^-$ could be, that whilst the charge of $Cl^-$ and $NO_3^-$ and the ionic strength of $NaCl$ and $NaNO_3$ containing buffers are identical, there could be differences in the Hofmeister activity[216] that influence the flexibility of the protein.

*Substrate binding stabilizes $Glt_{Tk}$ in the inward facing-conformation*

In detergent solution the sidedness is lost, which complicates the interpretation of the binding parameters. It is possible that in detergent solution a fraction of *apo*-$Glt_{Tk}$ has its external binding site exposed and another fraction the internal binding site. If there are no converging conformational changes towards the same occluded state upon substrate binding, the values determined for the $K_d$ represent a mean value for the affinity of the outward and inward oriented binding events. However, it is likely that conformational changes subsequent to the initial binding lead to a final state that does not discriminate anymore between the two alternative routes for binding, and a single value is determined.
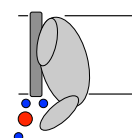
The kinetics of reaching the final state may be different, but such a difference would not affect the thermodynamic value for the $K_d$.

To differentiate between these events and to probe whether the affinity from either side of the membrane is different, it would be useful to fix the protein in the in- or outward facing states[192]. In an initial step, to obtain binding data for either side, we fixed the protein in an inward facing state similar to what has been done for $Glt_{Ph}$[192].

We observed a big difference in the effect of the cross-linkers $Hg^{2+}$ and $Cu^{2+}$. $Hg^{2+}$ binds fast and with high affinity to $Glt_{Tk}$. In the presence of substrates aggregation caused by $Hg^{2+}$ is reduced, which indicates that substrate binding facilitates the inward facing state with a form that is less prawn to aggregation. Additionally, $Hg^{2+}$ appeared to be a more efficient cross-linker (based on gel shift) and had very little effect on the number of binding sites (N). The binding affinity of L-aspartate to the $Hg^{2+}$ cross-linked transporter is comparable to the affinity of the *wt*. This is lower than for the uncross-linked mutant, which exhibited a four-fold lower affinity for aspartate than the *wt*, indicating that the cysteine substitution might hinder conformational rearrangements necessary for $Na^+$ and aspartate binding. Another possibility for the increased affinity of L-aspartate in the inward fixed transporter could be due to a higher affinity in the inward facing state (IFS). Such a binding asymmetry could be verified with an outward facing state (OFS) mutant.

In contrast to $Hg^{2+}$, $Cu^{2+}$ cross-linking was less efficient, and affected by the presence of substrates. The cross-linking efficiency was highest for the *apo* and sodium loaded states. This is in clear discrepancy to an earlier publication on $Glt_{Ph}$[192], where cross-linking in the presence of substrate and sodium occurred faster than for the *apo*-protein. The interpretation was that substrate binding pulls the transporter into the inward facing conformation. The difference of our results may be because the amino acid residues in $Glt_{Tk}$ are not ideally positioned to form a disulfide bridge, so the distance might be different and the movement into the IFS stronger than presented by the crystal structure of $Glt_{Ph}$[69]. Additionally, the cross-linked protein appeared to have lost the ability to bind aspartate. A possible explanation is that the cross-linked state is not a good mimic of the IFS, and the internal gate cannot open anymore. This result also differs from what was observed for $Hg^{2+}$ mediated cross-linked $Glt_{Ph}$[192]. Yet the direct disulfide bridge formation mediated by $Cu^{2+}$ cross-linking appears more restrictive than the $Hg^{2+}$ mediated cross-link, and the $Hg^{2+}$
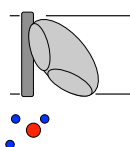
cross-link seemingly allows for more flexibility and movement of the transport domain. As consequence the substrate binding site might be more accessible with all binding sites remaining available upon cross-linking, and thus unchanged in the ITC experiment. This is in contrast to the Cu$^+$ mediated cross-link, where the number of binding sites is lower.

About a quarter of the CuPh cross-linked transporter remains uncross-linked, though the affinity for aspartate is lower than for the uncross-linked mutant. This is possibly because low affinity binding and a low N (< 0.4) make it difficult to determine the $K_d$ accurately. An explanation for the incomplete cross-link could be that some of the cysteine residues are oxidized to sulfoxides and cannot cross-link anymore.

Another explanation could be that the uncross-linked transporter is trapped in the OFS by asymmetric stretching and contraction as suggested by Jiang et al.[217]. Jiang et al. observed in EAAT1, that if two protomers were cross-linked via HP2 in the OFS, the third subunit resided in the IFS. If indeed, upon CuPh cross-linking, the uncross-linked protomer of Glt$_{Tk}$ is trapped in the OFS, substrate transport would be abolished. This could be probed with uptake experiments.

Alternatively, it is possible that the differences between Cu$^{2+}$ and Hg$^{2+}$ are caused by erroneous interpretation of the gel-shift that we used to assess the cross-linking efficiency. Possibly, the binding of Hg$^{2+}$ to the cysteines did not result in cross-linking, even though it caused a gel shift. Control experiments with single cysteine mutants could resolve this issue.

*The lipidic environment is important for the transport-function*

Even though the transport data is only preliminary it shows that Glt$_{Tk}$, even at temperatures much below its physiologically relevant temperature (60-100 °C), exhibits turnover rates comparable to those of the mammalian transporters EAAT1, 2, 4, and 5[175,182,187,218,219] which is ~1000-fold faster than reported for Glt$_{Ph}$[70]. Noteworthy, the apparent substrate affinity is lower in Glt$_{Tk}$ when compared with Glt$_{Ph}$. Minor differences could enable faster movement of the transport domain in Glt$_{Tk}$. A possibility on how this faster movement could be accomplished was proposed by a recent single molecule FRET study on Glt$_{Ph}$[106]: the mutation of two amino acids (K290A and G221A, Glt$_{Ph}$ numbering) resulted in an increased hydration of the transport and trimerization interface. Thereby increasing the
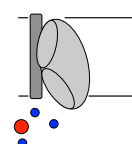
mobility of the transport domain accompanied by increased uptake rates. One of the mutated amino acids (K290 in $Glt_{Ph}$) is a glutamate in $Glt_{Tk}$ (E292). Another reason could be that the high affinity binding of aspartate in $Glt_{Ph}$ is connected to tight substrate binding, with resulting slow substrate release as has been suggested for EAAT5[188].

Additionally, our transport data reinforces the importance of the lipid environment on the function of the transporter as reported previously for $Glt_{Ph}$[209]. The influence of lipids on the function of glutamate transporters and membrane proteins in general are manifold and ranges from reconstitution efficiency, right-side-out orientation, structural stability and integrity, to the protein volume, and proper vertical positioning - not only due to the thickness of the membrane[209,220–224]. All these reasons are important for the proper function of membrane proteins and the specific requirements can vary amongst glutamate transporters. Though it must be noted that speed is not necessarily a measure for good transporter activity: fast transport rates might be accompanied by low affinity, while high affinity in turn is accompanied by slow transport, as has been proposed for the eukaryotic EAATs[188]. Future experiments should therefore address the transporter efficiency based on $K_M$ and $k_{cat}$, the reconstitution efficiency, and correct orientation of the transporter in membranes of various lipid-composition.

In summary our results show that $Glt_{Tk}$ is as $Glt_{Ph}$ a high affinity aspartate transporter, which binds sodium and L-aspartate in a 3:1 stoichiometry. Both transporters share many functional and mechanistic features, which therefore allows for direct comparison of their structures. But there are also conspicuous differences, especially in the transport rate. Such differences will allow finding the structural basis (amino acids) that determines the kinetic properties of the transporters in future work.
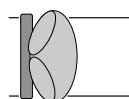
# Chapter 4

Crystal Structure of a Substrate-free Aspartate
Transporter

**Sonja Jensen[#], Albert Guskov[#], Stephan Rempel, Inga Hänelt, and Dirk Jan Slotboom**

[#]These authors contributed equally.
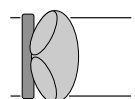
## Abstract

Archaeal glutamate transporter homologs catalyze the coupled uptake of aspartate and three sodium ions. After the delivery of the substrate and sodium ions to the cytoplasm, the empty binding site must reorient to the outward-facing conformation to reset the transporter. Here, we report a crystal structure of the substrate-free transporter $Glt_{Tk}$ from *Thermococcus kodakarensis*, which provides insight into the mechanism of this essential step in the translocation cycle.
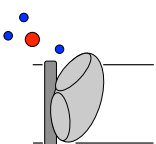
Glutamate transporters are secondary transporters found in many eukaryotes, bacteria and archaea[45]. In prokaryotes these transporters mediate the uptake of nutrients, whereas in mammals, where glutamate is a major excitatory neurotransmitter, they catalyze the neurotransmitter reuptake into neurons and glial cells that follows synaptic signal transduction. Maintaining a low extracellular concentration of the neurotransmitter is essential for sensitive signal transmission and for the prevention of neurotoxicity. The transporters couple the uptake of glutamate to the symport of cations: three sodium ions and one proton are co-transported by the neuronal and glial transporters[124]. After the substrate and cations are released into the cytoplasm, the empty binding site reorients to an outward-facing orientation. In mammalian transporters this reorientation is strictly coupled to the export of a potassium ion, but in prokaryotes no such coupling is required[70].

Structural information is available for the glutamate transporter homolog $Glt_{Ph}$ from the archaeon *Pyrococcus horikoshii*, which is selective for aspartate rather than glutamate and which couples the uptake of substrate to the symport of three sodium ions[15,69,70,99,128,189]. The protein is a homotrimer, with each protomer consisting of two domains. The trimerization domain mediates the subunit contacts, and the transport domain carries the binding sites for aspartate and sodium ions. Different crystal structures of substrate-bound $Glt_{Ph}$ have revealed that the trimerization domains form a stable scaffold[95,99,128,189]. The transport domains have been captured in three states: outward facing, intermediate and inward facing[69,99,189]. The structures suggest that the transport domains behave as rigid bodies and move across the membrane like an elevator to shuttle the substrate and coupled ions from one side to the other. Because the transporters are substrate loaded in all available crystal structures, the mechanism by which the empty (substrate-free) transporter reorients to the outward-facing position after delivery of the substrates to the cytoplasm remained elusive. To gain insight into this essential part of the transport cycle, we determined the structure of a substrate-free transporter.

We purified glutamate transporter homologs from several closely related archaea, using a protocol that yields the protein devoid of aspartate and sodium ions[128] (see also Methods). The reason that we did not focus exclusively on $Glt_{Ph}$ was to increase our chances of obtaining well-diffracting crystals. We obtained pure and stable preparations of $Glt_{Tk}$ from the thermophilic archaeon *T. kodakarensis*. $Glt_{Tk}$ shares 77% sequence identity with $Glt_{Ph}$, and all residues that interact with the substrate aspartate in $Glt_{Ph}$ are strictly conserved in
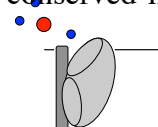
Glt$_{Tk}$ (figure 1.2). The residues that shape the two Na$^+$ binding sites found in the Glt$_{Ph}$ crystal structures are also conserved. The location of the third Na$^+$ binding site is still debated[146,148,149]. The two transporters are functionally similar as well. Just like Glt$_{Ph}$[99], Glt$_{Tk}$ is a sodium-coupled aspartate transporter that also accepts D-aspartate but not glutamate as substrate (figure 4.1). Importantly, we confirmed by isothermal titration calorimetry that our preparations of Glt$_{Tk}$ were free of Na$^+$ and aspartate (figure 4.2).
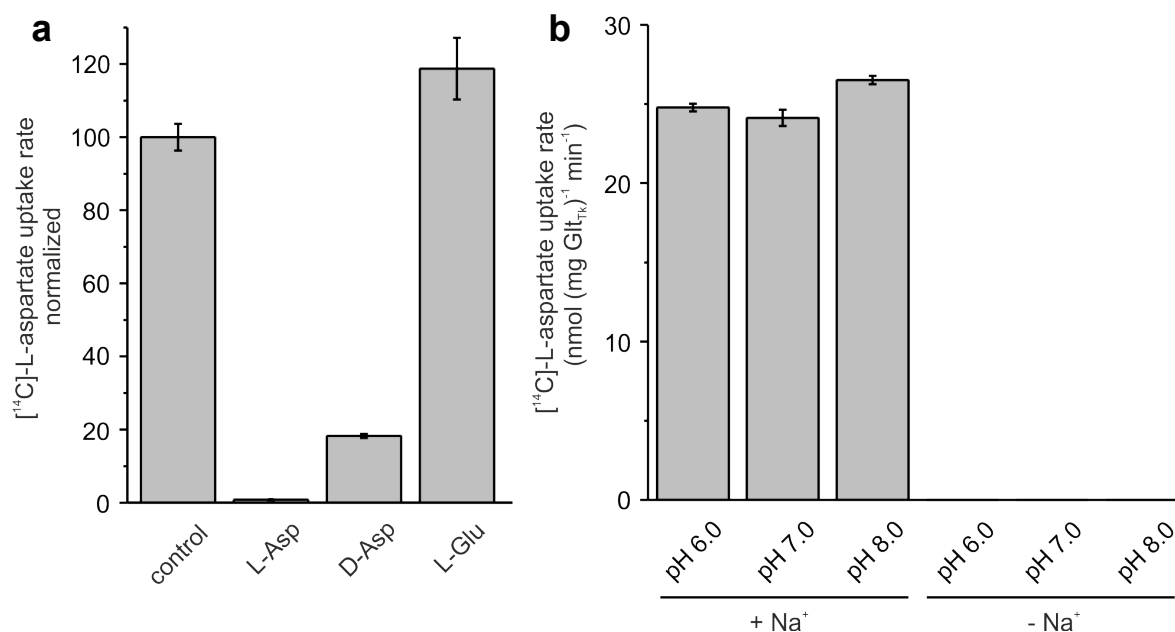


**Figure 4.1) Transport of aspartate by Glt$_{Tk}$.** The purified protein was reconstituted in proteoliposomes and uptake of L-aspartate was assayed. **(a)** Substrate specificity. The initial uptake rate of radiolabeled L-aspartate (0.23 μM) was measured in the absence (left bar) or presence of a 400-fold excess of the indicated, unlabeled amino acids. **(b)** Sodium and pH dependency. Proteoliposomes loaded with potassium phosphate buffer (50 mM, pH 7) were assayed for L-aspartate uptake using external buffers (50 mM sodium phosphate, left three bars; 50 mM TRIS/MES, right three bars) of different pH values. Transport of aspartate was dependent on sodium ions but not dependent on a proton gradient. Standard errors of the mean from triplicate experiments are shown. For the experiments in the absence of sodium ions the error bars are too small to be visible.

We solved the structure of *apo*-Glt$_{Tk}$ to a resolution of 3.0 Å (see supplementary table S4.1 for data collection and refinement statistics). The extensive sequence similarity between Glt$_{Ph}$ and Glt$_{Tk}$, as well as their functional resemblance, allowed for a comparison between the substrate-bound structures available for Glt$_{Ph}$ and the structure of the *apo*-protein of Glt$_{Tk}$. The overall structure of Glt$_{Tk}$ is very similar to that of Glt$_{Ph}$, with the transport domain in the outward-facing conformation (figure 4.3 a)[15,69]. The two helical hairpins
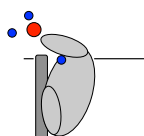
(HP1 and HP2) in the transport domain, which may form intra- and extracellular gates, respectively, occlude the substrate binding site in both $Glt_{Ph}$ and $Glt_{Tk}$ (figure 4.3 b).
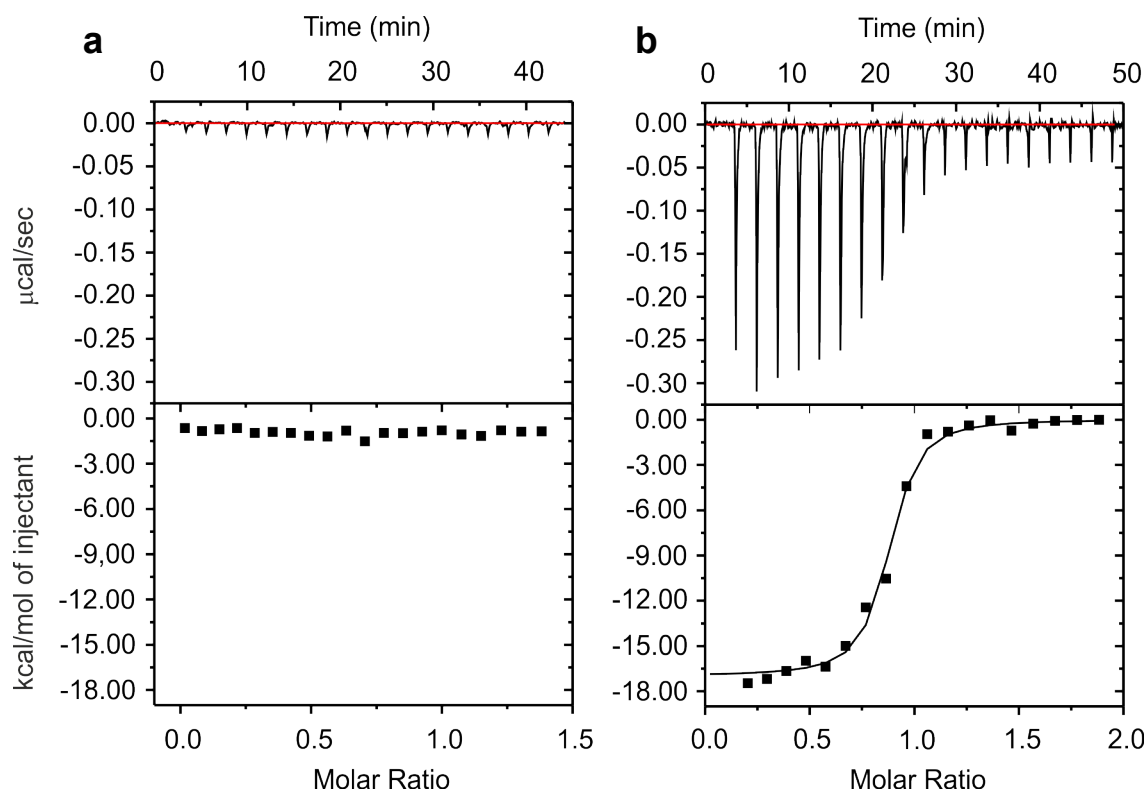


**Figure 4.2) Aspartate binding to $Glt_{Tk}$ assayed by isothermal titration calorimetry. (a)** and **(b)** show titrations of L-aspartate (0.2 nmol per addition) to 2.6 or 3.0 nmol $Glt_{Tk}$ in the absence and presence of 500 mM $Na^+$, respectively. The upper panels show the heat added to the cell over time with successive additions. The excess heat added per addition was integrated from the upper panel and plotted in the lower panel as function of the ratio of the concentrations of aspartate and $Glt_{Tk}$ in the cell. Aspartate binds only if $Na^+$ is present. This data shows that purified $Glt_{Tk}$ is devoid of $Na^+$ and aspartate.

Despite these similarities in global structure, there are crucial differences in the binding sites for aspartate and sodium ions. In the aspartate binding site, Arg401 of $Glt_{Tk}$ in transmembrane segment (TMS) 8 adopts a very different conformation from the equivalent Arg397 of $Glt_{Ph}$ (figure 4.5 and figure 4.6). This arginine is highly conserved in the glutamate transporter family and is essential for transport[109,115,225]. Compared to that in $Glt_{Ph}$, the guanidium group of Arg401 in $Glt_{Tk}$ is offset by ~4 Å, and its position overlaps that occupied by the substrate aspartate in $Glt_{Ph}$. Thus, in the empty carrier, the side chain of a highly conserved residue takes over the site occupied by the transported ligand in the loaded carrier. Because the overlap is not complete, we assume that water molecules fill up the rest of the empty binding site. The position of the guanidium group of Arg401 is
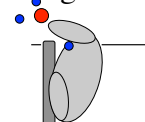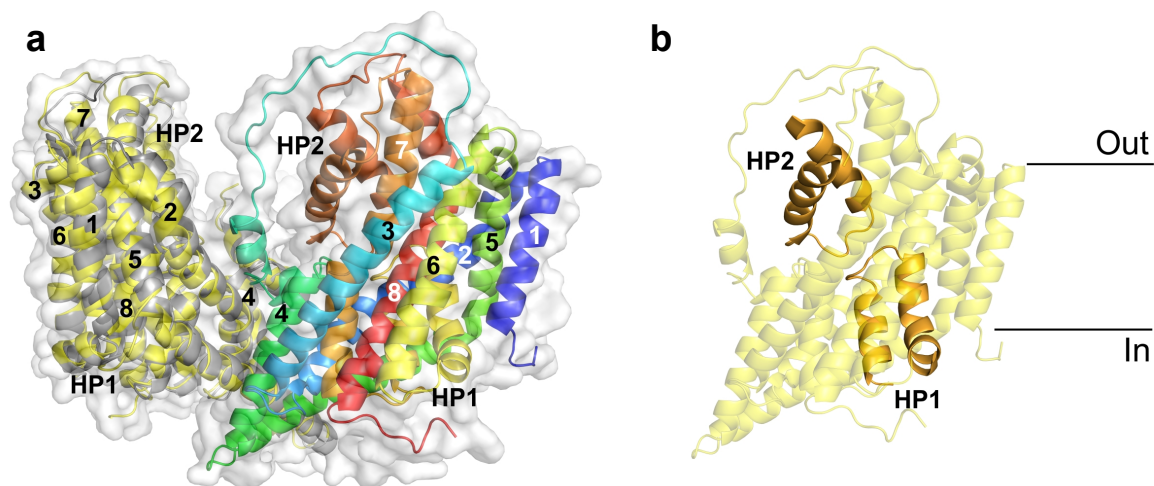
**Figure 4.3) Crystal structure of Glt$_{Tk}$.** **(a)** Left protomer; superposition of Glt$_{Tk}$ (yellow) with Glt$_{Ph}$ (gray, PDB code 2NWL)[69]. RMSDs: overall 1.31 Å, trimerization domain 0.84 Å, transport domain 1.43 Å, aspartate binding site 1.79 Å, sodium binding sites 2.72 Å. Right protomer: Glt$_{Tk}$ colored from blue (N-terminus) to red (C-terminus), as in figure 1.2. Transmembrane segments (TMS) and helical hairpins (HP) are labeled. **(b)** The two HPs occlude the binding site in Glt$_{Tk}$.

stabilized by an ionic interaction with conserved Asp398 (394, where the numbering in parentheses is for Glt$_{Ph}$). In substrate-bound Glt$_{Ph}$ this residue interacts with the amino group of the substrate aspartate (figure 4.6). The side chain *B*-factors of Arg401 are slightly higher than the average in the protein (supplementary table S4.2); this could be related to the dynamic role of Arg401, which should be able to reposition during the translocation cycle.
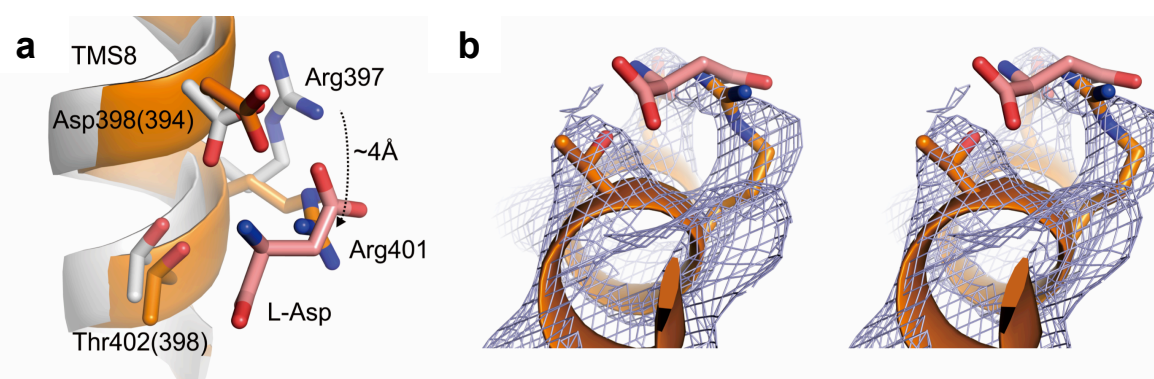


**Figure 4.4) Aspartate binding site**. **(a)** Comparison of the aspartate binding sites in Glt$_{Ph}$ and Glt$_{Tk}$. Relevant amino acid residues are shown as sticks and labeled and numbered as in Glt$_{Tk}$ (and as in Glt$_{Ph}$ in parentheses). The large shift of Arg401 (397) in TMS8 is indicated with an arrow. **(b)** Stereo image of the substrate binding site of Glt$_{Tk}$ with electron density (2 $F_o - F_c$ map, contoured at 1.2 σ). Glt$_{Tk}$ is shown in orange, Glt$_{Ph}$ is colored in gray, and the substrate L-aspartate present in Glt$_{Ph}$ is shown in light red to emphasize the clash with the position of Arg401 in Glt$_{Tk}$.
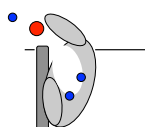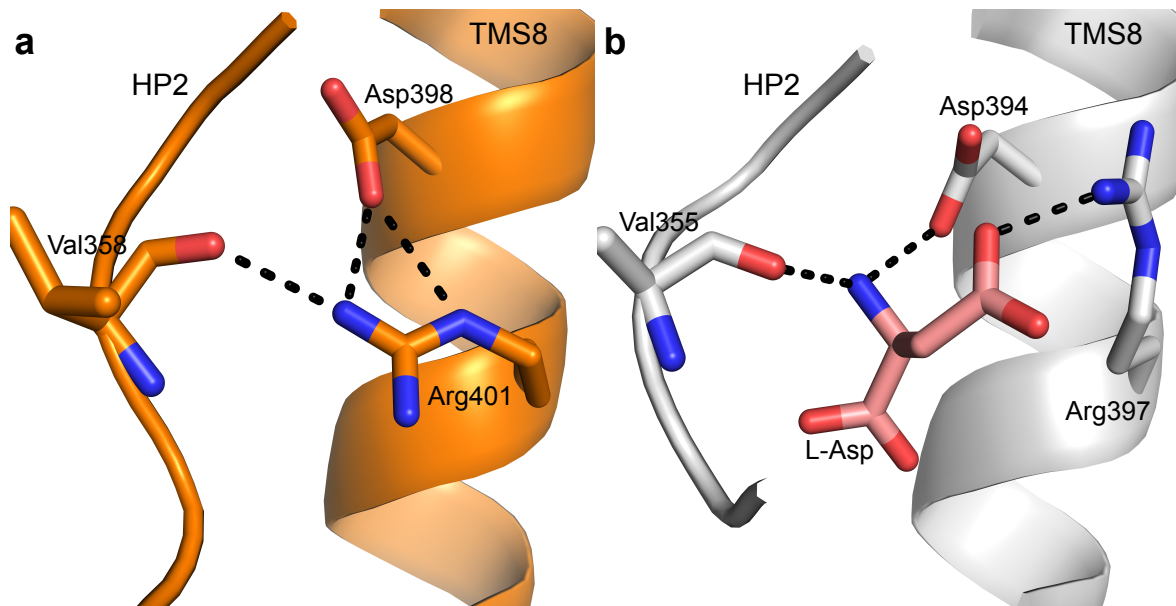
**Figure 4.5) Interaction network of Arg401 in Glt_Tk. (a)** Arg401 interacts with Asp398 in TMS8 and Val358 in HP2. **(b)** For comparison the equivalent residues in the binding site in Glt_Ph are shown. The three residues directly interact with the substrate L-aspartate. Colors as in figure 4.4.

The repositioning of Arg401 has another consequence as it breaks the cation-π interaction with Tyr320 (317) in TMS7 that is present in substrate-bound Glt_Ph (*cf*. ref. 15). This breakage allows for rearrangements in TMS7, notably of Tyr320 (317), Gln321 (318), and Thr317 (314) (figure 4.5 a). In Glt_Ph the location of the latter residue is stabilized by a hydrogen bond with the α-carboxylate of the substrate aspartate, but in the substrate-free transporter it can reorient, which also affects the region around Met314 (311) in TMS7 (see below). In the rat transporter GLT-1, the equivalents of Tyr320 and Gln321 (Tyr403 and Glu404, respectively) are essential for the coupling with potassium ions, which is required for reorientation of the empty carrier in mammalian glutamate transporters[66,133]. The rearrangement of residues around Arg401 in *apo*-Glt_Tk creates a pocket, which in the mammalian transporters may form a potassium binding site (figure 4.6 a). The structure provides an explanation for a key finding in the neuronal glutamate transporter EAAC1. When the equivalent of Arg401 (Arg447 in EAAC1) was mutated into cysteine, the protein could no longer bind or transport glutamate and aspartate, but it was still able to transport neutral amino acids. However, only exchange of the neutral amino acids could take place, and net transport was impaired, showing that the conserved arginine is crucial not only for the binding of acidic substrates but also for the reorientation of the empty carrier[109].
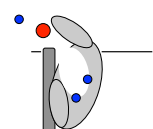
In both $Glt_{Tk}$ and $Glt_{Ph}$, TMS7 is partially unwound in the center of the membrane. The unwound part in $Glt_{Tk}$ has undergone a dramatic change of conformation around Met314, which is a highly conserved and functionally important residue[115,226]. The side chain of Met314 in the empty transporter points away from the binding site (figure 4.6 b-d) and is exposed to the lipid bilayer between Leu92 of TMS3 and Val349 of HP2. In $Glt_{Ph}$ the side chain of the equivalent Met311 points toward the binding site and is located between the two sodium binding sites that were found in the $Glt_{Ph}$ crystal structures.
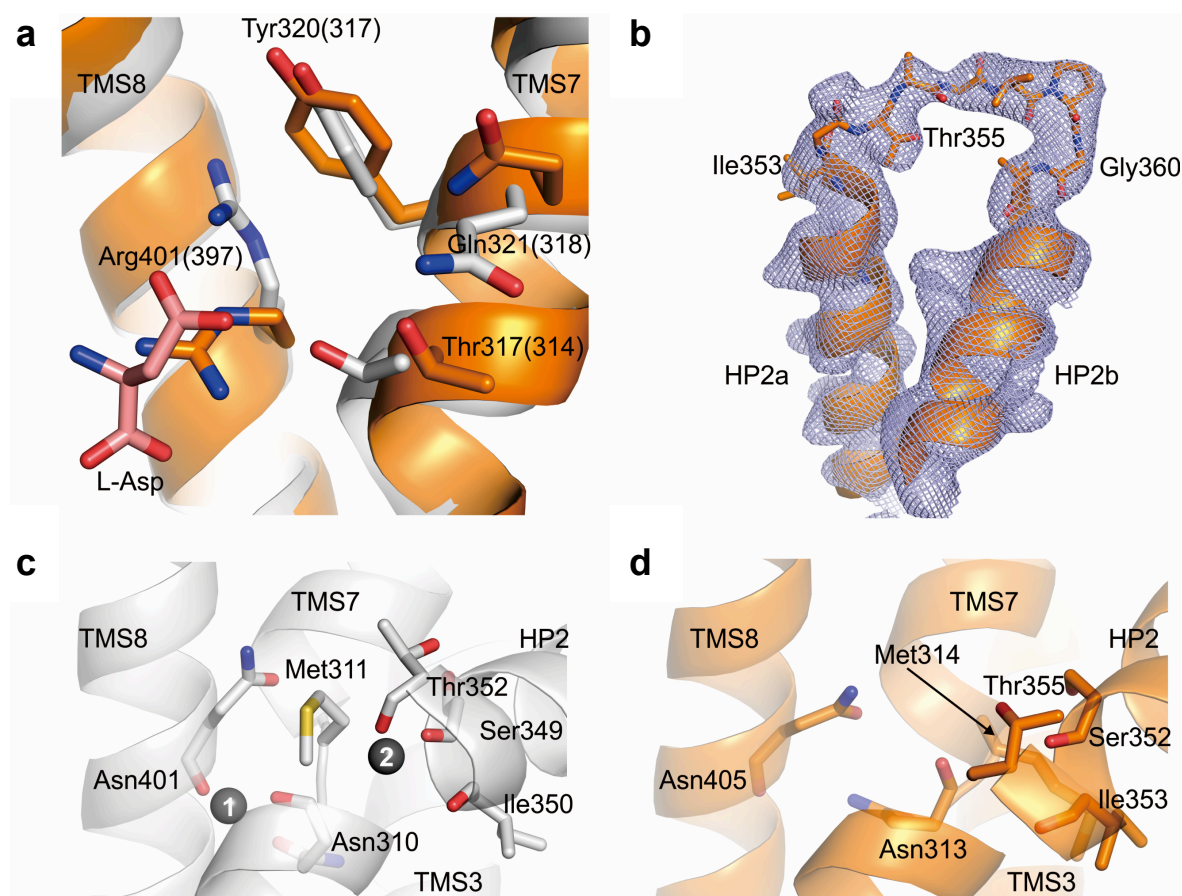


**Figure 4.6) Cation binding sites. (a)** Overlay of $Glt_{Tk}$, in orange, with $Glt_{Ph}$, in gray (the substrate L-aspartate is shown in light red). The cation-π interaction between Arg397 and Tyr317 of $Glt_{Ph}$ is disrupted in $Glt_{Tk}$ and a cavity is created, which could form a potassium binding site in the eukaryotic members of the glutamate transporter family. Numbering of residues is for $Glt_{Tk}$, with numbers for $Glt_{Ph}$ in parentheses. **(b)** Electron density of HP2 ($2 F_o − F_c$ map, contoured at 1.2 σ). **(c), (d)** Comparison of $Na^+$ binding sites of $Glt_{Ph}$ ((c), in gray) with $Glt_{Tk}$ ((d), in orange). The two $Na^+$ binding sites of $Glt_{Ph}$ are indicated with 1 and 2. Relevant residues are labeled and numbered according to the $Glt_{Ph}$ or $Glt_{Tk}$ sequence in (c) and (d), respectively.
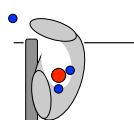
The change in conformation of the unwound part of TMS7 in $Glt_{Tk}$ directly affects the first $Na^+$ binding site, as the backbone carbonyl oxygen of Asn313 (310) is displaced and is no longer in a favorable position to coordinate a sodium ion. Similarly, the carbonyl oxygen of Asn405 (401) in $Glt_{Tk}$ is not properly oriented to bind the sodium ion. The second $Na^+$ binding site is also deformed in $Glt_{Tk}$. The backbone carbonyls of Ser352, Ile353, and Thr355 in HP2 that coordinate the second sodium ion in the $Glt_{Ph}$ structure are displaced by 4 Å, 1.8 Å, and 4.5 Å in $Glt_{Tk}$, thus impeding the binding of the cation (figure 4.6 c-d).
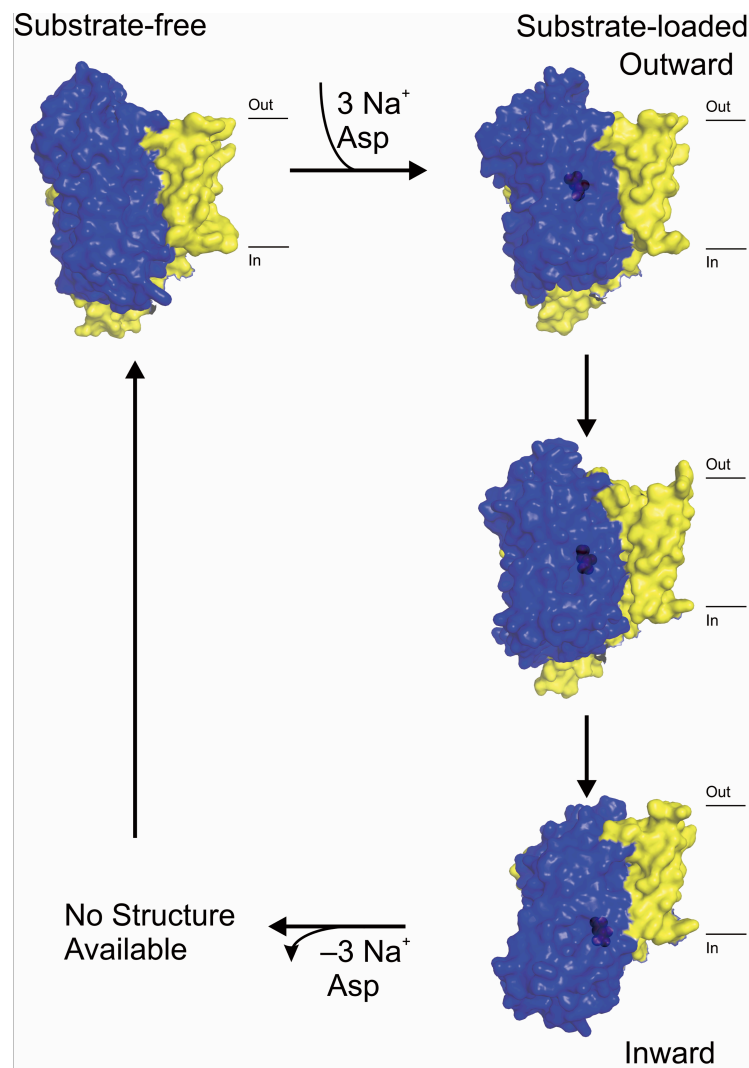


**Figure 4.7) Translocation cycle of archaeal aspartate transporters based on the available crystal structures.** Shown (clockwise from top right) are surface representations of a single subunit of the trimeric protein in the outward-facing substrate-loaded (PDB code 2NWL)[69], intermediate substrate-loaded (PDB code 3V8G)[189], inward-facing substrate-loaded (PDB code 3KBC)[99] and outward-facing substrate-free (current structure) states. No structures are available for the inward-facing and intermediate states of the substrate-free transporters. The trimerization domain is shown in yellow, the transport domain in blue and the substrate L-aspartate in purple.
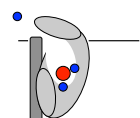
The structure of *apo*-$Glt_{Tk}$ provides an explanation for the mechanism of reorientation of the empty carrier. Because the overall structures of both the trimerization and the transport domains of the *apo*-protein are very similar to those of the corresponding domains in the substrate-loaded $Glt_{Ph}$, it is plausible that the movement of the transport domain across the membrane will take place in the empty carrier in the same manner as it does in the loaded carrier (figure 4.7). This hypothesis is supported by recent EPR experiments on $Glt_{Ph}$, which showed that the transport domain is structurally heterogeneous both in the *apo* and in the substrate-bound transporter, indicating a movement across the membrane in both conditions[86,96].

## Methods

### Chemicals

Restriction enzymes and antarctic phosphatase were purchased from New England BioLabs Inc., T4 DNA ligase from Thermo Scientific, [$^{14}$C]-L-aspartate (1.85 MBq, 7.4 GBq/mmol) from PerkinElmer and lipids from Avanti Polar Lipids Inc. L-Arabinose and ampicillin sodium salt were from Sigma-Aldrich. All chemicals were of analytical purity grade.

### DNA manipulation, protein purification and concentration determination

C-terminally His8-tagged $Glt_{Tk}$ was purchased from Geneart. $Glt_{Tk}$ was cloned into the pBAD24 vector using standard cloning methods. *Escherichia coli* MC1061 cells containing the plasmid were cultivated in LB medium (37 °C and 200 rpm), and protein was produced by inducing cells at an $OD_{600}$ of 0.8 with 0.05% L-arabinose for 3 h. Harvesting, membrane vesicle preparation, determination of total protein concentration and solubilization in n-dodecyl-β-D-maltopyranoside were done as described before[128]. To obtain *apo*-$Glt_{Tk}$, we used the procedure that also yielded *apo*-$Glt_{Ph}$, with minor modifications as described below[128]. The crucial difference between this purification procedure and the one used by the Gouaux and Boudker labs[15] is the omission of Na$^+$ from all buffers. In sodium-containing buffers, the substrate aspartate remains associated with the protein throughout the entire purification because the $k_{off}$ is very low. In the absence of sodium ions, the substrate aspartate is lost during the purification. After solubilization, the solution was subjected to ultracentrifugation for 30 min. at 4 °C, 265,000 g. The
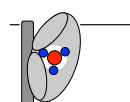
supernatant was incubated for 1 h on a rotating platform at 4 °C with 0.5 mL bed volume Ni-Sepharose (GE Healthcare) pre-equilibrated with 50 mM Tris HCl pH 8, 300 mM KCl, 0.15% n-decyl-β-D-maltopyranoside (DM), 15 mM imidazole pH 8. The solution was then loaded onto a Poly-Prep chromatography column (Bio-Rad), which was washed with 20 column volumes (CV) of 50 mM Tris HCl pH 8, 300 mM KCl, 0.15% DM, 60 mM imidazole pH 8. $Glt_{Tk}$ was eluted with 50 mM Tris HCl pH 8, 300 mM KCl, 0.15% DM, 500 mM imidazole pH 8. The protein was further purified by size exclusion chromatography (SEC) on a Superdex 200 10/300 GL (GE Healthcare) column using 10 mM HEPES-KOH pH 8, 100 mM KCl, 0.15% DM as running buffer. For crystallization trials the peak fractions were used. After purification, the protein concentration was determined by UV absorption (NanoDrop), using the molecular weight and extinction coefficient calculated by the ExPASy ProtParam tool (web.expasy.org/protparam/). The protein was concentrated to ~7 mg/mL using a spin concentrator (Vivaspin 2, 30,000 MWCO, PES membrane, Vivaproducts).

*Crystallization and structure determination*

The best diffracting crystals were obtained by the vapor diffusion method in hanging drop with a protein concentration of 7 mg/mL and a reservoir solution of 25% glycerol/polyethylene glycol (PEG) 4000/glycerol, 100 mM Tris/bicine pH 8.5, 60 mM $CaCl_2$/$MgCl_2$ and 0.5% n-octyl-β-D-glucopyranoside (OG). Data sets were collected at ESRF beamlines ID 23-1 and ID 29. Data processing was performed with XDS[227] with the highest resolution limit of 3.0 Å. The structure was solved with Phaser software using only one monomer of $Glt_{Ph}$ (PDB code: 2NWX)[69] as a search model. The refinement was done in PHENIX[228] with application of NCS and TLS restraints. To remove bias, several rounds of simulated annealing were performed. Manual correction and building was performed in Coot[229]. Structural figures were generated with PyMOL[83].

*Reconstitution and activity assays*

$Glt_{Tk}$ was reconstituted into liposomes consisting of a 3:1:1 mixture of 1,2-dioleoyl-sn-glycero-3-phosphoethanolamine (DOPE): 1,2-dioleoyl-sn-glycero-3-phosphocholine (DOPC): 1,2-di-(9Z- octadecenoyl)-sn-glycero-3-phospho-(1'-rac-glycerol) (DOPG) according to Hänelt et al.[96]. Transport assays were performed essentially as described before[128]. All assays were done at 30 °C with stirring, under iso-osmotic conditions.
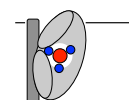
External buffer (50 mM sodium phosphate, pH 6, 7 or 8; or 50 mM Tris/MES, pH 6, 7, or 8), supplemented with 0.23 μM [$^{14}$C]-L-aspartate (PerkinElmer) and 0.6 μM valinomycin was mixed with the proteoliposomes containing 1 μg Glt$_{Tk}$ in a 100:1 (v/v) ratio. For substrate competition experiments a 400-fold excess of unlabeled L-aspartate, D-aspartate or L-glutamate was added to the external buffer. 200 μL samples were taken at each time point, transferred immediately into 2 mL ice-cold outside buffer and filtered over a 0.45-μm-pore-size filter (Protran Ba 85, Whatman). The filters were transferred to a 2 mL reaction tube, 2 mL scintillation liquid (Emulsifier Scintillator Plus, PerkinElmer) was added and the filters were allowed to dissolve. All samples were measured in a PerkinElmer Tri-Carb 2800RT liquid scintillation counter.

*ITC*

ITC experiments were performed at a constant temperature of 25 °C using an iTC200 calorimeter (MicroCal). The thermally equilibrated ITC cell was filled with 200 μl of purified Glt$_{Tk}$ (concentration 13–15 μM; in 10 mM HEPES/KOH, pH 8, 100 mM KCl, 0.15% DM with or without 500 mM NaCl). 100 μM aspartate (dissolved in the same buffer as the protein) was titrated into the cell in steps of 2 μL. Data was analyzed using the software provided by MicroCal.

**Accession codes**

Atomic coordinates and structure factors for the *Thermococcus kodakarensis* Glt$_{Tk}$ transporter in its substrate-free state are deposited in the Protein Data Bank under accession code 4KY0.

**Acknowledgments**
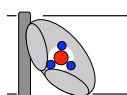
# Appendix to chapter 4

## Supplementary Tables

**Table S4.1) Data collection and refinement statistics.**

|  | $Glt_{Tk}$ native |
|---|---|
| **Data collection** | |
| Space group | P3221 |
| Cell dimensions | |
| $a, b, c$ (Å) | 117.57, 117.57, 309.51 |
| $\alpha, \beta, \gamma$ (°) | 90.00, 90.00, 120.00 |
| Resolution (Å) | 48.4 - 3.0 (3.1-3.0)* |
| $R_{mean}$ | 0.13 (1.18) |
| $I/\sigma I$ | 6.11 (1.1) |
| Completeness (%) | 99.8 (99.8) |
| Redundancy | 7 (7) |
|  | |
| **Refinement** | |
| Resolution (Å) | 3.0 |
| No. of reflections | 50526 |
| $R_{work}$ / $R_{free}$ (%) | 21.2 / 26.6 |
| No. of atoms | |
| Protein | 9308 |
| PEG | 52 |
| Water | - |
| $B$-factors | |
| Protein | 96.5 |
| PEG | 119.9 |
| Water | - |
| RMS deviations | |
| Bond lengths (Å) | 0.010 |
| Bond angles (°) | 1.510 |

\* Values in parentheses are for the highest-resolution shell.

RMS: Root-Mean-Square

*Chapter 4*
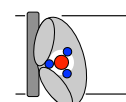
**Table S4.2) Comparison of *B*-factors in the Glt$_{Tk}$ structure.**

| Chain | Arg401 Side Chain | *B*-factors (Å$^2$) Average Side Chain | Range in Loops |
|-------|-------------------|----------------------------------------|----------------|
| A | 126.7 | 98.5 | 135 - 199 |
| B | 118.2 | 101.1 | 120 - 205 |
| C | 110.8 | 95.6 | 122 - 206 |
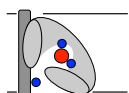
# Chapter 5

# Mechanism of Coupled Binding of Three Sodium Ions and Aspartate in the Glutamate Transporter Homolog $Glt_{Tk}$

**Albert Guskov[#], Sonja Jensen[#], Ignacio Faustino, Siewert J. Marrink and Dirk Jan Slotboom**

[#]These authors contributed equally.
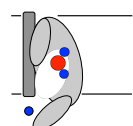
**Abstract**

Glutamate transporters catalyze the thermodynamically unfavorable transport of anionic amino acids across the cell membrane by coupling it to the downhill transport of cations. This coupling mechanism is still poorly understood, in part because the available crystal structures of these transporters are of relatively low resolution. Here we solve crystal structures of the archaeal transporter $Glt_{Tk}$ in the presence and absence of aspartate and use molecular dynamics simulations and binding assays to show how strict coupling between the binding of three sodium ions and aspartate takes place.
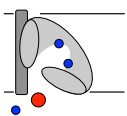
## Introduction

Glutamate transporters are found in Bacteria, Archaea and Eukarya. In vertebrates they guard the levels of the neurotransmitter glutamate in the synaptic cleft by pumping it (back) into neuronal and glial cells (reviewed in ref. 187, 233). The free energy stored in cation gradients across the membrane is utilized to accumulate the amino acid inside the cells. The eukaryotic proteins couple glutamate uptake to co-transport of three sodium ions and a proton, and counter-transport of a potassium ion[123–125].

Crystal structures are available for two similar archaeal homologs of the mammalian transporters (Glt$_{Ph}$ and Glt$_{Tk}$, which share 77% sequence identity, figures 1.2 and 5.1 a)[15,69,71,99,142]. The archaeal transporters also couple the cellular uptake of aspartate to the co-transport of sodium ions, but they do not use protons or potassium ions for co- or counter-transport[70]. A stoichiometry of three sodium ions per aspartate has been determined for Glt$_{Ph}$[128]. The crystal structures have provided a structural framework to explore the mechanism of transport, which has sparked a large amount of biochemical, electrophysiological, mutagenesis, and simulation studies on various members of the family. However, the resolution of the structural data has been too low to reveal the binding sites of the sodium ions, and therefore the coupling mechanism has remained poorly understood. Replacement of sodium by thallium ions allowed the use of the anomalous signal from the heavy atom to identify the potential locations of two of the three sodium binding sites in the low resolution structures[69]. Simulation studies indicated possible locations of the third sodium binding site[146,148,149], but no unequivocal solution was found, leaving the coupling mechanism unexplained.

Here, we present crystal structures, molecular dynamics simulations and substrate binding assays of Glt$_{Tk}$ to localize the sodium binding sites, and provide insight in the mechanism of coupling between sodium and aspartate binding.

## Results

*Overall structural characteristics of Glt$_{Tk}$*
We crystallized the archaeal glutamate transporter homolog from *Thermococcus kodakarensis* (Glt$_{Tk}$) in the presence of aspartate and sodium ions, solved its structure at 2.8
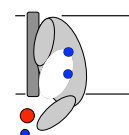
Å resolution (Glt$_{Tk}$$^{sub}$), and located three sodium sites. Isothermal titration calorimetry (ITC) experiments on aspartate binding in the presence of eight different sodium concentrations showed that Glt$_{Tk}$ indeed binds three sodium ions per aspartate molecule, the same number as Glt$_{Ph}$ (figure 3.3). In parallel we obtained improved crystals of the substrate-free form of Glt$_{Tk}$[71] that yielded a 2.7 Å resolution structure (Glt$_{Tk}$$^{apo}$) (see table 5.1 for data and refinement statistics). The two structures, each with better resolution and data quality than any previously determined one, provide a structural model for coupling between substrate and cation transport. Both structures have a very similar trimeric organization with the transport domains in an outward-occluded position (supplementary figure S5.1). There was well-defined electron density for all loops, as well as for the N-termini, which were not ordered in the Glt$_{Ph}$ crystals. Notably, we could model the entire loop between transmembrane helices 3 and 4, which is important for transport[231,232] (figure 5.1 b). This loop intimately wraps around the outer face of the transport domain, and appears to prevent excessive movements of helical hairpin 2 (HP2) away from the binding pocket, while allowing small-scale movements of HP2, which are required to provide access to the substrate and sodium binding sites (see below).

*Sodium and aspartate binding sites*

For all three sodium ions (Na1-3), as well as the aspartate molecule we observed well defined electron density in the Glt$_{Tk}$$^{sub}$ structure (figure 5.3 a–c). The positions of sodium ions in the two sites Na1 and Na2 (numbering of the sodium ion sites as in ref. 69) are in good agreement with the previously reported crystal structures[69], showing that thallium was indeed a good mimic for sodium in these sites (supplementary figure S5.2). Na1 is coordinated by the β-carboxylate of the conserved D409 residue (D405 in Glt$_{Ph}$, D454 in rat EAAT3, see figure 5.1 a for numbering) of Trans Membrane Segment (TMS) 8, and main chain carbonyls of G309, N313 from the unwound central region of TMS7, and N405 from TMS8 (figure 5.3 a and supplementary figure S5.3). Na2 is coordinated by main chain carbonyls (S352, I353, and T355) of HP2 connecting TMS7 and 8, and main chain carbonyl of T311 (TMS7) (figure 5.3 a and supplementary figure S5.3). The sulfur atom of M314 is within interacting distance (< 3 Å) to Na2, though the nature of this interaction is unclear. The proposal made by Boudker et al.[69] that the Tl$^+$ ion (used as a substitute of Na$^+$) forms favorable interactions with sulfur is unlikely to be the full explanation, because we also see the interaction in the presence of sodium instead of thallium. The unusual

coordination of Na2 by the methionine residue might be necessary for dynamic rearrangements of the binding site during the transport cycle. It was shown previously that the side chain of this methionine points away from the binding site in the substrate-free transporter, indicating that it must be highly mobile[71]. Furthermore, simulations have shown that Na2 is the last ion to bind during the substrate loading[148,149] and the first one to leave for substrate release, suggesting that the Na2 binding site might be of low affinity, which is supported by simulations presented below.

**Figure 5.1) Overview of the structure of Glt$_{Tk}$.** (a) Sequence alignment of the aspartate transporters Glt$_{Tk}$ from *Thermococcus kodakarensis* and Glt$_{Ph}$ from *Pyrococcus horikoshii* and the glutamate transporter EAAT3 from *Rattus norvegicus*. Identical residues between the archaeal proteins are colored red, those involved in Na1 binding in magenta, Na2 in green, and Na3 in blue respectively. N313 involved in coordination of both Na1 and Na3 is presented in purple. Bars above the sequences indicate helical segments and are colored in yellow and grey for the trimerization and transport domain, respectively. Loop 3–4 is indicated by the blue line, HP2 is shown in red. (b) Crystal structure of the substrate-loaded aspartate transporter Glt$_{Tk}$$^{sub}$ viewed from the extracellular side of the membrane shown in surface presentation. The trimerization domains are presented in yellow, the transport domains in gray, HP2 in red, and long loop 3–4 in blue.
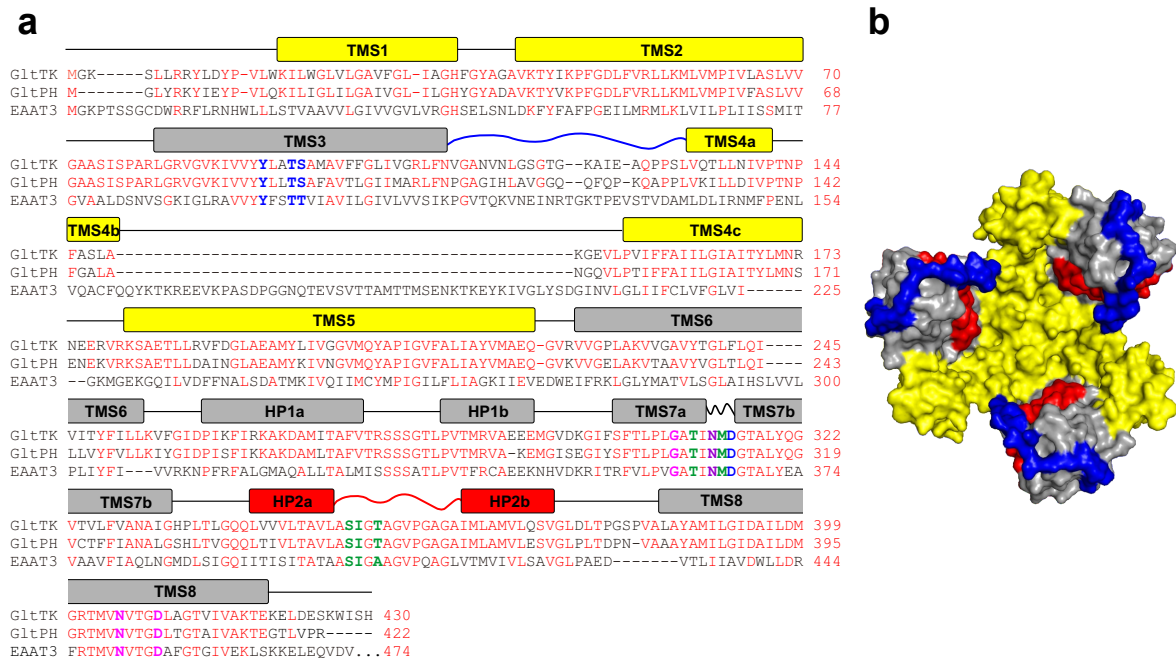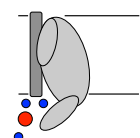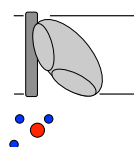
**Table 5.1) Data collection and refinement statistics.**

|  | $\text{Glt}_{\text{Tk}}^{\text{apo}}$ | $\text{Glt}_{\text{Tk}}^{\text{sub}}$ |
|---|---|---|
| **Data collection** |  |  |
| Space group | P3221 |  |
| Cell dimensions |  |  |
| $a, b, c$ (Å) | 116.0, 116.01, 308.5 |  |
| $\alpha, \beta, \gamma$ (°) | 90.00, 90.00, 120.00 |  |
| Resolution (Å) | 47.7 – 2.7 (2.78-2.7)* | 48.4 – 2.8 (2.87 – 2.8)* |
| $R_{mean}$ | 0.06 (0.74) | 0.07 (0.98) |
| $CC_{1/2}$ | 99.6 (36.0) | 99.8 (22.1) |
| $I/\sigma I$ | 11 (2.49) | 9.3 (1.3) |
| Completeness (%) | 79 (17.9) | 97.5 (96.0) |
| Redundancy | 3.4 | 3 |
|  |  |  |
| **Refinement** |  |  |
| Resolution (Å) | 2.7 | 2.8 |
| No. of reflections | 52,820 | 60,568 |
| $R_{work}$/ $R_{free}$ (%) | 19.8/ 23.7 | 21.3/ 24.3 |
| No. of atoms |  |  |
| Protein | 9,638 | 9,570 |
| PEG/ detergent | 278/ 40 | 508/ 99 |
| Ligand/ ion | - | 27/ 9 |
| Water | 60 | - |
| $B$-factors |  |  |
| Protein | 77.6 | 96.5 |
| PEG/ detergent | 114/ 132 | 118.4/ 137.7 |
| Ligand/ ion | - | 77.6/ 76.1 |
| Water | 69.9 | - |
| RMS deviations |  |  |
| Bond lengths (Å) | 0.008 | 0.008 |
| Bond angles (°) | 1.123 | 1.131 |

* Values in parentheses are for the highest-resolution shell.

RMS: Root-Mean-Square

*The third sodium binding site*

The third binding site is located between the unwound central region of helix 7 containing the essentially conserved NMDGT motif and TMS3, at a distance of ~8 Å from Na1, from which it is shielded by the side chain of N313 (figure 5.2 c). Na3 is coordinated by hydroxyl groups of T94 (T92 in Glt$_{Ph}$, T101 in EAAT3$_{rat}$) and S95 (S93 in Glt$_{Ph}$, T102 in EAAT3$_{rat}$) from TMS3; the carboxamide group of conserved N313 (N310 in Glt$_{Ph}$, N365 in EAAT3$_{rat}$); the side-chain carboxyl of D315 (D312 in Glt$_{Ph}$, D367 in EAAT3$_{rat}$); and the main chain carbonyl of Y91 (figure 5.2 and supplementary figure S5.3). The location of the third sodium binding site matches well with the site predicted in one of the published molecular dynamics simulations on Glt$_{Ph}$[148], and with mutagenesis studies on mammalian transporters[139,148,153,150,233].
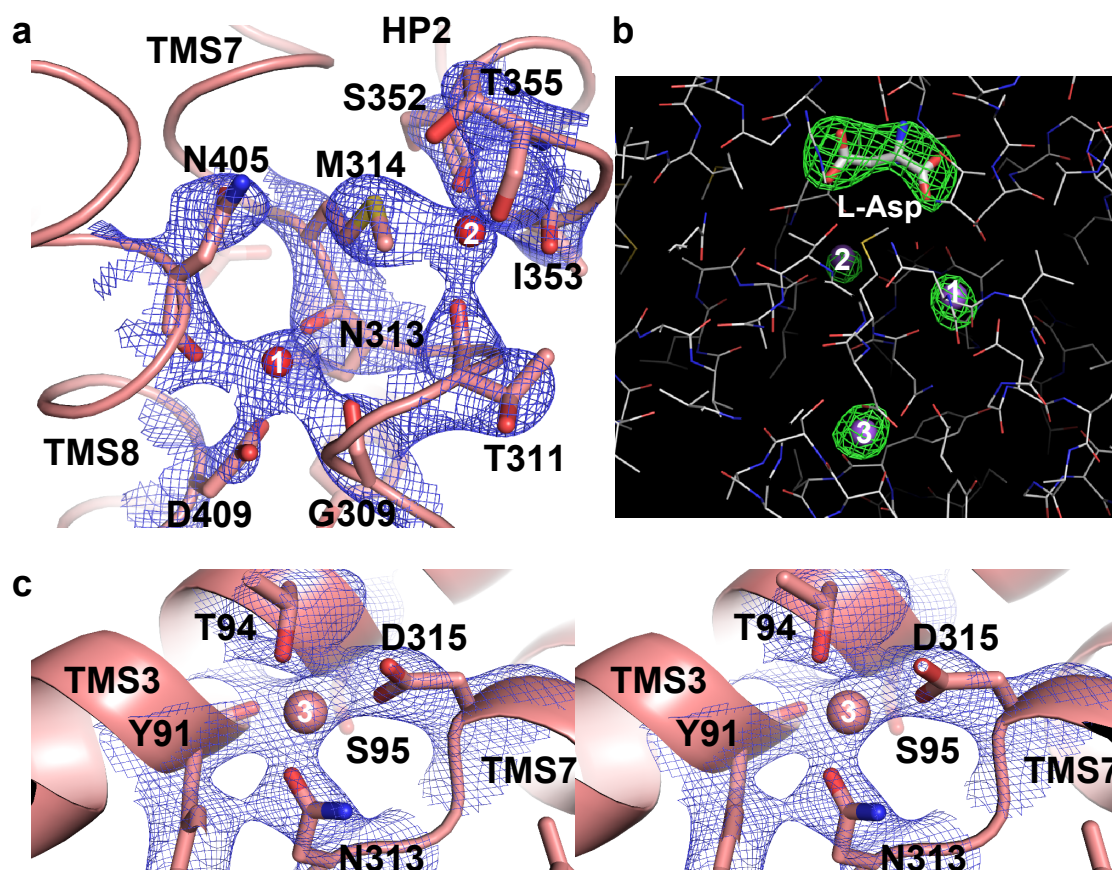


**Figure 5.2) Structure of Glt$_{Tk}$$^{sub}$ sodium binding sites. (a)** Sodium binding sites Na1 and Na2. The residues forming the sites are shown as sticks, sodium ions as spheres. The $2 F_o - F_c$ electron density is shown as blue mesh at 3 σ. **(b)** Composite omit map (simulated annealing protocol) for the substrates L-Asp (in stick presentation) and sodium ions (purple spheres), contoured at 3.5 σ. **(c)** Stereo-view of the Na3 site, depicted as in (a).

Of the three sodium ions, the interaction distances are the shortest for the third ion (~2.2–2.4 Å compared with ~2.5–2.7 Å for Na1 and Na2), which might indicate tighter binding of Na3 (supplementary table S5.1). Free energy calculations indeed show that sodium binds more tightly to Na3 than to the two other sites (supplementary table S5.2 and ref. 122). The higher binding affinity may explain why thallium could not replace sodium in the heavy-atom soaking experiment in $Glt_{Ph}$[69]. Moreover, the observed interaction distances for Na1 and Na2 are more similar to those typical for potassium ions, and $Tl^+$ is a very good mimic for $K^+$. It is also possible that steric hindrance prevented the larger $Tl^+$ ion (ionic radius of 1.64 Å versus 1.16 Å for $Na^+$) to enter the binding area for Na3.

*Interactivity between binding of sodium ions and aspartate*

The affinity of $Glt_{Ph}$ and $Glt_{Tk}$ for aspartate is strongly dependent on the sodium concentration[69,71,192] (chapter 2 and 3). In the mammalian transporters similar cooperativity between sodium and glutamate has been observed. In addition, sodium binding to $Glt_{Ph}$ in the absence of aspartate is also highly cooperative[192,210]. The structures of ligand loaded $Glt_{Tk}^{sub}$ and a new structure at 2.7 Å resolution of $Glt_{Tk}^{apo}$ provide a structural explanation for these observations. The most prominent difference between the two structures is the conformation of the conserved NMDGT motif in the central unwound region of TMS7 (figure 5.4 a), which is exemplified by the striking relocation of M314 from a position exposed to the lipid bilayer in the *apo*-state to the position as a ligand of Na2 in the substrate-bound state (figure 5.4 a and c). Sodium binding to N313 plays a crucial role in stabilizing the repositioned NMDGT region. The side-chain of N313 coordinates Na3, while its main chain carbonyl binds Na1 (figure 5.4 b and supplementary figure S5.3). Binding of one sodium ion repositions N313, which at the same time optimizes the geometry of the other sodium site, in line with the observed cooperativity in sodium binding.

In the repositioned NMDGT region of $Glt_{Tk}^{sub}$ G316 and T317 are located closer to TMS8 than in $Glt_{Tk}^{apo}$. The position of G316 is stabilized by a hydrogen bond to the side chain carboxamide of N405 in TMS8, which in turn binds Na1 via its backbone carbonyl, again contributing to the strong coupling between the movement of the NMDGT region and sodium binding. The movement places T317 in an optimal position for aspartate binding, which provides a structural explanation for cooperativity between $Na^+$ and aspartate

binding. In addition, the movement of T317 forces the side chain of R401 to reorient,
which creates space for aspartate binding, and places the guanidium group in an optimal
orientation to interact with the β-carboxylate of aspartate. In this way sodium binding
events in sites Na1 and Na3 not only interlink with each other, but also strongly affect the
affinity for aspartate. This coupling is further reinforced because binding of sodium to the
Na3 site leads to a movement of TMS3 (which contains three of the Na3 binding residues)
towards TMS7, thereby pushing T317 towards the aspartate binding position (figure 5.4 a).



**Figure 5.3) Mechanism of sodium-aspartate coupling. (a)** Superposition of $Glt_{Tk}^{sub}$ (yellow) and $Glt_{Tk}^{apo}$
(gray). Bound L-Asp is shown as blue sticks and sodium ions as purple spheres. Arrows represent the
movements during transition from the *apo* to the substrate-bound state. Note that parts of the protein, which
are not directly involved in substrate binding (for example, TMS2 and TMS5) do not undergo any noticeable
changes. **(b)** Interaction network between L-Asp (blue sticks) and sodium ions (purple spheres) mediated by
N313, M314, and N405 (in sticks); distances are given in Å (also see supplementary figure S5.3). **(c)** M314
in substrate-bound and substrate-free states with $2 F_o – F_c$ electron density countered at 3 σ (left) and without
density (right). In the *apo*-state two alternative conformations of the side chain are resolved, consistent with
the proposed inherent mobility of this residue.

After binding of Na1, Na3 and aspartate, Na2 is likely the last ion to bind[69,149,210]. The binding of Na2 is coupled to binding of the other two sodium ions and aspartate by the positioning of M314 at the center of the triangle formed by aspartate, Na1 and Na2 (figure 5.4 b), and by the conformation of the tip of HP2, which interacts both with aspartate and with Na2. Only after binding of Na2 can the transport domain reorient to the inward-facing state, because Na2 binding closes the gate formed by the tip of HP2. MD simulations indeed show that the tip of HP2 is one of the most flexible regions of the protein, and that Na2 relatively easily leaves this site (figure 5.4 and supplementary note 1).



**Figure 5.4) HP2 displays enhanced local flexibility.** Comparison of the protein atomic fluctuations averaged per residue in the presence/absence of the ligands in the binding site. Data was averaged from 100 ns during the MD simulations. The HP2 residues (in orange) involved in the gate opening showed enhanced local flexibility without the ligands (see also supplementary figure S5.5 for RMSD values of the backbone). The sequence indicates the amino acid residue of the protein; RMSF: Root-Mean-Square Fluctuation; RMSD: Root-Mean-Square Deviation.

## Discussion

The crystal structures and MD simulations presented here provide insight in the coupled binding of three sodium ions and aspartate. The work is fully consistent with a model for transport in which the cooperative binding of two sodium ions (Na1 and Na3) is followed by aspartate binding and finally binding of Na2. The order in which Na1 and Na3 bind may depend on an obligatory route of sodium ions from the Na1 site to the Na3 site[149]. The postulation of an obligatory route was based on the structure of substrate-bound Glt$_{Ph}$, which showed that the Na3 site could be accessed only via the cavity of the Na1 site. Because the affinity of the Na3 site is higher than that of the Na1 site, the Na3 site would fill up before the Na1 site. Our data are consistent with this binding order, but comparison of the substrate-bound structure with that of the *apo*-protein (which was not available at the time of the previous simulations) suggests that substantial conformational changes in the NMDGT region must take place upon sodium binding. Neither the Na1 nor the Na3 site is fully formed in the *apo*-state, and it is possible that an alternative access pathway may open upon repositioning of the NMDGT region and movements of the tip of HP2. In that case a random order of the binding of Na1 and Na3 may occur. Further simulations and experiments could clarify the issue. Finally, although the binding of three sodium ions to the sites identified here leads to a stable, crystallizable state, it is possible that also transient binding sites exist, which are briefly occupied while the Na$^+$ ions are en-route to their most stable positions[146].

## Methods

*Protein expression and purification*

*E. coli* MC1061 cells containing a pBAD24 derived plasmid for production of C-terminally His8-tagged Glt$_{Tk}$ were cultivated in LB medium (37 °C and 200 rpm), and expression was induced at an OD$_{600}$ of 0.8 with 0.05% L-arabinose for a period of 3 h. Harvesting, membrane vesicle preparation, determination of total protein concentration, and solubilization in n-Dodecyl-β-D-Maltopyranoside was done as described before[128]. To obtain *apo*-Glt$_{Tk}$ we omitted Na$^+$ from all buffers. After solubilization the solution was centrifuged for 30 min. at 4 °C, 265,000 g. The supernatant was incubated for 1 h on a rotating platform at 4 °C with Ni-Sepharose (GE Healthcare, 0.5 mL bed volume) pre-
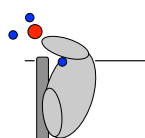
*Chapter 5*

equilibrated with 50 mM Tris HCl pH 8, 300 mM KCl, 0.15% n-Decyl-β-D-Maltopyranoside (DM), 15 mM Imidazole pH 8. The slurry was poured into a Poly-Prep chromatography column (BioRad), and washed with 10 mL of 50 mM Tris HCl pH 8, 300 mM KCl, 0.15% DM, 60 mM Imidazole pH 8. $Glt_{Tk}$ was eluted with 50 mM Tris HCl pH 8, 300 mM KCl, 0.15% DM, 500 mM Imidazole pH 8, and further purified by size exclusion chromatography (SEC) on a Superdex 200 10/300 GL column (GE Healthcare) equilibrated with buffer containing 10 mM Hepes KOH pH 8, 100 mM KCl, 0.15% DM. After purification the protein concentration was determined by UV absorption (NanoDrop), using the molecular weight and extinction coefficient calculated by the Expasy Protparam tool (web.expasy.org/protparam/). The protein was concentrated to ~7 mg/mL using a spin concentrator (Vivaspin 2, 30,000 MWCO, PES membrane, Vivaproducts). For purification of the substrate-loaded protein solubilization and purification buffers contained 300 mM $Na^+$ instead of $K^+$, and were supplemented with 10 μM L-aspartate.

*Isothermal titration calorimetry (ITC)*

ITC experiments were performed at a constant temperature of 25 °C using an iTC200 calorimeter (MicroCal). L-aspartate (dissolved in buffer containing 10 mM Hepes KOH pH 8, 100 mM KCl, 0.15% DM and indicated sodium concentrations) was titrated into a thermally equilibrated ITC cell filled with 250 μL of 3–20 μM $Glt_{Tk}$, dissolved in the same buffer. Data were analyzed using the ORIGIN-based software provided by MicroCal.

*Crystallization, data collection and structure determination*

Crystals of $Glt_{Tk}^{apo}$ and $Glt_{Tk}^{sub}$ were obtained by vapour diffusion technique (hanging drop) with the following conditions: 25% glycerol/PEG 4000, 100 mM Tris/Bicine pH 8.5, 60 mM $CaCl_2$/$MgCl_2$, 0.75–1% n-octyl-β-D-glucopyranoside (OG) and 20% PEG 400, 3% Xylitol, 50 mM $MgCl_2$, 150 mM NaCl, 100 mM Glycine pH 9 and 25% glycerol/PEG 4000, 100 mM Tris/Bicine pH 8.5, 60 mM $CaCl_2$/$MgCl_2$, respectively. Crystals were flash-frozen in liquid nitrogen, cryo-protected with Paraton-N and brought to the synchrotron for analysis. Data were collected at beam line X06SA (SLS, Villigen). In addition, we made many attempts to perform anomalous diffraction experiments via crystal soaking or co-crystallization with thallium salts but did not yield any useful results. Crystals of $Glt_{Tk}^{apo}$ and $Glt_{Tk}^{sub}$ diffracted up to 2.5 Å and 2.6 Å resolution; for $Glt_{Tk}^{apo}$ it was not possible to collect a fully complete dataset (overall completeness was 79%, see table 5.1). Data were

processed with XDS[227], and the structures were solved by Molecular Replacement with Phaser[234] using the previously published model of Glt$_{Tk}$ (PDB code 4KY0)[71]. Manual rebuilding was done with Coot[229] and refinement with Phenix refine[235]. Refined models were deposited into the PDB repository with the following IDs: 5DWY for Glt$_{Tk}$$^{apo}$ and 5E9S for Glt$_{Tk}$$^{sub}$, respectively. Images were prepared using Pymol[83] and LigPlot$^+$[236].

*Molecular dynamics simulations*

Two systems were simulated to assess the influence of the ligands in the dynamics of Glt$_{Tk}$: the holo system, which contained three sodium ions and aspartate in the binding site, and the same system, from which the ions and aspartate had been omitted. Atomistic MD simulations were carried out using the crystallographic model of Glt$_{Tk}$ (PDB code 4KY0)[71] embedded in a lipid membrane with explicit solvent. To this purpose we used the CHARMM Membrane Builder[237] and converted to Lipid14 PDB format[238]. Each of the original crystal structures was embedded in a lipid bilayer composed of 250 1- palmitoyl-2-oleoylphosphatidylcholine (POPC) lipids, solvated in aqueous solution with TIP3P water molecules[239] and 150 mM NaCl. The simulation systems contained a total of ~170,000 atoms. After the initial preparation, the systems were minimized and equilibrated as explained elsewhere[238]. After minimization, coordinates of the protein and ligands were fixed (10 kcal mol Å$^{-2}$) to allow for equilibration of the water and lipid densities, while increasing the temperature up to 303 K. In a second equilibration phase, the systems were relaxed without restraints for 20 ns. MD simulations were run with AMBER 14[240] (http://ambermd.org/) for another 80 ns using the NPT ensemble (1 atm, 303 K) with periodic boundary conditions and the Langevin thermostat.

*Free energy calculations*

We calculated the relative binding free energy of sodium ions at the Na1, Na2 and Na3 binding sites. In the case of Na1, we considered both: the case where no other ions were bound, and the case with the Na3 site already filled. For Na2, assumed to be the last site occupied, all other ligands were included in their binding sites (supplementary table S5.2).

The standard binding free energy can be decomposed as a sum of the translocation and translational free energy contributions:
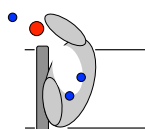
$$\Delta G_b = \Delta\Delta G_{int} + \Delta G_{tr} \tag{1}$$
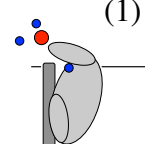
where the first term represents the contribution due to the difference in interaction energy of the ligand upon translocation from the bulk to the binding site while the second term represents the change in the translational energy upon binding. The latter is associated to the local fluctuations of the unrestrained $Na^+$ bound in the binding site[122,148,241], and was computed according to Heinzelmann et al.[122]. The first term, the free energy of translocation, is calculated using thermodynamic integration (TI) by transforming the bound $Na^+$ ion into a water molecule while transforming another water molecule into a $Na^+$ ion in the bulk. The transformation is done in three steps: first a decharging step, then a change in van der Waals and bonded interactions, and finally a recharging step. For each step, we used 11 values ($\lambda$) of l to go from 0 to 1 by increments of 0.1. Both a forward and a backward transformation were performed. At each l window, the system was first equilibrated for 0.5 ns and sampled for 1 ns. In all cases, the last snapshot of the unrestrained MD equilibration process was used as initial coordinates for the TI calculations. Calculation of the free energy can run into convergence issues unless the ligand is restrained to the protein through anchoring atoms in the binding site. We therefore used harmonic distance restraints between the sodium ion and the surrounding protein residues in the binding site. We verified that the effect of these conformational restraints was negligible (in the case of the Na1 and Na3 binding sites around 0.003 kcal/mol, and around 0.60 kcal/mol for the Na2 binding site). The convergence of the calculations was assessed by monitoring the cumulative averages of the free energy differences (supplementary figure 5.4). Given the smooth curves obtained, the free energy change associated to the transformation was calculated using the trapezoidal rule. Translocation free energies were calculated by averaging the values of the forward and backward transformations.

*Data availability*

All relevant data is available from the corresponding author upon reasonable request. The coordinates of the refined models and structure factors have been deposited into the PDB repository under: 5DWY for $Glt_{Tk}{}^{apo}$ and 5E9S for $Glt_{Tk}{}^{sub}$. The $Glt_{Tk}{}^{apo}$ structure (PDB code 4KY0)[71] was used as a molecular replacement model and for MD simulations.
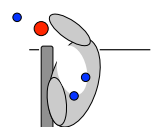
## Acknowledgments

## Author contributions

All authors designed experiments and simulations, analyzed data and wrote the manuscript, A.G. and S.J. performed experiments, I.F. performed simulations.

*Chapter 5*

# Appendix to chapter 5

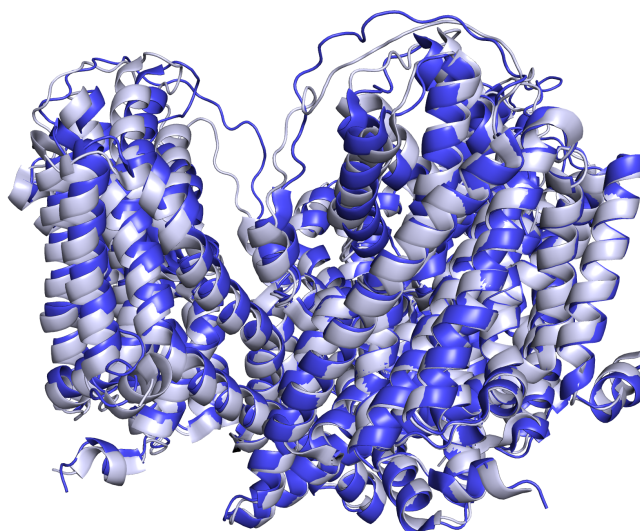## Supplementary Figures



**Figure S5.1) Superposition of Glt$_{Tk}^{sub}$ and Glt$_{Tk}^{apo}$.** Both structures represent the outward-facing conformation; Glt$_{Tk}^{sub}$ is shown in blue and Glt$_{Tk}^{apo}$ in light blue.
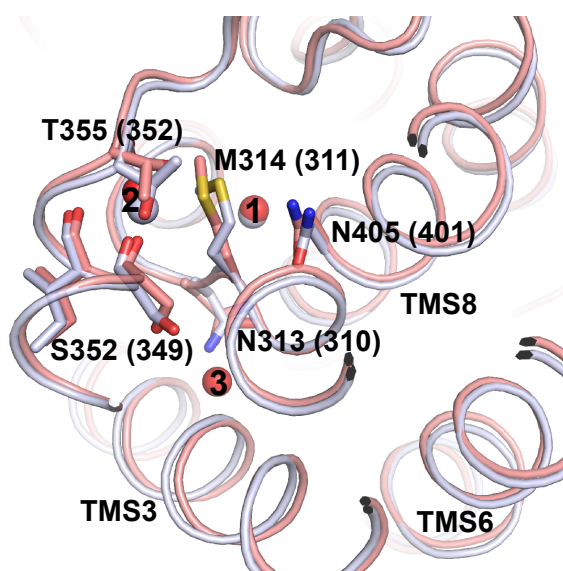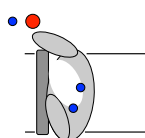


**Figure S5.2) Superposition of the sodium binding sites of Glt$_{Tk}^{sub}$ with Tl$^+$-bound Glt$_{Ph}$.** Glt$_{Tk}^{sub}$ presented in red and Tl$^+$-bound Glt$_{Ph}$ in gray (PDB code 2NWX)[69]. Binding sites for sodium and thallium numbered 1 to 3. Sites 1 and 2 are nearly identical in the substrate-loaded structures of Glt$_{Tk}$ and Glt$_{Ph}$; position 3 is observed only with sodium (this study).
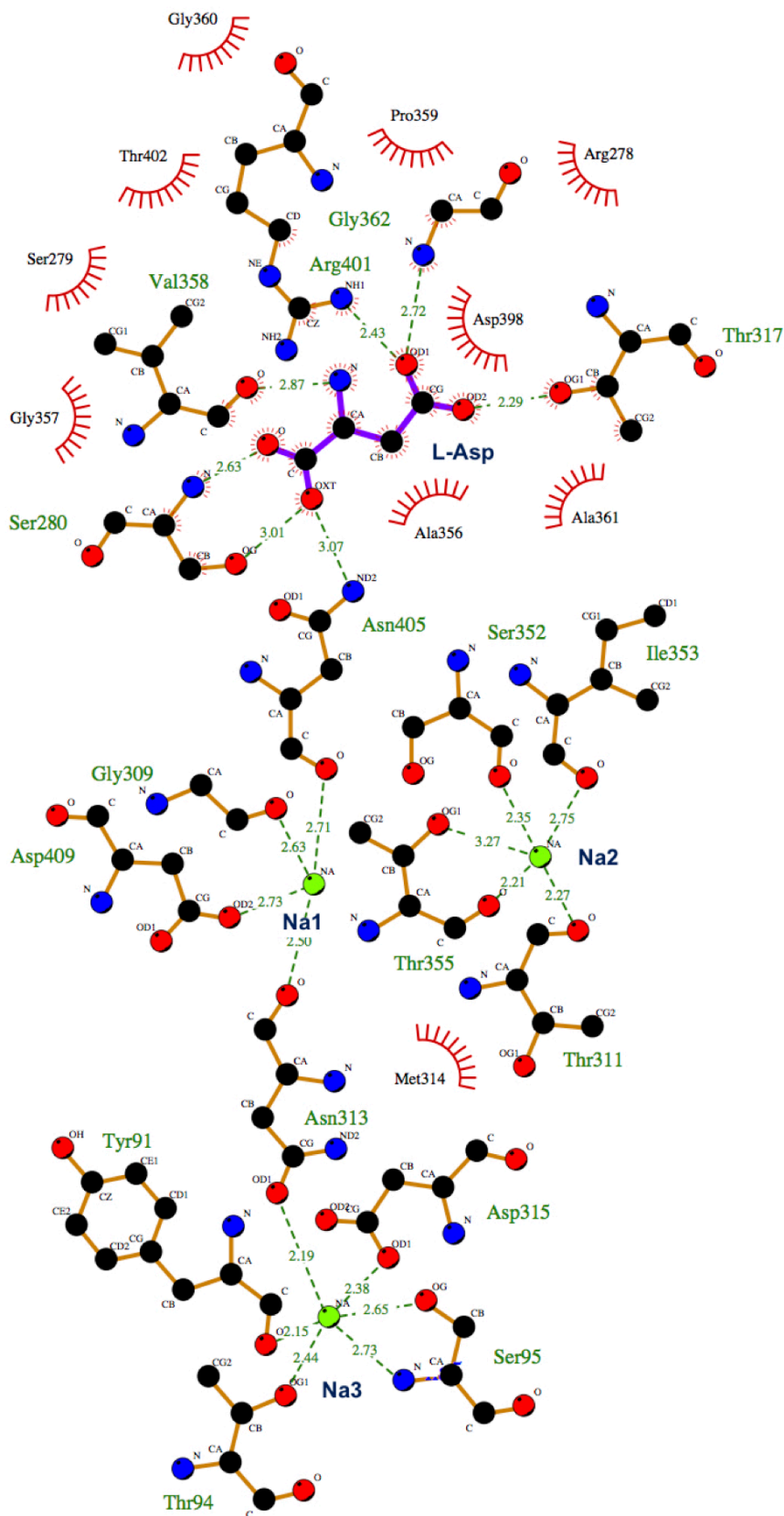
**Figure S5.3) Schematic representation of protein interactions with the ligands bound to Glt$_{Tk}$.** L-Asp is presented in purple, sodium ions (Na1-3) are shown in green. All distances in Å. Note the coupling between Na3, N313, Na1, N405, and L-Asp. Image was generated with LigPlot+[236].
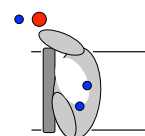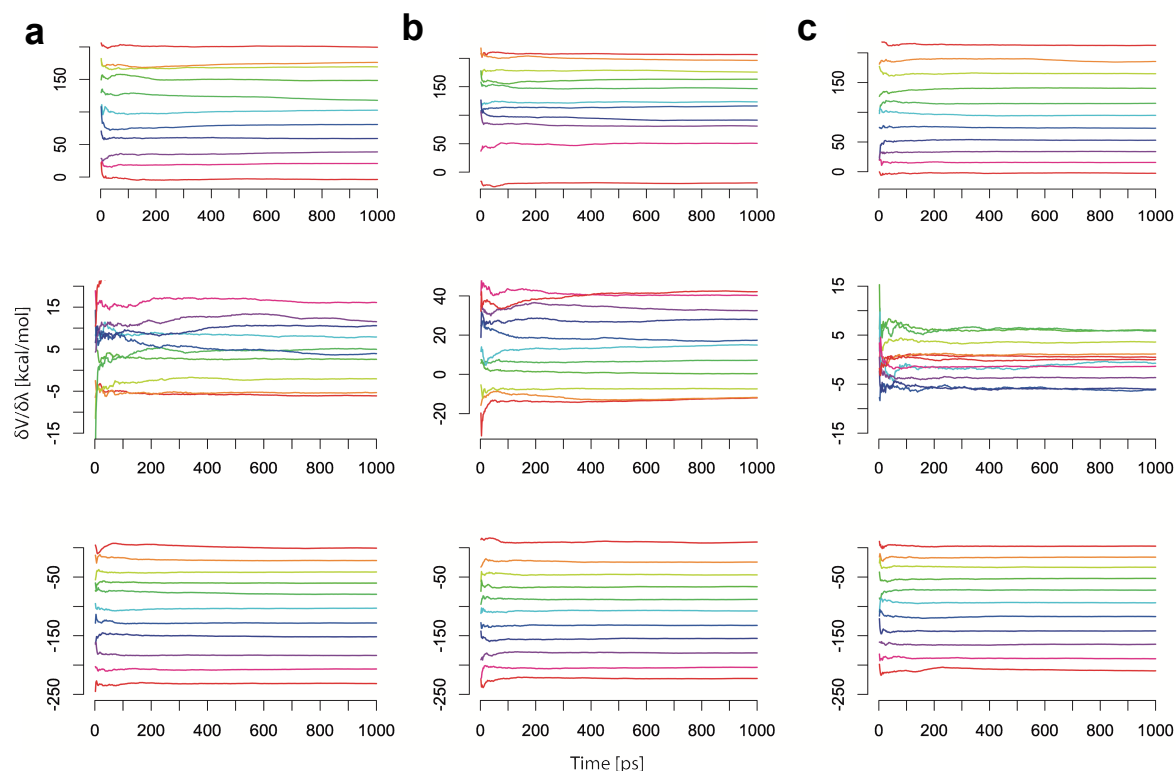
**Figure S5.4) Convergence analysis of the forward MD/TI calculations over time.** The values correspond to the time evolution of the cumulative $\delta V/\delta \lambda$ averages. Interaction free energy of Na2 **(a)** and Na3 **(b)** in the complex. **(c)** Interaction free energies for the Na$^+$ → H2O transformation in the bulk. Panels from top to bottom: discharging, van der Waals, and recharging transformations. Different colors stand for the eleven intermediate λ value.
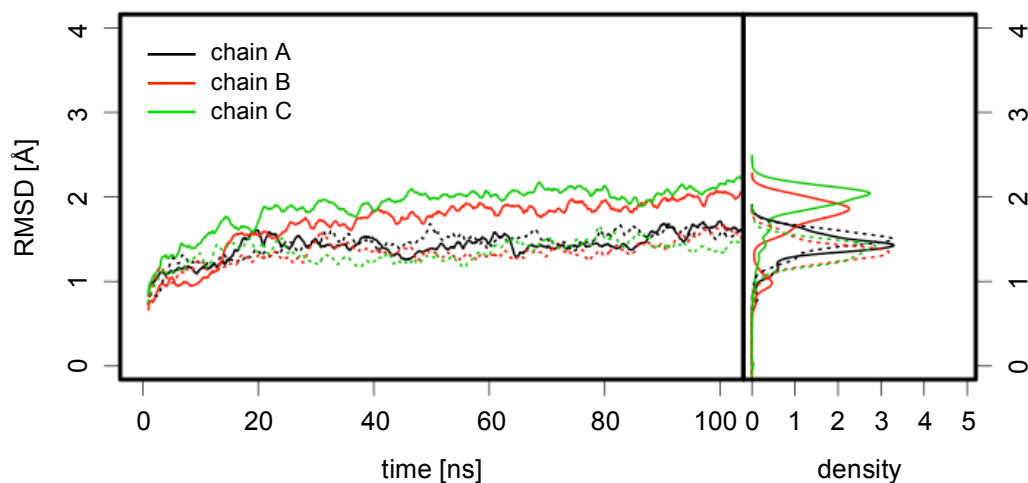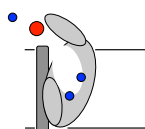


**Figure S5.5) RMSD of the protein backbone (Cα, N, O) during 100 ns of simulation for each monomer in the presence (solid lines) and absence (dashed lines) of ligands.** The systems showed no large conformational changes after 20 ns, which indicates that the models were stable on these time scales.

**Supplementary note 1**

*Impact of the ligands in the dynamics around the HP2 region*

The presence or absence of ligands in the binding site of Glt$_{Tk}$ showed differences at the local level. In these simulations where no restraints were applied, the average RMS values associated to the protein backbone were on the order of 2.0-3.1 Å and in general the presence/absence of the ligands has little effect at the global level (supplementary figure S5.5). However, as anticipated from previous studies[122,148], the absence of ligands in the binding site enhanced the fluctuations around the HP2 region as shown by the analysis of the protein residue fluctuations (figure 5.4). The relationship between the dynamics of the binding site and the HP2 hairpin was further supported by the rapid destabilization of Na2 in monomer B during the equilibration process.

In contrast to the less stable Na2 site, Na1 and Na3 are tightly bound within their binding sites. Five atoms coordinate the sodium ion in Na1, while 6 atoms coordinate the ion in the Na3 site. The ion-ligand distances for the Na1 and Na3 sites observed in this and other available crystal structures of aspartate transporter were maintained along the whole trajectory (supplementary table S5.1). Even in the absence of the Na$^+$ ion in the Na2 site of monomer B, the Na$^+$ coordination number and stability in the Na1 and Na3 sites were almost identical to the other two monomers (supplementary table S5.1), which indicates that the opening of the HP2 gate has a small impact on the Na1 and Na3 sites.

*Binding free energies*

Free energy differences were calculated for Na1, Na2, and Na3 binding sites. Relative Na$^+$ binding free energies revealed that the Na3 site is the most stable site. As shown in supplementary table S5.2, the free energy difference associated to the loss of translational entropy was similar for all Na$^+$ sites being around 5.0-5.3 kcal/mol. More importantly, the binding free energy of the Na3 site is -18 kcal/mol, implicating a strong binding site, whereas binding to the Na2 site is only weak at most (the affinity for water is actually larger, at least in the case we studied where all other sites are occupied). The explanation to this difference can be attributed to the higher coordination number for the Na$^+$ ion in the Na3 site (the Na$^+$ ion in Na2 site has one coordination atom less compared to the Na3 site) and also to the higher fluctuations of residues surrounding the Na2 site that are part of the
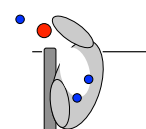
flexible HP2 hairpin. The Na1 site is also more stable than the Na2 site, but less stable compared to the Na3 site by about 7 kcal/mol. Note that the stability of the Na1 site is reduced when the Na3 site is already occupied, likely due to electrostatic repulsion between the bound ions. Although free energy calculations are very sensitive to the structure, simulation conditions and force field parameters, they provide useful information about the relative preference among the $Na^+$ sites. Our results, which are in the same line as previous free energy calculations[122,148], support the binding mechanism in which the Na2 site is the last to be filled during the extracellular half-cycle of glutamate/aspartate co-transport.

**Table S5.1) List of protein residues coordinating the three sodium ions in each monomer.**

|     |            | Monomer A |           | Monomer B |           | Monomer C |           |
|-----|------------|-----------|-----------|-----------|-----------|-----------|-----------|
|     |            | crystal   | MD        | crystal   | MD        | crystal   | MD        |
| **Na1** | Asn313 (O) | 2.4 | $2.4 \pm 0.1$ | 2.4 | $2.4 \pm 0.1$ | 2.6 | $2.5 \pm 0.2$ |
|     | Gly309 (O) | 2.5 | $2.4 \pm 0.1$ | 2.5 | $2.4 \pm 0.2$ | 2.6 | $2.5 \pm 0.2$ |
|     | Asn405 (O) | 2.5 | $2.4 \pm 0.2$ | 2.6 | $2.4 \pm 0.2$ | 2.5 | $7.2 \pm 0.3$ |
|     | Asp409 ($O_1$) | 2.8 | $2.3 \pm 0.1$ | 2.7 | $2.3 \pm 0.1$ | 2.7 | $2.3 \pm 0.1$ |
|     | Asp409 ($O_2$) | 2.7 | $2.3 \pm 0.1$ | 2.6 | $2.3 \pm 0.1$ | 2.6 | $2.4 \pm 0.1$ |
| **Na2** | Thr311 (O) | 2.3 | $2.4 \pm 0.2$ | 2.3 | (1) | 2.4 | $4.5 \pm 0.9$ |
|     | Met314 (O) | 2.8 | $5.2 \pm 0.4$ | 3.1 | (1) | 2.9 | $4.5 \pm 0.9$ |
|     | Ser352 (O) | 2.2 | $3.2 \pm 0.4$ | 2.4 | (1) | 2.2 | $4.6 \pm 0.4$ |
|     | Ile353 (O) | 2.5 | $2.4 \pm 0.2$ | 2.6 | (1) | 2.6 | $4.3 \pm 0.7$ |
|     | Thr355 (O) | 2.2 | $2.4 \pm 0.2$ | 2.3 | (1) | 2.1 | $2.5 \pm 0.3$ |
| **Na3** | Tyr91 (O) | 2.1 | $2.4 \pm 0.2$ | 2.2 | $2.4 \pm 0.1$ | 2.2 | $2.4 \pm 0.1$ |
|     | Thr94 (OG1) | 2.2 | $2.4 \pm 0.1$ | 2.4 | $2.4 \pm 0.1$ | 2.3 | $2.4 \pm 0.1$ |
|     | Ser95 (OG) | 2.6 | $2.8 \pm 0.4$ | 2.5 | $2.8 \pm 0.3$ | 2.4 | $2.8 \pm 0.4$ |
|     | Ser95 (N) | 2.2 | $3.0 \pm 0.2$ | 2.4 | $3.0 \pm 0.2$ | 2.5 | $3.0 \pm 0.2$ |
|     | Asn313 ($O_1$) | 2.7 | $2.3 \pm 0.1$ | 2.4 | $2.3 \pm 0.1$ | 2.3 | $2.3 \pm 0.1$ |
|     | Asp315 ($O_1$) | 2.0 | $2.3 \pm 0.3$ | 2.3 | $2.3 \pm 0.2$ | 2.3 | $2.4 \pm 0.3$ |

Average $Na^+$-O distances (in Å) obtained from 100 ns MD simulation. Values from MD simulation were compared with the distances in the crystallographic model. (1) No data was available for $Na^+$ ion in Na2 in monomer B since this left spontaneously the binding site.
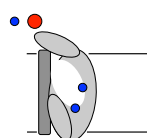
**Table S5.2) Binding free energies ($\Delta G_b$ in kcal/mol) for the sodium ions in Na1, Na2, and Na3 sites in the presence/absence of other ligands.**

|  | $-\Delta\Delta G_{int}$ (fwd) | $\Delta\Delta G_{int}$ (bwd) | $\Delta G_{tr}$ | $\Delta G_b$ |
|---|---|---|---|---|
| **Na2 (Na1, Na3, Asp)** | $1.3 \pm 3.6$ | $-4.3 \pm 3.6$ | 5.0 | $3.7 \pm 5.1$ |
| **Na3** | $-26.8 \pm 3.6$ | $-19.8 \pm 3.6$ | 5.3 | $-18.0 \pm 5.1$ |
| **Na1** | $-16.1 \pm 3.7$ | $-15.5 \pm 3.7$ | 5.1 | $-10.7 \pm 5.2$ |
| **Na1 (Na3)** | $-7.6 \pm 3.6$ | $-8.1 \pm 3.7$ | 5.0 | $-2.9 \pm 5.2$ |

The presence of other ligands in the binding site is shown in parentheses. $\Delta G_b$ is obtained as the sum of the translocation free energy of the ion from the bulk to the binding site, $\Delta\Delta G_{int}$ (averaged between the forward (fwd) and backward (bwd) transformation), and the change in translational free energy upon binding, $\Delta G_{tr}$. Negative values correspond to a spontaneous $H_2O \rightarrow Na^+$ transformation. The differences in the forward and reverse calculations can be due to minor rearrangements in the binding sites during the transformation process. Errors represent standard errors, obtained from block averaging.
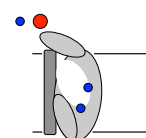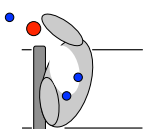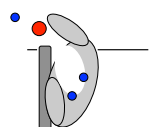
*Chapter 5*

# Chapter 6


## Summary, Conclusions, and Perspectives


**Sonja Jensen**

The smallest unit of all living organisms is the cell. Regardless of whether the cell belongs to an organism consisting of one or multiple cells, all cells are separated from their environment by at least one membrane. The membrane acts as barrier that shields the cell interior from the extracellular environment. In doing so, the membrane maintains the compositional integrity of the cell. However, in order to thrive, grow, and multiply cells have to take up nutrients, expel waste products, as well as sense and react on signals from the environment. This is facilitated by a great variety of membrane-associated proteins. Membrane transport proteins passively or actively move ions and molecules in and out of the cell. Chapter 1 provides a brief overview of membrane transport proteins (or transporters in short) with main focus on glutamate transporters and their homologs.

Glutamate transporters are secondary active transporters that couple the movement of negatively charged amino acids (glutamate and aspartate) to a pre-existing sodium and/or proton gradient[68,69,71,110–113,123–125]. The first chapter summarizes the current insights on substrate and cation binding and the transport mechanism of eukaryotic and prokaryotic glutamate transporters and glutamate transporter homologs and offers the framework of this thesis. Even though many functional and structural data on glutamate transporters was available by the start of my PhD project, crystal structures were available only for the glutamate transporter homolog $Glt_{Ph}$ from *Pyrococcus kodakarensis*. Additionally, all the crystal structures were in the substrate-loaded state. Therefore, it was unclear what the empty transporter would look like or how the protein would reorient after substrate delivery. Also, it was not clear yet how glutamate transporters coupled the translocation of substrate to the co-transport of ions, while avoiding ion or substrate leakage, especially since one of the sodium binding sites had not been unambiguously localized because structural information of sufficient quality was lacking[69,122,146,148,149]. This thesis focuses on how substrate and cation binding are linked in glutamate transporter homologs from Archaea. The data can be used to obtain better insight in other glutamate transporters, for instance the human ones. In this thesis biochemical methods and X-ray crystallography were combined to gain deeper insights into the mechanism of substrate and cation binding.

The best-studied and structurally characterized member of the glutamate transporter family is the sodium coupled aspartate transporter $Glt_{Ph}$. Tryptophan fluorescence based steady state and stopped-flow measurements on single tryptophan $Glt_{Ph}$ mutants (chapter 2) revealed that sodium binding is highly cooperative and precedes aspartate binding. Our
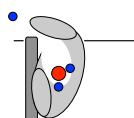
data show that at least two sodium ions bind in the absence of aspartate, whereas three sodium ions bind in the presence of aspartate[128] (chapter 3). The affinity for aspartate binding was dependent on the concentration of sodium. Vice versa the affinity for sodium binding was also increased in the presence of aspartate with aspartate pulling the transporter into the fully loaded state. The results show that, sodium and aspartate binding are mutually dependent in glutamate transporters. Additionally, the temperature dependence and derived high activation energy indicate that sodium binding to the *apo-transporter* is slow, of low affinity, and associated to relatively large structural rearrangements. Differently, aspartate binding in the presence of sodium was fast, of high affinity, and involved smaller conformational changes. This indicates that sodium binding is most likely the rate-limiting step during substrate binding.

The findings are well in-line with a binding mechanism in which two sodium ions bind prior to substrate binding with subsequent binding of the third sodium ion. Such a sequence of binding order was described for eukaryotic glutamate transporters[84,177] and has previously been proposed for $Glt_{Ph}$ by MD studies[92,122,149]. The study presented in chapter 2 confirms the binding of two sodium ions prior to aspartate binding but cannot exclude that all sodium ions (Na1-3) bind prior to aspartate binding.

In chapter 3 we used isothermal titration calorimetry and radiometric transport assays to biochemically analyze substrate binding to the archaeal aspartate transporter $Glt_{Tk}$ from *Thermoccoccus kodakarensis*. We found that $Glt_{Tk}$ is comparable to $Glt_{Ph}$ a sodium dependent aspartate transporter that binds at least three sodium ions together with one aspartate. The results show that $Glt_{Tk}$ and $Glt_{Ph}$ share not only a high sequence similarity (77% identity) but also the same cation and substrate preference. Additionally, all amino acid residues involved in substrate and cation binding are conserved in both transporters. This allows for direct comparison of the two transporters.

*The close proximity of substrate and cation binding sites links substrate and cation binding and is the key to productive binding and transport events*

Comparison of the crystal structures of $Glt_{Tk}$ in the substrate-free state (chapter 4) and fully loaded state (chapter 5) shows that none of the substrate or cation binding sites is present or fully formed in the unloaded transporter. Instead the functionally important residue R401[69,76,109,115,117] fills the space occupied by the substrate in the substrate-loaded structure[69]
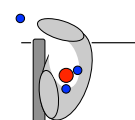
(chapter 5). As consequence of the conformation of R401 other residues involved in substrate and coupling ion coordination were relocated, resulting in disturbed substrate and sodium binding sites. The empty structure however, is as compact as the substrate-loaded transporter (chapter 4 and 5). This very likely enables the empty transporter to travel the membrane the same way as it does in the loaded state.

The structure of substrate and cation loaded $Glt_{Tk}$ (chapter 5), reveals the location of the substrate and all three sodium binding sites. In the structure substrate and coupling ions are bound in proximity to each other, although they do not directly interact. Binding of one sodium ion allosterically affects the binding sites of other sodium ions and the substrate binding site.
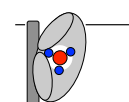
The crystal structures of substrate-free and substrate-loaded $Glt_{Tk}$ together with the functional data from chapter 1-3 indicate how the strict substrate and cation coupling of glutamate transporters is linked. Since none of the binding sites is (fully) formed in the unloaded state the first sodium ion binds with low affinity. The binding event repositions a conserved residue in TMS7 (N313, $Glt_{Tk}$ numbering), which coordinates Na3 and Na1 in the structure. Consequently repositioning of this residue aids in the creation of the next sodium binding site and further relocates the conserved NMDGT region of TMS7 that is involved in substrate and cation binding. This is in line with the observed cooperativity of sodium ion and substrate binding. The relocation of the NMDGT region also forces R401 to reorient and creates the space for aspartate binding. Further reorientations of amino acid residues in TMS3, TMS7, and TMS8 create the high affinity binding site for aspartate. Consistent with previous MD simulations[92,122] our MD studies suggest that Na2 binds as last sodium ion after substrate binding. Previous computational studies propose that binding of Na2 stabilizes the transporter in its loaded and occluded state[92], which allows the transporter to travel the membrane. Subsequently substrate and ions are released. Because Na2 is least stably bound with the weakest binding affinity amongst the coupling ions it likely leaves the binding site first. This in turn results in opening of the internal gate and subsequent exit of the substrate. As the substrate leaves the binding site R401 turns into the space previously occupied by the substrate. In consequence nearby amino acid residues in TMS3, TMS7 and TMS8 reorient, including those in the NMDGT region. This distorts all other sodium binding sites and results in the release of Na1 and Na3.
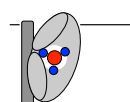
Thus the close proximity of all sodium binding sites and the substrate binding site allows for high cooperativity and coupling of substrate and coupling ions. While sodium binding is required for the creation of the substrate binding site, it is the substrate that closes the exterior gate, with another sodium ion stabilizing the occluded loaded state that is able to travel through the membrane. The combination of sodium-substrate-sodium binding shows how coupling is realized in glutamate transporters and how this coupling ensures productive transport without ion or substrate leakage.

*Substrate binding and transport speed is modulated by residues not directly involved in substrate and cation binding*

Chapter 1 summarizes some amino acid residues involved in substrate selectivity of glutamate transporters, with most of the residues being directly involved in substrate and cation coordination. In $Glt_{Tk}$ and $Glt_{Ph}$ all residues involved in substrate and cation binding are conserved, and the crystal structures of substrate-loaded and substrate-free $Glt_{Tk}$ and $Glt_{Ph}$ are merely identical. Therefore, slight differences in substrate spectrum and transport speed between both transporters suggest that also residues not directly involved in substrate and coupling ion coordination play a role in transporter functionality. While $Glt_{Ph}$ also binds serine, glutamate, and succinate with low affinity[69], $Glt_{Tk}$ binds none of these molecules but accepts the neutral amino acid asparagine as low affinity binder (chapter 3). Additionally, $Glt_{Tk}$ has a 20-fold lower affinity to aspartate than $Glt_{Ph}$, and the transport speed is three orders of magnitude higher in $Glt_{Tk}$ than in $Glt_{Ph}$. The slower uptake rate of $Glt_{Ph}$ might be related to the higher aspartate binding affinity with tight substrate binding and connected slower substrate release as suggested for the mammalian glutamate transporter EAAT5[188]. Another reason for the slow transport rates of $Glt_{Ph}$, compared to the mammalian transporters and $Glt_{Tk}$, was proposed by recent single molecule FRET studies[106]. Alanine mutations at position K290 and G221 in $Glt_{Ph}$ resulted in increased hydration of the transport and trimerization interface, and increased the mobility of the transport domain accompanied by increased uptake rates. Intriguingly, one of the mutated amino acids (K290 in $Glt_{Ph}$) is a glutamate in $Glt_{Tk}$ (E292). Whether enhanced hydration between trimerization and transport domain interface is the reason for faster transport in $Glt_{Tk}$ has to be elucidated by future mutational and computational studies.
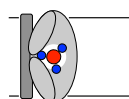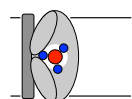
*Chapter 6*

*Perspectives*

This thesis answers some general questions on how substrate and cation binding are connected and was able to yield structures for the unloaded and substrate-loaded outward facing occluded states. The combination of all currently available functional, structural, and computational data of glutamate transporters resulted in a model of transport as described in chapter 1, figure 1.4. Yet not all states of the translocation cycle of glutamate transporters are structurally uncovered. Especially, high-resolution structures of new conformational states, such as partially sodium loaded or intermediate states, might reveal in which binding order all ligands (Na1, Na3, aspartate, and Na2 or Na3, Na1, aspartate, and Na2) bind. In order to identify the interior gate of glutamate transporters, it would be favorable to crystallize $Glt_{Tk}$ in a state with the interior gate opened. This could be accomplished by the use of substrate analogs, similar as reported for the co-crystallizsation of $Glt_{Ph}$ together with TBOA[69]. In the crystal structure TBOA arrested the exterior lid HP2 in open conformation, which therefore was able to be identified as exterior gate to the binding site[69]. The structures described in this thesis could serve as starting point for targeted drug design of suitable substrate analogs. Crystallization of $Glt_{Tk}$ in a lipidic environment using HILIDE[242] or lipidic cubic phase[243] might also yield novel conformations of the transporter.

Additionally, functional and structural data of other glutamate transporters or more distant family members as the neutral amino acid transporters and dicarboxylate transporters, are required to gain full insights into the determinants of substrate and cation selectivity and transporter functionality.

The content of this thesis concentrates on fundamental research. However, in the future better understanding of general functional, structural, and mechanistic properties of glutamate transporters might enable targeted drug design[244,245] to reduce or even prevent brain damage after ischemia[46,47]. During ischemia a lack of oxygen causes a change of the cation gradient over the membrane resulting in reversed functioning of glutamate transporters. Release of high concentrations of the neurotransmitter glutamate into the synaptic cleft then can lead to over-excitation of neurons resulting in cell death. The design of a small molecule that blocks the transporter might therefore prevent or reduce brain damage after ischemia. Additionally, better understanding of glutamate transporters also could foster drug development against symptoms of neurodegenerative diseases in which

malfunctioning of glutamate transporters seem to play a role, such as epilepsy, Huntington's, and Alzheimer's disease[48,56–58].
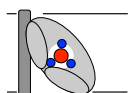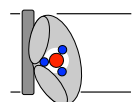
*Chapter 6*

# Chapter 7

## Nederlandse Samenvatting, Conclusies en Perspectieven

**Sonja Jensen**

De kleinste eenheid van alle levende organismen is de cel. Of deze cel nu alleen, of met meerdere cellen een organisme vormt, elke cel wordt door ten minste één membraan van zijn omgeving gescheiden. Dit membraan fungeert als een barrière die de inhoud van de cel van de extracellulaire omgeving afschermt. Op deze manier waarborgt de membraan de compositie en integriteit van de cel. Echter, om te gedijen, te groeien en te vermenigvuldigen, moet de cel voedingsstoffen opnemen, afvalproducten uitscheiden, en signalen uit de omgeving kunnen ontvangen en erop reageren. Dit wordt mogelijk gemaakt door een verscheidenheid aan membraan-geassocieerde eiwitten. Transporteiwitten in het membraan transporteren ionen en moleculen passief of actief in en uit de cel. Hoofdstuk 1 geeft een kort overzicht van de membraantransporteiwitten (of transporteurs in het kort), met de nadruk op glutamaattransporteurs en hun homologen.

Glutamaattransporteurs zijn secundair-actieve transporteurs die de beweging van negatief geladen aminozuren (glutamaat en aspartaat) koppelen aan een vooraf bestaande natrium- en/of protonen gradiënt[68,69,71,110–113,123–125]. Het eerste hoofdstuk geeft een overzicht van de huidige inzichten in het substraat- en kationbindingsmechanisme en het transportmechanisme van eukaryote en prokaryote glutamaattransporteurs en glutamaattransporteur homologen, en legt de fundering van dit proefschrift. Hoewel veel functionele en structurele informatie over glutamaattransporteurs voor het begin van mijn promotieonderzoek voorhanden was, waren kristalstructuren alleen beschikbaar voor de glutamaattransporteur homoloog Glt$_{Ph}$ van *Pyrococcus kodakarensis*. Bovendien waren alle beschikbare structuren in de substraatgebonden toestand. Hierdoor was het nog onduidelijk hoe de lege transporteur eruit zou zien en hoe de transporteur terug keert naar de andere kant van de membraan nadat het substraat getransporteerd en afgeleverd was. Ook was het niet duidelijk hoe glutamaattransporteurs de translocatie van het substraat koppelen aan het co-transport van ionen, terwijl tegelijkertijd lekkage van ionen of substraat vermeden wordt. Dit was voornamelijk een kwestie omdat, vanwege gebrek aan structurele informatie van voldoende hoge kwaliteit, één van de natriumbindingsplaatsen niet eenduidig gelokaliseerd was[69,122,146,148,149]. Dit proefschrift richt zich op hoe de binding van substraat en kationen met elkaar verbonden zijn in glutamaattransporteur homologen van archaea. De resultaten van het onderzoek aan deze homologen kunnen gebruikt worden om een beter inzicht in andere glutamaattransporteurs te verkrijgen, bijvoorbeeld de menselijke transporteurs. In dit proefschrift worden biochemische methoden en röntgenkristallografie
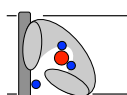
gecombineerd om meer inzicht te krijgen in het mechanisme van substraat- en kationenbinding.

Het best bestudeerde en structureel gekarakteriseerde lid van de glutamaattransporteur familie is de natrium:aspartaat transporteur Glt$_{Ph}$. Uit tryptofaan fluorescentie gebaseerde steady state en stopped-flow metingen aan Glt$_{Ph}$ mutanten die één enkele tryptofaan bevatten (hoofdstuk 2), is gebleken dat natriumbinding zeer coöperatief is en aan de binding van aspartaat voorafgaat. Onze gegevens tonen aan dat tenminste twee natriumionen in de afwezigheid van aspartaat binden, terwijl drie natriumionen in de aanwezigheid van aspartaat binden[128] (hoofdstuk 3). De affiniteit voor aspartaat was afhankelijk van de concentratie van de natriumionen. Omgekeerd was de affiniteit voor natrium ook verhoogd in de aanwezigheid van aspartaat, waarbij aspartaat de transporteur in de volledig geladen toestand trok. De resultaten tonen aan dat natrium- en aspartaatbinding in glutamaattransporteurs onderling afhankelijk zijn. Bovendien geven de temperatuurafhankelijkheid en de hiervan afgeleide hoge activeringsenergie aan dat natriumbinding aan de *apo*-transporteur langzaam en van lage affiniteit is, en vergezeld wordt door relatief grote structurele veranderingen. Daartegen is aspartaatbinding in aanwezigheid van natrium snel, van hoge affiniteit en zorgt het slechts voor kleine conformationele veranderingen. Dit geeft aan dat natriumbinding naar alle waarschijnlijkheid de snelheidsbeperkende stap is tijdens de substraatbinding.

Onze bevindingen kommen goed overeen met een bindingsmechanisme waarin eerst twee natriumionen binden voordat het substraat aspartaat bindt, gevolgd door de binding van het derde natriumion. Een dergelijke bindingsvolgorde werd eerder voor eukaryote glutamaattransporteurs beschreven[84,177], en was ook voor Glt$_{Ph}$ voorgesteld aan de hand van MD studies[92,122,149]. Het in hoofdstuk 2 beschreven onderzoek bevestigt de binding van twee natriumionen vóór aspartaatbinding, maar sluit niet uit dat alle natriumionen (Na1-3) binden voordat aspartaat bindt.

In hoofdstuk 3 hebben we gebruik gemaakt van isothermale titratie calorimetrie (ITC) en radiometrische transport assays om de substraatbinding in de archaeale aspartaattransporteur Glt$_{Tk}$ van *Thermoccoccus kodakarensis* biochemisch te karakteriseren. We vonden dat Glt$_{Tk}$, net als Glt$_{Ph}$, een natriumafhankelijk aspartaattransporteur is, die aspartaat samen met tenminste drie natriumionen bindt. De
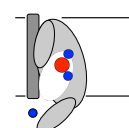
resultaten tonen aan dat Glt$_{Tk}$ en Glt$_{Ph}$ niet alleen een vergelijkbare aminozuursequentie hebben (77% identiek), maar ook dezelfde kation- en substraatvoorkeur. Daarnaast zijn in beide transporteurs alle aminozuren geconserveerd, die betrokken zijn bij de binding van het substraat en de kationen. Daarom is een directe vergelijking van Glt$_{Tk}$ en Glt$_{Ph}$ mogelijk.

*De dichte nabijheid van de substraat- en kationenbindingsplaatsen zorgt voor de koppeling van substraat- en kationbinding en is de sleutel voor een productieve stap in de transportcyclus*

Door de kristalstructuren van Glt$_{Tk}$ in substraat-vrije toestand (hoofdstuk 4) en volledig geladen toestand (hoofdstuk 5) met elkaar te vergelijken, is te zien dat geen van de substraat- of kationenbindingsplaatsen aanwezig of volledig gevormd is in de ongeladen transporteur. In plaats daarvan bezet het functioneel belangrijke residu R401[69,76,109,115,117] de ruimte die het substraat in de substraatgeladen structuur inneemt[69] (hoofdstuk 5). Als gevolg van deze conformatie die R401 aanneemt, zijn andere residuen die bij substraat- en natriumionencoördinatie betrokken zijn, verschoven. Dit betekent dat de substraat- en natriumbindingsplaatsen niet of niet volledig gevormd zijn. De ongeladen structuur is echter net zo compact als de substraatgeladen transporteur (hoofdstuk 4 en 5). Hierdoor kan de lege transporteur waarschijnlijk op dezelfde manier door de membraan reizen als in de geladen toestand.

De kristalstructuur van substraat- en kationgeladen Glt$_{Tk}$ (hoofdstuk 5) toont zowel de locatie van het substraat, als van alle drie natriumbindingsplaatsen. De structuur laat zien dat het substraat en de koppelingsionen zeer dicht bij  elkaar gebonden zitten. Dit maakt duidelijk waarom de binding van een natriumion allosterisch ook direct invloed heeft op de bindingsplaats van de andere natriumionen en de bindingsplaats van het substraat.

De kristalstructuren van substraat-vrij en substraatgeladen Glt$_{Tk}$ gecombineerd met de functionele data uit hoofdstuk 1-3 laten zien hoe de strikte koppeling van substraat en kationen tot stand komt. Aangezien in de ongeladen transporteur geen van de substraat- en natriumbindingsplaatsen (volledig) gevormd is, bindt het eerste natriumion met lage affiniteit. Deze natriumbinding leidt tot een conformationele verandering van een geconserveerd residu in TMS7 (N313, Glt$_{Tk}$ nummering). In de substraatgeladen structuur coördineert dit residu zowel Na3 als ook Na1. De conformationele verandering van dit
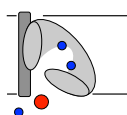
residu creëert de volgende natriumbindingsplaats en zorgt voor de verplaatsing van de geconserveerde NMDGT sequentie in TMS7, welke betrokken is bij het binden van het substraat en de kationen. De conformationele verandering van de residuen van de NMDGT sequentie dwingt vervolgens ook R401 om zich te verplaatsen en maakt zo de ruimte voor aspartaatbinding. Andere conformationele veranderingen van aminozuurresiduen in TMS3, TMS7 en TMS8 creëren vervolgens een bindingsplaats voor aspartaat, waar het met hoge affiniteit binden kan. In overeenstemming met eerdere MD simulaties[92,122], suggereert onze MD studie dat Na2 als laatste ligand bindt nadat substraatbinding heeft plaatsgevonden. Eerdere computergebaseerde studies stellen dat de binding van Na2 de transporteur in de geladen en gesloten toestand stabiliseert[92], in welke de transporteur het substraat door het membraan vervoeren kan. Aan de ander kant van het membraan worden vervolgens het substraat en de ionen vrijgelaten. Omdat Na2 het minst stabiel aan de transporteur gebonden is en de laagste bindingsaffiniteit bezit van alle koppelingsionen, is het waarschijnlijk dat het als eerste de bindingsplaats verlaat. Dit resulteert in het openen van de intracellulaire transporteurpoort, waarna het substraat losgelaten wordt. Wanneer het substraat de bindingsplaats verlaat, draait R401 in de ruimte waar voorheen het substraat gebonden zat. Als gevolg daarvan herschikken ook verdere residuen van TMS3, TMS7 en TMS8 zich, inclusief de residuen in de NMDGT sequentie, met als gevolg dat de andere twee natriumbindingsplaatsen verstoord worden en Na1 en Na3 vrijgelaten worden.

De nabijheid van alle natriumbindingsplaatsen en de substraatbindingsplaats zorgt dus voor de hoge coöperativiteit in natriumbinding en de koppeling van substraat- en natriumionenbinding. Terwijl natriumbinding voor het ontstaan van de substraatbindingsplaats zorgt, is het substraat nodig om de extracellulaire poort naar de bindingsplaats te sluiten. Het laatste natriumion stabiliseert vervolgens de transporteur in de gesloten en geladen toestand, waardoor de transporteur het substraat naar de andere kant van de membraan vervoeren kan. De combinatie van natrium-substraat-natrium binding toont hoe de koppeling wordt gerealiseerd in glutamaattransporteurs en hoe deze koppeling voor een productief transportproces zorgt, waarbij de lekkage van kationen of substraat vermeden wordt.
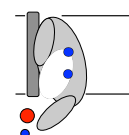
*Substraatbinding en transportsnelheid worden beïnvloed door aminozuurresiduen die niet rechtstreeks bij substraat- en kationbinding betrokken zijn*

Hoofdstuk 1 vat enkele aminozuurresiduen samen die invloed hebben op de substraatselectiviteit van glutamaattransporteurs, waarbij de meeste residuen rechtstreeks betrokken zijn bij de coördinatie van het substraat en de natriumionen. In $Glt_{Tk}$ en $Glt_{Ph}$ zijn alle aminozuren die het substraat en de natriumionen binden, geconserveerd en de kristalstructuren van $Glt_{Tk}$ en $Glt_{Ph}$ in de ongeladen en substraatgeladen toestand zijn vrijwel identiek. Kleine verschillen in het substraatspectrum en de transportsnelheid van beide transporteurs suggereren dat ook residuen die niet direct betrokken zijn bij de coördinatie van het substraat en de natriumionen, een rol spelen in de transporteurfunctionaliteit. Terwijl $Glt_{Ph}$ ook serine, glutamaat en succinaat met een lage affiniteit bindt[69], bindt $Glt_{Tk}$ geen van deze moleculen, maar kan het wel het neutrale aminozuur asparagine met lage affiniteit binden (hoofdstuk 3). Bovendien vertoont $Glt_{Tk}$ een 20-voudig lagere affiniteit voor aspartaat vergeleken met $Glt_{Ph}$, terwijl de transportsnelheid duizend keer hoger is in $Glt_{Tk}$ vergleken met $Glt_{Ph}$. Mogelijk is de tragere transportsnelheid van $Glt_{Ph}$ aan de hogere affiniteit voor aspartaat gerelateerd, waarbij de sterke substraatbinding ervoor zorgt dat het substraat alleen langzaam weer vrijkomt, zoals gesuggereerd wordt voor de dierlijke glutamaattransporteur EAAT5[188]. Een andere reden voor de langzame transportsnelheid van $Glt_{Ph}$ in vergelijking met die van dierlijke glutemaattransporteur en $Glt_{Tk}$, wordt in een recente single molecule FRET studie[106] voorgesteld. Alanine mutaties op de posities K290 en G221 in $Glt_{Ph}$ resulteerden in een verhoogde hydratatie van de transport- en trimerisatie-interface, wat de mobiliteit van het transportdomein verhoogd. Dit resulteert weer in een hogere transportsnelheid. Intrigerend is dat één van de aminozuren in de snellere $Glt_{Ph}$ mutant (K290 in $Glt_{Ph}$), een glutamaat is in $Glt_{Tk}$ (E292). Of de verbeterde hydratatie van de interface tussen het trimerisatie- en transportdomein de reden voor het snellere transport in $Glt_{Tk}$ is, moeten toekomstige mutatie en computationele studies uitwijzen.

*Perspectieven*

Dit proefschrift geeft antwoord op een aantal algemene vragen over hoe substraat- en kationenbinding met elkaar verbonden zijn, en leverde structuren voor de ongeladen en substraatgeladen toestand op – beide in naar buiten gerichte en gesloten conformatie. De analyse van alle momenteel beschikbare functionele, structurele en computationele data
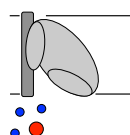
aangaande glutamaattransporteurs resulteerde in een transportmodel, dat beschreven is in hoofdstuk 1, figuur 1.4. Noch zijn echter niet alle staten van de transport cyclus van glutamaattransporteurs (structureel) opgehelderd. Vooral hoge resolutie structuren van niet eerder beschreven conformationele toestanden, zoals de gedeeltelijk natriumgeladen toestand of de overgangstoestanden, zouden kunnen aantonen in welke  volgorde alle liganden binden: eerst Na1, dan Na3, aspartaat en tot slot Na2, of eerst Na3, dan Na1, aspartaat en daarna Na2. Om de intracellulaire poort te identificeren, is het wenselijk om $Glt_{Tk}$ in een toestand te kristalliseren waarin de intracellulaire poort geopend is. Dit kan worden bereikt door gebruik te maken van substraatanalogen, zoals beschreven is voor de co-kristallisatie van $Glt_{Ph}$ met TBOA, dat tot de identificatie van de extracellulaire poort heeft geleid[9]. In de genoemde kristalstructuur dwingt de gebonden TBOA de extracellulaire poort HP2 in de geopende conformatie, waardoor deze dus geïdentificeerd worden kon als extracellulaire poort naar de substraat- en kationenbindingsplaats[9]. De in dit proefschrift beschreven structuren zouden als uitgangspunt voor het gerichte ontwerp van geschikte substraatanalogen kunnen dienen. Bovendien zou de kristallisatie van $Glt_{Tk}$ in een lipide-omgeving met behulp van HILIDE[242] of lipidic cubic phase[243] in de toekomst wellicht ook nieuwe conformaties van de transporteur kunnen opleveren.

Om een volledig inzicht in de bepalende factoren van substraat- en kationselectiviteit en transporteurfunctionaliteit te krijgen, zijn ook functionele en structurele gegevens nodig van andere glutamaattransporteurs en andere verre familieleden, zoals de neutrale aminozuurtransporteurs en dicarboxylaattransporteurs.

De inhoud van dit proefschrift is gericht op fundamenteel onderzoek. In de toekomst zou een beter begrip van de algemene functionele, structurele en mechanistische eigenschappen van glutamaattransporteurs ertoe kunnen leiden gericht geneesmiddelen te ontwerpen[244,245] om de hersenschade na een beroerte te verminderen of tegen te gaan[46,47]. De schade ontstaat door een zuurstofgebrek tijdens de beroerte en heeft een verandering in de kationgradiënt tot gevolg. Hierdoor werken de transporteiwitten voor de neurotransmitter glutamaat in omgekeerde richting, waardoor zenuwcellen overgestimuleerd raken en uiteindelijk afsterven. Het ontwikkelen van een klein molecuul dat de transporteur tijdelijk blokkeert, zou de hersenschade na een beroerte kunnen verminderen. Daarnaast zou een beter begrip van glutamaattransporteurs de ontwikkeling van geneesmiddelen tegen de symptomen van
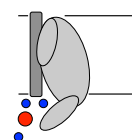
neurodegeneratieve ziekten, zoals epilepsie, Huntington en Alzheimer, waarbij het disfunctioneren van glutamaattransporteurs een rol lijkt te spelen, kunnen bevorderen[48,56–58].
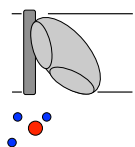
# References

1)   van den Bogaart, G., Krasnikov, V., and Poolman, B. (2007) Dual-color fluorescence-burst analysis to probe protein efflux through the mechanosensitive channel MscL. *Biophys. J. 92*, 1233–1240.

2)   Cho, H.-C., and Backx, P. H. (2001) Three-Dimensional Structure of the $K^+$ Channel Pore: Basis for Ion Selectivity and Permeability, in *Potassium Channels in Cardiovascular Biology* (Archer, S. L., and Rusch, N., Eds.) 1st ed., 17–35. Springer US, New York.

3)   Jardetzky, O. (1966) Simple allosteric model for membrane pumps. *Nature 211*, 969–970.

4)   Raffaello, A., de Stefani, D., and Rizzuto, R. (2012) The mitochondrial $Ca^{2+}$ uniporter. *Cell Calcium 52*, 16–21.

5)   Deng, D., Xu, C., Sun, P., Wu, J., Yan, C., Hu, M., and Yan, N. (2014) Crystal structure of the human glucose transporter GLUT1. *Nature 510*, 121–125.

6)   Rees, D. C., Johnson, E., and Lewinson, O. (2009) ABC transporters: the power to change. *Nat. Rev. Mol. Cell Biol. 10*, 218–27.

7)   Davidson, A. L., Dassa, E., Orelle, C., and Chen, J. (2008) Structure, function, and evolution of bacterial ATP-binding cassette systems. *Microbiol. Mol. Biol. Rev. 72*, 317–364.

8)   ter Beek, J., Guskov, A., and Slotboom, D. J. (2014) Structural diversity of ABC transporters. *J. Gen. Physiol. 143*, 419–435.

9)   Birrell, J. A., and Hirst, J. (2013) Investigation of NADH binding, hydride transfer, and $NAD^+$ dissociation during NADH oxidation by mitochondrial complex I using modified nicotinamide nucleotides. *Biochemistry 52*, 4048–4055.

10)  Saier, M. H. (2000) A functional-phylogenetic classification system for transmembrane solute transporters. *Microbiol. Mol. Biol. Rev. 64*, 354–411.

11)  Marger, M. D., and Saier, M. H. (1993) A major superfamily of transmembrane facilitators that catalyse uniport, symport and antiport. *Trends Biochem. Sci. 18*, 13–20.

12)  Huang, Y. (2003) Structure and Mechanism of the Glycerol-3-Phosphate Transporter from *Escherichia coli*. *Science 301*, 616–620.

13)  Abramson, J., Smirnova, I., Kasho, V., Verner, G., Kaback, H. R., and Iwata, S. (2003) Structure and mechanism of the lactose permease of *Escherichia coli*. *Science 301*, 610–615.

14)  Slotboom, D. J., Konings, W. N., and Lolkema, J. S. (1999) Structural features of the glutamate transporter family. *Microbiol. Mol. Biol. Rev. 63*, 293–307.
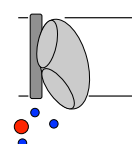
15)     Yernool, D., Boudker, O., Jin, Y., and Gouaux, E. (2004) Structure of a glutamate transporter homologue from *Pyrococcus horikoshii*. *Nature 431*, 811–818.

16)     Youn, J. W., Jolkver, E., Krämer, R., Marin, K., and Wendisch, V. F. (2009) Characterization of the dicarboxylate transporter DctA in *Corynebacterium glutamicum*. *J. Bacteriol. 191*, 5480–5488.

17)     Groeneveld, M., Detert Oude Weme, R. G. J., Duurkens, R. H., and Slotboom, D. J. (2010) Biochemical characterization of the C4-dicarboxylate transporter DctA from *Bacillus subtilis*. *J. Bacteriol. 192*, 2900–2907.

18)     Davies, S. J., Golby, P., Omrani, D., Broad, S. A., Harrington, V. L., Guest, J. R., Kelly, D. J., and Andrews, S. C. (1999) Inactivation and regulation of the aerobic C4-dicarboxylate transport (dctA) gene of *Escherichia coli*. *J. Bacteriol. 181*, 5624–5635.

19)     Yurgel, S. N., and Kahn, M. L. (2005) *Sinorhizobium meliloti* dctA mutants with partial ability to transport dicarboxylic acids. *J. Bacteriol. 187*, 1161–1172.

20)     Kekuda, R., Prasad, P. D., Fei, Y. J., Torres-Zamorano, V., Sinha, S., Yang-Feng, T. L., Leibach, F. H., and Ganapathy, V. (1996) Cloning of the sodium-dependent, broad-scope, neutral amino acid transporter B$^o$ from a human placental choriocarcinoma cell line. *J. Biol. Chem. 271*, 18657–18661.

21)     Deutch, C. E., Spahija, I., and Wagner, C. E. (2014) Susceptibility of *Escherichia coli* to the toxic L-proline analogue L-selenaproline is dependent on two L-cystine transport systems. *J. Appl. Microbiol. 117*, 1487–1499.

22)     Burguière, P., Auger, S., Hullo, M. F., Danchin, A., and Martin-Verstraete, I. (2004) Three different systems participate in L-cystine uptake in *Bacillus subtilis*. *J. Bacteriol. 186*, 4875–4884.

23)     Kim, Y.-M., Ogawa, W., Tamai, E., Kuroda, T., Mizushima, T., and Tsuchiya, T. (2002) Purification, reconstitution, and characterization of Na$^+$/serine symporter, SstT, of *Escherichia coli*. *J. Biochem. 132*, 71–76.

24)     Groeneveld, M., Duurkens, R., and Slotboom, D. J. (2010) Biochemical characterisation of three prokaryal glutamate transporter homologues. *Mech. prokaryotic glutamate Transp. Homol.* Ipskamp drukker, Groningen.

25)     Arriza, J. L., Kavanaugh, M. P., Fairman, W. a, Wu, Y. N., Murdoch, G. H., North, R. a, and Amara, S. G. (1993) Cloning and Expression of a Human Neutral Amino Acid Transporter with Structural Similarity to the Glutamate Transporter Gene Family. *J. Biol. Chem. 268*, 15329–15332.

26)     Shafqat, S., Tamarappoo, B. K., Kilberg, M. S., Puranam, R. S., McNamara, J. O., Guadaño-Ferraz, A., and Fremeau, R. T. (1993) Cloning and expression of a novel Na$^+$-dependent neutral amino acid transporter structurally related to mammalian Na$^+$/glutamate cotransporters. *J. Biol. Chem. 268*, 15351–15355.

27)     Utsunomiya-Tate, N., Endou, H., and Kanai, Y. (1996) Cloning and functional characterization of a system ASC-like Na$^+$-dependent neutral amino acid transporter. *J Biol Chem 271*, 14883–14890.

28)     Tamarappoo, B. K., McDonald, K. K., and Kilberg, M. S. (1996) Expressed human hippocampal ASCT1 amino acid transporter exhibits a pH- dependent change in substrate specificity. *Biochim. Acta 1279*, 131–136.

29)     Vadgama, J. V., and Christensen, H. N. (1984) Wide distribution of pH-dependent service of
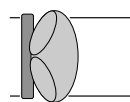
transport system ASC for both anionic and zwitterionic amino acids. *J. Biol. Chem. 259*, 3648–3652.

30) Makowske, M., and Christensen, H. N. (1982) Hepatic transport system interconverted by protonation from service for neutral to service for anionic amino acids. *J. Biol. Chem. 257*, 14635–14638.

31) Goujon, M., McWilliam, H., Li, W., Valentin, F., Squizzato, S., Paern, J., and Lopez, R. (2010) A new bioinformatics analysis tools framework at EMBL-EBI. *Nucleic Acids Res. 38*, 695–699.

32) Sievers, F., Wilm, A., Dineen, D., Gibson, T. J., Karplus, K., Li, W., Lopez, R., McWilliam, H., Remmert, M., Söding, J., Thompson, J. D., and Higgins, D. G. (2011) Fast, scalable generation of high-quality protein multiple sequence alignments using Clustal Omega. *Mol. Syst. Biol. 7*, 539.

33) Scalise, M., Pochini, L., Pingitore, P., Hedfalk, K., and Indiveri, C. (2015) Cysteine is not a substrate but a specific modulator of human ASCT2 (SLC1A5) transporter. *FEBS Lett. 589*, 3617–3623.

34) Grewer, C., and Grabsch, E. (2004) New inhibitors for the neutral amino acid transporter ASCT2 reveal its Na$^+$-dependent anion leak. *J. Physiol. 557*, 747–759.

35) Oppedisano, F., Pochini, L., Galluccio, M., and Indiveri, C. (2007) The glutamine/amino acid transporter (ASCT2) reconstituted in liposomes: Transport mechanism, regulation by ATP and characterization of the glutamine/glutamate antiport. *Biochim. Biophys. Acta - Biomembr. 1768*, 291–298.

36) Kawano, T., Takuwa, K., and Nakajima, T. (1996) Molecular cloning of a cDNA for the glutamate transporter of the nematode *Caenorhabditis elegans*. *Biochem Biophys Res Commun 228*, 415–420.

37) Kawano, T., Takuwa, K., Kuniyoshi, H., Juni, N., Nakajima, T., Yamamoto, D., and Kimura, Y. (1999) Cloning and characterization of a *Drosophila melanogaster* cDNA encoding a glutamate transporter. *Biosci Biotechnol Biochem 63*, 2042–2044.

38) Donly, C., Richman, A., and Hawkins, E. (1997) Molecular Cloning and Functional Expression of an Insect High-Affinity Na$^+$-Dependent Glutamate Transporter. *Eur. J. 248*, 535–542.

39) Eliasof, S., Arriza, J. L., Leighton, B. H., Amara, S. G., and Kavanaugh, M. P. (1998) Localization and function of five glutamate transporters cloned from the salamander retina. *Vision Res. 38*, 1443–1454.

40) Sato, K., Inaba, M., Suwa, Y., Matsuu, a, Hikasa, Y., Ono, K., and Kagota, K. (2000) Inherited defects of sodium-dependent glutamate transport mediated by glutamate/aspartate transporter in canine red cells due to a decreased level of transporter protein expression. *J Biol Chem 275*, 6620–6627.

41) Kanai, Y., and Hediger, M. A. (1992) Primary structure and functional characterization of a high-affinity glutamate transporter. *Nature 360*, 467–471.

42) Tanaka, K. (1993) Expression cloning of a rat glutamate transporter. *Neurosci. Res. 16*, 149–153.

43) Kirschner, M. A., Copeland, N. G., Gilbert, D. J., Jenkins, N. A., and Amara, S. G. (1994) Mouse excitatory amino acid transporter EAAT2: isolation, characterization, and proximity to neuroexcitability loci on mouse chromosome 2. *Genomics 24*, 218–224.

44) Arriza, J. L., Fairman, W. a, Wadiche, J. I., Murdoch, G. H., Kavanaugh, M. P., and Amara, S. G. (1994) Functional comparisons of three glutamate transporter subtypes cloned from human motor
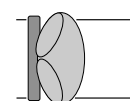
cortex. *J. Neurosci. 14*, 5559–5569.

45)    Danbolt, N. C. (2001) Glutamate uptake. *Prog. Neurobiol. 65*, 1–105.

46)    Lai, T. W., Zhang, S., and Wang, Y. T. (2014) Excitotoxicity and stroke: Identifying novel targets
       for neuroprotection. *Prog. Neurobiol. 115*, 157-188.

47)    Camacho, A., and Massieu, L. (2006) Role of glutamate transporters in the clearance and release of
       glutamate during ischemia and its relation to neuronal death. *Arch. Med. Res. 37*, 11-18.

48)    Hynd, M. R., Scott, H. L., and Dodd, P. R. (2004) Glutamate-mediated excitotoxicity and
       neurodegeneration in Alzheimer's disease. *Neurochem. Int. 45*, 583-595.

49)    Bridges, R. J., and Esslinger, C. S. (2005) The excitatory amino acid transporters: Pharmacological
       insights on substrate and inhibitor specificity of the EAAT subtypes. *Pharmacol. Ther. 107*, 271–
       285.

50)    Asztely, F., Erdemli, G., and Kullmann, D. M. (1997) Extrasynaptic glutamate spillover in the
       hippocampus: Dependence on temperature and the role of active glutamate uptake. *Neuron 18*, 281–
       293.

51)    Diamond, J. S. (2002) A broad view of glutamate spillover. *Nat. Neurosci. 5*, 291–292.

52)    Castagna, M., Shayakul, C., Trotti, D., Sacchi, V. F., Harvey, W. R., and Hediger, M. a. (1997)
       Molecular characteristics of mammalian and insect amino acid transporters: implications for amino
       acid homeostasis. *J. Exp. Biol. 200*, 269–286.

53)    Dehnes, Y., Chaudhry, F. a, Ullensvang, K., Lehre, K. P., Storm-Mathisen, J., and Danbolt, N. C.
       (1998) The glutamate transporter EAAT4 in rat cerebellar Purkinje cells: a glutamate-gated chloride
       channel concentrated near the synapse in parts of the dendritic membrane facing astroglia. *J.
       Neurosci. 18*, 3606–3619.

54)    Auger, C., and Attwell, D. (2000) Fast removal of synaptic glutamate by postsynaptic transporters.
       *Neuron 28*, 547–558.

55)    Li, S., Mallory, M., Alford, M., Tanaka, S., and Masliah, E. (1997) Glutamate transporter alterations
       in Alzheimer disease are possibly associated with abnormal APP expression. *J Neuropathol Exp
       Neurol 56*, 901–911.

56)    Scott, H. A., Gebhardt, F. M., Mitrovic, A. D., Vandenberg, R. J., and Dodd, P. R. (2011) Glutamate
       transporter variants reduce glutamate uptake in Alzheimer's disease. *Neurobiol. Aging 32*, 553.e1-
       11.

57)    Estrada-Sánchez, A. M., and Rebec, G. V. (2012) Corticostriatal dysfunction and glutamate
       transporter 1 (GLT1) in Huntington's disease: Interactions between neurons and astrocytes. *Basal
       Ganglia 2*, 57–66.

58)    Janjua, N. A., Itano, T., Kugoh, T., Hosokawa, K., Nakano, M., Matsui, H., and Hatase, O. (1992)
       Familial increase in plasma glutamic acid in epilepsy. *Epilepsy Res. 11*, 37–44.

59)    Tanaka, K. (1997) Epilepsy and Exacerbation of Brain Injury in Mice Lacking the Glutamate
       Transporter GLT-1. *Science (80-. ). 276*, 1699–1702.

60)    Rothstein, J. D., Dykes-Hoberg, M., Pardo, C. A., Bristol, L. A., Jin, L., Kuncl, R. W., Kanai, Y.,
       Hediger, M. A., Wang, Y., Schielke, J. P., and Welty, D. F. (1996) Knockout of glutamate
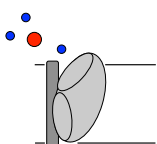
transporters reveals a major role for astroglial transport in excitotoxicity and clearance of glutamate. *Neuron 16*, 675–686.

61) Pines, G., and Danbolt NC, Bjørås M, Zhang Y, Bendahan A, Eide L, Koepsell H, Storm-Mathisen J, Seeberg E, K. B. (1992) Cloning and expression of a rat brain L-glutamate transporter. *Nature 360*, 464–467.

62) Storck, T., Schulte, S., Hofmann, K., and Stoffel, W. (1992) Structure, expression, and functional analysis of a Na$^+$-dependent glutamate/aspartate transporter from rat brain. *Proc. Natl. Acad. Sci. U. S. A. 89*, 10955–10959.

63) Fairman, W. A., Vandenberg, R. J., Arriza, J. L., Kavanaugh, M. P., and Amara, S. G. (1995) An excitatory amino-acid transporter with properties of a ligand-gated chloride channel. *Nature 375*, 599-603.

64) Arriza, J. L., Eliasof, S., Kavanaugh, M. P., and Amara, S. G. (1997) Excitatory amino acid transporter 5, a retinal glutamate transporter coupled to a chloride conductance. *Proc. Natl. Acad. Sci. U. S. A. 94*, 4155–4160.

65) Kanner, B. I., and Bendahan, a. (1982) Binding order of substrates to the sodium and potassium ion coupled L-glutamic acid transporter from rat brain. *Biochemistry 21*, 6327–6330.

66) Kavanaugh, M. P., Bendahan, A., Zerangue, N., Zhang, Y., and Kanner, B. I. (1997) Mutation of an amino acid residue influencing potassium coupling in the glutamate transporter GLT-1 induces obligate exchange. *J. Biol. Chem. 272*, 1703–1708.

67) Pines, G., and Kanner, B. I. (1990) Counterflow of L-glutamate in plasma membrane vesicles and reconstituted preparations from rat brain. *Biochemistry 29*, 11209–11214.

68) Raunser, S., Appel, M., Ganea, C., Geldmacher-Kaufer, U., Fendler, K., and Kühlbrandt, W. (2006) Structure and function of prokaryotic glutamate transporters from *Escherichia coli* and *Pyrococcus horikoshii*. *Biochemistry 45*, 12796–12805.

69) Boudker, O., Ryan, R. M., Yernool, D., Shimamoto, K., and Gouaux, E. (2007) Coupling substrate and ion binding to extracellular gate of a sodium-dependent aspartate transporter. *Nature 445*, 387–393.

70) Ryan, R. M., Compton, E. L. R., and Mindell, J. a. (2009) Functional Characterization of a Na$^+$-dependent Aspartate Transporter from *Pyrococcus horikoshii*. *J. Biol. Chem. 284*, 17540–17548.

71) Jensen, S., Guskov, A., Rempel, S., Hänelt, I., and Slotboom, D. J. (2013) Crystal structure of a substrate-free aspartate transporter. *Nat. Struct. Mol. Biol. 20*, 1224–1226.

72) Guskov, A., Jensen, S., Faustino, I., and Marrink, S. J. (2016) Mechanism of coupled transport of three sodium ions and aspartate in the glutamate transporter homologue Glt$_{Tk}$. *Nat. Commun. 7*, 13420.

73) Gendreau, S., Voswinkel, S., Torres-Salazar, D., Lang, N., Heidtmann, H., Detro-Dassen, S., Schmalzing, G., Hidalgo, P., and Fahlke, C. (2004) A trimeric quaternary structure is conserved in bacterial and human glutamate transporters. *J. Biol. Chem. 279*, 39505–39512.

74) Yernool, D., Boudker, O., Folta-Stogniew, E., and Gouaux, E. (2003) Trimeric Subunit Stoichiometry of the Glutamate Transporters from *Bacillus caldotenax* and *Bacillus*
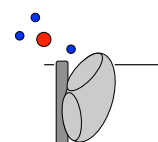
*stearothermophilus*. *Biochemistry 42*, 12981–12988.

75) Haugeto, O., Ullensvang, K., Levy, L. M., Chaudhry, F. a., Honore, T., Nielsen, M., Lehre, K. P., Danbolt, N. C., and Honoré, T. (1996) Brain Glutamate Transporter Proteins Form Homomultimers. *J. Biol. Chem. 271*, 27715–27722.

76) Grewer, C., Balani, P., Weidenfeller, C., Bartusel, T., Tao, Z., and Rauen, T. (2005) The individual subunits of the glutamate transporter EAAC1 homotrimer function independently of each other. *Biochemistry 44*, 11913–11923.

77) Nothmann, D., Leinenweber, A., Torres-Salazar, D., Kovermann, P., Hotzy, J., Gameiro, A., Grewer, C., and Fahlke, C. (2011) Hetero-oligomerization of neuronal glutamate transporters. *J. Biol. Chem. 286*, 3935–3943.

78) Slotboom, D. J., Sobczak, I., Konings, W. N., and Lolkema, J. S. (1999) A conserved serine-rich stretch in the glutamate transporter family forms a substrate-sensitive reentrant loop. *Proc. Natl. Acad. Sci. U. S. A. 96*, 14282–14287.

79) Grunewald, M., and Kanner, B. I. (2000) The accessibility of a novel reentrant loop of the glutamate transporter GLT-1 is restricted by its substrate. *J Biol Chem 275*, 9684–9689.

80) Brocke, L., Bendahan, A., Grunewald, M., and Kanner, B. I. (2002) Proximity of two oppositely oriented reentrant loops in the glutamate transporter GLT-1 identified by paired cysteine mutagenesis. *J. Biol. Chem. 277*, 3985–3992.

81) Leighton, B. H., Seal, R. P., Watts, S. D., Skyba, M. O., and Amara, S. G. (2006) Structural rearrangements at the translocation pore of the human glutamate transporter, EAAT1. *J. Biol. Chem. 281*, 29788–29796.

82) Qu, S., and Kanner, B. I. (2008) Substrates and non-transportable analogues induce structural rearrangements at the extracellular entrance of the glial glutamate transporter GLT-1/EAAT2. *J. Biol. Chem. 283*, 26391–26400.

83) DeLano, W. L. (2010) The PyMOL Molecular Graphics System, Version 1.8. *Schrödinger LLC* http://www.pymol.org.

84) Koch, H. P., Hubbard, J. M., and Larsson, H. P. (2007) Voltage-independent sodium-binding events reported by the 4B-4C loop in the human glutamate transporter excitatory amino acid transporter 3. *J. Biol. Chem. 282*, 24547–24553.

85) Erkens, G. B., Hänelt, I., Goudsmits, J. M. H., Slotboom, D. J., and van Oijen, A. M. (2013) Unsynchronised subunit motion in single trimeric sodium-coupled aspartate transporters. *Nature 502*, 119–123.

86) Georgieva, E. R., Borbat, P. P., Ginter, C., Freed, J. H., Boudker, O., and Georgieva, E. R., Borbat, P. P., Ginter, C., Freed, J. H., Boudker, O. (2013) Conformational ensemble of the sodium-coupled aspartate transporter. *Nat. Struct. Mol. Biol. 20*, 215–221.

87) Koch, H. P. (2005) Small-Scale Molecular Motions Accomplish Glutamate Uptake in Human Glutamate Transporters. *J. Neurosci. 25*, 1730–1736.

88) Leary, G. P., Stone, E. F., Holley, D. C., and Kavanaugh, M. P. (2007) The glutamate and chloride permeation pathways are colocalized in individual neuronal glutamate transporter subunits. *J.*
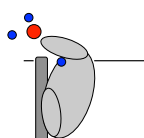
*Neurosci. 27*, 2938–2942.

89) Koch, H. P., Lane Brown, R., and Larsson, H. P. (2007) The Glutamate-Activated Anion Conductance in Excitatory Amino Acid Transporters Is Gated Independently by the Individual Subunits. *J. Neurosci. 27*, 2943–2947.

90) Rong, X., Zomot, E., Zhang, X., and Qu, S. (2014) Investigating Substrate-Induced Motion between the Scaffold and Transport Domains in the Glutamate Transporter EAAT1. *Mol. Pharmacol. 86*, 657–664.

91) Focke, P. J., Moenne-Loccoz, P., and Larsson, H. P. (2011) Opposite movement of the external gate of a glutamate transporter homolog upon binding cotransported sodium compared with substrate. *J. Neurosci. 31*, 6255–6262.

92) Huang, Z., and Tajkhorshid, E. (2008) Dynamics of the extracellular gate and ion-substrate coupling in the glutamate transporter. *Biophys. J. 95*, 2292–2300.

93) Shrivastava, I. H., Jiang, J., Amara, S. G., and Bahar, I. (2008) Time-resolved Mechanism of Extracellular Gate Opening and Substrate Binding in a Glutamate Transporter. *J. Biol. Chem. 283*, 28680–28690.

94) Silverstein, N., Ewers, D., Forrest, L. R., Fahlke, C., and Kanner, B. I. (2015) Molecular Determinants of Substrate Specificity in Sodium-Coupled Glutamate Transporters. *J. Biol. Chem. 290*, 28988-28996.

95) Groeneveld, M., and Slotboom, D. J. (2007) Rigidity of the Subunit Interfaces of the Trimeric Glutamate Transporter GltT During Translocation. *J. Mol. Biol. 372*, 565–570.

96) Hänelt, I., Wunnicke, D., Bordignon, E., Steinhoff, H.-J., and Slotboom, D. J. (2013) Conformational heterogeneity of the aspartate transporter $Glt_{Ph}$. *Nat. Struct. Mol. Biol. 20*, 210–214.

97) Ryan, R. M., Mitrovic, a. D., and Vandenberg, R. J. (2004) The Chloride Permeation Pathway of a Glutamate Transporter and Its Proximity to the Glutamate Translocation Pathway. *J. Biol. Chem. 279*, 20742–20751.

98) Crisman, T. J., Qu, S., Kanner, B. I., and Forrest, L. R. (2009) Inward-facing conformation of glutamate transporters as revealed by their inverted-topology structural repeats. *Proc. Natl. Acad. Sci. U. S. A. 106*, 20752–20757.

99) Reyes, N., Ginter, C., and Boudker, O. (2009) Transport mechanism of a bacterial homologue of glutamate transporters. *Nature 462*, 880–885.

100) DeChancie, J., Shrivastava, I. H., and Bahar, I. (2011) The mechanism of substrate release by the aspartate transporter $Glt_{Ph}$: insights from simulations. *Mol. Biosyst. 7*, 832–842.

101) Mulligan, C., Fenollar-Ferrer, C., Fitzgerald, G. A., Vergara-Jaque, A., Kaufmann, D., Li, Y., Forrest, L. R., and Mindell, J. A. (2016) The bacterial dicarboxylate transporter VcINDY uses a two-domain elevator-type mechanism. *Nat. Struct. Mol. Biol. 23*, 256–263.

102) Lee, C., Kang, H. J., von Ballmoos, C., Newstead, S., Uzdavinys, P., Dotson, D. L., Iwata, S., Beckstein, O., Cameron, A. D., and Drew, D. (2013) A two-domain elevator mechanism for sodium/proton antiport. *Nature 501*, 573–577.

103) Hu, N.-J., Iwata, S., Cameron, A. D., and Drew, D. (2011) Crystal structure of a bacterial homologue
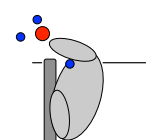
of the bile acid sodium symporter ASBT. *Nature 478*, 408–411.

104) Vergara-Jaque, A., Fenollar-Ferrer, C., Kaufmann, D., and Forrest, L. R. (2015) Repeat-swap homology modeling of secondary active transporters: updated protocol and prediction of elevator-type mechanisms. *Front. Pharmacol. 6*, 1–12.

105) Grazioso, G., Limongelli, V., Branduardi, D., Novellino, E., De Micheli, C., Cavalli, A., and Parrinello, M. (2012) Investigating the mechanism of substrate uptake and release in the glutamate transporter homologue Glt$_{Ph}$ through metadynamics simulations. *J. Am. Chem. Soc. 134*, 453–63.

106) Akyuz, N., Georgieva, E. R., Zhou, Z., Stolzenberg, S., Cuendet, M. a, Khelashvili, G., Altman, R. B., Terry, D. S., Freed, J. H., Weinstein, H., Boudker, O., and Blanchard, S. C. (2015) Transport domain unlocking sets the uptake rate of an aspartate transporter. *Nature 518*, 68–73.

107) Zomot, E., and Bahar, I. (2013) Intracellular Gating in an Inward-facing State of Aspartate Transporter Glt$_{Ph}$ Is Regulated by the Movements of the Helical Hairpin HP2. *J. Biol. Chem. 288*, 8231–8237.

108) Esslinger, C. S., Agarwal, S., Gerdes, J., Wilson, P. a., Davis, E. S., Awes, A. N., O'Brien, E., Mavencamp, T., Koch, H. P., Poulsen, D. J., Rhoderick, J. F., Chamberlin, a. R., Kavanaugh, M. P., and Bridges, R. J. (2005) The substituted aspartate analogue L-β-*threo*-benzyl-aspartate preferentially inhibits the neuronal excitatory amino acid transporter EAAT3. *Neuropharmacology 49*, 850–861.

109) Bendahan, a. (2000) Arginine 447 Plays a Pivotal Role in Substrate Interactions in a Neuronal Glutamate Transporter. *J. Biol. Chem. 275*, 37436–37442.

110) Gaillard, I., Slotboom, D. J., Knol, J., Lolkema, J. S., and Konings, W. N. (1996) Purification and reconstitution of the glutamate carrier GltT of the thermophilic bacterium *Bacillus stearothermophilus*. *Biochemistry 35*, 6150–6156.

111) Tolner, B., Poolman, B., Wallace, B., and Konings, W. N. (1992) Revised nucleotide sequence of the gltP gene, which encodes the proton-glutamate-aspartate transport protein of *Escherichia coli*. *J. Bacteriol. 174*, 2391–2393.

112) Tolner, B., Ubbink-Kok, T., Poolman, B., and Konings, W. N. (1995) Cation-selectivity of the L-glutamate transporters of *Escherichia coli*, *Bacillus stearothermophilus* and *Bacillus caldotenax*: dependence on the environment in which the proteins are expressed. *Mol Microbiol 18*, 123–133.

113) Tolner, B., Ubbink-Kok, T., Poolman, B., and Konings, W. N. (1995) Characterization of the proton/glutamate symport protein of *Bacillus subtilis* and its functional expression in *Escherichia coli*. *J. Bacteriol. 177*, 2863–2869.

114) Seal, R. P., and Amara, S. G. (1998) A reentrant loop domain in the glutamate carrier EAAT1 participates in substrate binding and translocation. *Neuron 21*, 1487–1498.

115) Seal, R. P., Leighton, B. H., and Amara, S. G. (2000) A model for the topology of excitatory amino acid transporters determined by the extracellular accessibility of substituted cysteines. *Neuron 25*, 695–706.

116) Conradt, M., and Stoffel, W. (1995) Functional analysis of the high affinity, Na$^+$-dependent glutamate transporter GLAST-1 by site-directed mutagenesis. *J. Biol. Chem. 270*, 25207–25212.
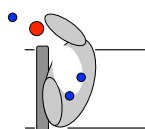
117) Scopelliti, A. J., Ryan, R. M., and Vandenberg, R. J. (2013) Molecular determinants for functional differences between alanine-serine-cysteine transporter 1 and other glutamate transporter family members. *J. Biol. Chem. 288*, 8250–8257.

118) Dang, V., Penjwini, M., Viswanath, V., and Staubli, U. (2016) D-Serine Is a Substrate for Neutral Amino Acid Transporters ASCT1/SLC1A4 and ASCT2/SLC1A5, and Is Transported by Both Subtypes in Rat Hippocampal Astrocyte Cultures. *PLoS One 11*, e0156551.

119) Zerangue, N., and Kavanaugh, M. P. (1996) ASCT-1 is a neutral amino acid exchanger with chloride channel activity. *J. Biol. Chem. 271*, 27991–27994.

120) Teichman, S., and Kanner, B. I. (2007) Aspartate-444 is essential for productive substrate interactions in a neuronal glutamate transporter. *J. Gen. Physiol. 129*, 527–539.

121) Wang, H., Rascoe, A. M., Holley, D. C., Gouaux, E., and Kavanaugh, M. P. (2013) Novel dicarboxylate selectivity in an insect glutamate transporter homolog. *PLoS One 8*, e70947.

122) Heinzelmann, G., Baştuğ, T., and Kuyucak, S. (2011) Free Energy Simulations of Ligand Binding to the Aspartate Transporter Glt$_{Ph}$. *Biophys. J. 101*, 2380–2388.

123) Levy, L. M., Warr, O., and Attwell, D. (1998) Stoichiometry of the glial glutamate transporter GLT-1 expressed inducibly in a Chinese hamster ovary cell line selected for low endogenous Na$^+$-dependent glutamate uptake. *J. Neurosci. 18*, 9620–9628.

124) Zerangue, N., and Kavanaugh, M. P. (1996) Flux coupling in a neuronal glutamate transporter. *Nature, 383*, 634-637.

125) Owe, S. G., Marcaggi, P., and Attwell, D. (2006) The ionic stoichiometry of the GLAST glutamate transporter in salamander retinal glia. *J. Physiol. 577*, 591–599.

126) Ogawa, W., Kim, Y. M., Mizushima, T., and Tsuchiya, T. (1998) Cloning and expression of the gene for the Na$^+$-coupled serine transporter from *Escherichia coli* and characteristics of the transporter. *J. Bacteriol. 180*, 6749–6752.

127) Dashper, S. G., Brownfield, L., Slakeski, N., Zilm, P. S., Rogers, A. H., and Reynolds, E. C. (2001) Sodium ion-driven serine/threonine transport in *Porphyromonas gingivalis*. *J. Bacteriol. 183*, 4142–4148.

128) Groeneveld, M., and Slotboom, D. J. (2010) Na$^+$:Aspartate coupling stoichiometry in the glutamate transporter homologue Glt$_{Ph}$. *Biochemistry 49*, 3511–3513.

129) De Vrij, W., Bulthuis, R. A., Van Iwaarden, P. R., and Konings, W. N. (1989) Mechanism of glutamate transport in membrane vesicles from *Bacillus stearothermophilus*. *J. Bacteriol. 171*, 1118–1125.

130) Borre, L., and Kanner, B. I. (2001) Coupled, but Not Uncoupled, Fluxes in a Neuronal Glutamate Transporter Can Be Activated by Lithium Ions. *J. Biol. Chem. 276*, 40396–40401.

131) Machtens, J.-P., Kovermann, P., and Fahlke, C. (2011) Substrate-dependent gating of anion channels associated with excitatory amino acid transporter 4. *J. Biol. Chem. 286*, 23780–23788.

132) Grunewald, M., and Kanner, B. (1995) Conformational Changes Monitored on Glutamate Transporter Glt-1 Indicate the Existence of Two Neurotransmitter-bound States. *J. Biol. Chem. 270*, 17017-17024.
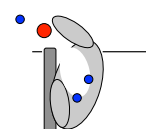
133)  Zhang, Y., Bendahan, A., Zarbiv, R., Kavanaugh, M. P., and Kanner, B. I. (1998) Molecular determinant of ion selectivity of a ($Na^+$ + $K^+$)-coupled rat brain glutamate transporter. *Proc. Natl. Acad. Sci. U. S. A. 95*, 751–755.

134)  Zhang, Y., and Kanner, B. I. (1999) Two serine residues of the glutamate transporter GLT-1 are crucial for coupling the fluxes of sodium and the neurotransmitter. *Proc. Natl. Acad. Sci. U. S. A. 96*, 1710–1715.

135)  Teichman, S., Qu, S., and Kanner, B. I. (2009) The equivalent of a thallium binding residue from an archeal homolog controls cation interactions in brain glutamate transporters. *Proc. Natl. Acad. Sci. U. S. A. 106*, 14297–14302.

136)  Teichman, S., Qu, S., and Kanner, B. I. (2012) Conserved asparagine residue located in binding pocket controls cation selectivity and substrate interactions in neuronal glutamate transporter. *J. Biol. Chem. 287*, 17198–17205.

137)  Huang, S., Ryan, R. M., and Vandenberg, R. J. (2009) The role of cation binding in determining substrate selectivity of glutamate transporters. *J. Biol. Chem. 284*, 4510–4515.

138)  Tao, Z., Gameiro, A., and Grewer, C. (2008) Thallium ions can replace both sodium and potassium ions in the glutamate transporter EAAC1. *Biochemistry 47*, 12923–12930.

139)  Zarbiv, R., Grunewald, M., Kavanaugh, M. P., and Kanner, B. I. (1998) Cysteine scanning of the surroundings of an alkali-ion binding site of the glutamate transporter GLT-1 reveals a conformationally sensitive residue. *J. Biol. Chem. 273*, 14231–14237.

140)  Tao, Z., and Grewer, C. (2007) Cooperation of the Conserved Aspartate 439 and Bound Amino Acid Substrate Is Important for High-Affinity $Na^+$ Binding to the Glutamate Transporter EAAC1. *J. Gen. Physiol. 129*, 331–344.

141)  Scopelliti, A. J., Heinzelmann, G., Kuyucak, S., Ryan, R. M., and Vandenberg, R. J. (2014) $Na^+$ Interactions with the Neutral Amino Acid Transporter ASCT1. *J. Biol. Chem. 289*, 17468–17479.

142)  Verdon, G. G., Oh, S., Serio, R., and Boudker, O. (2014) Coupled ion binding and structural transitions along the transport cycle of glutamate transporters. *Elife*, 3:e02283.

143)  Venkatesan, S., Saha, K., Sohail, A., Sandtner, W., Freissmuth, M., Ecker, G. F., Sitte, H. H., and Stockner, T. (2015) Refinement of the Central Steps of Substrate Transport by the Aspartate Transporter $Glt_{Ph}$: Elucidating the Role of the Na2 Sodium Binding Site. *PLOS Comput. Biol. 11*, e1004551.

144)  Holley, D. C., and Kavanaugh, M. P. (2009) Interactions of alkali cations with glutamate transporters. *Philos. Trans. R. Soc. Lond. B. Biol. Sci. 364*, 155–161.

145)  Gu, Y., Shrivastava, I. H., Amara, S. G., and Bahar, I. (2009) Molecular simulations elucidate the substrate translocation pathway in a glutamate transporter. *Proc. Natl. Acad. Sci. U. S. A. 106*, 2589–2594.

146)  Larsson, H. P., Wang, X., Lev, B., Baconguis, I., Caplan, D. a, Vyleta, N. P., Koch, H. P., Diez-Sampedro, A., and Noskov, S. Y. (2010) Evidence for a third sodium-binding site in glutamate transporters suggests an ion/substrate coupling model. *Proc. Natl. Acad. Sci. U. S. A. 107*, 13912–13917.
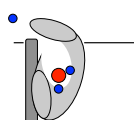
147) Heinzelmann, G., and Kuyucak, S. (2014) Molecular dynamics simulations of the mammalian glutamate transporter EAAT3. *PLoS One 9*, e92089.

148) Bastug, T., Heinzelmann, G., Kuyucak, S., Salim, M., Vandenberg, R. J., and Ryan, R. M. (2012) Position of the third $Na^+$ site in the aspartate transporter $Glt_{Ph}$ and the human glutamate transporter, EAAT1. *PLoS One 7*, e33058.

149) Huang, Z., and Tajkhorshid, E. (2010) Identification of the Third $Na^+$ Site and the Sequence of Extracellular Binding Events in the Glutamate Transporter. *Biophys. J. 99*, 1416–1425.

150) Tao, Z., Rosental, N., Kanner, B. I., Gameiro, A., Mwaura, J., and Grewer, C. (2010) Mechanism of Cation Binding to the Glutamate Transporter EAAC1 Probed with Mutation of the Conserved Amino Acid Residue Thr101. *J. Biol. Chem. 285*, 17725–17733.

151) Pines G., Zhang Y., K. B. I. (1995) Glutamate 404 is involved in the substrate discrimination of GLT-1, a $(Na^+ + K^+)$-coupled glutamate transporter from rat brain. *J. Biol. Chem. 270*, 17093-17097.

152) Rosental, N., Bendahan, A., and Kanner, B. I. (2006) Multiple Consequences of Mutating Two Conserved β-Bridge Forming Residues in the Translocation Cycle of a Neuronal Glutamate Transporter. *J. Biol. Chem. 281*, 27905–27915.

153) Tao, Z., Zhang, Z., and Grewer, C. (2006) Neutralization of the aspartic acid residue Asp-367, but not Asp-454, inhibits binding of $Na^+$ to the glutamate-free form and cycling of the glutamate transporter EAAC1. *J. Biol. Chem. 281*, 10263–10272.

154) Erecinska, M. I., Wantorsky, D., and Wilson, D. F. (1983) Aspartate transport in synaptosomes from rat brain. *J. Biol. Chem. 258*, 9069–9077.

155) Bouvier, M., Szatkowski, M., Amato, A., and Attwell, D. (1992) The glial cell glutamate uptake carrier countertransports pH-changing anions. *Nature 360*, 471–474.

156) Zerangue, N., and Kavanaugh, M. P. (1996) Interaction of L-cysteine with a human excitatory amino acid transporter. *J. Physiol. 493 (Pt 2)*, 419–423.

157) Watzke, N., Rauen, T., Bamberg, E., and Grewer, C. (2000) On the mechanism of proton transport by the neuronal excitatory amino acid carrier 1. *J. Gen. Physiol. 116*, 609–622.

158) Zhang, Y., Pines, G., and Kanner, B. I. (1994) Histidine 326 is critical for the function of GLT-1, a $(Na^+ + K^+)$-coupled glutamate transporter from rat brain. *J Biol Chem 269*, 19573–19577.

159) Padant, E., Sarkart, H. K., Viitanent, P. V, Pooniant, M. S., and Kabackt, H. R. (1985) Site-specific mutagenesis of histidien residues in the lac permease of *Escherichia coli*. *Proc. Natl. Acad. Sci. U. S. A. 82*, 6765–6768.

160) Tao, Z., and Grewer, C. (2005) The conserved histidine 295 does not contribute to proton cotransport by the glutamate transporter EAAC1. *Biochemistry 44*, 3466–3476.

161) Grewer, C. (2003) Is the Glutamate Residue Glu-373 the Proton Acceptor of the Excitatory Amino Acid Carrier 1? *J. Biol. Chem. 278*, 2585–2592.

162) Heinzelmann, G., and Kuyucak, S. (2014) Molecular Dynamics Simulations Elucidate the Mechanism of Proton Transport in the Glutamate Transporter EAAT3. *Biophys. J. 106*, 2675–2683.

163) Mwaura, J., Tao, Z., James, H., Albers, T., Schwartz, A., and Grewer, C. (2012) Protonation State of a Conserved Acidic Amino Acid Involved in $Na^+$ Binding to the Glutamate Transporter EAAC1.
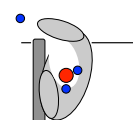
*ACS Chem. Neurosci. 3*, 1073–1083.

164) Rosental, N., Gameiro, A., Grewer, C., and Kanner, B. I. (2011) A conserved aspartate residue located at the extracellular end of the binding pocket controls cation interactions in brain glutamate transporters. *J. Biol. Chem. 286*, 41381–41390.

165) Sarantis, M., Everett, K., and Attwell, D. (1988) A presynaptic action of glutamate at the cone output synapse. *Nature 332*, 451–453.

166) Wadiche, J. I., Amara, S. G., and Kavanaugh, M. P. (1995) Ion fluxes associated with excitatory amino acid transport. *Neuron 15*, 721–728.

167) Machtens, J.-P., Kortzak, D., Lansche, C., Leinenweber, A., Kilian, P., Begemann, B., Zachariae, U., Ewers, D., de Groot, B. L., Briones, R., and Fahlke, C. (2015) Mechanisms of Anion Conduction by Coupled Glutamate Transporters. *Cell 160*, 542–553.

168) Bröer, a, Wagner, C., Lang, F., and Bröer, S. (2000) Neutral amino acid transporter ASCT2 displays substrate-induced Na$^+$ exchange and a substrate-gated anion conductance. *Biochem. J. 346 (Pt 3)*, 705–710.

169) Billups, B., Rossi, D., and Attwell, D. (1996) Anion conductance behavior of the glutamate uptake carrier in salamander retinal glial cells. *J. Neurosci. 16*, 6722–6731.

170) Grant, G. B., and Dowling, J. E. (1995) A glutamate-activated chloride current in cone-driven ON bipolar cells of the white perch retina. *J. Neurosci. 15*, 3852–3862.

171) Picaud, S. a, Larsson, H. P., Grant, G. B., Lecar, H., and Werblin, F. S. (1995) Glutamate-gated chloride channel with glutamate-transporter-like properties in cone photoreceptors of the tiger salamander. *J. Neurophysiol. 74*, 1760–1771.

172) Borre, L., Kavanaugh, M. P., and Kanner, B. I. (2002) Dynamic Equilibrium between Coupled and Uncoupled Modes of a Neuronal Glutamate Transporter. *J. Biol. Chem. 277*, 13501–13507.

173) Ryan, R. M., and Vandenberg, R. J. (2002) Distinct conformational states mediate the transport and anion channel properties of the glutamate transporter EAAT-1. *J. Biol. Chem. 277*, 13494–13500.

174) Seal, R. P., Shigeri, Y., Eliasof, S., Leighton, B. H., and Amara, S. G. (2001) Sulfhydryl modification of V449C in the glutamate transporter EAAT1 abolishes substrate transport but not the substrate-gated anion conductance. *Proc. Natl. Acad. Sci. U. S. A. 98*, 15324–15329.

175) Wadiche, J. I., and Kavanaugh, M. P. (1998) Macroscopic and microscopic properties of a cloned glutamate transporter/chloride channel. *J. Neurosci. 18*, 7650–7661.

176) Huang, S., and Vandenberg, R. J. (2007) Mutations in transmembrane domains 5 and 7 of the human excitatory amino acid transporter 1 affect the substrate-activated anion channel. *Biochemistry 46*, 9685–9692.

177) Bergles, D. E., Tzingounis, A. V, and Jahr, C. E. (2002) Comparison of coupled and uncoupled currents during glutamate uptake by GLT-1 transporters. *J. Neurosci. 22*, 10153–10162.

178) Otis, T. S., and Kavanaugh, M. P. (2000) Isolation of current components and partial reaction cycles in the glial glutamate transporter EAAT2. *J. Neurosci. 20*, 2749–2757.

179) Larsson, H. P., Picaud, S. A., Werblin, F. S., and Lecar, H. (1996) Noise analysis of the glutamate-activated current in photoreceptors. *Biophys. J. 70*, 733–742.
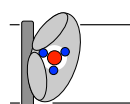
180) Melzer, N., Biela, A., and Fahlke, C. (2003) Glutamate modifies ion conduction and voltage-dependent gating of excitatory amino acid transporter-associated anion channels. *J. Biol. Chem. 278*, 50112–50119.

181) Kovermann, P., Machtens, J. P., Ewers, D., and Fahlke, C. (2010) A conserved aspartate determines pore properties of anion channels associated with Excitatory Amino Acid Transporter 4 (EAAT4). *J. Biol. Chem. 285*, 23676–23686.

182) Vandenberg, R. J., and Ryan, R. M. (2013) Mechanisms of Glutamate Transport. *Physiol. Rev. 93*, 1621–1657.

183) Ryan, R. M., and Mindell, J. a. (2007) The uncoupled chloride conductance of a bacterial glutamate transporter homolog. *Nat. Struct. Mol. Biol. 14*, 365–371.

184) Veruki, M. L., Mørkve, S. H., and Hartveit, E. (2006) Activation of a presynaptic glutamate transporter regulates synaptic transmission through electrical signaling. *Nat. Neurosci. 9*, 1388–1396.

185) Wersinger, E., Schwab, Y., Sahel, J.-A., Rendon, A., Pow, D. V, Picaud, S., and Roux, M. J. (2006) The glutamate transporter EAAT5 works as a presynaptic receptor in mouse rod bipolar cells. *J. Physiol. 577*, 221–234.

186) Cater, R. J., Ryan, R. M., and Vandenberg, R. J. (2016) The Split Personality of Glutamate Transporters: A Chloride Channel and a Transporter. *Neurochem. Res. 41*, 593-599.

187) Mim, C. (2005) The Glutamate Transporter Subtypes EAAT4 and EAATs 1-3 Transport Glutamate with Dramatically Different Kinetics and Voltage Dependence but Share a Common Uptake Mechanism. *J. Gen. Physiol. 126*, 571–589.

188) Gameiro, A., Braams, S., Rauen, T., and Grewer, C. (2011) The discovery of slowness: low-capacity transport and slow anion channel gating by the glutamate transporter EAAT5. *Biophys. J. 100*, 2623–2632.

189) Verdon, G., and Boudker, O. (2012) Crystal structure of an asymmetric trimer of a bacterial glutamate transporter homolog. *Nat. Struct. Mol. Biol. 19*, 355–357.

190) Cater, R. J., Vandenberg, R. J., and Ryan, R. M. (2014) The Domain Interface of the Human Glutamate Transporter EAAT1 Mediates Chloride Permeation. *Biophys. J. 107*, 621–629.

191) Hotzy, J., Machtens, J.-P., and Fahlke, C. (2012) Neutralizing aspartate 83 modifies substrate translocation of excitatory amino acid transporter 3 (EAAT3) glutamate transporters. *J. Biol. Chem. 287*, 20016–20026.

192) Reyes, N., Oh, S., and Boudker, O. (2013) Binding thermodynamics of a glutamate transporter homolog. *Nat. Struct. Mol. Biol. 20*, 634–640.

193) Heinzelmann, G., Bastug, T., and Kuyucak, S. (2013) Mechanism and energetics of ligand release in the aspartate transporter Glt$_{Ph}$. *J. Phys. Chem. B 117*, 5486–5496.

194) Larsson, H. P., Tzingounis, A. V, Koch, H. P., and Kavanaugh, M. P. (2004) Fluorometric measurements of conformational changes in glutamate transporters. *Proc. Natl. Acad. Sci. U. S. A. 101*, 3951–3956.

195) Petsko, G. a. (2006) An introduction to modeling structure from sequence. *Curr. Protoc.*
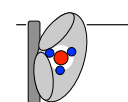
*Bioinformatics Chapter 5*, Unit 5.1.

196) Søndergaard, C. R., Garrett, A. E., Carstensen, T., Pollastri, G., and Nielsen, J. E. (2009) Structural artifacts in protein-ligand X-ray structures: Implications for the development of docking scoring functions. *J. Med. Chem. 52*, 5673–5684.

197) Blow, D. M. (2002) Outline of crystallography for biologists 1st ed. Oxford University Press, Oxford.

198) Walton, E. B., and VanVliet, K. J. (2006) Equilibration of experimentally determined protein structures for molecular dynamics simulation. *Phys. Rev. E. Stat. Nonlin. Soft. Matter Phys. 74*, 061901.

199) Meller, J. (2001) Molecular Dynamics. *Encycl. Life Sci.* 1–8.

200) Wieder, M., Perricone, U., Seidel, T., Boresch, S., and Langer, T. (2016) Comparing pharmacophore models derived from crystal structures and from molecular dynamics simulations. *Monatshefte für Chemie 147*, 553–563.

201) Tzingounis, A. V., and Wadiche, J. I. (2007) Glutamate transporters: confining runaway excitation by shaping synaptic transmission. *Nat. Rev. Neurosci. 8*, 935–947.

202) Kanai, Y., Nussberger, S., Romero, M. F., Boron, W. F., Hebert, S. C., and Hediger, M. A. (1995) Electrogenic properties of the epithelial and neuronal high affinity glutamate transporter. *J. Biol. Chem. 270*, 16561–16568.

203) Watzke, N., Bamberg, E., and Grewer, C. (2001) Early intermediates in the transport cycle of the neuronal excitatory amino acid carrier EAAC1. *J. Gen. Physiol. 117*, 547–562.

204) Erkens, G. B., and Slotboom, D. J. (2010) Biochemical characterization of ThiT from *Lactococcus lactis*: A thiamin transporter with picomolar substrate binding affinity. *Biochemistry 49*, 3203–3212.

205) Ewers, D., Becher, T., Machtens, J.-P., Weyand, I., and Fahlke, C. (2013) Induced fit substrate binding to an archeal glutamate transporter homologue. *Proc. Natl. Acad. Sci. U. S. A. 110*, 12486–12491.

206) Akyuz, N., Altman, R. B., Blanchard, S. C., and Boudker, O. (2013) Transport dynamics in a glutamate transporter homologue. *Nature 502*, 114–118.

207) Focke, P. J., Annen, A. W., and Valiyaveetil, F. I. (2015) Engineering the glutamate transporter homolog Glt$_{Ph}$ using protein semisynthesis. *Biochemist*ry 54, 1694-1702.

208) Lolkema, J. S., and Slotboom, D.-J. (2015) The Hill analysis and co-ion-driven transporter kinetics. *J. Gen. Physiol. 145*, 565–574.

209) McIlwain, B. C., Vandenberg, R. J., and Ryan, R. M. (2015) Transport Rates of a Glutamate Transporter Homologue Are Influenced by the Lipid Bilayer. *J. Biol. Chem. 290*, 9780–9788.

210) Hänelt, I., Jensen, S., Wunnicke, D., and Slotboom, D. J. (2015) Low Affinity and Slow Na$^+$ Binding Precedes High Affinity Aspartate Binding in the Secondary-active Transporter Glt$_{Ph}$. *J. Biol. Chem. 290*, 15962–15972.

211) Menaker, D., Bendahan, A., and Kanner, B. I. (2006) The substrate specificity of a neuronal glutamate transporter is determined by the nature of the coupling ion. *J Neurochem. 99*, 20–28.

212) Simonin, A., Montalbetti, N., Gyimesi, G., Pujol-Giménez, J., and Hediger, M. A. (2015) The
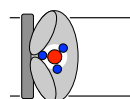
Hydroxyl Side Chain of a Highly Conserved Serine Residue is Required for Cation Selectivity and Substrate Transport in the Glial Glutamate Transporter GLT-1/SLC1A2. *J. Biol. Chem. 290*, 30464-30474.

213)   Torres-Salazar, D., and Fahlke, C. (2007) Neuronal glutamate transporters vary in substrate transport rate but not in unitary anion channel conductance. *J. Biol. Chem. 282*, 34719–34726.

214)   Otis, T. S., and Jahr, C. E. (1998) Anion currents and predicted glutamate flux through a neuronal glutamate transporter. *J. Neurosci. 18*, 7099–7110.

215)   Ryan, R. M., and Vandenberg, R. J. (2005) A channel in a transporter. *Clin. Exp. Pharmacol. Physiol. 32*, 1–6.

216)   Baldwin, R. L. (1996) How Hofmeister Interactions Affect Protein Stability. *Biopghys. J. 71*, 2056–2063.

217)   Jiang, J., Shrivastava, I. H., Watts, S. D., Bahar, I., and Amara, S. G. (2011) Large collective motions regulate the functional properties of glutamate transporter trimers. *Proc. Natl. Acad. Sci. U. S. A. 108*, 15141–15146.

218)   Grewer, C., Watzke, N., Wiessner, M., and Rauen, T. (2000) Glutamate translocation of the neuronal glutamate transporter EAAC1 occurs within milliseconds. *Proc. Natl. Acad. Sci. U. S. A. 97*, 9706–9711.

219)   Wadiche, J. I., Arriza, J. L., Amara, S. G., and Kavanaugh, M. P. (1995) Kinetics of a human glutamate transporter. *Neuron 14*, 1019–1027.

220)   Lee, A. G. (2004) How lipids affect the activities of integral membrane proteins. *Biochim. Biophys. Acta - Biomembr. 1666*, 62-87.

221)   Palsdottir, H., and Hunte, C. (2004) Lipids in membrane protein structures. *Biochim. Biophys. Acta - Biomembr. 1666*, 2-18.

222)   Dowhan, W., and Bogdanov, M. (2012) Molecular genetic and biochemical approaches for defining lipid-dependent membrane protein folding. *Biochim. Biophys. Acta - Biomembr. 1818*, 1097-1107.

223)   Phillips, R., Ursell, T., Wiggins, P., and Sens, P. (2009) Emerging roles for lipids in shaping membrane-protein function. *Nature 459*, 379–385.

224)   Bogdanov, M., and Dowhan, W. (2012) Lipid-dependent generation of dual topology for a membrane protein. *J. Biol. Chem. 287*, 37939–37948.

225)   Slotboom, D. J., Konings, W. N., Lolkema, J. S. (2001) Cysteine-scanning Mutagenesis Reveals a Highly Amphipathic, Pore-lining Membrane-spanning Helix in the Glutamate Transporter GltT. *J. Biol. Chem. 276*, 10775–10781.

226)   Rosental, N., and Kanner, B. I. (2010) A conserved methionine residue controls the substrate selectivity of a neuronal glutamate transporter. *J. Biol. Chem. 285*, 21241–21248.

227)   Kabsch, W. (2010) XDS. *Acta Crystallogr. Sect. D Biol. Crystallogr. 66*, 125–132.

228)   Adams, P. D., Afonine, P. V., Bunkóczi, G., Chen, V. B., Davis, I. W., Echols, N., Headd, J. J., Hung, L. W., Kapral, G. J., Grosse-Kunstleve, R. W., McCoy, A. J., Moriarty, N. W., Oeffner, R., Read, R. J., Richardson, D. C., Richardson, J. S., Terwilliger, T. C., and Zwart, P. H. (2010) PHENIX: A comprehensive Python-based system for macromolecular structure solution. *Acta*
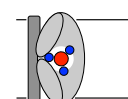
*Crystallogr. Sect. D Biol. Crystallogr. 66*, 213–221.

229)  Emsley, P., and Cowtan, K. (2004) Coot: Model-building tools for molecular graphics. *Acta Crystallogr. Sect. D Biol. Crystallogr. 60*, 2126–2132.

230)  Grewer, C., Gameiro, A., and Rauen, T. (2014) SLC1 glutamate transporters. *Pflügers Arch. - Eur. J. Physiol. 466*, 3–24.

231)  Compton, E. L. R., Taylor, E. M., and Mindell, J. a. (2010) The 3-4 loop of an archaeal glutamate transporter homolog experiences ligand-induced structural changes and is essential for transport. *Proc. Natl. Acad. Sci. U. S. A. 107*, 12840–12845.

232)  Mulligan, C., and Mindell, J. a. (2013) Mechanism of Transport Modulation by an Extracellular Loop in an Archaeal Excitatory Amino Acid Transporter (EAAT) Homolog. *J. Biol. Chem. 288*, 35266–35276.

233)  Silverstein, N., Crisman, T. J., Forrest, L. R., and Kanner, B. I. (2013) Cysteine scanning mutagenesis of transmembrane helix 3 of a brain glutamate transporter reveals two conformationally sensitive positions. *J. Biol. Chem. 288*, 964–973.

234)  McCoy, A. J., Grosse-Kunstleve, R. W., Adams, P. D., Winn, M. D., Storoni, L. C., and Read, R. J. (2007)   Phaser crystallographic software. *J. Appl. Crystallogr. 40*, 658–674.

235)  Afonine, P. V., Grosse-Kunstleve, R. W., Echols, N., Headd, J. J., Moriarty, N. W., Mustyakimov, M., Terwilliger, T. C., Urzhumtsev, A., Zwart, P. H., and Adams, P. D. (2012) Towards automated crystallographic structure refinement with phenix. refine. *Acta Crystallogr. Sect. D Biol. Crystallogr. 68*, 352–367.

236)  Laskowski, R. A., and Swindells, M. B. (2011) LigPlot+: Multiple ligand-protein interaction diagrams for drug discovery. *J. Chem. Inf. Model. 51*, 2778–2786.

237)  Jo, S., Lim, J. B., Klauda, J. B., and Im, W. (2009) CHARMM-GUI membrane builder for mixed bilayers and its application to yeast membranes. *Biophys. J. 97*, 50–58.

238)  Dickson, C. J., Madej, B. D., Skjevik, ??ge A., Betz, R. M., Teigen, K., Gould, I. R., and Walker, R. C. (2014) Lipid14: The amber lipid force field. *J. Chem. Theory Comput. 10*, 865–879.

239)  Jorgensen, W. L., Chandrasekhar, J., Madura, J. D., Impey, R. W., and Klein, M. L. (1983) Comparison of simple potential functions for simulating liquid water. *J. Chem. Phys. 79*, 926.

240)  Case, D. A., Babin, V., Berryman, J. T., Betz, R. M., Cai, Q., Cerutti, D. S., Cheatham, III, T. E., Darden, T. A., Duke, R. E., Gohlke, H., Goetz, A. W., Gusarov, S., Homeyer, N., Janowski, P., Kaus, J., Kolossváry, I., Kovalenko, A., Lee, T. S., LeGrand, S., Luchko, T., Luo, R., Madej, B., Merz, K. M., Paesani, F., Roe, D. R., Roitberg, A., Sagui, C., Salomon-Ferrer, R., Seabra, G., Simmerling, C. L., Smith, W., Swails, J., Walker, R. C., Wang, J., Wolf, R. M., Wu, X., Kollman, P. A., Kollman, W. and P. A., Duke, H. Gohlke, A.W. Goetz, S. Gusarov, N. Homeyer, P. Janowski, J. Kaus, I. Kolossváry, A. K., T.S. Lee, S. LeGrand, T. Luchko, R. Luo, B. Madej, K.M. Merz, F. Paesani, D.R. Roe, A. Roitberg, C. S., R. Salomon-Ferrer, G. Seabra, C.L. Simmerling, W. Smith, J. Swails, R.C. Walker, J. Wang, R.M. Wolf, X., and Kollman, W. and P. A. (2014) AMBER 14. *Univ. California, San Fr.*

241)  Karplus, M., and Kushick, J. N. (1981) Method for estimating the configurational entropy of
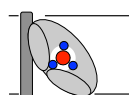
macromolecules. *Macromolecules 14*, 325–332.

242) Gourdon, P., Andersen, J. L., Hein, K. L., Bublitz, M., Pedersen, B. P., Liu, X. Y., Yatime, L., Nyblom, M., Nielsen, T. T., Olesen, C., Møller, J. V., Nissen, P., and Morth, J. P. (2011) HiLiDe - systematic approach to membrane protein crystallization in lipid and detergent. *Cryst. Growth Des. 11*, 2098–2106.

243) Caffrey, M., Li, D., and Dukkipati, A. (2012) Membrane protein structure determination using crystallography and lipidic mesophases: Recent advances and successes. *Biochemistry 51*, 6266–6288.

244) Verma, S., and Prabhakar, Y. S. (2015) Target based drug design - a reality in virtual sphere. *Curr. Med. Chem. 22*, 1603–1630.

245) Sliwoski, G., Kothiwale, S., Meiler, J., and Lowe, E. W. (2013) Computational Methods in Drug Discovery. *Pharmacol. Rev. 66*, 334–395.

246) Borre, L., and Kanner, B. I. (2004) Arginine 445 controls the coupling between glutamate and cations in the neuronal transporter EAAC-1. *J. Biol. Chem. 279*, 2513–2519.
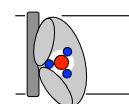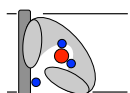
# List of Publications

Guskov, A.*, <u>Jensen, S.</u>*, Faustino, I., and Marrink, S. J. (2016) Mechanism of coupled transport of three sodium ions and aspartate in the glutamate transporter homologue $Glt_{Tk}$. *Nat. Commun. 7*, 13420.

Hänelt, I.*, <u>Jensen, S.</u>*, Wunnicke, D., and Slotboom, D. J. (2015) Low Affinity and Slow $Na^+$ Binding Precedes High Affinity Aspartate Binding in the Secondary-active Transporter $Glt_{Ph}$. *J. Biol. Chem. 290*, 15962–15972.

<u>Jensen, S.</u>*, Guskov, A.*, Rempel, S., Hänelt, I., and Slotboom, D. J. (2013) Crystal structure of a substrate-free aspartate transporter. *Nat. Struct. Mol. Biol. 20*, 1224–1226.

*: Shared first authorship
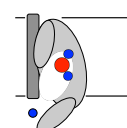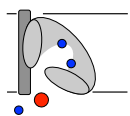
# Acknowledgments

Now an exciting, challenging, and fantastic time comes to its end. Throughout the past couple of years I was able to work not only on an amazing project but also met and worked with many interesting and wonderful people that helped me master my PhD. This chapter is dedicated to my family, friends, and colleagues that enriched my life in and outside of academia.

First of all I want to thank my promotor **Dirk**. Thank you for giving me the chance to work on the glutamate transporter project. Your enthusiasm about this project convinced me to join the group and work on the topic. I really feel honored that you entrusted me with the project that you have been working on during your own PhD research. I was happy to find in you a supervisor that truly was interested in the project and excited about every new result and break through. Your ability to explain even the most complicated things in a way that everyone could understand it is amazing and absolutely inspiring.

I also would like to thank my reading committee (Prof. dr. **A.J.M. Driessen**, Prof. dr. **R. Dutzler**, Prof. dr. **B. Poolman**) for taking the time to carefully read my thesis, for the encouraging comments, and for the constructive suggestions that helped me to improve the content.

**Albert**, you accompanied me during the first synchrotron trips and taught me how to collect data sets. Also, when I went alone to the synchrotron you were always online and ready to offer support. Often it felt like watching a magician when you processed the data: twinning or not - you always managed to get the best out of it. Thank you!

**Stefan**, **Łukasz**, **Nynke**, and **Gianluca**, I was lucky to have you as my bachelor and master students. I enjoyed working with you all and have learned a lot from you. Thank you for your help on the glutamate transporters!

Dear **Faizah**, I got to know you during my final project in the X-ray group, when I was still studying biology. We both were setting up plates. Half a year later I started my PhD research and was happy to find in you a wonderful colleague and friend. Now you have returned to Indonesia and surely I will visit you there one day.

**Trijnia**, we started our PhD projects almost at the same time, and for half a year we shared the same office and lab. Thank you for all the laughter we had together, for helping me set up my laptop, and installing most of the programs that I needed for my PhD research.

**Dorith**, about one month after I started my PhD project you joined the Membrane Enzymology group. Together we discovered Groningen. Thank you for the nice conversations, some great baking experiments, and your support in the lab.

I also would like to thank **Sarah**, **Evelyn**, and **Jonas** for their advice and friendship throughout the past years. Thanks to you life was never boring. Jonas with you I could always joke around and I enjoyed our singing sessions in the lab. Sarah and Evelyn, you managed to get me interested into playing settlers. At this point I also would like to thank the current settlers crew **Karin**, **Rianne**, **Wenxuan**, and **Gea** for the delicious dishes and evenings full of fun while playing settlers.

**Franz** and **Raj**, when I was working late I was seldom alone: I could count on one of you to be around too. We often tried to beat each other on not being the last to leave, but I think there was never a clear winner.

**Joana**, in my third year you joined the group and worked on glutamate transporters for a while. Thank you for the great time working together.

**Ignacio**, thank you for performing the MD simulations and for your patience.
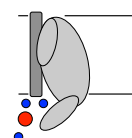
I also would like to thank current and previous members of the Membrane Enzymology group that I had the pleasure to work with, share my office with, and that had direct or indirect influence on my PhD but have not already been mentioned (in alphabetical order): **Alisa**, **Andreija**, **Anna**, **Annemarie**, **Anton**, **Arnold**, **Artem**, **Astri**, **Boqun**, **Christoffer**, **Duygu**, **Frans**, **Gemma**, **Guus**, **Hendrik**, **Jan-Peter**, **Jeanette**, **Jelger**, **Łukasz**, **MacDonald**, **Marina**, **Martyna**, **Marysia**, **Michael**, **Nadia**, **Nobina**, **Patricia**, **Pranav**, **Ruslan**, **Ryan**, **Stephanie**, **Tjeerd**, **Valentina**, **Wojtek**, and **Yustina**. Thank you for your advice, support, encouraging words, useful feedback and comments, and inspiration. Additionally, I want to thank all previous and current members of the Membrane Enzymology group for creating a welcoming and creative work environment.

**Cyntia**, **Marco**, **Paulien**, **Daniël**, **Jennifer**, and **Manuel** thank you for enriching my life outside of university.

Furthermore, I want to thank my **family** for their support, patience, and for believing in me. Heartfelt thanks also to my Dutch family: Beste **André** en **Dineke** – Pa en Ma, bedankt dat jullie mij met open armen opgenomen hebben en er altijd voor me waren. Bedankt voor jullie interesse in mijn onderzoek, jullie zijn de beste schoonouders die ik mij kan wensen.

Last but not least I want to thank you **Edwin**. You were there for me whenever I needed you. Thank you for cooking dinner, picking me up from work when it was getting late, cheering me up, and sharing my joy. You kept me grounded and gave me wings to fly. Thank you for your support, patience, and love. You are my best friend and I am so lucky to have you in my life.